Cost Effective Expansion Planning

Mathematical optimization models to support large scale offshore wind deployment

Stephen Hardy

Supervisors:
Prof. dr. ir. D. Van Hertem
Dr. dipl.-ing. H. Ergun

Dissertation presented in partial
fulfillment of the requirements for the
degree of Doctor of Engineering
Science (PhD): Electrical Engineering

June 2023

Cost Effective Expansion Planning

Mathematical optimization models to support large scale offshore wind deployment

Stephen HARDY

Examination committee:
Prof. dr. ir. P. Wollants, chair
Prof. dr. ir. D. Van Hertem, supervisor
Dr. dipl.-ing. H. Ergun, supervisor
Prof. dr. ir. R. Sabariego
Prof. dr. ir. J. Meyers
Prof. dr. ir. L. Meeus   (KUL/Florence School of regulation)
Prof. dr. ir. B. Kazemtabrizi
  (Durham University)
Prof. dr. ir. E. Prieto-Araujo
  (Universitat Politècnica de Catalunya (UPC))
Ir. Kristof Van Brusselen
  (Parkwind)

June 2023

Preface

PhDs are hard. Anyone who says differently is selling something. It is fair to say I didn't realize how hard it would be when almost five years ago, my wife Akari and I decided to move out to Belgium and take on the challenge. If I am completely honest, we did it for the visa. We wanted to move to Europe and getting a company to sponsor a visa is much harder than getting a University to do the same. Don't get me wrong, getting the opportunity to work with offshore wind and do a deep dive into the incredible world of optimization was a big carrot but I didn't really understand at the start what I was getting into. To me, it was simply an interesting job opportunity that happened to be in academia, which meant a visa would be easier to acquire. Now, nearing the end of this chapter of our lives we are left looking back at a period of time that will shape our future more than we would have ever expected. My first and deepest debt of gratitude is owed to the most important human in my life, my incredible partner, the one who has been there from start to finish and has supported me through thick and thin. Thank you for your love and patience Akari, without you, this wasn't possible.

Next, I want to express my deep gratitude to Dr Hakan Ergun. Throughout my working career, it has been one job after another where I have felt thrown to the wolves. Left with little direction and outsized expectations. While many say this is how we grow, in my case it was too much. I disliked my jobs and ended up leaving them before I could become proficient. This has made me somewhat of a jack-of-all-trades, master of none. What I have needed and have been searching for is a mentor, somebody I deeply respected for their ability and who was willing to take the time to teach me. This is what I finally found with Hakan and I am most grateful for, I could not have had a better supervisor. Between our bi-weekly updates and Friday beers on the lawn, Hakan set up a great work environment. I hope one day to have as positive an impact on another's career as he has had on mine. I feel truly lucky to have had his guidance throughout this process.

Prof. Dirk Van Hertem has been an exceptional leader to the research group. While I tend to think of Dirk as my "boss" and Hakan my supervisor, there is no better boss to have than Dirk. Those lucky enough to be in his care experience the benefits of having a supervisor that truly cares for his employee's wellbeing. This was especially apparent during a time dominated by the pandemic. I am particularly grateful to Dirk for his flexibility regarding working arrangements. When visa renewal requirements meant Akari needed to return to Japan, Dirk encouraged me to investigate possible Japanese University collaborations. This lead to the very rewarding work performed in chapter 7 of this thesis completed in part at Kyushuu University. Without Hakan and Dirk as supervisors, I am unsure I could have made it this far. They have both changed my life for the better and I am deeply appreciative.

I owe a debt of gratitude to Stijn Hendrix and Toni Dalmau at Enersynt for keeping the office door open for me at all times – even giving me my own keys. This connection to industry was very important in keeping the research grounded in reality. As Stijn was my supervisor along with Kristof Van Brusselen at CG power systems before it's bankruptcy forced me to switch over to KU Leuven, he has been involved in the project from the start. The many discussions on practical applications as well as needs in industry has been invaluable.

Of course, for hiring me in the first place and starting me on this journey I owe to Kristof Van Brusselen. Thank you for taking the risk and staying on throughout the PhD within the advisory committee. I have been very lucky to have a wonderful advisory committee throughout the process. Prof. Ruth Sabariego, T.A.ing your finite element modelling course was an incredible challenge but it was a truly enjoyable experience due to your incredible patience and guidance. Prof. Eduardo Prieto-Araujo, from the very beginning of the InnoDC project your leadership was essential in sending me down the right research path.

As mentioned the work of chapter 7 was performed in collaboration with Kyushuu University in Japan under the guidance of profs. Andreas Themelis and Kaoru Yamamoto. Due to the generosity of both Andreas-san and Kaoru-san my time at KyuDai was incredibly enjoyable and fruitful. Thanks to this collaboration including the many long meetings with Andreas going over the syntactical presentation of my generation and expansion planning formulation I was able to improve dramatically my ability to formulate and effectively communicate to others concisely my optimization models.

This research has been funded under one EU project and a Flemish project, the InnoDC and Cordoba projects. The InnoDC project was what got me to Europe in the first place and funded the first three years of research, for this I am truly grateful. To all the early stage researchers, thanks for the many amazing times. Although they were cut artificially short due to the pandemic

I will forever cherish the connections and lifelong friendships made. Manon Davies, your incredible management of the project made it possible to both develop as a researcher while fully enjoying the experience of interacting with friends from all areas of the world throughout the many partner countries in the EU. It was a very rewarding experience. To all the project partners in Cordoba, thank you for the wonderful collaborations, I look forward to the many more over the next year of the project!

Finally, thanks to my many colleagues at the KU Leuven. Both fellow researchers as well as the incredible support staff at ESAT. I am hesitant to single out names as there are so many who helped in so many ways but a particular thanks must be mentioned to Katja Schils for handling all the administration including my many contract and visa renewals as well as Veronica Lucero Ortega for all the IT support. Also to Jens Moschner and Kris Baert for the great conversations at Friday beers which managed to keep me at least partially sane during the pandemic lockdowns.

To my parents, Bruce and Laurie Hardy.
I hope one day to be as good a parent as you were to me.
Thank you.

Abstract

Effective long term planning of offshore generation and transmission infrastructure in the North Sea is key for the efficient development of Europe's offshore wind resources, an essential component to reach our climate commitments. Planning approaches have been proposed within industry and academia. These approaches are generally grouped into either generation expansion planning or transmission network expansion planning. In Europe's liberalized energy markets, the responsibility for generation expansion lies with private industry, while regulated entities oversee transmission system expansion. One of the challenges in this context is the possible conflict of objectives between these entities, with private investors prioritizing profit maximization and regulated entities responsible for ensuring the reliability and affordability of the electricity supply. As such, to consider either generation or transmission expansion planning in isolation from the other can be problematic. Rather, an integrated approach is more appropriate, one that can simultaneously consider the objectives of all stakeholders involved. Such modelling in the context of offshore wind expansion planning is still lacking and is a principle focus of the work in this thesis.

The rapid pace at which offshore wind technology has evolved further complicates offshore planning. Planning models have failed to keep pace. Over the last thirty years, the capacity of offshore wind farms has increased by orders of magnitude, multiple concessions are placed side by side, and locations farther out to sea are utilized. Still, planning approaches at the power plant scale have tended to focus heavily on collection circuit topology optimization while assuming a radial transmission connection to shore. These planning models have not tended to consider the possibility of a transmission system design based on multiple neighboring concessions. The high level offshore expansion planning models have largely missed this scale as well, rather focusing on trans-national network expansion such as the planning of HVDC interconnectors. The gap in between these two scales is of particular interest when considering an integrated approach as it is the transitional piece that links models suited for low level collection circuit optimization with those for high level trans-national grid planning.

This thesis proposes a comprehensive planning methodology that addresses the integration of offshore wind generation and the interconnection of energy markets. The methodology covers a broad range of planning levels, including medium voltage collection circuits up to HVDC interconnectors. This approach allows the incorporation of various energy market models to investigate their impact on offshore generation and expansion planning. At the highest transmission capacity level, the proposed methodology employs a step-wise, least regret generation and transmission network expansion formulation that considers hybrid offshore assets and market design. At the medium capacity transmission level, the methodology includes a mathematical framework that describes the combinatorial search space of the problem, classical and heuristic based approaches to efficiently traverse the search space, a machine learning clustering approach for handling very large offshore development regions, and a candidate offshore substation placement methodology that considers spatial constraints. Finally, the methodology reviews state-of-the-art classical and heuristic optimization techniques at the collection circuit level, with a particular focus on the integration of the medium voltage network with the proposed high voltage network optimization.

In summary, this thesis presents a novel and comprehensive approach to offshore wind expansion planning that addresses the challenges of integrating different energy market models and considers the objectives of all stakeholders involved, from private investors to regulated entities. The proposed methodology fills a critical gap in the existing planning models and provides a valuable tool for the effective long-term planning of offshore generation and transmission infrastructure in the North Sea, which is key for the efficient development of Europe's offshore wind resources and the achievement of our climate commitments.

Beknopte samenvatting

Effectieve langetermijnplanning van offshore-opwekkings- en transmissie-infrastructuur in de Noordzee is essentieel voor de efficiënte ontwikkeling van Europa's offshore windenergie, een essentieel onderdeel om onze klimaatdoelstellingen te halen. Zowel binnen industrie als academische wereld zijn hiervoor reeds verschillende planningsbenaderingen voorgesteld. Deze benaderingen worden over het algemeen gegroepeerd in enerzijds planning voor de uitbreiding van de opwekkingscapaciteit en anderzijds planning voor de uitbreiding van transmissienetwerken. In de geliberaliseerde energiemarkten van Europa ligt de verantwoordelijkheid voor de uitbreiding van de opwekking bij de particuliere industrie, terwijl gereguleerde entiteiten toezicht houden op de uitbreiding van het transmissiesysteem. Een van de uitdagingen in deze context is de mogelijke verkeerde afstemming van doelstellingen tussen deze entiteiten, waarbij particuliere investeerders prioriteit geven aan winstmaximalisatie en gereguleerde entiteiten verantwoordelijk zijn voor het waarborgen van de betrouwbaarheid en betaalbaarheid van de elektriciteitsvoorziening. Als zodanig kan het problematisch zijn om zowel de planning voor de uitbereiding van de opwekkingscapaciteit als transmissienetwerken los van elkaar te beschouwen. Veeleer is een geïntegreerde aanpak geschikter die tegelijkertijd rekening houdt met de doelstellingen van alle betrokken belanghebbenden. Een dergelijke modellering in de context van offshore wind-uitbreidingsplanning ontbreekt nog en is een hoofdfocus van het werk in dit proefschrift.

Het snelle tempo waarin netwerk- en offshore windtechnologie zich heeft ontwikkeld maakt offshore planning nog complexer waardoor huidige planningsmodellen geen rekening houden met deze recente ontwikkelingen. De afgelopen dertig jaar is de capaciteit van offshore windparken exponentieel toegenomen, zijn meerdere concessies naast elkaar uitgebouwd en zijn locaties steeds verder op zee in gebruik genomen. Toch hebben planningsbenaderingen op de schaal van offshore windparken de neiging zich sterk te concentreren op optimalisatie van de topologie van het verzamelcircuit, terwijl wordt uitgegaan van een radiale transmissieverbinding met de kust. Deze planningsmodellen negeren de

mogelijkheid van een transmissiesysteemontwerp op basis van meerdere naburige concessies. De planningsmodellen voor offshore-uitbreiding op hoog niveau hebben deze schaal ook grotendeels gemist aangezien ze zich richten op transnationale netwerkuitbreiding, zoals de planning van HVDC-interconnectoren. De kloof tussen deze twee schalen is van bijzonder belang bij het overwegen van een geïntegreerde aanpak waarbij modellen die geschikt zijn voor optimalisatie van het verzamelcircuit gekoppeld worden met die voor transnationale netplanning.

Dit proefschrift stelt een alomvattende planningsmethodiek voor die zich richt op de integratie van offshore windopwekking en de onderlinge verbinding van energiemarkten. De methodologie omvat een breed scala aan planningsniveaus, waaronder middenspanningsverzamelcircuits tot HVDC-interconnectoren. Deze aanpak maakt het mogelijk om verschillende energiemarktmodellen te integreren om hun impact op offshore-opwekkings- en uitbreidingsplanning te onderzoeken. Op het hoogste transmissiecapaciteitsniveau maakt de voorgestelde methodologie gebruik van een stapsgewijze, minst spijt opwekkings- en transmissienetwerk-uitbreidingsformulering die rekening houdt met hybride offshore-activa en marktontwerp. Op het transmissieniveau met gemiddelde capaciteit omvat de methodologie een wiskundig raamwerk dat enerzijds de combinatorische zoekruimte van het probleem beschrijft, alsook klassieke en op heuristiek gebaseerde benaderingen om de zoekruimte efficiënt te doorkruisen, een machine learning-clusteringsbenadering voor het omgaan met zeer grote offshore-ontwikkelingsregio's, en een kandidaat plaatsingsmethode voor offshore onderstations die rekening houdt met ruimtelijke beperkingen. Ten slotte bespreekt de methodologie state-of-the-art klassieke en heuristische optimalisatietechnieken op het niveau van het verzamelcircuit met bijzondere aandacht voor de integratie van het middenspanningsnetwerk met de voorgestelde optimalisatie van het hoogspanningsnetwerk.

Samenvattend presenteert dit proefschrift een nieuwe en alomvattende benadering van de uitbreidingsplanning van offshore windenergie die de uitdagingen van de integratie van verschillende energiemarktmodellen aanpakt en rekening houdt met de doelstellingen van alle betrokken belanghebbenden, van particuliere investeerders tot gereguleerde entiteiten. De voorgestelde methodologie vult een kritieke leemte in de bestaande planningsmodellen en biedt een waardevol instrument voor de effectieve langetermijnplanning van offshore-opwekkings- en transmissie-infrastructuur in de Noordzee, wat essentieel is voor de efficiënte ontwikkeling van Europa's offshore windenergie en de verwezenlijking van onze klimaatdoelstellingen.

Abbreviations

ARM	Association Rule Mining.
CAPEX	Capital Expenditures.
EEA	Exclusive Economic Area.
EENT	Expected Energy Not Transmitted.
ENTSO-E	European Network of Transmission System Operators for Electricity.
GA	Genetic Algorithm.
GATE	Generation And Transmission Expansion.
GEP	Generation Expansion Planning.
HMD	Home Market Design.
HOA	Hybrid Offshore Asset.
HVAC	High Voltage Alternating Current.
HVDC	High Voltage Direct Current.
IEC	International Electrotechnical Commission.
LCOE	Levelized Cost of Energy.
LFAC	Low Frequency Alternating Current.
MILP	Mixed Integer Linear Programming.
MINLP	Mixed Integer Non-Linear Programming.
MIP	Mixed Integer Program.
MIQP	Mixed Integer Quadratic Programming.
MPC-AC	Mid Point Compensated HVAC.
MVAC	Medium Voltage Alternating Current.
nOBZ	nodal Offshore Bidding Zone.
NPV	Net Present Value.
NTC	Net Transfer Capacity.
OPEX	Operating Expenditure.
OSS	Offshore Substation.
OW-EP	Offshore Wind Expansion Planning.
OW-GATE	Offshore Wind Generation And Transmission Expansion Planning.
OW-TNEP	Offshore Wind Transmission Network Expansion Planning.

OWPP	Offshore Wind Power Plant.
PCC	Point of Common Coupling.
RC	Route Cost.
RCC	Route Capital Cost.
RES	Renewable Energy Source.
RLC	Route Loss Cost.
TC	Terminal Cost.
TCC	Terminal Capital Cost.
TLC	Terminal Loss Cost.
TNEP	Transmission Network Expansion Planning.
TSO	Transmission System Operator.
TYNDP	Ten Year Network Development Plan.
VOLL	Value Of Lost Load.
zOBZ	zonal Offshore Bidding Zone.

List of Symbols

Special notation:

- $x : n$ (x located at node n).
- $x : mn$ (x located on directed edge mn).
- $x : {mn}$ (x located on undirected edge mn).
- Candidate and existing infrastructure are differentiated by tildes and overlines, e.g. $\widetilde{g}$ is a candidate and $\bar{g}$ is an existing generator.
- Sub and super scripts written in italics refer to variables, while identifiers are written in roman font.

$\mathcal{A}^{\mathrm{br}}$	Balancing responsible optimization variables
$\mathcal{A}^{\mathrm{te}}$	Transmission expansion optimization variables
$\mathcal{A}_{\mathrm{j}}$	Storage developer optimization variables
$\mathcal{A}_{\mathrm{o}}$	Transmission developer optimization variables
$\mathcal{A}_{\mathrm{w}}$	OWPP developer optimization variables
$\alpha^{\ell,\mathrm{br}}$	Intra-zonal candidate line binary decision variable
$\alpha^{\ell,\mathrm{te}}$	Inter-zonal candidate line binary decision variable
α^{ℓ}	Candidate line binary decision variable
$\boldsymbol{A}$	Set of binary strings for OWPPs
$\boldsymbol{B}$	Set of combinations of OWPPs
$\boldsymbol{C}$	Set of compliment combinations of OWPPs
$\boldsymbol{E}$	Set of k-combinations of combinations of OWPPs
$\boldsymbol{H}$	Exhaustive set of combinations of OWPPs
$\boldsymbol{T}^{\mathrm{B}}$	Basis set of topologies
$\boldsymbol{T}^{\mathrm{E}}$	k-combinations set of radial topologies
$\boldsymbol{T}^{\mathrm{FR}}$	Optimal set of k-combinations of radial topologies
$\boldsymbol{T}^{\mathrm{H}}$	Optimal set of single export cable radial topologies
$\Delta\theta^{\mathrm{max}}$	Maximum voltage angle difference
$\Delta E^{\mathrm{j,max}}$	Change in storage capacity
δI^{ζ}	Converter expansion investment
δI^{g}	Generation expansion investment

δI^{j}	Storage expansion investment
$\Delta P^{\mathrm{g,max}}$	Change in generation capacity
$\Delta P^{\zeta,\mathrm{max}}$	Change in converter capacity
$\mathcal{E}$	Set of all (directed) edges
$\mathcal{E}^{\mathrm{AC}}$	Set of AC network edges
$\mathcal{E}^{\mathrm{DC}}$	Set of DC network edges
$\mathcal{E}^{\mathrm{br}}$	Set of intra-zonal edges
$\mathcal{E}^{\mathrm{te}}$	Set of inter-zonal edges
$\mathcal{E}^{\mathrm{AC\text{-}DC}}$	Set of all edges between AC and DC networks
ϵ	Error in eliminated connections
$\eta^{\mathrm{j,abs}}$	Charge efficiency of storage
$\eta^{\mathrm{j,inj}}$	Discharge efficiency of storage
$\bar{\mathcal{S}}_{\mathrm{g}}$	Set of existing generators
$\bar{\mathcal{S}}_{\ell}$	Set of existing transmission lines
γ^{j}	Self-discharge rate
κ	Member of the population of OWPP connections
λ	Market clearing price
$\mathcal{D}$	Database of items
$\mathcal{G}^{\mathrm{AC}}$	HVAC grid
$\mathcal{G}^{\mathrm{CC}}$	Collection circuit
$\mathcal{G}^{\mathrm{DC}}$	HVDC grid
$\mathcal{G}^{\mathrm{L}}$	High capacity grid
$\mathcal{G}^{\mathrm{M}}$	Medium capacity grid
$\mathcal{G}^{\mathrm{S}}$	Low capacity grid
$\mathcal{U}$	Social welfare
$\mathcal{N}$	Set of all nodes
$\mathcal{N}^{\mathrm{AC}}$	Set of all AC nodes
$\mathcal{N}^{\mathrm{DC}}$	Set of all DC nodes
Ω	Set of candidate OSS locations
π_s	Probability of scenario s
Ψ^{g}	RES generator time series
Ψ^{u}	Demand time series
ρ	Wind energy density
$\mathcal{S}_{\mathrm{g}}$	Set of all generators
$\mathcal{S}_{\mathrm{j}}$	Set of storage devices
$\mathcal{S}_{\ell}$	Set of all transmission lines
$\mathcal{S}_{\mathrm{s}}$	Set of scenarios
$\mathcal{S}_{\mathrm{t}}$	Set of hours
$\mathcal{S}_{\mathrm{u}}$	Set of demands
$\mathcal{S}_{\mathrm{y}}$	Set of years
τ	Transformer ratio
θ	Voltage angle

θ^{max}	Maximum voltage angle
θ^{min}	Minimum voltage angle
ϱ	Percentage of eliminated connections
$\widehat{E^{\mathrm{j,max}}}$	Maximum expansion capacity of candidate storage
$\widehat{P^{\mathrm{g,max}}}$	Maximum expansion capacity of candidate generators
$\widehat{P^{\zeta,\mathrm{max}}}$	Maximum expansion capacity of candidate converters
$\xi^{\mathrm{j,c}}$	Maximum charge rate
$\xi^{\mathrm{j,d}}$	Maximum discharge rate
$\mathcal{Z}$	Set of market zones
ζ	Sea depth
A^{g}	Area of an OWPP
A^{mv}	Area of cost effective MV connections
b	Transmission line susceptance
C^{g}	Generator bid price
C^{u}	Consumer bid price
D	Set of PCCs
$E^{\mathrm{j,max}}$	Maximum capacity of candidate storage
E^{j}	Capacity of candidate storage
f^{H}	NPV scalar for hourly revenues
f^{Y}	NPV scalar for yearly revenues
G	Set of OWPPs
K	Population of OWPP connections
L^{ζ}	Converter loss factor
P	Confidence
p	Support
$P^{\ell,\mathrm{max}}$	Maximum transmission line power
P^{ℓ}	Instantaneous Transmission line power
$P^{\mathrm{g,max}}$	Maximum generator power
P^{g}	Instantaneous generator power
$P^{\mathrm{j,abs}}$	Instantaneous storage charging power
$P^{\mathrm{j,inj}}$	Instantaneous storage discharging power
$P^{\mathrm{u,max}}$	Maximum demand power
P^{u}	Instantaneous demand power
$P^{\zeta,\mathrm{max}}$	Maximum converter power
$P^{\zeta,\mathrm{AC}}$	Instantaneous AC side converter power
$P^{\zeta,\mathrm{DC}}$	Instantaneous DC side converter power
$P^{\zeta,\mathrm{loss}}$	Instantaneous converter power losses
R	Set of shortest paths
r	Shortest path
T	Hours per simulation year
t_j	Topology j
V	Set of voltage levels

X, Y Sets of items

Contents

List of Figures

List of Tables

Chapter 1

Introduction

1.1 Context

"Code red for humanity!" - UN Secretary General Guterres, in summarizing the sixth assessment report by the Intergovernmental Panel on Climate Change (IPCC), released in August of 2021. Guterres followed this by outlining the necessary actions required to decarbonize the world economy, including a quadrupling of wind and solar generation by 2030 and a net zero economy by 2050 [1]. According to the International Renewable Energy Agency, to limit global warming to 1.5^oC, the proportion of wind and solar making up the electricity mix will have to be around 90% by 2050. Currently, the percentage is around 26% [2]. Furthermore, demand for electricity is growing and is projected to more than double by 2050 [3].

Since the publication of "Climate impact of increasing atmospheric carbon dioxide" by Hansen et al [4] over forty years ago, climate scientists and an engaged populace have been pushing governments with ever increasing urgency to enact meaningful CO_2 emissions reduction policies in order to stem the worst effects of climate change. Finally, in 2015, the first universal and legally binding global climate change agreement was signed by 196 countries at the COP21 summit in Paris, France. 'The Paris Agreement' commits signatories to a nationally determined contribution aimed at stemming global greenhouse gas emissions and limiting global temperature rise to 2^oC [5].

In the EU, climate policy is evolving towards ever stricter targets in an attempt to meet its global climate commitments. In 2009, the 20-20-20 climate and energy package was passed, committing EU member states to a 20% reduction

in greenhouse gas emissions relative to 1990 levels, an energy system powered by 20% Renewable Energy Sources (RESs) and a 20% increase in energy efficiency by 2020. In 2014, the package was updated to a 40% greenhouse gas reduction and 32% RES penetration and increased efficiency by 2030. 2019 brought the introduction of the Green new deal aiming to make Europe the first carbon neutral continent by 2050. At the core of the Green new deal are the fit-for-55 policy proposals that aim to reduce carbon emissions by 55% by 2030 through a combination of increased RES, energy efficiency measures, alternative liquid fuels and market mechanisms [3].

Achieving carbon neutrality in Europe, in no small part, means transitioning our electrical energy infrastructure away from fossil fuels and towards RES. Recent events, specifically the Russian invasion of Ukraine, has only compounded this need. In response to the invasion, the EU released the REpowerEU plan, setting even more ambitious targets for RES than those in the fit-for-55 proposals. REpowerEU increases renewable generation targets to 45% by 2030, up from 40%, as well as expanding funding for hydrogen storage and other energy infrastructure projects [6].

1.2 Motivation

The offshore wind industry has evolved at an incredibly rapid pace over the last thirty years. Today's multi gigawatt offshore wind power plants are a far cry from the world's first offshore wind farm commissioned off the coast of Vindeby island, Denmark in 1991. Vindeby wind farm consisted of eleven – 54 m high, 450 kW turbines [7]. By contrast, turbines today can be over 200 m tall and produce up to 15 MW each [8]. The world's largest offshore wind power plant today; Horn Sea 2, has a capacity of 1.3 GW [9].

The success of offshore wind, despite the increased difficulty of building at sea, can be attributed, in part, to some advantages over it's already highly successful onshore sibling. Out to sea the wind is stronger and more reliable resulting in higher capacity factors. Furthermore, permitting is simpler as it does not lie in anyone's backyard. Coupling these advantages with economies of scale has managed to bring the Levelized Cost of Energy (LCOE) for offshore wind down to between 60 and 112 €/MWh making it a highly competitive electricity generating source [10]. In fact, according to [11] the era of subsidy-free offshore wind in markets such as the UK, Germany and the Netherlands is already upon us.

Europe has led the way in offshore wind development. Currently 28.4 GW of the world's 56 GW of offshore wind installations lie in European waters [12, 13].

Until 2021 the UK had held the record of most installed capacity at 13.6 GW. As of 2022 however, China has claimed the top spot after an astounding 17 GW of new installations in 2021. The total installed capacity in China is now rivalling that of the entire EU at 24.8 GW [13]. Indeed, by the end of 2022 it seems Europe will have lost it's top spot in terms of installed capacity to China. But Europe has ambitious climate goals and if the targets of the Green new deal can be met, it may once again claim this title by the end of the decade [13].

According to the Green new deal, a carbon free energy system will require 240 to 450 GW of offshore wind by 2050. The largest concentration, 212 GW, is expected to be built within the North Sea. The North Sea's geography, in the heart of Europe, surrounded by Belgium, the Netherlands, Germany, Denmark, Norway, France and the UK, make it not only an excellent candidate for large concentrations of offshore wind but also for increasing the interconnectedness of the European energy system and the integration of energy markets. In fact, pairing stochastic RES with increased cross border connections is natural. Geographically linking disparate regions contributes to less volatility in terms of both generation and load profiles. This relationship is demonstrated in Fig. 1.1 where the combined solar and offshore wind generation from the UK, Belgium and Denmark are shown.
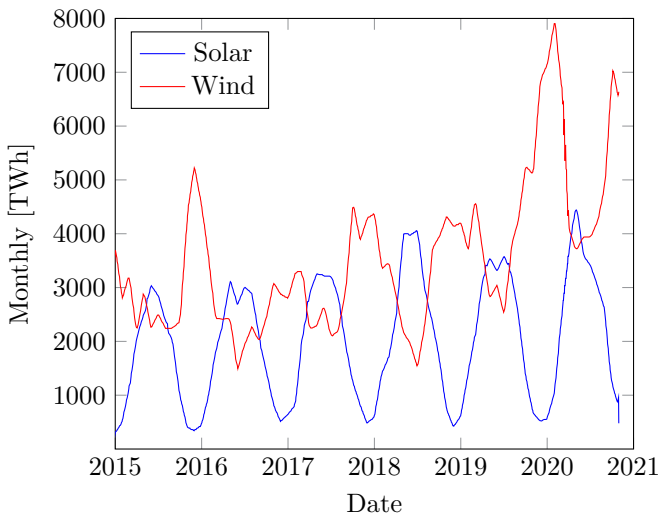
Figure 1.1: Anti-correlation between solar and wind RES from the UK, Belgium and Denmark combined [14].

The anti-correlation between different sources of renewable generation demonstrates that decarbonizing the energy system is not only a case of replacing carbon generating sources with carbon free RESs but also a case of re-enforcing and expanding the current transmission network. The required expansions are by no means small either. Considering just the North Sea and an eventual 212 GW of offshore wind, we will need to build over 100 connections of 2 GW each. There is growing consensus that an offshore grid of such a scale would need to be a meshed High Voltage Direct Current (HVDC) grid [15–18]. Not simply from a transmission capacity perspective but also from a technical perspective as many issues raised by a high penetration of renewables can be mitigated by HVDC grids [19]. The results from this thesis, too, support the conclusion that HVDC is an indispensable technology in our quest to expand renewable generation.

Luckily, recent advancements in HVDC technology, such as voltage source converters and DC protection devices have transitioned a meshed HVDC grid from a technology of the near future to a technology of the now [20]. In fact, a four-terminal HVDC grid has already been demonstrated in Zhangbei China [21]. Europe too, has made steps in this direction. Many point to point HVDC connections exist and new projects such as the proposed 6 GW windpower booster in Germany show development is moving in this direction [22].

To summarize the state of play, to achieve the desired climate targets we have established that we need a rapid expansion of Offshore Wind Power Plants (OWPPs) coupled with the reinforcement and expansion of the transmission network. And in light of recent technological advancements, the best choice of transmission technology is a meshed HVDC network. But how does one effectively take on such a massive undertaking? A basic requirement is high quality tools for offshore planning. Such tools are essential in the development of a road map such as the European Network of Transmission System Operators for Electricity (ENTSO-E)'s Ten Year Network Development Plan (TYNDP). Every two years a new TYNDP is released identifying key infrastructure projects for development. Releasing an updated development plan every two years is no accident as current planning methods are known to be lacking and the ability to incorporate more refined methods and tools is necessary and anticipated.

The TYNDP for 2022 is currently under public consultation and the official release will be in 2023 [23]. Fig. 1.2 shows a map of planned transmission and storage projects. Of the 141 transmission projects, 52 are offshore and include interconnectors, Hybrid Offshore Assets (HOAs) and OWPP connections. In the context of generation expansion needs, ENTSO-E estimates the total installed onshore and offshore wind, and solar power generation capacity under different future scenarios as shown in Table 1.1. We can observe a wide range of projected capacities are specified. This is an effect of the different modelling scenarios.
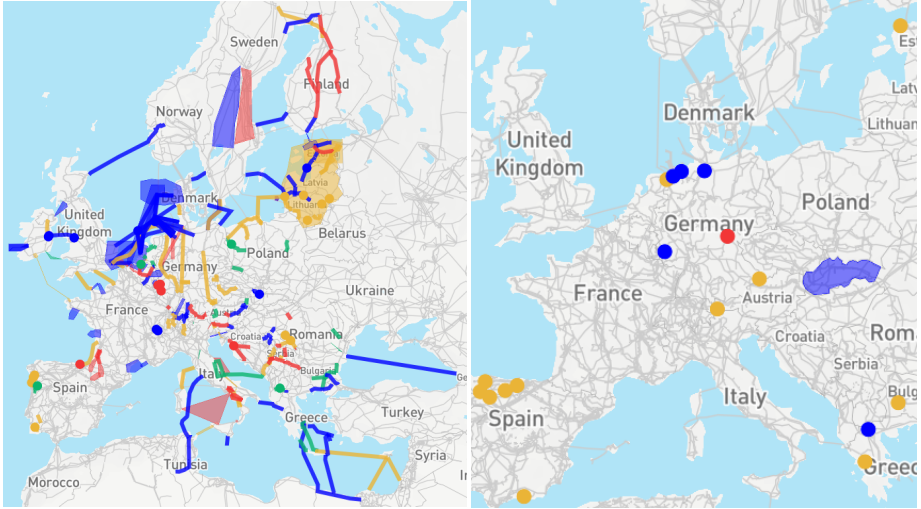
(a) Transmission projects.   (b) Storage projects.

Figure 1.2: Transmission and storage projects from TYNDP 2022. If only on area is displayed the transmission route of the project is still unknown. Blue is under consideration, red is planned but not yet in permitting, yellow is in permitting, green is under construction [23].

Table 1.1: Projected RES generation by type in GW for the EU27 [23].

Type	2030	2040	2050
Onshore wind	250–400	350–600	600–800
Offshore wind	90–100	150–300	250–350
Solar	350–660	500–1350	1050–2150

As such, an offshore planning methodology able to consider different future scenarios is essential and must be incorporated in the future.

Despite the many existing and planned projects for RES expansions, we are still a long way from meeting our climate commitments and our concrete plans lag well behind our vision of where need to be. For example, scenarios put forward within the TYNDP estimate the demand for hydrogen in the EU will be between 426 and 1063 TWh by 2040. Yet none of the 23 currently planned storage projects involve hydrogen [23]. It is estimated that investments in electrical infrastructure of one trillion USD annually, every year, till 2050 will be needed to meet net zero [2,3]. Such an enormous sum will only grow if proper planning is not executed in a timely manner. To ensure Europe invests in the correct

generation and transmission infrastructure at the right time, it is essential we continue to develop and refine advanced long term planning and optimization tools, providing decision makers with the best data and evidence available to effectively and efficiently plan for Europe's carbon free energy future.

1.3 Scope

1.3.1 Basic definitions
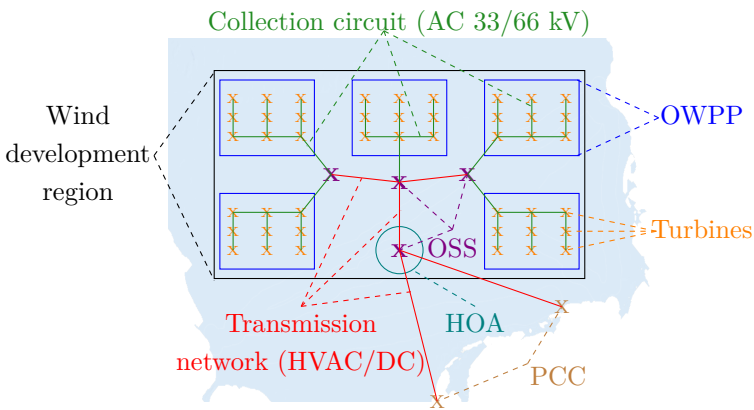
Figure 1.3: Basic definitions of common terms used for describing offshore infrastructure.

The following definitions visualized in Fig. 1.3 are used throughout the thesis:

- **Collection circuit**: the collection circuit is the offshore electrical network that gathers the energy generated at the wind turbines within an OWPP and connects it to the greater transmission network as a whole. The collection circuit can be integrated with the transmission system through an OSS or directly to the PCC. Typically, collection circuits operate at voltage levels of 33 and 66 kV, with modern OWPPs utilizing the higher 66 kV level. As next-generation turbines are introduced, it is likely that OWPPs will transition to even higher voltage levels, such as 132 kV.

- **HOA (Hybrid Offshore Asset)**: A multi-functional piece of offshore infrastructure that combines two or more traditionally independent assets such as storage, inter-connectors and OWPPs into a single hybrid asset.

- **OSS (Offshore Sub Station)**: OSS is a term used to describe any substation located offshore, regardless of its size or functionality. An OSS may serve various functions, ranging from a simple collection platform to a more complex "energy island". In most cases, an OSS is constructed to facilitate a transition between different transmission technologies or voltage levels, such as from medium voltage to high voltage alternating current or from alternating current to direct current transmission.

- **OWPP (Offshore Wind Power Plant)**: An OWPP is a collection of two or more offshore wind turbines, connected via a collection circuit and operated by a single entity. It is important to note that, in this context, an OWPP does not necessarily include an OSS, which, instead is lumped in with the offshore transmission network. In this text the terms "offshore wind farm" and "OWPP" are used interchangeably. The term "OWPP concession" refers specifically to the surface area that contains the OWPP.

- **PCC (Point of Common Coupling)**: A PCC refers to a substation located onshore that serves as a transition point between the offshore and onshore power networks.

- **Transmission network**: The offshore transmission network encompasses all electrical infrastructure up to the PCC that forms both the HVAC and HVDC networks. This includes OSSs but excludes OWPPs and collection circuits. As part of the transmission network, the term "export cable" is used to refer to an offshore transmission cable with a single point connected to a PCC. While the term "feeder" is used to refer to an offshore transmission cable with at least one end connected directly to an OWPP via an OSS. The term "inter-connector" is an offshore transmission cable where the ends terminate in different market zones.

- **Turbines**: An offshore wind turbine is a large-scale device used to convert wind energy to electrical energy. Typically, an offshore wind turbine consists of a tower, blades, nacelle, and other components mounted on either a fixed or floating foundation. At the time of writing, the highest capacity offshore wind turbines in existence have a capacity of approximately 15 MW. In the near future, however, it is expected that turbines with capacities as high as 20 MW or more will become available.

- **Wind development region**: A wind development region refers to an area offshore reserved for the development of one or more OWPPs.

Throughout the thesis, different stakeholders related to offshore development are discussed and are defined as follows:

- **Wind farm developer**: A wind farm developer is an individual or a company that specializes in the planning, design, construction, and operation of wind energy projects. In the context of this thesis it is considered an agent with the objective of profit maximization by developing offshore wind energy.

- **Storage developer**: A storage developer is an individual or a company that specializes in the planning, design, construction, and operation of energy storage systems. In the context of this thesis it is considered an agent with the objective of profit maximization by developing energy storage system.

- **Offshore transmission system developer**: An offshore transmission system developer is a regulated entity that specializes in the planning, design, construction, and operation of transmission systems. In the context of this thesis it is considered an agent with the objective of social welfare maximization through the development of the offshore transmission system.

1.3.2 Context

As the importance of an effective energy transition is high, there are several research projects focused on the development of tools for offshore wind and its enabling technologies that have been funded by the European Commission. These include PROMOTioN [24], MEDOW [25], FlexPlan [26] and InnoDC [27]. This work has been performed in the context of work package 1: "Components of DC grids and wind farms" of the InnoDC project and work package 1: "Optimization models for modular design of hybrid offshore assets" of the Cordoba project. These work packages focused on the development of long term planning and optimization tools for offshore wind farms and HVDC grids.[1]

1.3.3 Research questions

The overall objective (OG) of the thesis can be summarized as:

- OG: developing a holistic, step-wise, multi-period, expansion planning methodology and tool set that considers the uncertainty of long term

planning for offshore wind farms and transmission networks. This overall objective is illustrated in Fig. 1.4. As the optimization of the MVAC collection circuit has been the subject of significant interest in previous literature. This thesis primarily aims to develop strategies for levels 1 and 2 of the network, and to consolidate these distinct issues into a unified framework.
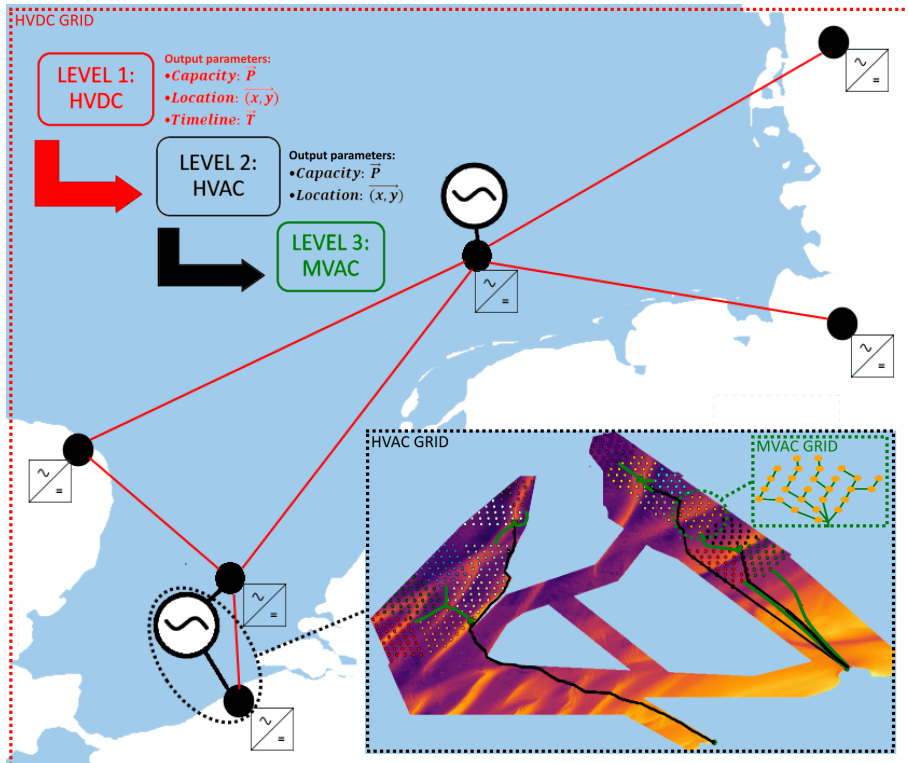
Figure 1.4: Illustration of the over arching framework for multi-level, step-wise planning of offshore transmission and generation expansion.

The overall objective is divided into individual thesis objectives that are in line with the technical goals of the project work packages and are defined as:

- Holistic long term expansion planning:
  - O1: Provide a comprehensive summary of the current state of the art in relation to offshore generation and transmission expansion planning models.

- O2: Propose a general methodology for generation and expansion planning considering collection circuits, intra-national and transnational networks.

- Wind farm transmission networks:

  - O3: Develop models for the various technological options (HVAC, HVDC, etc.) available for connecting OWPPs to shore considering reliability of transmission components and turn them into a planning tool for techno-economically optimizing radial wind farm grid connections.

- Offshore High Voltage Alternating Current (HVAC) transmission networks considering multiple wind farms:

  - O4: Develop an approach for green field transmission network expansion of offshore wind development regions. The choice of technology, the number and location of Offshore Substations (OSSs), the required location and capacity of transmission infrastructure and the topological layout of the network should be specified.

  - O5: Develop decomposition or size reduction strategies that can be employed in the case of large intractable systems.

  - O6: Develop methods of addressing the highly non-linear physical constraints associated with marine spatial planning and hydrography.

- Offshore HVDC grids and energy markets:

  - O7: Develop a planning tool for modular, step-wise design of transnational generation and transmission expansion planning under uncertainty.

  - O8: Develop a methodology for analyzing different energy market models in the context of expansion planning.

Research objectives one through nine are addressed in chapters three through seven and Appendices A and B.

1.4 Contributions

The contributions of the thesis, as with the objectives can be sub-divided into three major categories:

- Holistic long term expansion planning:

– Cn1: A general framework for linking high-level Generation And Transmission Expansion (GATE) planning with the lower-level localized planning models for OWPP collection and transmission systems. This framework fills a gap within the literature between large scale expansion planning models that consider lumped localized grids and the small scale planning tools geared at individual OWPPs.

- Offshore HVAC transmission networks considering multiple wind farms:

    – Cn2: A novel mathematical description of the combinatorial search space of large regions consisting of multiple OWPPs. A greedy search algorithm for determining the optimal number and location of OSSs, transmission topology and infrastructure sizing for large regions consisting of multiple OWPPs (J1).

    – Cn3: A novel approach to search space reduction of very large offshore wind regions through the application of the supervised machine learning approach of association rule mining to clusters of OWPP concessions by eliminating unlikely interconnections (J2).

    – Cn4: An algorithm for determining candidate OSS locations when considering bathymetry, restricted zones and optimal cable routing (C4).

- Offshore HVDC grids and energy markets:

    – Cn5: A methodology/tool for offshore GATE planning considering HOAs. This is in the form of a stochastic mixed integer, multi-period, linear program (J3).

    – Cn6: A methodology/tool for comparing market structures (zonal and nodal) within a GATE planning problem. This is in the form of a multi-level extension to the GATE formulation (J3).

1.5 Publications

1.5.1 Publications included in the thesis

Peer reviewed journals

- J1: **Stephen Hardy**, Hakan Ergun, Dirk Van Hertem, "A Greedy Algorithm for Optimizing Offshore Wind Transmission Topologies," IEEE Transactions On Power Systems - November 2021.

- J2: **Stephen Hardy**, Hakan Ergun, Dirk Van Hertem, "Application of Association Rule Mining in Offshore HVAC Transmission Topology Optimization," Journal Electric Power Systems Research - July 2022.

- J3: **Stephen Hardy**, Hakan Ergun, Dirk Van Hertem, "Generation and transmission expansion planning under Zonal and Nodal market mechanisms," IEEE Transactions on Energy Markets, Policy and Regulation. – under review.

International conferences

- C1: **Stephen Hardy**, Hakan Ergun, Dirk Van Hertem, Stijn Hendrix, Kristof Van Brusselen, "Techno-Economic Analysis of HVAC, HVDC and OFAC Offshore Wind Power Connections." 2019 IEEE Milan PowerTech.

- C2: **Stephen Hardy**, Hakan Ergun, Dirk Van Hertem, "A Techno-Economic Analysis of meshed Topologies of Offshore Wind HVAC Transmission." 2021 IEEE Madrid PowerTech.

- C3: **Stephen Hardy**, Hakan Ergun, Dirk Van Hertem, "Application of Association Rule Mining in Offshore HVAC Transmission Topology Optimization" PSCC 2022 Porto, Portugal.

- C4: **Stephen Hardy**, Hakan Ergun, Dirk Van Hertem, "A Methodology for Offshore Transmission System Optimization Considering Spatial Constraints," 2023 IEEE Belgrade PowerTech – under review.

1.5.2 Publications not included in the thesis

Peer reviewed journals

- J4: Chandra Kant Jat, **Stephen Hardy**, Jay Kumar Dave, Hakan Ergun, Dirk Van Hertem, "Cost Effectiveness of a Multi-Terminal HVDC Demonstration Grid in the North Sea: Off-shore Bidding Zone Strategy For Wind Generators," Applied Energy – under review.

International conferences

- C5: **Stephen Hardy**, Hakan Ergun, Dirk Van Hertem, Kristof Van Brusselen, "A Techno-Economic MILP Optimization of Multiple Offshore Wind Concessions." 2nd International Conference on Large-Scale Grid Integration of Renewable Energy in India.

The relationship between thesis chapters, the objectives, thesis contributions and scientific publications is summarized in Table 1.2.

Table 1.2: Relationship between thesis chapters, research objectives, thesis contributions and scientific publications.

Chapters	Objectives	Contributions	Publications
Ch2	O1	-	-
Ch3	O2	Cn1	-
Ch4	O4	Cn2	J1
Ch5	O5	Cn3	J2
Ch6	O6	Cn4	C4
Ch7	O7	Cn5	J3
Ch7	O8	Cn6	J3
Appendix A/B	O3	-	C1, C2

O: objective, Cn: contribution, C: conference paper, J: journal paper

1.6   Thesis structure

The thesis structure is summarized in Fig. 1.5. In chapter 2 the necessary background for the reader to understand the remaining chapters is presented. It introduces the general field of long term planning and optimization before going into detail on the specific topic of expansion planning. A thorough review of the state of the art in the topic is provided.

In chapter 3, the overall methodology proposed for long term planning and optimization of offshore wind farms and transmission networks is presented. As can be seen in Fig. 1.5, the chapter leads into the work performed in chapters 4 through 7, allowing a brief introduction of each of the topics covered and how they interact with each other in a holistic planning approach.

In chapter 4, HVAC transmission network planning when considering development zones consisting of multiple neighbouring OWPPs is discussed. A mathematical model describing the combinatorial search space is presented. This is followed by the description of a greedy algorithm for efficiently searching the space for the optimal radial transmission topology.

In chapter 5, modelling large problem sizes is addressed. A hybrid search algorithm that combines greedy search with a method of search space reduction based on the machine learning method of association rule mining is presented, bring previously intractable problem sizes into the feasible space.

Chapter 1
Introduction

Chapter 2
Background/State of the art

Chapter 3
Structure of proposed offshore wind expansion planning methodology

Chapter 4
HVAC transmission considering
multiple OWPPs

Chapter 5
HVAC transmission planning of
very large offshore developments

Chapter 6
HVAC transmission planning
considering spatial constraints

Appendix A/B
Economics of offshore transmission

Chapter 7
Generation and transmission
expansion planning in nodal
and zonal market structures

Chapter 8
Conclusions and future work

Figure 1.5: Thesis structure

In chapter 6, the proposed optimization method is extended to deal with the highly non-linear but binding physical constraints of marine spatial planning and bathymetry. A candidate OSS locating algorithm is presented as well as a Mixed Integer Program (MIP) that extends the planning approach to include multiple candidate onshore connection points.

In chapter 7, a multi-period, step-wise, stochastic-scenario based mixed integer GATE planning model is developed. The planning model considers the possibility of HOAs, finding the optimal capacity and layout of transmission infrastructure, storage and OWPPs. The possibility of both HVAC and HVDC transmission is considered. Additionally, expansion planning is performed under different energy market structures, allowing for a comparison between nodal and zonal markets such as home market designs and offshore bidding zones.

In chapter 8, the main conclusions of the work are summarized and suggestions for future work on offshore wind expansion planning are presented.

In Appendices A/B a review of various technologies available for connecting OWPPs to the grid is provided. A techno-economic model is derived, which is used in part or in whole within chapters 4 through 7. The economic model is useful for understanding how quantities such as reliability are accounted for within the proposed methodology. A solution space describing the optimal choice of technology and voltage level given an OWPP capacity and transmission distance is presented. In appendix A, only radial connections for single OWPPs are discussed, while in appendix B, the benefits of making meshed connections between neighbouring OWPPs is investigated. A range as a function of relative location and capacity of the OWPPs is derived and discussed.

Chapter 2

Power system expansion planning

2.1 Introduction

Long term planning and optimization in power systems are highly related disciplines. When planning the long term development of a power system it is useful to study what an optimal (or highly optimized) power system looks like. One can then take educated decisions to steer the development of the existing power system towards a network that meets future needs efficiently.

When one approaches planning with this perspective, an optimization model is an essential tool that guides the decision making process. Power system expansion planning models are optimization models that focus on the following investment decisions in relation to the power system:

- What expansions or refurbishments of the transmission network are required and when should they be completed?

- What additional generation is required, where should it be located and when should it be built?

These questions are motivated by an evolving power system, e.g. aging infrastructure, increasing demand or the construction of new RESs far away from load centres or traditional centralized generating facilities.

The Offshore Wind Expansion Planning (OW-EP) problem is a special case of the general expansion planning problem that focuses specifically on wind generation and transmission network expansion offshore. The problem can be broken down into macro siting of OWPPs, micro-siting of turbines and electrical topology optimization. Micro siting refers to the placement of individual turbines and macro siting is the determination of the outer boundary within which the turbines are placed. This work focuses on electrical topology optimization. Macro siting of OWPPs is not explicitly investigated, however, some insight is provided. Micro siting is not considered.

The objective of the problem is to identify the optimal offshore topological configuration of power system infrastructure that meets current and future power system requirements with the highest net benefits. The solution space specifies locational information, build schedule and the technical specifications of infrastructure including the following:

- Number, capacity and location of OWPPs.

- Voltage level and frequency of the collection circuit and transmission system (alternating current or direct current).

- Number, capacity and location of OSSs and Point of Common Couplings (PCCs).

- Type, rating and location of all cables, converters, transformers, switch-gear and compensation equipment.

- Topology of the collection circuit including groupings of wind turbines and connections to and within the OSSs.

- Topology of the transmission system including connections among OSSs, with the PCCs and interconnectors.

2.2   Solution methods

In this text the term *solution method* is used to refer to a broad category of algorithms, e.g. meta-heuristics or mathematical optimization, while *formulation* refers to a specific implementation for a specific application of a solution method. Solution methods are therefore a general tool box which can be drawn upon in order to solve a wide range of problems in power systems including that of expansion planning. As power systems are highly complex however, no single solution method is suited to the wide range of problems encountered. As such, a range of solution methods exist, and it is the challenge of the designer

to understand when one method is more appropriate than another. Solution methods can be broadly sorted into six categories:

1. Brute force optimization

2. Heuristic optimization (e.g. Dijkstra's algorithm, Greedy algorithm, A* algorithm, etc.)

3. Meta-heuristics optimization (e.g. genetic algorithm, particle swarm optimization, Monte Carlo search, etc.)

4. Machine learning optimization (Supervised/unsupervised learning, neural networks, etc.)

5. Mathematical optimization (Non linear programming, convex optimization, mixed integer linear program, etc.)

6. Hybrid approaches (two or more combinations of any of the above)

Brute force optimization involves calculating every possibility within a defined search space and selecting the best one. A brute force approach has the advantage of guaranteeing global optimality but the disadvantage of poor scaleability. Brute force optimization should only be considered when the number of options, e.g. decision variables, is small. An example of where brute force optimization may be used in power systems is in the sizing of an export cable by comparing the cost of all available export cables. As the number of possible cable sizes is quite small a brute force approach is likely the easiest method. Brute force optimization is applied in this thesis within appendix A.

Heuristic optimization involves the application of purpose built rules (an algorithm) to traverse a search space towards an optimized solution. Heuristics in general do not guarantee a globally optimal solution, however, if specific conditions can be met a global solution can be obtained. Examples of heuristics that provide globally optimal solutions are a greedy search satisfying the "greedy stays ahead principle" or the A* algorithm with an admissible distance heuristic [29]. The major advantage of heuristic optimization is its speed and scalability as it exhibits polynomial time execution [30].

Heuristics are used throughout power system optimization, often without even being recognized as such. For example, we may choose to size a transmission line within a transmission expansion study by providing three candidate lines as options. One line with an ampacity at the expected power flow and then one at 90 % and the other at 110 % of expected power flow. We are employing an "educated guess" to limit the search space and reduce the number of required transmission lines being analyzed. Under the right conditions this could be

a valid assumption, however, we must recognize that unless the underlying heuristic can be proven optimal, any certificate of global optimality obtained is no longer valid for the entire search space but rather a reduced one. For practical engineering problems such as transmission planning, the complexity requires that all globally optimal approaches be built upon a foundation of simplifying heuristics (assumptions) such as this. As such, it is important to understand that a globally optimal solution to a mathematically defined search space may not be the global optimal for the physical problem that is being approximated. Heuristic optimization is applied in this thesis within chapter 4.

Meta-heuristics provide a flexible and reusable structure, usually in algorithmic form, to heuristically optimize a problem. As in the case of simple heuristics there is no guarantee of global optimality. One of the most widely used meta-heuristics in power system planning is the Genetic Algorithm (GA) [30,31] which is an algorithm based on the science of evolution whereby parent populations are crossed with each other to form new generations of offspring. Random mutations are also occasionally introduced. The new generations are tested for fitness and then only the strongest members are permitted to reproduce and create the next generation. Over the course of many generations, a set of attributes emerge as the defining characteristics of the fittest individual(s). These attributes are the set of heuristics the meta-heuristic has discovered. When applying meta-heuristics it is important to find the right balance between deterministic and stochastic behaviour in order to converge within a reasonable time without getting easily stuck in a local minima. A representative implementation of meta-heuristic optimization in relation to power systems can be found in [32].

Machine learning uses data sets to train computers how to recognize patterns that can be used for classification or prediction. There are two major categories of machine learning, supervised and unsupervised learning. Supervised learning uses labelled data, unsupervised learning does not. Machine learning algorithms, like meta-heuristics, provide a method of finding a set of rules that can be used to improve on an objective. Some machine learning approaches, such as the highly popular neural networks, can have the drawback of being opaque "black boxes" that provide solutions based on inputs with little to no insight in regard to internal operations. In light of the aforementioned limitation, there has been an increase in interest in physics-informed neural network models, as evidenced by research such as that presented in [33]. These models leverage information obtained from the governing equations to train a neural network. However, as with any neural network, overfitting to the data is a potential concern. To address this challenge, techniques such as cross-validation or regularization [34] can be employed. As with heuristics and meta-heuristics, there is no guarantee of global optimality provided by machine learning models [35].

Machine learning is data driven and so its application to power systems naturally occurs in areas rich with data. Renewable generation is one such area. Wind generation for example is often represented by a lengthy time series. Computationally, it can be impractical to use the entire time series however, and so a reduced representative set is desirable. Machine learning clustering algorithms such as K-means or K-mediods are well suited to this task [36]. Clustering is by no means the only application. Machine learning applied to power system optimization is among the most active branches of research in the field with new applications being discovered all the time [37]. Machine learning optimization is applied in this thesis within chapter 5.

Mathematical optimization, also called mathematical programming, is a branch of applied mathematics dedicated to the identification of an optimal element within a specified space of alternatives with respect to pre-defined criteria. Sub-branches of mathematical optimization are defined based on characteristics of the problem under investigation, e.g. Mixed Integer Linear Programming (MILP), convex optimization, Mixed Integer Quadratic Programming (MIQP) and Mixed Integer Non-Linear Programming (MINLP). Mathematical optimization has the advantage of providing a transparent formulation, one that under well defined conditions, can guarantee global optimality. Even in the absence of global optimality, upper and lower bounds can be obtained providing a measure of the solution quality. The main drawbacks are a lack of flexibility within the structure and the need for an external solver. Some popular solver algorithms for mathematical optimization are listed in Table 2.1. The application of

Table 2.1: Popular solvers for mathematical programs [38].

Problem type	Solver algorithm
linear program	Interior point method, Simplex method
MIP/MIQP	Branch and cut, Branch and bound
MINLP	Reduced gradient method

mathematical optimization in power systems is widespread. Examples include optimal power flow, expansion planning, energy market modelling and system restoration to name just a few [39, 40]. Mathematical optimization is applied in this thesis within chapter 7.

Finally, a hybrid solution method can be used. Hybrid optimization combines two or more of the previously discussed methods. Arguably for practical problems this is the only feasible approach as even in the most detailed formulations heuristics in the form of simplifying assumptions will be combined with another approach. Hybrid optimization is applied throughout this thesis with a particularly representative example found within chapter 6. In Table 2.2 a summary

of the most important considerations when deciding on a solution method to a particular problem is provided.

Table 2.2: Comparison of solution approaches.

Method	Pros	Cons
Heuristics	- Polynomial time execution. - No external solver required. - Provides a feasible initial solution or primal bound.	- Mostly finds local minima. - Is purpose built for each application.
Meta-heuristics	- Flexible and reusable modelling structure. - No external solver required. - Provides a feasible initial solution or primal bound.	- Convergence is not guaranteed. - Computation times are uncertain. - No measurement of the solution quality.
Machine learning	- Easily clusters and classifies data. - Results improve over time. - Flexible and reusable modelling structure.	- Training may require large amounts of data and time. - Solutions can be difficult to interpret. - Overfitting is possible.
Mathematical optimization	- Upper and lower bound on solution. - Transparent formulations. - New constraints are easily added.	Requires an external solver. - Strict modelling structure. - Computation time is hard to predict.

2.3   Basic expansion planning formulation

All of the solution methods presented in the previous section can and have been turned into specific formulations to solve expansion planning problems. Some examples of heuristic formulations are [41, 42]. In this regard, chapter 4 of this thesis develops a heuristic approach to offshore transmission system planning when considering multiple neighboring OWPPs. As for meta-heuristics, using a GA as in [43] is the most common, but an array of other algorithms such as simulated annealing [44], particle swarm [45] or tabu search [46] to name just a few have been used. Approaches involving machine learning are comparatively new and less common [47]. This may be primarily due to a lack of appropriate data sets needed for training models. In section 5.2 an alternative approach that relies on synthetic data sets is proposed as part of this thesis. In what follows, however, the primary focus will be on mathematical formulations as these are the most transparent and therefore most important for understanding.

2.3.1   Mathematical formulation

In mathematical optimization the expansion planning problem is formulated into an objective function, for example the maximization of social welfare or minimization of cost etc., and a set of constraints describing the search space within which the solution is contained. Constraints are equalities or inequalities that describe physical or technical limitations, financial considerations or regulatory requirements among other things. The general form of the expansion planning problem can be written as:

$$\min_{\mathbf{x}} f(\mathbf{x}) \tag{2.1}$$

subject to

$$g_i(\mathbf{x}) = 0, i = 1, ..., m \tag{2.1a}$$

$$h_i(\mathbf{x}) \leq 0, i = 1, ..., n \tag{2.1b}$$

The objective is to find the values of the set of decision variables $\mathbf{x} = (x_1, ..., x_l)$ that minimizes (2.1) subject to equality constraints (2.1a) and inequality constraints (2.1b). The characteristics of the formulation, e.g. convexity, non-linearities, continuous or binary decisions etc., determine what solution algorithm is appropriate for the problem. A non exhaustive list of solution algorithms used in expansion planning include linear programs [48], non-linear programs [49], mixed integer programs [50], stochastic programs [51] and dynamic programs [52].

The first application of mathematical optimization to expansion planning is attributed to a 1970 paper by Garver et. al. [48] in which a linear program was used to solve the Transmission Network Expansion Planning (TNEP) problem. Since this time, much research has been devoted to developing solution approaches based on mathematical programming. Problem formulations for expansion planning can generally be grouped into three categories:

- The Transmission Network Expansion Planning (TNEP) problem,

- The Generation Expansion Planning (GEP) problem,

- The Generation And Transmission Expansion Planning (GATE) problem.

In the first two formulations, the questions of transmission and generation expansion are treated independently of one another. In the third formulation, transmission and generation expansion planning are done simultaneously.

Naturally, decisions regarding network and generation investments are highly inter-related, however, considering simultaneous expansion is computationally expensive and so opting for separate TNEP and GEP formulations versus a GATE formulation may at times be done out of necessity. Beyond computational practicalities, however, the utility of a particular modelling formulation may also be dependent on the particular entity that is making the decision and what the ultimate objective is for the investment. Transmission and generation investments are performed within the context of a regulation and a local energy market. The regulatory framework defines the division of authority in terms of ability to make investment decisions.

In a liberalized energy market such as Europe or North America, the decision making authority is typically split between a centrally regulated entity for the transmission network and the private sector for generation. This is due to inherently monopolistic characteristics of a transmission network. The cost of infrastructure is high, access is sought by all and duplicate, competing infrastructure is undesirable.

Objective function

In the EU, Transmission System Operators (TSOs) are tasked with maintaining and expanding their respective national transmission networks. The objective of TSOs when expanding the transmission network is the maximization of social welfare. On the other hand, generation expansion is done by private industry, where generation investment decisions are based on profit maximization. These objectives can at times be conflicting or market incentives may be improperly aligned. As such, a third independent entity, the national regulators, have the dual mandate of ensuring market incentives for expansion plans of both transmission and generation infrastructure align with the objective of maximizing societal social welfare [39, 53].

Considering the above, the details of the objective can be somewhat case dependant, however, we can still say that in general, the objective is to maximize benefits and minimize costs over the lifetime of the system. An example objective could therefore be:

$$\min_{\mathbf{x}}(C^{\text{TOTAL}} - B^{\text{TOTAL}}) \tag{2.2}$$

where total costs (C^{TOTAL}) are defined as the sum of Capital Expenditures (CAPEX) (C^{CPX}), maintenance (C^{MNT}), losses (C^{LOSS}) and Expected Energy Not Transmitted (EENT) (C^{EENT}) due to unavailability as in:

$$C^{\text{TOTAL}} = C^{\text{CPX}} + \sum_{i=1}^{life}\left(C_i^{\text{LOSS}} + C_i^{\text{MNT}} + C_i^{\text{EENT}}\right) \tag{2.3}$$

and total benefits (B^{TOTAL}) are defined as the sum of generator profits (B^{GENS}), gross consumer surplus (B^{GCS}) and congestion rent (B^{RENT}) as in:

$$B^{\text{TOTAL}} = \sum_{i=1}^{life} \left(B_i^{\text{GENS}} + B_i^{\text{GCS}} + B_i^{\text{RENT}} \right). \qquad (2.4)$$

Constraints

Power Flow constraints

In a mathematical formulation of expansion planning, the search space is defined by a set of constraints. While certain constraints may be case specific, constraints describing the physics of the system are not, i.e. system power flow must satisfy Kirchhoff's laws. The power flow constraints as well as some typical technical constraints of the system are discussed below. For simplicity, static constraints (considering only a single time step), are presented.

We consider a transmission network $\mathcal{T}$ consisting of nodes (buses) $\mathcal{N}$ and edges $\mathcal{E} \subseteq \mathcal{N} \times \mathcal{N}$. A set of existing ($\mathcal{S}_\ell$) and candidate ($\tilde{S}_\ell$) transmission lines connect nodes of the network. Sets of existing generators ($\mathcal{S}_{\text{g}}$), candidate generators ($\tilde{S}_{\text{g}}$) and loads (S_{d}) are located at nodes throughout the network. We describe the active and reactive power flows through the transmission lines of the network by the power flow equations. The bus injection formulation of the power flow equations are:

$$P_{l:mn} = |U_m|^2 g_{l:\{mn\}} - |U_m||U_n|(g_{l:\{mn\}} \cos(\theta_m - \theta_n) + b_{l:\{mn\}} \sin(\theta_m - \theta_n)), \qquad (2.5a)$$

$$Q_{l:mn} = |U_m||U_n|(b_{l:\{mn\}} \cos(\theta_m - \theta_n) + g_{l:\{mn\}} \sin(\theta_m - \theta_n)) - |U_m|^2 b_{l:\{mn\}}, \qquad (2.5b)$$

$$\forall l \in \mathcal{S}_{\ell:\{mn\}}, \forall (mn) \in \mathcal{E}.$$

Where $P_{l:mn}$ and $Q_{l:mn}$ are the AC active and reactive power flowing on existing transmission lines $l \in \mathcal{S}_{\ell:\{mn\}}$ from node m to n. $|U_m|$ and θ_m are the voltage magnitude and phase angle at node m. $b_{l:\{mn\}}$ and $g_{l:\{mn\}}$ are the susceptance and conductance of line l between m and n respectively. In the case of the candidate lines $l \in \tilde{S}_\ell$, (2.5) must be adapted by multiplying each sub-equation by a binary decision variable (α) for the candidate line as in:

$$\tilde{P}_{l:mn} = \alpha_{l:\{mn\}} \cdot P_{l:mn}, \tag{2.6a}$$

$$\tilde{Q}_{l:mn} = \alpha_{l:\{mn\}} \cdot Q_{l:mn}, \tag{2.6b}$$

$$\forall l \in \mathcal{S}_{\tilde{\ell}:\{mn\}}, \forall (mn) \in \mathcal{E}, \alpha_{l:\{mn\}} \in \{0,1\}.$$

The second physical law that must be satisfied is Kirchhoff's current law. Kirchhoff's current law states that the sum of current into a node must be equal to the sum of current exiting the same node. In expansion planning formulations this is expressed as the following nodal power balance constraint:

$$\sum_{g \in \mathcal{S}_{g:m}} P_g + \sum_{\tilde{g} \in \tilde{S}_{g:m}} P_{\tilde{g}} - \sum_{d \in S_{d:m}} P_d = \sum_{\substack{l \in \mathcal{S}_{\ell:\{mn\}}, \\ n \in \mathcal{N}_m}} P_{l:mn} + \sum_{\substack{\tilde{l} \in \mathcal{S}_{\tilde{\ell}:\{mn\}}, \\ n \in \mathcal{N}_m}} P_{\tilde{l}:mn} \tag{2.7a}$$

$$\sum_{g \in \mathcal{S}_{g:m}} Q_g + \sum_{\tilde{g} \in \tilde{S}_{g:m}} Q_{\tilde{g}} - \sum_{d \in S_{d:m}} Q_d = \sum_{\substack{l \in \mathcal{S}_{\ell:\{mn\}}, \\ n \in \mathcal{N}_m}} Q_{l:mn} + \sum_{\substack{\tilde{l} \in \mathcal{S}_{\tilde{\ell}:\{mn\}}, \\ n \in \mathcal{N}_m}} Q_{\tilde{l}:mn} \tag{2.7b}$$

$$\forall m \in \mathcal{N}, \text{ where } \mathcal{N}_m = \{n \in \mathcal{N} : mn \in \mathcal{E}\}$$

The equation requires that at each node m, the balance between generation (existing and candidate) and demand shown on the left hand side equals the sum of complex power flowing in and out of the node on transmission lines shown on the right hand side. In the continuous version of the problem (no binary variables), the dual variables $(\lambda_m^p, \lambda_m^q)$ of (2.7) are the so called shadow prices. They represent the localized marginal price of supplying one additional unit of real or reactive power to the node. In market models λ_m^p is typically taken as the nodal clearing price.

Technical constraints

Additional network constraints that must be considered are listed in (2.8). (2.8a) restricts the nodal voltage magnitude to an acceptable range. In a typical power system this is between 90% and 110% of nominal voltage. (2.8b), (2.8c), (2.8d) and (2.8e) ensure that existing and candidate generators remain within safe operating limits for both real and reactive power. (2.8f) and (2.8g) restrict candidate generation expansion to an upper limit.

In this formulation candidate generation is modelled as a continuous variable. In more advanced formulations, discrete decisions regarding generation may be required for modelling characteristics related to unit commitment e.g. ramping rates, minimum and maximum up and down times, minimum stable operating points, etc. [40]. (2.8h) and (2.8i) ensure that existing and candidate lines remain within safe operating limits for both real and reactive power. (2.8j) and (2.8k) ensure the divergence of nodal voltage angles does not exceed safe operational limits for pairs of nodes connected via existing and candidate lines respectively. Under normal operation this is less than 10-15°. It is common practise to set $\theta^{\max}$, and $\theta^{\min}$ to $+/-\pi$ [39]. The last constraint (2.8l) defines a reference angle to guarantee a unique solution.

$$|U_m^{min}| \leq |U_m| \leq |U_m^{max}| \quad \forall m \in \mathcal{N} \tag{2.8a}$$

$$0 \leq P_g \leq P_g^{max} \quad \forall g \in \mathcal{S}_{\mathrm{g}} \tag{2.8b}$$

$$-Q_g^{max} \leq Q_g \leq Q_g^{max} \quad \forall g \in \mathcal{S}_{\mathrm{g}} \tag{2.8c}$$

$$0 \leq P_{\tilde{g}} \leq P_{\tilde{g}}^{max} \quad \forall \tilde{g} \in \tilde{S}_{\mathrm{g}} \tag{2.8d}$$

$$-Q_{\tilde{g}}^{max} \leq Q_{\tilde{g}} \leq Q_{\tilde{g}}^{max} \quad \forall \tilde{g} \in \tilde{S}_{\mathrm{g}} \tag{2.8e}$$

$$0 \leq P_{\tilde{g}}^{max} \leq \widehat{P_{\tilde{g}}^{max}} \quad \forall \tilde{g} \in \tilde{S}_{\mathrm{g}} \tag{2.8f}$$

$$-\widehat{Q_{\tilde{g}}^{max}} \leq Q_{\tilde{g}}^{max} \leq \widehat{Q_{\tilde{g}}^{max}} \quad \forall \tilde{g} \in \tilde{S}_{\mathrm{g}} \tag{2.8g}$$

$$0 \leq P_{l:mn}^2 + Q_{l:mn}^2 \leq (S_{l:mn}^{max})^2 \quad \forall l \in \mathcal{S}_{\ell:\{mn\}}, \forall mn \in \mathcal{E} \tag{2.8h}$$

$$0 \leq P_{\tilde{l}:mn}^2 + Q_{\tilde{l}:mn}^2 \leq (S_{\tilde{l}:mn}^{max})^2 \quad \forall \tilde{l} \in \mathcal{S}_{\tilde{\ell}:\{mn\}}, \forall mn \in \mathcal{E} \tag{2.8i}$$

$$\theta^{\min} \leq \theta_m - \theta_n \leq \theta^{\max} \quad \forall mn \in \mathcal{E} \tag{2.8j}$$

$$\theta^{\min} \leq \alpha_{\tilde{l}:\{mn\}}(\theta_m - \theta_n) \leq \theta^{\max} \quad \forall \tilde{l} \in \mathcal{S}_{\tilde{\ell}:\{mn\}}, \forall mn \in \mathcal{E} \tag{2.8k}$$

$$\theta_1 = 0 \tag{2.8l}$$

Linear DC approximation

As the presented constraints, particularly the power flow equations, are both non-linear and non convex, an unmodified formulation is very difficult to solve. As such, it is common to use either a relaxed or approximated version of the
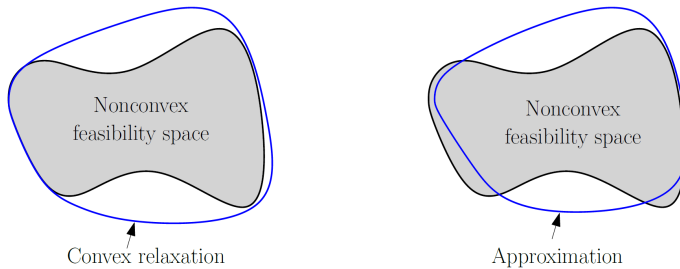
Figure 2.1: Approximation versus relaxation [54].

equations. Relaxations and approximations are modelling strategies whereby a similar, but easier to solve version of the original problem is solved to gain insight into the solution of the original formulation. Relaxed versions of the power flow equations are derived in such a manner as to ensure the entire search space is included within the relaxed search space. An approximation on the other hand makes no such guarantee and may exclude regions of the original search space, potentially even excluding the globally optimal point. This concept is illustrated in Fig. 2.1. Although, relaxations guarantee the optimal point remains within the search space, it does not guarantee the optimal point or even a feasible point will be found. As such, it should not be assumed that a relaxation will provide a better solution than an approximation. Rather, the purpose of both approaches is to provide a tractable version of the original problem. Relaxations of the power flow equations include quadratic convex [55], SOC [56] and SDP [57]. Approximations include network flow and the linear programming LPAC and DC formulations [58].

To conduct a comprehensive comparison of the available formulations, we direct readers to the outstanding study conducted in [59]. This work provides an extensive evaluation of the DC, LPAC, two-SOC, quadratic convex, SDP, and "AC" formulations across various numerical examples. The study demonstrates that selecting an optimal formulation is a nuanced decision, contingent upon the specific problem at hand, without a clear winner in general. Nevertheless, as problem size expands, a discernible trend in computational complexity emerges.

In this regard, the DC formulation emerges as the frontrunner, exhibiting superior computational efficiency. On average, the computation time is shown to be more than one order of magnitude faster than its closest rival, the LPAC formulation. Moreover, as problem sizes increase, the performance gap becomes more pronounced, underscoring the superior scalability of the DC formulation. Considering that the computational challenge in expansion planning primarily arises from the number of binary variables, it is noteworthy that the problem

addressed in this work entails several thousand binary decisions, while the largest test case explored in [59] encompassed less than 200 binary candidate investment decisions. Consequently, the DC formulation has been selected.

Furthermore, it is important to highlight that the objective of this thesis does not encompass comparing various approximations and relaxations. Thus, due to its exceptional computational efficiency and well-established track record, only the DC approximation has been implemented and discussed in the subsequent sections. However, it is worth mentioning that certain limitations are associated with this approximation and have been identified in [60].

The DC approximation is based on three practical observations within an HVAC transmission system under typical operating conditions.

1. Transmission line resistance is small compared to the reactance.

2. The divergence in voltage angles between nodes of a network is small.

3. The voltage magnitudes remain close to 1 PU.

Based on these observations we make the following simplifying assumptions:

1. The terms containing conductances (g) can be neglected i.e. $g = 0$.

2. The cosine and sine functions can be approximated by one and the difference between the angles in radians respectively i.e. $\cos(\theta_m - \theta_n) \approx 1$, $\sin(\theta_m - \theta_n) \approx \theta_m - \theta_n$.

3. All voltage magnitudes can be approximated as one PU i.e. $|U_m| = 1$.

By applying these assumptions and performing some algebraic manipulations we can obtain the following linear approximation of the power flow equations:

$$P_{l:mn} = b_{l:\{mn\}}(\theta_m - \theta_n) \qquad \forall l \in S_{\ell:\{mn\}}, \forall mn \in \mathcal{E}.$$
$$P_{\tilde{l}:mn} = b_{\tilde{l}:\{mn\}}(\theta_{\tilde{l}:mn} - \theta_{\tilde{l}:nm}) \quad \forall \tilde{l} \in S_{\tilde{\ell}:\{mn\}}, \forall mn \in \mathcal{E}.$$
$$(2.9)$$

Where $\theta_{\tilde{l}:mn}$ and $\theta_{\tilde{l}:nm}$ are dummy voltage angles associated with each candidate line. By defining these angles we can eliminate the non-linearity in (2.8k) by replacing it with the following two constraints:

$$\theta^{\min} \leq \theta_{\tilde{l}:mn} - \theta_{\tilde{l}:nm} \leq \theta^{\max} \quad \forall \tilde{l} \in S_{\tilde{\ell}:\{mn\}}, \forall mn \in \mathcal{E}. \qquad (2.10a)$$

$$|\theta_{\tilde{l}:mn} - \theta_m| \leq (1 - \alpha_{\tilde{l}:\{mn\}}) \cdot M \quad \forall \tilde{l} \in S_{\tilde{\ell}:\{mn\}}, \forall mn \in \mathcal{E}. \qquad (2.10b)$$

Here, M is a sufficiently large angle ensuring (2.10b) is a non-binding constraint when $\alpha = 0$ and locking the dummy angle to the existing voltage angle when $\alpha = 1$. As only real power is considered in the approximation, constraints (2.7b), (2.8c) and (2.8e) are no longer applicable. Furthermore (2.8h) and (2.8i) simplify to:

$$-P_{l:mn}^{max} \leq P_{l:mn} \leq P_{l:mn}^{max} \quad \forall l \in \mathcal{S}_\ell \qquad (2.11a)$$

$$-\alpha_{\tilde{l}:\{mn\}} P_{\tilde{l}:mn}^{max} \leq P_{\tilde{l}:mn} \leq \alpha_{\tilde{l}:\{mn\}} P_{\tilde{l}:mn}^{max} \quad \forall \tilde{l} \in \tilde{S}_\ell \qquad (2.11b)$$

The linear DC approximation of the deterministic and static GATE planning problem is summarized as:

$$\min_{\boldsymbol{x}} \mathbf{c}^\top \boldsymbol{x}, \text{ subject to:} \qquad (2.12)$$

$$(2.8b), (2.8d), (2.8f), (2.8j), (2.8l), (2.9), (2.10), (2.11),$$

where $\mathbf{c}^\top$ is a vector of coefficients and $\boldsymbol{x}$ are the optimization variables.

2.3.2 Deterministic and static GATE example problem
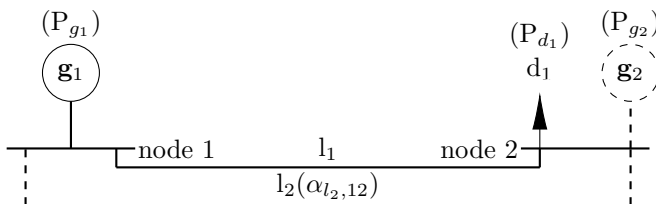
Figure 2.2: Illustrative two node example electrical grid.

To illustrate the basics of the formulation we will introduce a simple two node example grid as in Fig. 2.2 and solve a deterministic and static GATE problem subject to DC power flow (2.12). The figure shows two nodes 1 and 2 connected by an existing transmission line l_1 and a candidate transmission line l_2. At node 1 there is existing generator G_1 and at node 2 there is a candidate generator

G_2 as well as demand d. $\alpha_{l_2,12}$ is a binary decision variable that is one when l_2 is active and zero otherwise.

1. g_1 is a 75 MW generator. The production cost is 100 €/MWh.

2. g_2 is a candidate generator up to 25 MW. The production cost is 95 €/MWh. The annualized cost to construct g_2 45 k€/MW.

3. d_1 is a load of 60 MW. The cost to shed load is 105 €/MWh.

4. l_1 is an existing transmission line of capacity 50 MW. The per unit susceptance is 500 PU.

5. l_2 is a candidate transmission line of capacity 15 MW. The per unit susceptance is 150 PU. The annualized cost to construct l_2 20 k€/MW.

6. The base voltage is 100 kV, the base power is 1 MW.

We define the following objective of minimizing the sum of yearly costs:

$$\min_{\boldsymbol{x}} 8760(100P_{g_1} + 95P_{g_2} + 105P_{d_1}) + 45000P_{g_2}^{max} + 20000\alpha_{l_2,12},$$
$$\boldsymbol{x} = (P_{g_1}, P_{g_2}, P_{d_1}, P_{g_2}^{max}, \theta_1, \theta_2, \alpha_{l_2,12})$$

subject to:

$$P_{l_1:12} = 500(\theta_1 - \theta_2) \tag{2.13a}$$

$$P_{l_2:12} = 150(\theta_{l_2:12} - \theta_{l_2:21}) \tag{2.13b}$$

$$P_{l_1:21} = 500(\theta_2 - \theta_1) \tag{2.13c}$$

$$P_{l_2:21} = 150(\theta_{l_2:21} - \theta_{l_2:12}) \tag{2.13d}$$

$$P_{g_1} + P_{l_1:12} + P_{l_2:12} = 0 \tag{2.13e}$$

$$P_{g_2} + P_{l_1:21} + P_{l_2:21} = 60 - P_{d_1} \tag{2.13f}$$

$$0 \leq P_{g_1} \leq 75 \tag{2.13g}$$

$$0 \leq P_{g_2}^{max} \leq 25 \tag{2.13h}$$

$$0 \leq P_{g_2} \leq P_{g_2}^{max} \tag{2.13i}$$

$$-50 \leq P_{l_1:12} \leq 50 \tag{2.13j}$$

$$-50 \leq P_{l_1:21} \leq 50 \tag{2.13k}$$

$$-15\alpha_{l_2:\{12\}} \leq P_{l_2,12} \leq 15\alpha_{l_2:\{12\}} \tag{2.13l}$$

$$-15\alpha_{l_2:\{12\}} \leq P_{l_2,21} \leq 15\alpha_{l_2:\{12\}} \tag{2.13m}$$

$$-\pi \leq \theta_2 \leq \pi \tag{2.13n}$$

$$-\pi \leq \theta_{l_2:12} \leq \pi \tag{2.13o}$$

$$-\pi \leq \theta_{l_2:21} \leq \pi \tag{2.13p}$$

$$|\theta_{l_2:12} - \theta_1| \leq (1 - \alpha_{l_2:\{12\}}) \cdot M \tag{2.13q}$$

$$|\theta_{l_2:21} - \theta_2| \leq (1 - \alpha_{l_2:\{12\}}) \cdot M \tag{2.13r}$$

$$\theta_1 = 0 \tag{2.13s}$$

In Fig. 2.3 the solution space of the problem is shown. The optimal point lies at $\alpha_{l_2:\{12\}} = 0$, $P_{g_2}^{max} = 10\,\text{MW}$, $P_{g_1} = 50\,\text{MW}$, $P_{g_2} = 10\,\text{MW}$, $P_{d_1} = 0\,\text{MW}$, $\theta_2 = 0.1\,\text{rad}$.
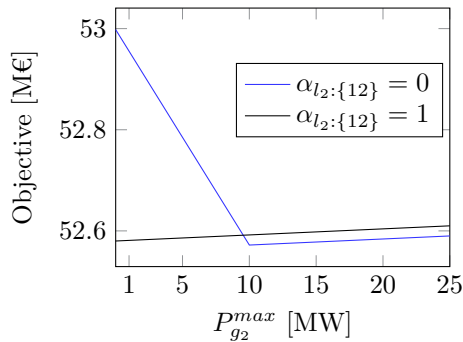
Figure 2.3: Solution space of two node example problem.

2.4 State of the art

2.4.1 Overview

Offshore Wind Expansion Planning (OW-EP) shares much in common with traditional expansion planning and the basic formulation discussed thus far is an excellent starting point. Some differences of particular importance, however, do exist. They are the increased reactive power flows in AC submarine cables

compared to overhead lines and the green (or only lightly browned) field nature of the problem. The increased reactive power in AC submarine cables shifts the techno-economic optimal in favor of HVDC at shorter distances and lower power levels when compared to onshore overhead lines. More details in this regard are provided in appendix A. The green field nature, or lack of existing power infrastructure, complicates expansion planning as decision variables become unconstrained and grow in number rapidly experiencing a combinatorial explosion, leading to computational difficulties. This is discussed in further detail in chapter 4.

The complexity of the OW-EP problem is dependant on the features considered within the formulation. Some complicating features such as accounting for losses, reliability and stochasticity are shared with traditional expansion planning. On top of these, however, there are drivers specific to the offshore case such as:

- The types of collection circuits considered

  - e.g. radial, branched, or meshed.

- Whether the number and location of OSSs is known apriori or are additional decision variables.

- The need to avoid obstacles or restricted zones, where electrical infrastructure is not permitted.

- The need to limit cable crossings.

- The consideration of wake losses.

In the following, the state-of-the-art in dealing with these various drivers of complexity is discussed. In Table 2.3 a summary of research articles that consider explicitly the problem of OW-EP is provided. The articles are sorted by solution approach and whether they apply to the collection circuit, transmission system or both. The articles listed in the table do not include applicable methods from related fields.

Table 2.3: Grid level studied and solution method of literature on OW-EP.

Grid level	Heuristic	Meta-heuristic	Mathematical
Collection	[61–67]	[32, 68–79]	[80–93]
Collection/ transmission	[94, 95]	[96–101]	[102, 103]
Transmission	[104]	[105]	[106–109]
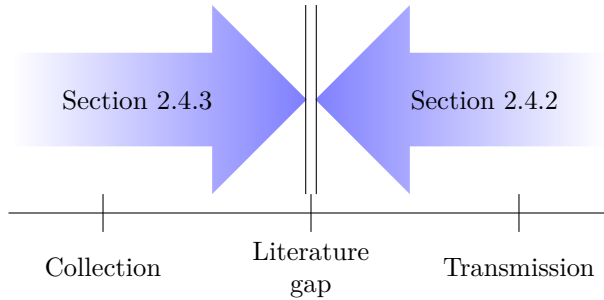
Figure 2.4: Literature on the state-of-the-art of the OW-EP problem

First, we can see that a wide cross section of solution algorithms have been applied including heuristics, meta-heuristics and mathematical programs. Second, we see that most research has tended to focus on the collection circuit, with about two thirds of articles found on the topic ignoring the transmission system entirely. Opting instead to focus on the problem of inter-array cable optimization and OSS placement from the perspective of the collection circuit. As single OWPPs connected via a radial export cable to shore have dominated the industry for much of its history this is not a surprising observation. As the industry shifts, however, to meshed offshore HVDC grids and larger offshore generating regions consisting of multiple OWPPs, energy islands and HOAs this is sure to change.

Luckily, the lack of research on the transmission level of OW-EP is less pronounced as it first appears, as the existing articles that do focus on transmission level expansion planning [104–109] demonstrate a high similarity with the traditional onshore expansion planning formulation already introduced in section 2.3. A comprehensive literature review therefore consists of advanced formulations of the traditional onshore expansion planning problem to form an upper (high level) boundary of knowledge. These are presented in section 2.4.2. This is then followed by a review in section 2.4.3 of advanced formulations specific to the OW-EP problem. As these formulations have a heavy focus on the collection circuit level of optimization, they provide the bottom up (low level) boundary of available approaches to the problem. The identified gap in literature exists at the transition between the upper and lower level models. These are the methods required to link high and low level approaches effectively. This identified gap is illustrated in Fig. 2.4 and is the focus of chapter 4.

2.4.2   Advanced formulations of traditional expansion planning

Traditional expansion planning problems are commonly formulated taking either a central planner's perspective as in [52, 110] or a market perspective as in [111, 112]. Equilibrium modelling such as [113, 114] has been used to model competition between stake holders. The equivalency of equilibrium and optimization formulations is established by demonstrating identical Karush-Kuhn-Tucker optimality conditions [115].

From an energy market perspective, the market can be settled at different time intervals. Futures, day-ahead and intra-day balancing markets exist. The futures market generally spans a week to several years in advance. Day-ahead markets typically close at noon the day before energy is dispatched. The shortest time frame is the balancing market where trading is performed an hour to minutes before real time dispatch. Complementarity based formulations such as [116, 117] and bi-level programming approaches such as [118, 119] are frequently applied when solving expansion planning problems considering the energy market.

Deciding on an appropriate modelling time span is another important consideration, generally expansion planning is a long term endeavor. The lifespan of transmission infrastructure is in the neighborhood of 40 to 50 years. New transmission lines typically have construction times ranging from half a year up to two years and new generating facilities typically take even longer to build, ranging from two to five years [39]. Investment decisions are therefore, multi-year undertakings. To capture this behavior, dynamic, multi-period expansion planning formulations such as [52] are used. This naturally comes at the price of increased complexity, however. An appropriate trade-off between less computationally expensive static formulations such as [120, 121] and a dynamic formulation must therefore be struck.

When planning over such a long time horizon, high levels of uncertainty are involved. It can be useful to sort the uncertainties by the timeframe to which they apply. Short term (less than a year) uncertainties include variations in demand and production capacity e.g. RESs, equipment failure or outages and market related uncertainties such as unknown bidding strategies. Long term (greater than a year) uncertainties include: the expansion, contraction or change in geographic distribution of production or demand, changing operational costs, an increasing cost to borrow i.e. interest rate hikes, or increased extreme weather events.

To incorporate the uncertainties in expansion planning problems, techniques such as stochastic programming and robust optimization can be used. The "best" approach depends on what is known of the uncertainties in question.

A review of uncertainty modelling in power system optimization is presented in [122]. Stochastic programming is a scenario based method and has the advantage of being able to capture the future operating conditions of the power system as well as the evolution of uncertainty over time. Examples of stochastic programming in expansion planning are [51, 111, 112].

Unfortunately, the uncertainty space can be vast, requiring large numbers of scenarios resulting in intractability. In this situation, it may be possible to apply a decomposition technique. Benders decomposition is by far the most commonly applied but by no means the only one. Some examples of expansion planning using Benders decomposition and stochastic programming can be found here [112, 123]. An overview of different decomposition techniques in optimization is provided in [40]. A comparison of decomposition techniques applied to the TNEP problem can be found in [124].

In certain situations it may be difficult to create accurate scenarios to describe the uncertainty. For example, future RES generation scenarios are frequently based on historical data [125]. Unfortunately, a remote region proposed for new RES production may have a very limited history of data collection or the data available is of very poor quality. Poor scenario generation can affect investment decisions significantly [125]. In such situations, using robust optimization techniques to model the distribution of uncertainties may be more appropriate. It can be easier to know the distribution of uncertainty versus an accurate scenario based description [126]. Some examples of expansion planning formulations using robust optimization are [127–129].

A drawback of robust optimization is that it is a worst case analysis and may result in a too conservative solution. In this situation adaptive robust optimization such as [130] or chance constraints such as [131] may be more appropriate. A flowchart summarizing the major decisions in determining an appropriate formulation for the expansion planning problem is presented in block diagram of Fig. 2.5.
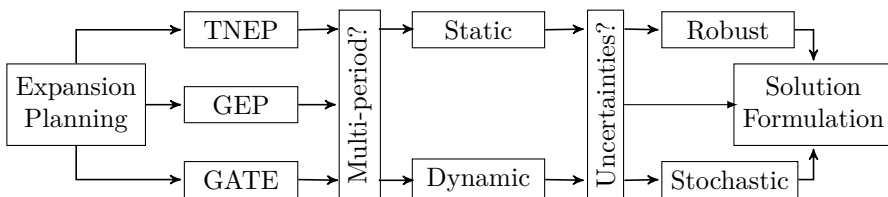
Figure 2.5: Expansion planning block diagram for deciding a solution method.

2.4.3   Advanced formulations of offshore wind expansion planning

Radial topologies

The assumption to restrict collection circuit topologies to radial configurations only is common [32, 63, 68, 132]. After all, radial topologies are the most common in practise [38]. On top of radiality these examples also assume no wind stochasticity, network power flow, no power losses, no restricted zones or obstacles and no wake effect. As these represent the lowest level of complexity, it is a good opportunity to contrast the different solution approaches.

In [63] a heuristic based on the Clarke and Wright savings algorithm is developed as well as a hop indexed binary integer program. The two models are compared on three real world OWPPs. The largest of which is 88 turbines with 2 OSSs. The heuristic is shown to perform quite well, finding solutions on average only 2% more expensive than the binary integer program. It is the computational results, however, that demonstrate the primary strength of heuristics. On the largest problem size, the binary integer program takes an hour before being terminated with a small optimality gap while the worst case computation time for the heuristic is 60 ms.

Contrasting these two formulations with the GA implemented in [32], we see the flexibility provided in the meta-heuristic modelling structure. The most notable difference between [32] and [63] is the comprehensive cost model that is implemented. Cables, switchgear, OSSs and even turbine mounted transformers are accounted for versus a simple lumped cable length cost model. This highlights the important consideration when selecting a solution method whereby desirable characteristics such as computation time, a guarantee of global optimality or the detail in which the search space is described may be mutually exclusive trade-offs between methods.

Branched topologies

The topological complexity can be increased by allowing branching in radial circuits. This can result in lower overall cost [91]. Heuristic formulations that allow branching are [67] and [65]. Examples of meta-heuristics are a particle swarm optimization in [74] and a GA in [69]. The introduction of Steiner nodes in [61] allows branching at nodes other than turbines. Although interesting this falls into the category of "In theory there is no difference between theory and practise. In practise there is". Practically speaking branching should be restricted to wind turbine nodes where switchgear is located, however, the

concept of Steiner nodes is still important as it can be useful in other ways such as in avoiding no-go zones. This is discussed further below.

Mathematical programs that include branched topologies are a MILP [82], a stochastic, MILP using Benders decomposition [102] and a MIQP [84]. Unfortunately, this last model proved computationally impractical and was therefore linearized. Finally, of particular note, is [85], a MINLP formulation of the problem. This formulation is perhaps, the most complete in terms of capturing problem complexity while retaining tractability. It accounts for electrical losses, wind stochasticity and reliability. An example problem of 100 turbines is solved. Since it is non-convex however, global optimality is not guaranteed. The approach relies on Benders decomposition.

Meshed topologies

The final step regarding the complexity of the collection circuit topology is achieved by allowing looped or fully meshed layouts. System reliability should be considered in these formulations, else the additional CAPEX cannot be justified and the radial solution is selected. The majority of formulations that consider meshed collection circuits are meta-heuristics. Examples include [79, 101], both are GAs and [64] is an ant colony optimization. In [95] a heuristic formulation using a multiple travelling salesmen approach that permits single looped topologies is presented. Mathematical formulations that consider meshed configurations are [103] and [102]. Both are based on the same underlying model using Benders decomposition. The later improves on the first through scenario aggregation, relaxed Benders cuts and reliability via the technique of progressive contingency incorporation [88].

Reliability

Several approaches to account for reliability exist. In [133] a deterministic technique that introduces the metric of Generation Ratio Availability is proposed. This same metric is applied to DC collection systems in [134]. A probabilistic approach using scenario based stochastic programming is used in [83, 103]. The same authors improve on this via the progressive contingency incorporation method mentioned previously in [88]. Another probabilistic approach is with Monte Carlo simulations as in [132]. Finally, the authors of [135] use a multi-state Markhov model to represent reliability and propose a strategy based on the universal generating function to split the network and retain computational tractability.

Wind stochasticity

The simplest models do not account for wind stochasticity and assume an average value [68, 79, 101, 136]. More advanced models account for the stochasticity of wind speed, and yet even more advanced models, stochasticity in both speed and direction [132]. According to [38], however, direction is only important in micro siting problems not electrical topology optimization. The most straight forward approach to include wind speed stochasticity is via historical time series as in [85]. This approach is further improved using a probabilistic approach with stochastic scenarios in [82, 83, 102]. Monte Carlo simulations are used in [132].

Power flow

Power flow can be modelled to various degrees of complexity. The simplest approach is a transportation model which is found in most of the formulations surveyed, e.g. [65, 67, 74, 76, 77, 81, 82, 86, 87, 91]. In the opposite extreme is the non-linear, non-convex formulation of the power flow equations, that captures the full non linearity of the problem. Most models that implement such formulations are not true optimizations as they only consider a few set topologies [132, 137]. The exception to this being [85], the MINLP mentioned above. Between these two extremes are the approximations and relaxations mentioned in section 2.3.1. Of these approaches, only quadratic convex [84] and the DCOPF were found to have been explicitly applied to the OW-EP problem. DCOPF examples can be found in [68, 79, 101, 102].

Losses

Electrical losses in the transmission system consume between 1% and 3% of generation [137]. There are several approaches for incorporating electrical losses with varying degrees of complexity and accuracy. In a MILP they have been incorporated by pre-processing as in [82] or by an iterative, Benders decomposition based approach as in [102]. In [138] a piece-wise linear approach is used. Examples of quadratic loss models are found in [79, 83–85] and full AC loss model in [137].

Variable number or position of OSSs within the topology

Most problems assume a single OSS at a predefined location. When increasing the number of OSSs there are three degrees of freedom: the number, location

and capacity. To the best knowledge of the author there is no work that has combined all three degrees of freedom in a single model. The most complex models manage only two of these as variables, number and location, at a single time. In the case of linear cost models, the OSS capacity constraint can be handled by fixing the OSS capacity to the maximum feasible value to avoid the exclusion of viable search space and then down sizing based on the resulting solution. When more comprehensive cost models such as [139] are required this approach may not be sufficient.

The first variation on this problem worth mentioning is when the number of OSSs is increased above one but number, location and capacity remain input parameters. This problem formulation involves first assigning turbines to the OSSs such that no turbine is assigned to more than one OSS and the capacities of all OSSs are respected. Following this, the electrical topology is optimized for each OSS grouping. A mathematical formulation [63] and a heuristic based [67] formulation that solve this problem directly were identified. The heavy computational burden of this approach is discussed in [67]. The problem can also be solved in steps. The first is to assign turbines to OSSs either by mathematical programming [61] or with clustering algorithms [140]. After assignment, the electrical topology can be determined using an appropriate approach already discussed. Iteratively solving these steps, while updating the complementary problem at each iteration until convergence, was done in [76].

A problem variation with a further level of complexity is allowing the number of substations to change but having fixed locations as in [99]. The inverse where the OSS number is a decision variable but the possible locations are parameters is solved in [88, 102] with an MILP and a stochastic program respectively. This is done heuristicly in [87]. Finally, formulations with both location and number of OSSs as variables can be found. This is a particularly difficult problem. To cope with the complexity multi step approaches are used. In [89] this is done with an MILP, in [75] a GA, in [96] particle swarm optimization and in [95] a hierarchical heuristic.

Cable crossing

Avoiding cable crossings is desirable, particularly within the collection grid. At higher capacities with multiple PCCs, avoiding them entirely is not possible. An example of a no cable crossing implementation using the minimum spanning tree heuristic is found in [73]. For meta-heuristics the Bently-Ottman algorithm [141] is a recommended approach [30]. In mathematical formulations this is accomplished using lazy call backs in [63, 82, 86, 87, 91].

Obstacles and restricted zones

Considering obstacles or restricted zones is a challenge. Two approaches for this are found. The first uses Steiner nodes to create convex boundaries surrounding obstacles as in [82, 86]. This method may not be suitable however for complex obstacles as a convex hull over non-convex areas can result in sub optimal solutions. To remedy this, a hybrid MIP and route finding algorithm is proposed in [142]. A variation of the restricted zone formulations is the inclusion of ocean bathymetry for cable routing. The only formulation reviewed that considers bathymetry uses Dijkstra's shortest path algorithm coupled with weighted regions [67]. In the onshore case it is shown that transmission routing over terrain using the A^* algorithm versus Dijkstra's algorithm is five to ten times more computationally efficient [143, 144]. Dealing with obstacles and restricted zones is the focus of chapter 6.

Wake effects

In general wake effects are not considered within the OW-EP formulations. It is most relevant in the micro-siting problem [30, 38]. Notable exceptions to this are the minimum spanning tree algorithm in [65] that accounts for wake losses, and [80] that proposes a collection grid topology optimization heuristic that considers micro siting as part of the objective function. In both formulations the linear Katic-Jensen [145] wake model is used. This is the most common simple wake model in the literature. An alternative approach called vertex packing is used in [146], however [38] advises against its use due to oversimplification. In micro-siting applications linear models are unlikely to capture wake behaviour sufficiently well. In such a case a computational fluid dynamics model such as [147] that directly solves the Navier-Stokes partial differential equations numerically is more appropriate.

2.4.4 Thesis positioning relative to the current state of play

In this thesis a framework is proposed that integrates state of the art models and methods developed within the scope of this research. The framework interlinks multiple models, each designed to address a specific aspect of power generation and transmission system expansion. Whenever possible, state of the art models from existing literature are utilized, but in instances where the literature lacks suitable solutions, the thesis introduces its own contributions.

In the context of the offshore wind expansion planning problem features discussed in this chapter, chapter 3 of the thesis briefly introduces the pre-processing

approach adopted for addressing losses, wind stochasticity, and reliability within the economic model, with a full description provided in Appendix A. Chapter 4 tackles the challenge of determining the transmission topology when the number of optimal OSS sites is variable and their positions are undetermined. Chapter 5 expands upon this methodology to address large-scale systems. Chapter 6 presents a methodology for overcoming obstacles and restricted zones. In chapters 4 to 6, only radial connection topologies are considered. In chapter 7 the possible topological configurations are expanded to include meshed topologies, long-term uncertainty is considered, and energy market design options addressed.

Throughout the chapters, test cases are presented to both investigate the performance of the proposed approaches and to place the methods in context relative to the current state of play of offshore development in the EU. In this context much reference is made towards the projects proposed within the TYNDP and readers interested in a broader context than that provided in this thesis are referred to this excellent resource [23]. It is worth, however, specifically highlighting several projects directly as they play an out-sized role in relation to the presented test cases. In Table 2.4 these projects are listed along with direct references to their project pages. The offshore development

Table 2.4: North Sea TYNDP projects inspiring test grids

Project	Type	Location	ref.
MOG II	OWPP	BE	[148]
Belgian energy island	HOA	BE	[149]
NeuConnect	HVDC Inter-connector	DE, UK	[150]
Nautilus	HVDC Inter-connector	BE, UK	[151]
Triton Link	HVDC Inter-connector	BE, DK	[152]
Aminth Energy	HVDC Inter-connector	DK, UK	[153]
North Sea Wind Power Hub	HOA	DE, DK, NL	[154]

landscape in the North Sea is a dynamic and rapidly evolving environment, as exemplified by the first two projects listed. For much of this research project the solution proposed for the Belgian offshore development zone was an extension to the modular offshore grid [148]. However, a competing proposal to construct an energy island [149] gained traction in 2021 and was eventually adopted [155]. Furthermore, the proposed wind generation to be added in the Princess Elizabeth zone where the energy island is to be located has increased from 2.1 GW in 2021 to 3.5 GW today [156]. As such, the test cases that are presented in chapters 4 through 6 in relation to the Belgian offshore neglect some of the most recent developments.

Chapter 7 takes a broader view of the North Sea, encompassing the integration of a simple energy market model for the various national energy markets surrounding the region. Thus, the inter-connectivity of markets and HOAs become significant considerations. The test case in Chapter 7 therefore, drew inspiration from the various HVDC interconnector projects and proposed HOAs in Table 2.4.

2.5   Conclusions

Power system expansion planning is a specific topic in the broader field of planning and optimization theory, where the objective is to expand generation and transmission in a cost-optimal manner to effectively meet current and future power needs. Three general categories of expansion planning formulations are found, focusing solely on transmission system expansion planning, solely on generation expansion planning, or attempting to perform both simultaneously.

There are various solution approaches that can be used to find solutions to the problem, including brute force, heuristic optimization, meta-heuristic optimization, machine learning, and mathematical optimization. Hybrid approaches also exist that combine two or more of these solution approaches at once. In practical systems, hybrid approaches are mostly always used, as simplifying assumptions (heuristics) need to be combined with a more sophisticated approach, such as mathematical optimization, to ensure tractability. The complexity of the problem grows with the number of problem features considered, such as system losses, reliability, stochasticity, or multi-periodicity.

The OW-EP problem represents a unique challenge in power system expansion planning that aims to identify the optimal expansion plan for offshore transmission networks, encompassing OWPPs. It is important to note that this problem exhibits distinct characteristics when compared to the general power system expansion planning problem, including the increased reactive power in subsea cabling versus overhead lines and the green field nature of the offshore environment, i.e. the lack of an existing network. Nonetheless, similar solution approaches can be applied to both the general and specific cases, although the complexity of the OW-EP problem can be further compounded by additional problem features such as the type of collection circuits considered, the number and location of the OSSs, marine spatial planning constraints, the need to limit cable crossings, and the wake effect.

The state-of-the-art techniques for addressing the various problem features of the OW-EP problem, as well as references to representative implementations of these techniques, are summarized in Table 2.5. In several cases, multiple

techniques have been developed for a given feature and are ordered from least computationally intensive to most. For instance, the least computationally expensive method for accounting for losses is to handle them as a pre-processing step, while the most intensive method involves calculating the full non-linear AC losses of power flow. This ordering generally corresponds to an increase in modeling accuracy as well. Whenever appropriate, example implementations using classical formulations are provided in blue, meta-heuristics in green, and heuristics in red. References in black are for miscellaneous methods that do not fit specifically into any of these three solution methods (e.g. [136] is a finite element model).

Table 2.5: Summary of state-of-the-art techniques for the OW-EP problem and representative implementations. References in blue are for classical formulations, green meta-heuristics, red heuristics and black other techniques.

Losses	Topologies	Wind stochasticity	Uncertainty	Power flow
pre-process	predefined	deterministic	robust optimization	transport
[82]	[68]	[91] [32] [63]	[127]	[82] [32] [63]
linear	radial	sampling	ARO	DCOPF
[142]	[63] [32] [132]	[102]	[130]	[102] [68]
iterative	branched	PDF	chance constraints	ACOPF
[102]	[102] [69] [67]	[82]	[131]	[85] [137]
quadratic	steiner nodes	simulation	stochastic	
[85] [65]	[61]	[85] [132]	[51]	
AC	meshed			
[137]	[103] [101] [95]			

Reliability	Wake	No-go zones	OSS	Cable crossings
deterministic	vertex packing	steiner nodes	>1, fixed position	forbidden edge sets
[133]	[146]	[82]	[63] [67]	[73]
probabilistic	Katic-Jansen	shortest path	variable position	lazy call back
[102] [157]	[65]	[142]	[89] [75] [95]	[82]
monte carlo	CFD			
[132]	[136]			

	Time	Decomposition	Bathymetry	
	static	transmisison	weighted edge graph	
	[120]	[112]	[67]	
	dynamic	collection		
	[52]	[103]		

Through this extensive review of current literature, two critical gaps that require further investigation have been identified. The first pertains to the transition between traditional high-level expansion planning models that focus on transnational grid expansion and the low-level models used for planning collection circuits and simple transmission networks of isolated, radially connected OWPPs.

While previous research in offshore expansion planning has largely focused on the collection circuit problem, the recent rapid development in the offshore wind industry has created a gap in state-of-the-art planning models. To address this, a transmission network expansion model focused on the intermediate capacity network, which fits between existing high and low-level models is developed in chapters 4, 5, and 6.

The second gap identified pertains to the macro scale, where the structure of the energy market dictates the distribution of benefits among stakeholders. While state-of-the-art expansion planning models have been developed for a market structure known a priori, none were found to effectively address the initial decision of what market structure should be implemented. This creates a significant challenge for developers, particularly as the industry moves towards a meshed offshore HVDC grid, which lacks a clearly defined energy market structure for developers to reliably predict future revenues. This high level of uncertainty translates directly to higher costs of development. As such, chapter 7 will focus on developing an offshore wind generation and transmission expansion planning model that considers the market structure as part of the decision-making process. Such a model will help formulate a market-aware strategy that addresses these uncertainties and provides developers with a reliable basis for predicting future revenues.

In the subsequent chapter, a framework that builds upon the findings of this thesis, emphasizing accuracy and efficiency, will be proposed for the OW-EP problem.

Chapter 3

Structure of the proposed offshore wind expansion planning methodology

3.1 Introduction

This chapter presents an overview of the proposed methodology for OW-EP. It provides an over-arching framework for expansion of generation and transmission from single OWPPs up to a high capacity meshed HVDC grid. The framework links together several different models, each developed for a specific aspect of the generation and transmission system expansion. When there is existing research that is appropriate for the application, the state-of-the-art model from existing literature is recommended. When there is a gap in the literature and the solution has been the subject of research within this thesis, the chapter's work is briefly introduced and the reader is directed to the appropriate section for more details.

In the last part of the chapter the domain within which the methodology operates is described through discussion on the most relevant data sources available. The proposed methodology is a multi-level, step-wise, stochastic, Offshore Wind Generation And Transmission Expansion Planning (OW-GATE) model that permits a holistic planning approach to HOAs, market design, HVAC and HVDC transmission and collection circuit design.
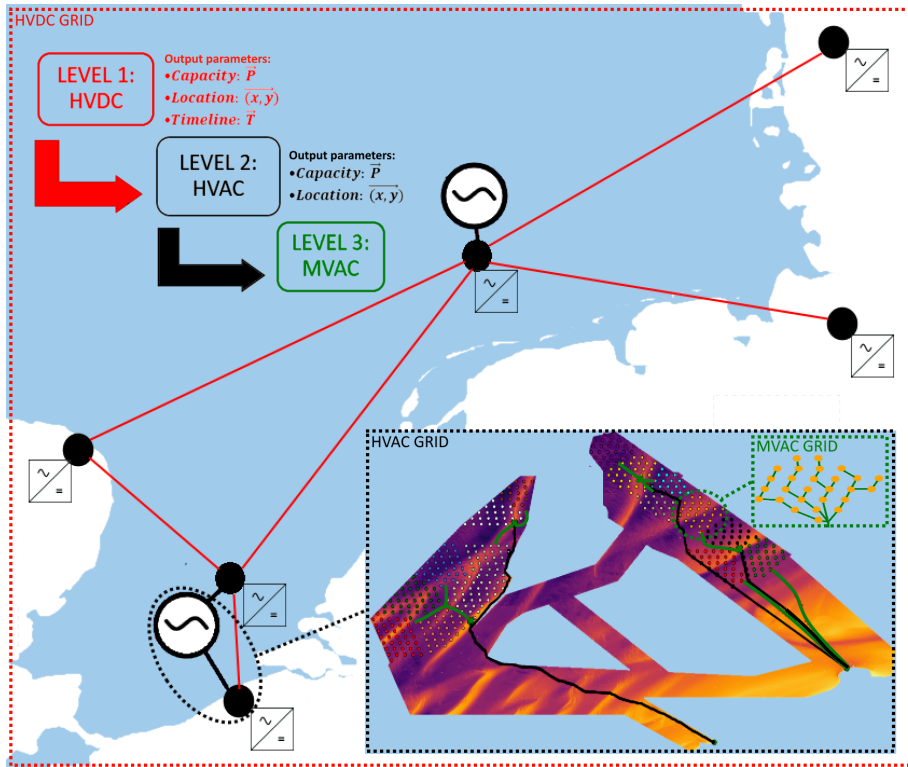
Figure 3.1: Illustration of the over-arching framework for multi-level, step-wise planning of offshore transmission and generation expansion.

3.2 Divide and conquer

A broad overview of this methodology is shown in Fig. 3.1. The offshore electrical transmission infrastructure of interest, spans three voltage/technology levels:

- Level 1: $\mathcal{G}^{\mathrm{DC}}$ The HVDC transmission system.

- Level 2: $\mathcal{G}^{\mathrm{AC}}$ The HVAC transmission system ($> 66\,\mathrm{kV}$ AC[1]).

- Level 3: $\mathcal{G}^{\mathrm{CC}}$ The OWPP collection circuit (typically $\leq 66\,\mathrm{kV}$ AC).

---

[1]66 kV is used as a separation in this work as it corresponds to current offshore wind farm collection systems, however, in the future higher voltages such as 132 kV are expected.

At level $\mathcal{G}^{\mathrm{DC}}$, the primary objective is to find the sizing and topological layout of HVDC transmission lines as well as the number and location of converter stations that maximizes system social welfare. Converter stations may be located onshore or offshore and occur at the transition between the existing grid and or either of the candidate AC networks. The simplest HVDC system is a single OWPP radially connected to shore via an offshore rectifying station and onshore inverter station. A complicated HVDC network is multi-terminal, meshed, spans multiple energy markets and connects large regions of offshore generation consisting of many OWPPs and possibly other components such as storage or loads. Level $\mathcal{G}^{\mathrm{DC}}$ is the highest capacity network of the three levels.

At level $\mathcal{G}^{\mathrm{AC}}$, the primary objective is the sizing and topological configuration of HVAC transmission lines as well as the number and location of OSSs that maximizes system social welfare. Points of coupling with the existing network and the HVDC network must also be decided. As with the HVDC grid, the simplest HVAC system is an OWPP with a single OSS connected via a radial export cable to a point of coupling onshore. The complexity of the HVAC network grows combinatorially with the number of OWPPs and points of coupling that are considered. Level $\mathcal{G}^{\mathrm{AC}}$ is the medium capacity network of the three levels.

At level $\mathcal{G}^{\mathrm{CC}}$, the primary objective is the sizing and topological configuration of the inter-turbine cabling as well as the number and location of MV/HV OSSs that maximizes OWPP profit. For OWPPs that are near to shore, the collection circuit may connect directly to a point of coupling of the existing network. The simplest collection circuit consists of strings of radially connected turbines. More complicated layouts with meshing are used to increase reliability. level $\mathcal{G}^{\mathrm{CC}}$ is the lowest capacity network of the three levels. A summary of the three grid levels' objectives and the desired infrastructure is provided in Table 3.1.

	Objective (maximize)	Output
$\mathcal{G}^{\mathrm{DC}}$	Social welfare	Sizing and topological configuration of HVDC transmission lines and number/location of converter stations
$\mathcal{G}^{\mathrm{AC}}$	Social welfare	Sizing and topological configuration of HVAC transmission lines and number/location of OSS
$\mathcal{G}^{\mathrm{CC}}$	OWPP profit	Sizing and topological configuration of the inter-turbine cabling and number/location of OSS

Table 3.1: Summary of grid level objectives and outputs.

A divide and conquer approach to the OW-EP problem is adopted. A set of subproblems are defined with the hope that the combination of the optimized
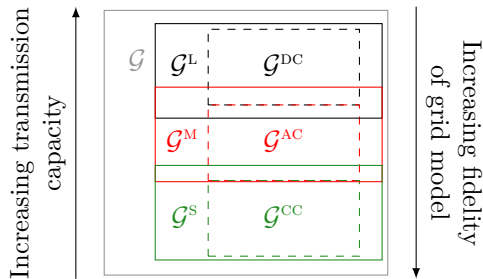
Figure 3.2: Technological domains of sub-grids of $\mathcal{G}$. Transmission capacity and the fidelity of the grid model have an inverse relationship.

subproblems approaches the optimal solution of the full size problem. The complete network is the union of all three voltage levels: $\mathcal{G} = \mathcal{G}^{\mathrm{CC}} \cup \mathcal{G}^{\mathrm{AC}} \cup \mathcal{G}^{\mathrm{DC}}$. Infrastructure at all or only a subset of the three levels forms the solution space of a particular problem. Dividing the problem along voltage or technological lines is logical. Unfortunately, the line between economic HVAC and HVDC transmission is not easily defined. As such a strict division along these lines may result in sub-optimal topologies. This is discussed further in Appendices A and B.

A better definition for subproblems of $\mathcal{G}$ is along the lines made by the intended transmission capacity and the changing fidelity of the underlying grid models. In this work these sub-grid models are defined as: $\mathcal{G} = \mathcal{G}^{\mathrm{S}} \cup \mathcal{G}^{\mathrm{M}} \cup \mathcal{G}^{\mathrm{L}}$. Where $\mathcal{G}^{\mathrm{S}}$ is the lowest capacity grid, $\mathcal{G}^{\mathrm{L}}$ the highest capacity and $\mathcal{G}^{\mathrm{M}}$ has a capacity between these extremes. With this division, $\mathcal{G}^{\mathrm{S}}$ essentially maps to $\mathcal{G}^{\mathrm{CC}}$ with the line blurring as higher collection circuit voltages are considered. Both $\mathcal{G}^{\mathrm{M}}$ and $\mathcal{G}^{\mathrm{L}}$ can be composed of both HVAC or HVDC, although it is assumed that $\mathcal{G}^{\mathrm{M}}$ is more likely to be a majority HVAC transmission and $\mathcal{G}^{\mathrm{L}}$ HVDC. It can be helpful to think of these three sub-grids in terms of national borders, $\mathcal{G}^{\mathrm{L}}$ being the transnational grid, $\mathcal{G}^{\mathrm{M}}$ the national grid and $\mathcal{G}^{\mathrm{S}}$ the sub-transmission or distribution network. The technological domains of sub-grids are displayed in Fig. 3.2.

As noted the fidelity with which the grid can be represented has an inverse relationship with the transmission capacity. This is due to the computational limitations of the model. To illustrate this concept, consider Fig. 3.3, which depicts a common point **P** as seen from different subproblems. When viewed from the perspective of the coarsest subproblem, grid $\mathcal{G}^{\mathrm{L}}$, all offshore wind power plants (OWPPs) within a certain region are lumped together and represented as a single point source, **P**. In the medium grid $\mathcal{G}^{\mathrm{M}}$, separate OWPPs are identified, $G_1, ..., G_n$, but individual turbines are clustered to a single point source. Finally,

in the finest grid $\mathcal{G}^{\mathrm{S}}$, each individual turbine, $g_1, ..., g_n$, is modeled separately.

The boundary point **P** frequently corresponds to a transition between voltage levels. In offshore wind, this boundary occurs in the OSSs. The locations of OSSs are therefore complicating decision variables that must be shared across the different grid levels. A common criterion used for positioning OSSs is to minimize cable length. Unfortunately, shortening the cable length for one level can result in longer cable lengths for another level, leading to a trade-off. To address this issue, a top-down approach can be used to solve the problem incrementally, first by adjusting the location of OSSs at a macro scale, and then at a micro scale as the grid fidelity increases. The sub-grids are solved in the order of $\mathcal{G}^{\mathrm{L}}$, $\mathcal{G}^{\mathrm{M}}$, $\mathcal{G}^{\mathrm{S}}$.
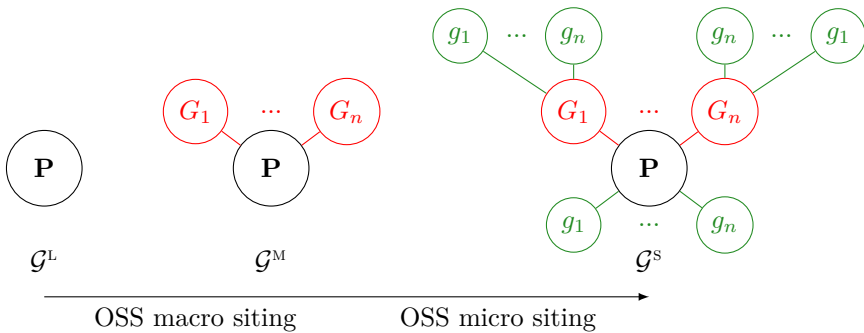
Figure 3.3: Boundary point **P** as seen from $\mathcal{G}^{\mathrm{S}}$, $\mathcal{G}^{\mathrm{M}}$ and $\mathcal{G}^{\mathrm{L}}$. $\mathcal{G}^{\mathrm{CC}}$ (green), $\mathcal{G}^{\mathrm{AC}}$ (red) and $\mathcal{G}^{\mathrm{DC}}$ (black)

3.3 Timeline of power system planning

Approaching the problem in this top down manner, jibes well with the expected planning horizons of each sub-grid. The time scale at which OW-EP applies is shown in Fig. 3.4. $\mathcal{G}^{\mathrm{L}}$ falls into the long term planning category, $\mathcal{G}^{\mathrm{S}}$ into the medium term and $\mathcal{G}^{\mathrm{M}}$ straddles the two.

The divide and conquer approach is extended to the network levels which are further broken down into subproblems as in Fig. 3.5. Each subproblem has a unique objective. The font chosen for each subproblem in the figure indicates its relevance to this thesis. Subproblems in bold are the primary focus of this thesis. Those in normal font are fully outside the scope. Subproblems in italic are not covered in detail but some insights have been provided.
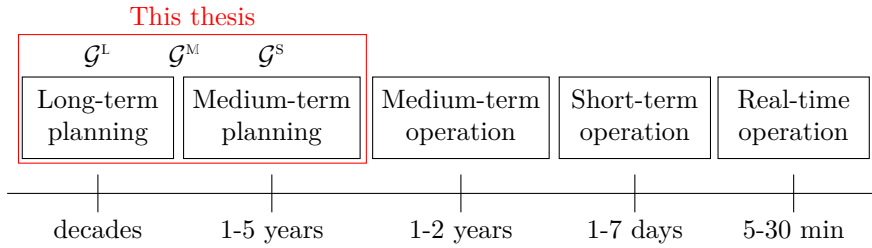
Figure 3.4: Time scale of power system planning and operation [158].

When solving the subproblems, ordering is important. Certain problems must be solved sequentially while others can be done in parallel. In Fig. 3.6 the time dependence of the subproblems is presented. In total six sequential stages are needed. The color coding is a legend for the schematic on the right side of the figure. This figure shows a one-line diagram of a toy example of an offshore transmission system connecting five OWPPs to two PCCs onshore.

To illustrate the planning process effectively, planning stages one through six will be discussed in reference to this toy problem. Each subproblem will be introduced in the order they are to be executed, systematically expanding the offshore transmission network. To begin, the boundary conditions on the domain are specified. We consider a green field problem therefore no offshore network exists. We do assume, however, there are some predetermined areas which have been ear-marked for offshore wind development. In our toy problem, this is the region enclosed by a dashed rectangle 3.6 - right). We also assume the locations of possible onshore PCCs have been determined apriori.

In **planning stage one** subproblem L.1 to L.4 are solved answering the following questions:

- What are the generation capacities and macro locations of the OWPPs?

- What is the topology of $\mathcal{G}^{\mathrm{L}}$?

- What are the capacities and macro locations of $\mathcal{G}^{\mathrm{L}}$ OSSs?

- What is the construction timeline?

In our toy problem (Fig. 3.6 - right), this result is illustrated in black and includes the following:
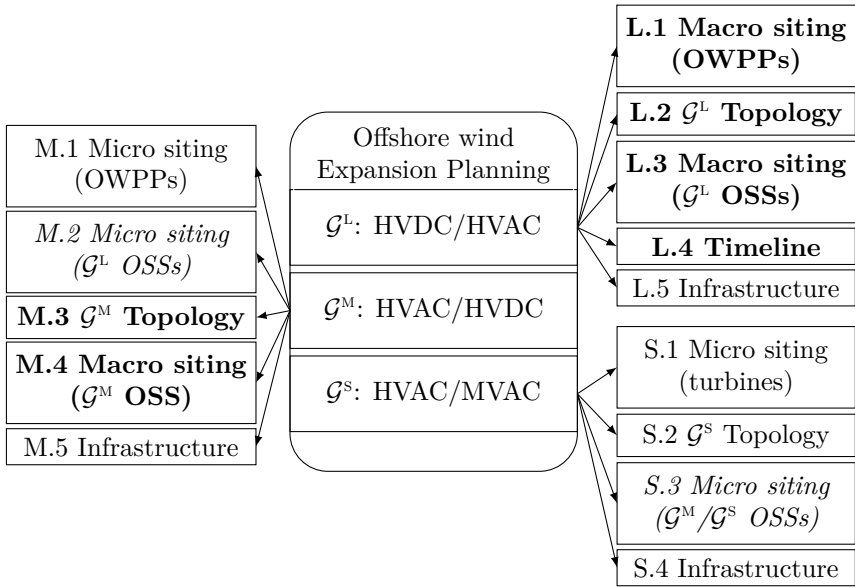
Figure 3.5: Divide and conquer approach to the offshore wind expansion planning problem. Subproblems in bold are within the scope of this thesis, regular font are outside and italic are not covered in detail but some insights are provided.
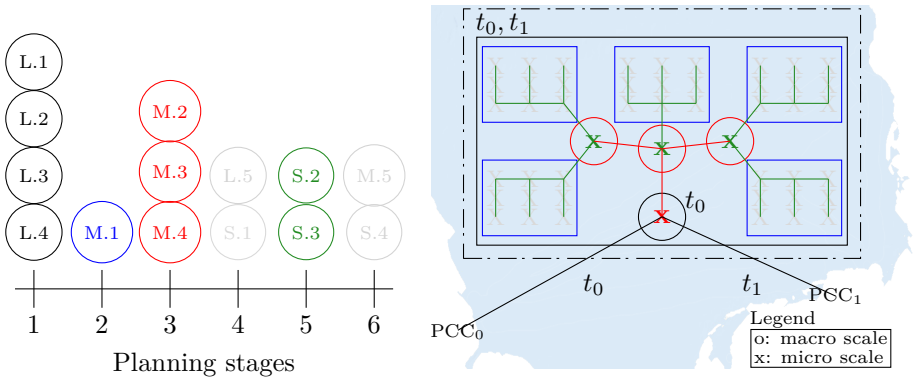
Figure 3.6: Step by step development. Sequential and parallel subproblem execution (left). Color coded toy-problem (right). Colors in the toy problem match those of subproblems L.1–S.4 (L.5, M.5 and S.4 not shown).

- The capacity of offshore generation: the surface area enclosed by the solid black rectangle. The relationship between the area and the capacity is:

$$A^{\mathrm{wg}} = \frac{P^{\mathrm{wg}}}{\rho},\tag{3.1}$$

  where P^{wg} is the desired generation capacity of the region and ρ is the average wind power density of the region.

- The transmission topology: an HVDC network consisting of a single OSS connected to two PCCs. Onshore and offshore converters and cable capacities are specified.

- The macro location of the OSS: the area of the black circle.

- The timeline to develop the project: the OSS is built in t_0 and connected to PCC_0 in the same period. An additional connection to the PCC_1 is built in t_1.

Notice the precise boundaries (or even number) of OWPP concessions are not yet defined. Neither is the exact location of the OSS. At this level the goal is to only define these quantities on a macro scale. There is a high degree of interdependence between all these aspects of the solution space and answering them in unison is desirable. Fortunately, there is an existing formulation discussed in section 2.4.2 that meets our needs, the multi-period GATE planning problem. This formulation is the topic of chapter 7.

In **planning stage two** subproblem M.1 is solved. The objective of this subproblem is to finalize the outer boundaries of the OWPP concessions. Within our toy problem the desired results are shown in blue as five boxes indicating five future concessions. Siting OWPP concessions on a micro scale requires the consideration of many factors such as wind resources, physical constraints such as cable routing, marine spatial planning, environmental requirements, soil conditions, bathymetry, available technology, available ports, existing supply lines and available vessel types. Within this work, the micro siting of concessions is not investigated and when necessary assumed to be known apriori.

In **planning stage three** subproblem M.2 to M.4 are solved answering the following questions:

- What is the micro siting locations of the $\mathcal{G}^{\mathrm{L}}$ OSSs?

- What is the topology of $\mathcal{G}^{\mathrm{M}}$?

- What are the capacities and macro locations of $\mathcal{G}^{\mathrm{M}}$ OSSs?

In our toy problem the solution is illustrated in red.

- The micro location of the $\mathcal{G}^{\mathrm{L}}$ HVDC OSSs is indicated by the red cross.

- The topology of $\mathcal{G}^{\mathrm{M}}$ consists of three MV/HV OSSs, two of which are servicing two of the five OWPPs each and a third that only services a single OWPP. The third OSS is acting as a central hub with connections to all other substations, including the HVDC station.

- The macro locations of the OSSs: the area of the red circles.

High level specifications for major transmission components are determined at this stage, including the OSSs, transformers and cable capacities. Problems M.2 through M.4 can be solved simultaneously as a TNEP problem. Formulating this TNEP is the topic of chapters 4 through 6.

In **planning stage four** subproblems L.5 and S.1 are solved. In subproblem L.5 the final optimization of the $\mathcal{G}^{\mathrm{L}}$ infrastructure is done. This is the stage where detailed thermal and electromagnetic design is carried out, which is out of the scope of this thesis. However, below, in planning stage six, a brief discussion on the topic is presented as it applies to infrastructure at all grid levels. Subproblem S.1 is the micro siting problem of the wind turbines within the OWPP concessions. Micro siting turbines is a an optimization of the physical location of turbines. Turbine layout has traditionally focused on minimizing wake losses while considering physical constraints such as spatial planning and soil conditions. This subproblem as previously discussed is not within the scope of work. A representative solution space however, is displayed in our toy problem as grey x's.

In **planning stage five** subproblems S.2 and S.3 are solved. The objective of S.2 is to determine the layout of the OWPP collection circuit. Specifications for components are determined, particularly the cable capacities and associated amount of switch gear (if branching or meshing). Subproblem S.3 finalizes the location of the MV/HVAC OSSs specified within a previous planning stage. Physical constraints such as cable routing, marine spatial planning, environmental requirements, soil conditions and bathymetry to name a few are to be considered. S.2 and S.3 can be solved simultaneously using a formulation presented in section 2.4.3. As collection circuit optimization is the most heavily researched part of offshore topology optimization no further work on this topic was carried out within this thesis.

In **planning stage six** subproblems M.5 and S.4 are solved. As with stage L.5, this is the point where detailed thermal and electromagnetic equipment design should be performed prior to actually breaking ground on the construction sight. The objective is the optimal sizing of components such as cables,

transformers, converters etc. Equipment must be sized to meet power system requirements while minimizing lifetime costs and ensuring that the thermal ratings of components are respected. The temperature of equipment is calculated by modelling the physics of the system subject to the expected load profile. The degree of detail to which these two aspects are modelled dictates the complexity of the modelling method and therefore the computational cost.

Modelling the partial differential equations directly on complex geometries with an approach such as the finite element method provides the highest fidelity physics. This can provide valuable insights into objectives such as loss minimization. But, such detail comes at a high computational price and is therefore only applicable after expansion planning has occurred and infrastructure is narrowed down to the final few options. A thermo-electric equivalent model [159,160] may be deemed a more acceptable trade-off, capturing higher physical detail than a standard parametric model such as those from the International Electrotechnical Commission (IEC) [161] or CIGRE [162], but with substantially reduced computation time.

Load profiles can be modelled as static or dynamic. The traditional approach used in the IEC standard assumes a static load profile [161]. But OWPPs are highly fluctuating sources with capacity factors in the neighbourhood of 40 %. Assuming a constant rated output can result in a conservative approach to sizing that is expensive. Dynamic sizing attempts to remedy this deficiency by modelling the fluctuating nature of RESs when calculating the thermal limit. The IEC proposes a simple step function [163] and CIGRE a slightly more sophisticated four step RMS signal in [164]. Adapting such an approach to accept a probabilistic wind distribution would improve accuracy and seems relatively easy to implement, however, this would of course come at the expense of higher computation time. In [165] a method using dynamic temperature sensing with a thermo-electric equivalent is proposed for export cables. If computation time is not a concern, the full dynamic time series of the expected load profile can be considered.

3.4   Optimization input data

Using high quality input data to describe the domain and boundary conditions is essential. Six major categories of data are identified: meteorological data, energy market data, grid data (onshore and offshore), hydrographic data, economic data and regulatory/technological data. These categories can each be further broken down into sub-categories of data that are more or less useful depending on the grid level optimization being performed. Input data used in this thesis and

the level at which it was most useful is depicted in Fig. 3.7. When describing certain features of the domain there may be several data types to chose from, some more appropriate than others given the specifics of the problem. In this section a brief description of the most relevant input data is presented.
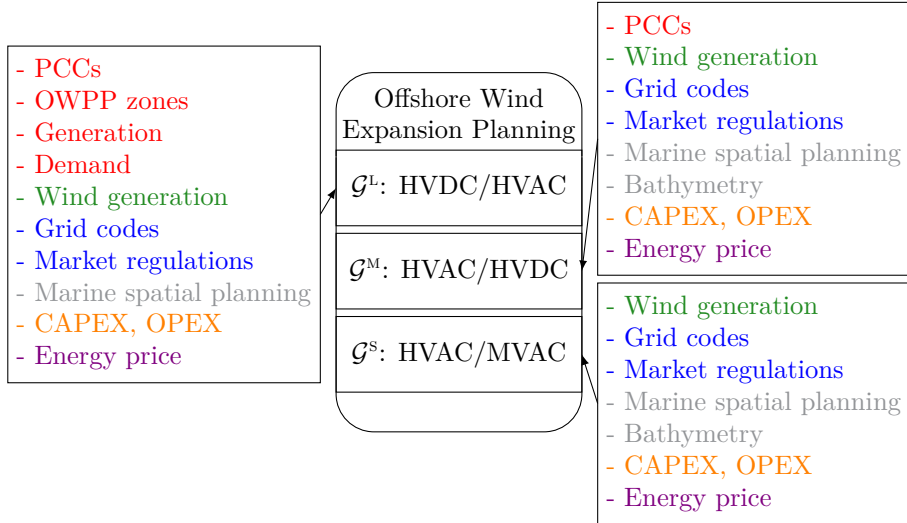
Figure 3.7: List of input data collected to describe each level of the offshore wind expansion planning problem. Color legend: Grid data (red), Meteorological data (green), regulatory/technological data (blue), Hydrographic data (gray), Economic data (orange), Energy market data (purple).

Meteorological data

Accurately estimating the power generation of RESs is essential in expansion planning, however, due to the stochastic nature of RESs this can be a challenge. Two possible approaches for OWPPs adopted within this thesis are presented below. The two methods depend on two different base data sets. A comparison of the generation forecasts obtained by each set described below is displayed in Fig. 3.8.

Method one (in blue) uses historic offshore wind generation data e.g. from the ENTSO-E transparency platform [166]. The benefit of using such data is the additional information contained in the time series, particularly the OWPP power curve, wake effect and system reliability, since these are imprinted on the data as reduced generation. When using this type of data, it is essential when

normalizing to have an accurate value for installed capacity. This can be more difficult than it seems as new installations are being commissioned regularly. As such, using a single value based on the installed capacity at the start or end of year can result in an over or under estimation of annual production.
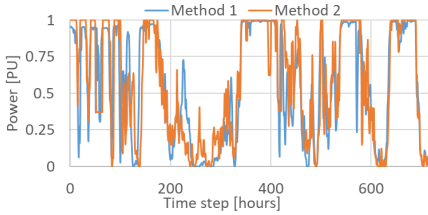
Figure 3.8: January 2018 generation time series for Belgium offshore. ENTSO-E generation data [167] (Method 1) and CorWind simulation results [168] (Method 2).
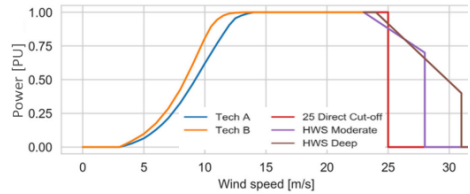
Figure 3.9: Plant level power curve with different shut down characteristics [169].

Method two (in orange) uses meteorological data, such as those generated by the CorWind software [168]. To calculate power generation, a power curve such as in Fig. 3.9 must be assumed. This has the added advantage of permitting the analysis of turbine specific factors such as the different approaches to storm shut down in the figure. For locations where there is no existing generation, using meterological data may be the only data based option available for assessing OWPP yield. Of course, probibalistic methods such as in [170] are also a possibility. Typically, manufacturers are reluctant to share turbine power curves due to intellectual property concerns necessitating the reliance on generic wind power curves.

In Table 3.2 a comparison of the production forecasts for the Belgium offshore region obtained by each method is provided. Method 1 reflects the actual production recorded on the ENTSO-E transparency platform. Method 2 is obtained using the CorWind software. In this case, the projected annual yield using meteorological data results in an over-estimation of almost 10 %. This is on the low end as far as over-estimation when neglecting wake, electrical and down time losses as according to [171], wake losses alone can reduce OWPP output by 10-20 %. In this work method 1 is used in chapter 7 and method 2 in chapters 4 through 6, as the effect of losses and reliability of the system is accounted for explicitly in these chapters.

Table 3.2: Comparison of production forecasts for Belgium 2018 using method 1 and method 2.

Method	Capacity factor [%]	Yearly yield [MWh]	Difference [%]
1	38.6	3384	-
2	42.2	3697	9.26

Energy market data

Accurately modeling the price of energy is essential when calculating the revenue of OWPPs. Three approaches have been found. The first is the simplest which is to assume a given, average future value for each zone. This approach is used in chapters 4 through 6. The second approach is slightly more sophisticated. In this approach, instead of using a static value, a time series of historical energy prices such as is available from ENTSO-E [166] is used. This approach was used in [172], a publication produced as part of the Cordoba project but not included within this thesis. Calculating revenue in this way has the advantage over a static value of capturing temporal correlations with other data, such as the RES generation time series and demand time series. Of course, this comes at the expense of increased complexity.

Unfortunately, this approach still has its limitations. As the investment advice goes "past performance is not indicative of future results" neither are past energy prices indicative of future energy prices. In Europe, in 2022, this statement is more true than ever as electricity prices have increased almost an order of magnitude in the last two years. For reference, in Fig. 3.10, the average yearly Belgian wholesale energy price since 2015 is shown. Obviously, using pre-2021 prices to predict revenues in 2021 and 2022 is not realistic. Furthermore, historical clearing prices are a function of the available generation, demand and congestion in the system at that time. In expansion planning it is desirable to model how the energy price will change given the construction of new generating sources and transmission lines as well as changing demand over time.

The third approach used in this work attempts to overcome the shortcomings of the previous methods by modelling economic dispatch. In this approach grid data from [173] is used to model available generating sources, system congestion and demand. The LCOE for each source [174] is then used to calculate the marginal cost of energy within each market zone. In this way, as grid expansion occurs and new generation, demand and transmission lines are added, the clearing price evolves in lock step. This approach is used in chapter 7.
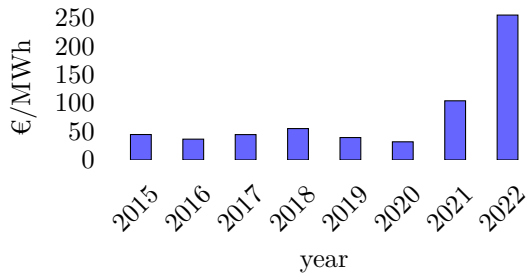
Figure 3.10: Average annual wholesale electricity price in Belgium 2015 to 2022. Note: 2022 only includes prices up to September.

Grid data

Offshore expansion planning depends on the existing and future onshore electrical grid. The principal source of grid data used in this work is from either open academic test networks or the ENTSO-E TYNDP [173] which is updated every two years to reflect the current state of the European grid as well as possible future expansion scenarios. The existing grid data is summarized in Fig. 3.11. Modelling the onshore grid in full detail is not computationally feasible. As such a reduced grid model consisting of the type and capacity of generation and demand within each market zone and inter-market congestion in the form of Net Transfer Capacitys (NTCs) is used.
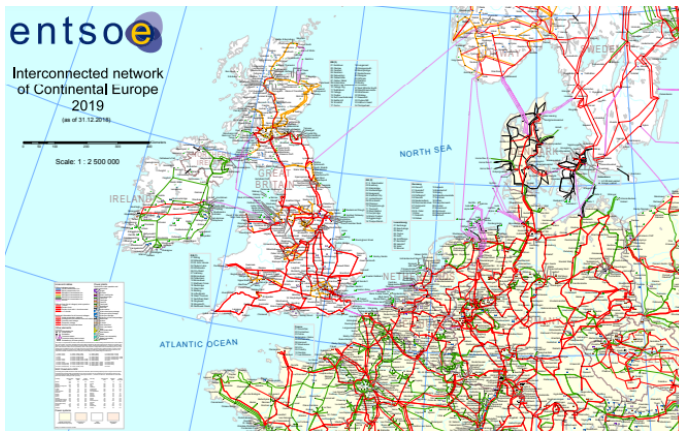
Figure 3.11: ENTSO-E Interconnected network of continental Europe 2019 [175].

Hydrographic data

The North Sea spans 570000 km^2 and is bordered by Norway, Denmark, the UK, the Netherlands, Belgium, France and Germany. The sea depth varies greatly along its geographic features. Notable features are vast banks, such as the 17600 km^2 Dogger bank with a depth in the low tens of meters, and the devil's hole and Norwegian trenches with depths in the hundreds of meters. The deepest point in the North Sea is in Norwegian waters at 725 m. Even within small areas the depth can vary significantly. For example, the 3447 km^2 Belgian Exclusive Economic Area (EEA) is criss-crossed by 23 sand banks. The peaks of the sand banks sit around 5 to 15 meters below the surface while the valleys 25 to 35 meters [176]. This change is significant, it is estimated in [177] that an increase in depth of 20 meters results in a 177 % increase in the cost of offshore foundations.

In addition to water depth, marine spatial planning in the North Sea cannot be ignored during expansion planning. As can be seen in Fig. 3.12, some regions of the North Sea can be highly congested, with areas reserved for shipping, environmental protection, fisheries, military, existing OWPPs, pipelines, cabling and more. Furthermore, a history of warfare has left hazards such as unexploded ordinances littering the sea floor. In chapter 6 the impact of hydrography is discussed.
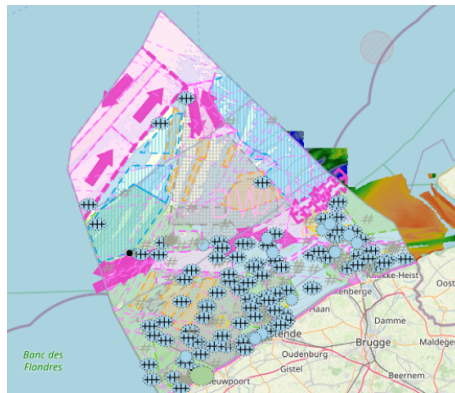
Figure 3.12: Hydrography and marine spatial plan of the Belgian continental shelf [176]. For markup details please refer to the source map in the reference.

Regulatory and technological data

Technological limitations and government regulations are among the most uncertain and challenging constraints to define, in particular on a longer time horizon. While current technological limits are straightforward to understand, anticipating what will be achievable in two or three decades into the future, and at what cost, is not.

Regulations can also be difficult to properly define for a couple reasons: regional differences and shifts in policy. Europe has invested much time towards EU-wide harmonization. The trans-national electricity network codes [178] are set by the European Commission with input from the ENTSO-E and the Agency for the Cooperation of Energy Regulators (ACER). In addition to these trans-national authorities, stakeholders at the national levels, including TSOs, National Regulatory Authorities (NRA) and member state governments among others are given the opportunity to participate in their development. The guidelines are legally binding and cover three major categories:

- Market and trading regulations including:

    - Capacity allocation and congestion management: (EU) 2015/1222
    - Forward capacity allocation: (EU) 2016/1719
    - Balancing: (EU) 2017/2195

- Connection and system operation regulations including

    - Emergency and restoration: (EU) 2017/2196
    - Demand connection: (EU) 2016/1388
    - Requirements for generators: (EU) 2016/631
    - High-voltage direct current: (EU) 2016/1447
    - System operation: (EU) 2017/1485

- Regulation on conditions for accessing the network for cross-border electricity exchanges (EC) 714/2009

Progress towards EU-wide harmonization is good, but regional difference do (and likely always will) exist. Some, such as the various dimensionning incidents across synchronous zones, which dictate the maximum loss of in-feed can have a significant and direct impact on possible transmission topologies in the North Sea. The values for different synchronous regions are set at 1.8 GW in Great Britain, 1.45 GW in the Nordic power system and 3 GW in continental Europe. Other differences such as offshore transmission development in Europe being

the responsibility of TSOs versus an Offshore Transmission Operator (OFTO) in the UK [179] has a more indirect impact which is difficult to quantify.

Furthermore, regulations are subject to change, creating uncertainty for developers. A particularly impactful example of this is the exit of the UK from the European internal energy market as part of Brexit in January of 2021 [180]. A consequence of this, is that capacity allocation in interconnectors linking the UK and the EU can no longer be done via an implicit auction but rather an explicit auction must be held, reducing the efficiency of the process [180]. Furthermore, current regulations are likely only an interim solution as post-Brexit negotiations between the EU and UK are on-going [181].

This has significantly clouded the regulatory landscape, leaving planners and developers unsure of what the future will bring in terms of energy market integration with the UK. Developers of HOAs, such as Elia's energy island [182], that combines offshore wind with interconnectors (one between the UK and Belgium), face high uncertainty, which drives up costs. Due to the uncertainty associated with the regulatory and technological future, this thesis takes the approach of considering these as soft constraints which can change over time. As such, the models attempt to be as general as possible in this regard and ignore much of the regional differences. For example, implicit energy coupling, as it is between any member of the EU internal energy market, is assumed between the EU and the UK. Should the modelling approach be adopted in future in a more specific context, then at that time the appropriate regional regulations should be considered.

Cost data

The main data sources used in this work are gathered from commercial projects [183–188]. Unfortunately, the uncertainty of offshore development costs are very high. For example, in [183] the range for an offshore 2 GW HVDC converter station is between 390-530 M€, in [184] the same station is estimated to be between 740-900 M€, while [185] estimates 595-1030 M€. The large variation in estimates is caused by several factors. First, companies are hesitant to share detailed cost information out of fear of loosing a competitive advantage. Second, reported costs often lack detail as to what is included. The low range cost reported in [184] for example, includes installation for the substructure but likely not the installation cost of the topside plant including the HVDC converter itself. Third, installation costs offshore are significant, often accounting for around 50% of CAPEX. Installation costs are project specific and can vary substantially based on factors such as soil conditions, water depth, available ports, time of year and vessel availability [183]. Finally, current macro economic

conditions are very uncertain. Disruptions in supply chains due to the ongoing pandemic, war in Ukraine, deteriorating trade relations with China, increasing costs of lending by central banks and record high inflation all contribute to uncertainty. As such, the highest source of error within this work is attributed to the cost data. An error of +/- 30 % is assumed as in [184], however, even this may be an underestimate.

3.5 Cost modelling

In this section, a brief introduction to the cost model is presented, for a more detailed presentation, the reader is directed to Appendix A. The developed cost model attempts to capture the non-linear and discontinuous effects associated with infrastructure investment. The most influential non-linearity requiring consideration is that of the reactive power flows within HVAC cables. The relationship between distance, capacity and transmission voltage is presented in Fig. 3.13. Notice that at standard transmission frequency (50 Hz), transmission
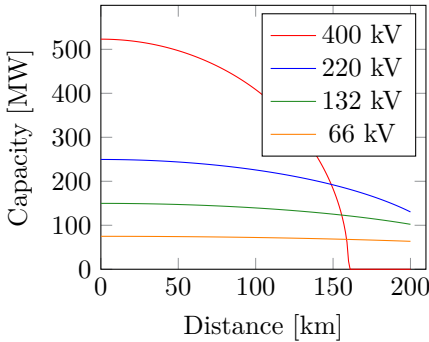
Figure 3.13: 500mm^2 AC cable capacity dependence on voltage and distance.
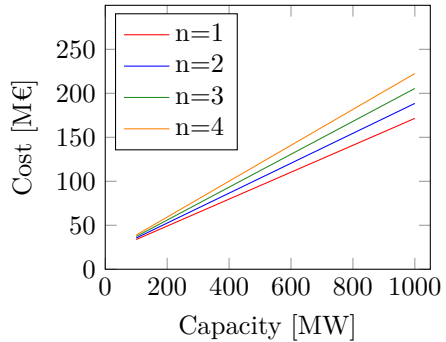
Figure 3.14: OSS cost considering capacity and redundancy. (depth: 30m)

at voltages above 220 kV is severely limited by distance. This is due to the reactive power flows being proportional to the square of the transmission voltage. Another non-linearity occurs when considering the trade-off between an investment in redundant paths (reliability) and CAPEX. For example, when considering redundancy at the OSS, the cost function becomes discontinuous as in Fig. 3.14 due to parallel paths being integer quantities.

On top of CAPEX, transmission investment should consider Operating Expenditures (OPEXs), such as corrective maintenance, losses and EENT. The model accounts for these quantities as in the data structure displayed in Fig.

3.15. Transmission system costs are broken down into several contributing costs. First, Terminal Costs (TCs) and Route Costs (RCs) are differentiated. TCs are distance independent costs associated to a node, for example an OSS and its components. RCs are costs tied to the cabling and depend on distance. TCs and RCs are then further subdivided into CAPEXs and OPEXs. All up front costs for equipment and installation are grouped into CAPEXs. The terms Terminal Capital Costs (TCCs) and Route Capital Costs (RCCs) are used for CAPEXs while Terminal Loss Costs (TLCs) and Route Loss Costs (RLCs) are used for OPEXs.
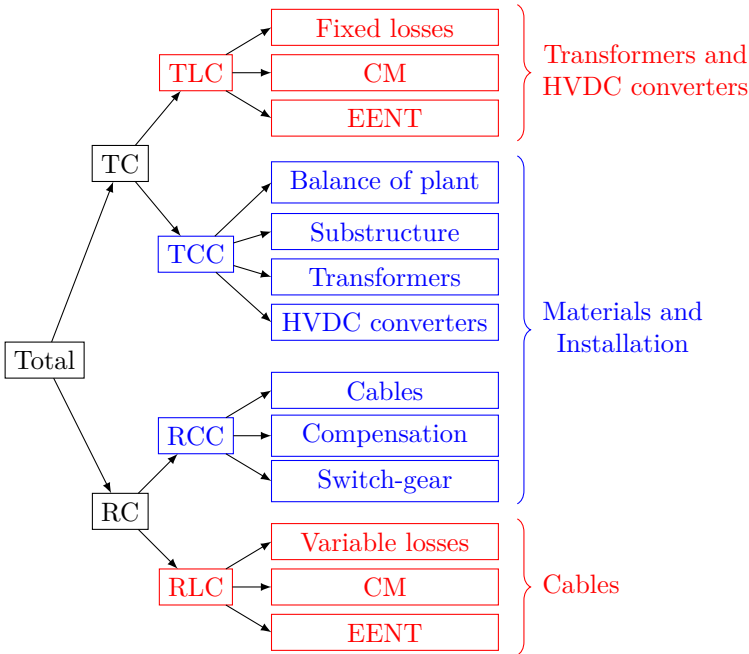
Figure 3.15: Hierarchy of the cost model. CAPEX is in blue. OPEX is in red.

3.5.1 Capital expenditures

The CAPEX functions presented below use a superscript notation to avoid unnecessary repetition of equations. The xx notation is a place holder identifier that varies based on the transmission technology chosen. The cost of a specific technological solution can be determined by replacing xx with *AC* for HVAC or *DC* for HVDC and choosing the relevant cost parameter. All cost parameters are listed in Table A.3 of Appendix A.

Route capital costs

Subsea transmission is complicated by high reactive power flows within alternating current cables that increase with network frequency, transmission voltage and distance as in:

$$Q^{\text{XX}} = 2\pi \cdot f^{\text{XX}} \cdot q_{cbl}^{\text{XX}} \cdot (V^{\text{XX}})^2 \cdot l_{cbl}^{\text{XX}} \cdot n_{cbl}^{\text{XX}}, \tag{3.2}$$

where, f is the network frequency in Hz, V the transmission voltage in kV, q_{cbl} the capacitance of the cable in F/km, l_{cbl} is the cable length in km and n_{cbl} is the number of cables in parallel.

It is typical to distribute reactive power compensation 50% onshore and 50% offshore. With this distribution the remaining cable capacity available for real power transfer is calculated as in:

$$P_{cbl}^{\text{XX}} = \sqrt{(S_{cbl}^{\text{XX}})^2 - \left(\frac{Q^{\text{XX}}}{2}\right)^2}. \tag{3.3}$$

The cost of supplying this compensation is estimated as:

$$C_q^{\text{XX}} = \frac{c_{oss}^{\text{XX}} Q^{\text{XX}}}{2} + \frac{c_{ss}^{\text{XX}} Q^{\text{XX}}}{2}, \tag{3.4}$$

where c_{oss} and c_{ss} are the per unit costs for offshore and onshore reactive compensation respectively. The cost of supplying and installing the cable is given by:

$$C_{cbl}^{\text{XX}} = n_{cbl}^{\text{XX}} \cdot c_{cbl}^{\text{XX}} \cdot l_{cbl}^{\text{XX}} \tag{3.5}$$

where c_{cbl}^{XX} is the per unit length cost in €/km. The total RCC is the sum of the cable and reactive power compensation as in:

$$RCC^{\text{XX}} = C_q^{\text{XX}} + C_{cbl}^{\text{XX}}. \tag{3.6}$$

Terminal capital costs

TCC is the sum of the costs for the offshore and onshore substations. The cost of an OSS has three principle drivers, the capacity, the level of redundancy (parallel paths), and water depth. This relationship is expressed as:

$$C_{oss}^{\text{XX}} = \sigma(\zeta)(\overline{c_{oss}^{\text{XX}}} + (1 + \beta_{oss}^{\text{XX}} \cdot (n_{oss}^{\text{XX}} - 2))(\widetilde{c_{oss}^{\text{XX}}} + \widetilde{c_{oss}^{\text{XX}'}}) \cdot P_{oss}^{\text{XX}} \cdot \alpha^{\text{XX}}),$$
$$\text{where } \sigma(\zeta) = 0.0136 \cdot (\zeta - 17) + 0.7676 \tag{3.7}$$

where n_{oss} is the number of parallel paths, β_{oss} is the penalization factor for greater than two parallel paths, $\overline{c_{oss}}$ is the fixed OSS cost, $\widetilde{c_{oss}}$ is the variable substructure cost, $\widetilde{c'_{oss}}$ is the variable balance of plant cost, P_{oss} is the substation capacity and ζ is the sea floor depth. α is a scaling factor for Low Frequency Alternating Current (LFAC) which is discussed within the Appendix. For HVAC and HVDC networks this value is always equal to one.

In an onshore substation, no substructure is required therefore increased reliability does not result in a substantial increase in steel and concrete as it does offshore. As such, n-1 reliability is assumed and the simpler cost function:

$$C_{ss}^{\text{XX}} = \beta_{ss}^{\text{XX}} \cdot (P_{ss}^{\text{XX}})^{\gamma^{\text{XX}}} \tag{3.8}$$

is used.

3.5.2 Operational expenditures

Losses

Equipment losses are modelled as the sum of variable losses in the cables (RLC) and fixed losses in the transformers and converters (TLC). Variable losses capture the I^2R losses in cables. Both alternating current and direct current cables are modelled with the same equation:

$$RLC^{\text{XX}} = \left(\frac{P_{oss}^{\text{XX}} \cdot \eta_{oss}^{\text{XX}}}{n_{cbl}^{\text{XX}} \cdot V^{\text{XX}}} \right)^2 \cdot r_{cbl}^{\text{XX}} \cdot l_{cbl}^{\text{XX}} \cdot n_{cbl}^{\text{XX}} \cdot T \cdot E \cdot \delta, \tag{3.9}$$

where r_{cbl} is the cable resistance in Ω/km and η_{oss} is the conversion efficiency of the OSS in percent. The alternating current resistance is used for alternating current cables and direct current resistance for direct current cables. T, E and δ are the operational lifetime (25 years), energy price (90€/MWh) and load loss factor.

The load loss factor is a function of the square of the per unit power generation profile as in:

$$\delta = \frac{\sum\limits_{t=0}^{T} (S_{g,t}^{\text{pu}})^2}{T}. \tag{3.10}$$

Fixed losses occur in the transformers and converters. They are the magnetic core losses in the transformers and the switching losses in the converters. The fixed losses for offshore and onshore components are given by equations 3.11 and 3.12. η_{ss} is the onshore substation conversion efficiency.

$$TLC_{oss}^{\text{XX}} = P_{pcc}^{\text{XX}} \cdot (1 - \eta_{oss}^{\text{XX}}) \cdot T \cdot E \cdot \delta \tag{3.11}$$

$$TLC_{ss}^{\text{XX}} = (P_{pcc}^{\text{XX}} \cdot T \cdot E \cdot \delta - RLC^{\text{XX}})(1 - \eta_{ss}^{\text{XX}}) \qquad (3.12)$$

Reliability

System reliability is considered in terms of corrective maintenance and EENT. Corrective maintenance is considered post fault, meaning it is the cost of replacing or repairing faulty equipment. Preventative maintenance is not considered within the scope. Yearly corrective maintenance is calculated using the mean time to repair (μ), failure rate (λ) and mean cost per repair (ξ) as in (3.13) [139]. The parameters for transformers, converters and cables are given in the Appendix in Table A.4. Corrective maintenance for the remaining components is not considered. The total corrective maintenance is obtained by summing over the Net Present Value (NPV) of all years within the lifetime of the project.

$$CM_y = \left[\frac{n_{oss}^{\text{XX}} \cdot \xi_{oss}^{\text{XX}}}{\frac{1}{\lambda_{oss}^{\text{XX}}} + \frac{\mu_{oss}^{\text{XX}}}{8760}} + \frac{n_{cbl}^{\text{XX}} \cdot \xi_{cbl}^{\text{XX}}}{\frac{1}{\lambda_{cbl}^{\text{XX}}} + \frac{\mu_{cbl}^{\text{XX}}}{8760}} + \frac{n_{ss}^{\text{XX}} \cdot \xi_{ss}^{\text{XX}}}{\frac{1}{\lambda_{ss}^{\text{XX}}} + \frac{\mu_{ss}^{\text{XX}}}{8760}} \right] \qquad (3.13)$$

The second component of reliability considered is EENT. Additional EENT is available wind energy that must be curtailed due to system capacity constraints. The system capacity may be constrained intentionally through under sizing of equipment or due to component failure. ΔEENT is calculated as follows: consider contingency i with constrained capacity, P_i^{cons}, and probability of occurrence, π_i^{cons}, the per unit ΔEENT is given by:

$$\Delta EENT_i^{\text{PU}} = \text{A}_i^{\text{cons}} \cdot \pi_i^{\text{cons}}. \qquad (3.14)$$

Where A_i^{cons} is the area under the OWPP generation power curve and above the constrained capacity P_i^{cons}. The power generation profile is obtained using meteorological data and the CorWind software [168]. Summing over all contingencies and multiplying by the OWPP peak capacity gives the yearly EENT. The cost of EENT is then obtained by summing the NPV of each year within the lifetime.

Constrained capacities and their probabilities are calculated from capacity outage probability tables for all considered contingencies. The capacity outage probability table of a single piece of equipment is calculated as follows. A piece of equipment x has capacity, P_x. The number of possible states N_x of the equipment is modelled as binary (1: functional, 0: broken). The availability of

the piece of equipment A_x, is given by:

$$A_x = \frac{1}{1 + \lambda_x \cdot \frac{\mu_x}{8760}}.$$ (3.15)

The resulting capacity outage probability table is as in Table 3.3. To construct

Table 3.3: Example capacity outage probability table.

State (i)	Capacity ($P_{x,i}^{\text{cons}}$)	Probability ($\pi_{x,i}^{\text{cons}}$)
1	P_x	A_x
0	0	1-A_x

a capacity outage probability table for an entire system, convolution of all component capacity outage probability tables is done as in:

$$P_k =: \begin{cases} P_{x,i} + P_{y,j} & \text{Parallel} \\ min(P_{x,i}, P_{y,j}) & \text{Series} \end{cases}$$

$$\pi_k = \pi_{x,i} \cdot \pi_{y,j}$$ (3.16)

$$\text{where } i = \{1, .., N_x\}, j = \{1, .., N_y\}, k = \{1, ..., N_x \cdot N_y\}$$

If after combining two tables, two rows k have identical capacities, they are combined into a single row with a common capacity and a probability equal to the sum of the individual probabilities.

3.5.3 Applicable range per transmission technology

Using the presented model while considering a simple radial connection to shore, an applicable range for the different transmission options is established. Note, the proposed model is simple and the exact range for the technologies is highly dependant on available data thus the presented ranges should be understood as only very rough estimates. The transmission options considered are 66 kV Medium Voltage Alternating Current (MVAC), 132 kV, 220 kV and 400 kV HVAC, 220 kV Mid Point Compensated HVAC (MPC-AC) and 500 kV HVDC. The resulting technological solution space is shown in Fig. 3.16. Above 500 MW a relatively stable relation appears where a connection made at 66 kV is the lowest cost option up to about 60 km, between 60 and 125 km it is better to transmit at 220 kV and once 125 km has been surpassed, HVDC becomes the best option. Below 500 MW the relationship complicates. At very low power levels the 66 kV range increases to a maximum of 125 km at 100 MW. The
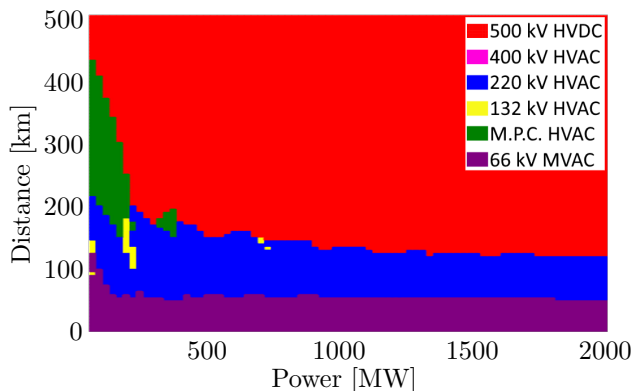
Figure 3.16: Range of optimal technology for a point to point connection considering: 66 kV collection circuit, 132 kV/220 kV/400 kV HVAC, 220 kV mid-point compensated HVAC, 500 kV HVDC.

range of 220 kV HVAC also increases. The highest viable distance is at 225 km at 100 MW. In very few instances 132 kV becomes the optimal choice. The range of MPC-AC starts around 150 km and reaches it's maximum feasible range near 425 km. The optimal choice of technology in the lower range of OWPP capacity appears complicated, however, it is likely that this complicated technological solution space is more of a product of poor data availability than a truly varied technological optimal. At low capacities, the relative jump between single cable sizes can have a substantial impact on the cost, e.g. choosing between a cable of 100 MW and 150 MW to transmit 110 MW. At higher capacities as cables start to be placed in parallel to meet the load, the relative jump between available options decreases. This jump between available sizes can be reduced by considering an exhaustive list of available conductor sizes from multiple manufacturers as well as both aluminium and copper options.

A surprising result is perhaps the complete lack of an optimal range for 400 kV HVAC transmission. In reality, however, this result is expected. First, as was demonstrated in Fig. 3.13 the available capacity of an HVAC cable for real power drops with the square of the voltage as distance increases. This means that the advantages gained of higher capacity and lower losses that make a higher transmission voltage appealing for overhead lines are offset at higher distances by reactive power flows. This fact alone would perhaps not completely eliminate 400 kV from the technological solution space but there is also the fact that due to higher insulating requirements 3-core 400 kV cables are not available, making the cost of installation significantly higher than at lower transmission

voltages.

Considering the high value associated with standardization the results support the idea that only three transmission technologies need be considered offshore: 66 kV collection circuits, 220 kV HVAC transmission and 500 kV HVDC. In certain edge cases mid-point compensated HVAC may prove useful. In the upcoming chapters, optimization approaches are developed, first for the OW-TNEP problem at grid level $\mathcal{G}^m$ and then for the OW-GATE planning problem at grid level $\mathcal{G}^l$. Unless explicitly stated, equipment sizing and costs are calculated using the presented method, although the considered technological options do vary. In chapters 4, 5 and 6 only AC transmission options (excluding MPC-AC) are considered, while in chapter 7 both HVDC and HVAC are considered.

3.6   Conclusions

This chapter provides a comprehensive, high level, overview of the proposed methodology for OW-GATE planning, which is the central focus of this thesis. The methodology adopts a divide and conquer approach that partitions the transmission network into three levels based on transmission capacity, and then further breaks each one of these levels down into a collection of fourteen steps grouped into six planning stages. Each stage having to be done sequentially.

The offshore grid is expanded in a top-down manner by following the six sequential planning stages, where the higher capacity levels determine the size, macro location, and build schedule of the lower levels, while the lower levels define the final location of the infrastructure on the boundary between levels. To execute the steps of each planning stage, the literature's state-of-the-art approaches are suggested, or if an effective approach is lacking then the proposed solution is introduced and the relevant chapters of the thesis referred to for full details.

Following the description of the methodology, a brief description of the most relevant input data is presented, that which was found most useful for describing the search space at a high level. The data are grouped into five categories: grid data, meteorological data, regulatory/technological data, hydrographic data, energy market data and cost data. The most relevant data for a given grid level is defined. If multiple modeling options exist based on multiple data sources, the approaches' strengths and weaknesses are presented.

The final section of the chapter, presents in brief the cost modelling strategy developed for the proposed optimization methods found in the following chapters. The cost model attempts to capture the nonlinear effects associated with integer

quantities of equipment and the high reactive power flows found in AC sub-sea cabling. The method describes an approach for approximating OPEX (losses, corrective maintenance and EENT) a priori when the assumption of a radial topology is made. Considering this model, a range for different available transmission technologies and voltages is derived. The range indicates that the only voltages and technologies that need be considered are 66 and 220 kV HVAC and 500 kV HVDC.

In the subsequent chapters, the specific optimization models developed for grids $\mathcal{G}^{\mathrm{m}}$ and $\mathcal{G}^{\mathrm{l}}$ are presented. Chapters 4, 5, and 6 are dedicated to $\mathcal{G}^{\mathrm{m}}$, while Chapter 7 focuses on $\mathcal{G}^{\mathrm{l}}$. These chapters serve as the substantive core of the research conducted within this thesis. It is important to note that, in order to ensure clarity and avoid any potential misinterpretation, only the individual optimization approaches have been developed and tested. As a result, a comprehensive fourteen-step test case illustrating the entire optimization process, from start to finish as described in this chapter, is not provided. The decision to omit such an example was primarily due to the substantial time required to properly build and test such a case. Moreover, considering that the expansion planning process encompasses a medium to long-term timeline, it is not imperative to solve all steps within the methodology simultaneously. The crucial aspect lies in maintaining the proper order and ensuring that a plan is established for grid $\mathcal{G}^{\mathrm{l}}$ before addressing grid $\mathcal{G}^{\mathrm{m}}$, and finally grid $\mathcal{G}^{\mathrm{s}}$.

Chapter 4

HVAC transmission considering multiple OWPPs

4.1 Introduction

This chapter[1] presents the Offshore Wind Transmission Network Expansion Planning (OW-TNEP) formulation for planning stages M.3 and M.4 to bridge the literature gap between the presented state of the art high-level expansion planning models that focus on transnational grid expansion and the low-level models used for planning collection circuits and simple transmission networks of isolated, radially connected OWPPs. Thus, an OW-TNEP model focusing on the intermediate capacity network, that considers multiple neighbouring OWPPs has been developed.

The objective of planning stages M.3 and M.4 is to determine the transmission topology and macro site of OSSs at grid level $\mathcal{G}^{\mathrm{M}}$. The proposed formulation takes the form of a greedy algorithm, which was initially developed in [189]. Before moving into the proposed formulation however, some further background on what makes this problem difficult is helpful.

A key difference between a traditional TNEP problem and the OW-TNEP problem is the green field nature of the offshore network. As there is no (or

---

[1]The work of this chapter has been published as: *Stephen Hardy, Hakan Ergun and Dirk Van Hertem, 'A Greedy Algorithm for Optimizing Offshore Wind Transmission Topologies.',* in the Journal IEEE Transactions on Power Sytems. The content of the paper has been modified here to make it consistent with the other chapters of this dissertation. The first author is the main author of the paper.

very minimal) existing grid and no geographic features restricting possible build sites, the search space has very few constraints. As such, spanning the search space with a candidate grid results in a very high number of binary decision variables that very quickly results in an intractable problem size.

Table 4.1: Belgian OWPP and PCC locations.

Label	Name	Longitude	Latitude	Euclidean distance to PCC [km]
PCC	Zeebrugge	3.18361	51.32694	-
0	Norther	3.01583	51.52806	25.21
1	Thortonbank	2.94499	51.54999	29.81
2	Rentel	2.93997	51.59	33.77
3	Northwind	2.90097	51.61897	37.92
4	Seastar	2.85997	51.63	40.47
5	Nobelwind (Belwind)	2.80997	51.667	45.81
6	Northwester	2.757	51.68597	49.65
7	Mermaid	2.74	51.71997	53.4
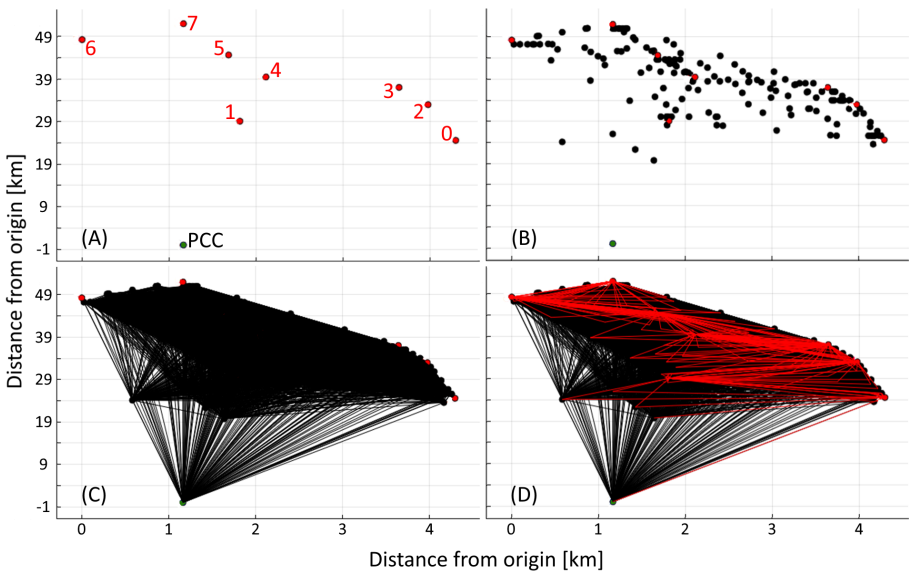
Figure 4.1: (A) 8-250 MVA OWPPs and PCC. (B) Candidate OSSs. (C) HVAC candidate grid. (D) MVAC candidate grid.

This is most easily understood through a practical example. We will do this by modelling the Belgian offshore development zone one, as a new, to be developed area. We approximate the 2.3 GW region with 8-250 MW OWPPs located at the approximate locations of the existing OWPPs. To do this, we start by taking the coordinates of the OWPPs and a single PCC at Zeebrugge as specified in Table 4.1 and project them onto a Cartesian plane[2] as shown in Fig. 4.1(A).

In order to layout a candidate offshore grid, it is necessary to define some locations for candidate OSSs. However, as there is no existing network and the sea (without considering bathymetry or spatial planning constraints) is identical everywhere, there are no constraints on where the OSSs could be placed. This is very different than the onshore case. Although not computationally very efficient, for intuitively illustrating the size of the resulting problem, we can use a k-1 nearest neighbors approach which was developed by the authors at the initial stages of this research [190][3]. In the algorithm, n candidate OSSs are placed along the straight line paths connecting the OWPPs to each other and the PCC.

The pseudo code for the algorithm is provided in Algorithm 1, where G is the set of OWPP locations and d is the PCC location. For our example problem, placement begins on the line between the furthest OWPP (7 in Fig. 4.1(A)) and the 2nd furthest (6 in Fig. 4.1(A)). Next, OSSs are placed between the 7th and the 5th furthest. This continues, until the line between the 7th OWPP and the PCC has candidate OSSs added. This process is then repeated for the line between OWPP 6 and 5, 6 and 4 and so on. The final path to contain any candidate OSSs is between OWPP 0 and the PCC. Setting $n = 5$ candidate OSSs for OWPP to OWPP lines ($\approx$ 0.5-1 OSS/km) and $n = 2$ candidate OSSs for OWPP to PCC lines results in 156 candidate OSSs. This is reduced to 141 by eliminating duplicated locations. The final set of candidate OSS locations is shown in Fig. 4.1(B).

Now that the candidate OSS locations are specified, candidate HVAC and MVAC transmission lines need to be defined. The number of candidate transmission lines, all of which are binary decision variables, climbs combinatorally and very quickly creates an intractable problem, especially when considering multiple voltage levels. In Fig. 4.1(C) and 4.1(D) the resulting candidate grids are shown for HVAC and MVAC networks respectively when considering MVAC levels of

---

[2]The GPS co-ordinates are transformed into Cartesian co-ordinates by rotating the principal axis to align with the y axis and shifting linearly all co-ordinates into the first quadrant. The original GPS co-ordinates of the origin were at latitude: 51.320628 and longitude: 3.169166.

[3]*Stephen Hardy, Hakan Ergun, Dirk Van Hertem, Kristof Van Brusselen, 'A Techno-Economic MILP Optimization of Multiple Offshore Wind Concessions.', in 2nd International Conference on Large-Scale Grid Integration of Renewable Energy in India.*

Algorithm 1: k-1 nearest neighbour Algorithm

Input: G, d, n

Output: Candidate OSS locations: Ω

1 **Function** NearestNeighbours(G, d, n):

2     $Q \leftarrow order(G)$# Order OWPPs from closest to furthest from PCC

3     $Q.push(d)$# Place the PCC at the start of the ordered queue

4     $k = length(Q)$# Initialize k equal to the last index of Q

5   **while** $(k \neq 1)$ **do**

6        $q_k = Q.remove(k)$# Remove the kth element of Q

7   **for** q_i *in* Q **do**

8           $\Omega_{k,i} \leftarrow CandidateOSS(q_k, q_i, n)$

9           $\Omega_k = (\Omega_k \cup \Omega_{k,i})$

10        $\Omega = (\Omega \cup \Omega_k)$

11        $k = k - 1$

12     $Prune(\Omega)$# Remove all duplicates in Ω

13   **return** Ω

14

15 **Function** CandidateOSS(q_k, q_i, n):

16     $l_{k,i} = LineBetween(q_k, q_i)$# Find line connecting points q_k and q_i

17     $S_{k,i} = DivideLine(l_{k,i}, n)$# Divide line into n-1 equal sections

18     $\Omega_{k,i} = Npoints(S_{k,i})$# Keep n terminal points from sections $S_{k,i}$

19   **return** $\Omega_{k,i}$

---

33 kV and 66 kV and HVAC levels of 132 kV, 220 kV and 400 kV. The number of candidate transmission lines required is summarized in Table 4.2.

Table 4.2: Candidate Lines.

Type	Start	End	Number of Lines
MVAC	OWPP	OSS	1120
MVAC	OWPP	PCC	8
HVAC	OSS	OSS	39173
HVAC	OSS	PCC	665
Total			40966

This is not a feasible problem size today. To solve such a TNEP problem, a sequential MILP algorithm is presented in [190][3]. The algorithm divides the problem into subproblems based on voltage levels and OSS clusters, gradually combining solution topologies together until a final "optimal" topology is found. This algorithm will not be elaborated on in this work as it is not a recommended

approach, but presenting the problem structure as it was first investigated does provide essential background on the motivation for the work that follows. Without an effective way to reduce the number of binary decision variables for candidate equipment offshore, the traditional TNEP formulation as is used onshore is not an effective approach.

4.2 TNEP formulation

4.2.1 Overview

The objective of the proposed formulation for OW-TNEP is to determine the transmission topology and macro site the OSSs at grid level $\mathcal{G}^{\mathrm{M}}$ from a cost and reliability perspective. The cost model implemented is presented in Appendix A. The major steps of the formulation, which are further elaborated in the following sections, are summarized in Fig. 4.2.

Define the optimization domain as in section 4.2.2.
Find the basis set $\boldsymbol{T}^{\mathrm{B}}$ as in section 1.
Find set $\boldsymbol{T}^{\mathrm{H}}$ using greedy search as in section 4.2.4
Find the optimal transmission topology $t^{\mathrm{fr}*}$ as in section 4.2.5.
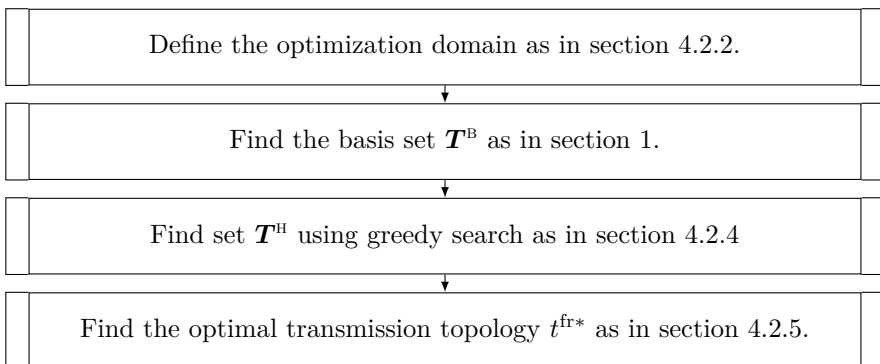
Figure 4.2: Overview of OW-TNEP formulation.

4.2.2 Domain and boundary conditions

The domain consists of existing network nodes $n \in \mathcal{N}$, candidate network nodes $\widetilde{n} \in \widetilde{\mathcal{N}}$ and directed candidate edges $e \in \mathcal{E}$. PCCs, $d \in D$, are defined by their geographic location, n_d^{d}, a maximum connection capacity, $P_d^{\mathrm{d,max}}$, and a network voltage, V_d^{d}. Similarly, OWPPs, $g \in G$, are defined by their geographic position, n_g^{g}, a max generation capacity of $P_g^{\mathrm{g,max}}$, a per-unit power profile time series Ψ_g^{g} and a surface area, A_g^{g}. The surface area is modelled as a perfect circle centered

around n_g^{g} and is calculated by taking the ratio of $P_g^{\mathrm{g,max}}$ and ρ_g, where ρ_g is the wind energy density of location n_g^{g}. The OWPPs are ordered by euclidean distance relative to the PCC, starting at 0 for the OWPP nearest to the PCC.

Candidate infrastructure consists of OSSs, $\omega \in \Omega$, located at a candidate node $\widetilde{n_\omega^{\mathrm{o}}}$ and transmission lines, $\ell_{mn} \in \mathcal{S}_{\ell:\mathrm{e}}$ on candidate edge e. Candidate edges exist between all combinations of existing and candidate nodes except OWPP nodes, i.e. OWPPs can only be connected to eachother via an OSS.

Ψ_g^{g} is generated using the CorWind software [168]. CorWind applies advanced stochastic and re-analysis techniques to the historical meteorological data of the WRF model [191]. CorWind accounts for both fluctuations and forecast error, providing a realistic and geographically relevant generation time series up to a one minute resolution. In this work hourly resolution is used.

Power flow

The optimal topology is a priori assumed to be radial in nature, i.e. a minimum spanning tree. As such unidirectional network power flow is assumed. Power is generated at an OWPP and flows toward a PCC via a transmission network. The term downstream is used to refer to the direction towards the PCC while upstream is towards an OWPP.

OWPPs are assumed to operate at 66 kV. As such 66 kV, medium voltage transmission lines connect an OWPP to either an OSS or a PCC. Medium voltage transmission lines must have a capacity capable of safely carrying the peak capacity of the OWPP which it serves i.e. $P_{mn}^{\ell,max} = P_{g:m}^{\mathrm{g,max}}$. The power flow in a medium voltage transmission line is defined to flow from a root node m to a destination node n and is calculated for a given time step t as $P_{mn,t}^{\ell} = \Psi_{g:m,t}^{\mathrm{g}} P_{g:m}^{\mathrm{g,max}}$.

The capacity of an OSS located at node n is determined by taking the sum of all incoming transmission lines as in $P_{\omega:n}^{\mathrm{o,max}} = \sum_{i=0}^{m} P_{in}^{\ell,max}$. Similarly the power flow at time t is calculated as in $P_{\omega:n,t}^{\mathrm{o}} = \sum_{i=0}^{m} P_{in,t}^{\ell}$. The power injection at onshore PCCs is calculated in an identical manner: $P_{d:n,t}^{\mathrm{d}} = \sum_{i=0}^{m} P_{in,t}^{\ell}$. Of course the constraint $P_{d:n,t}^{\mathrm{d}} \leq P_{d:n}^{\mathrm{d,max}}$ must be respected for all t.

High voltage transmission lines connect an OSS to either another OSS or a PCC. The capacity and power flow in high voltage transmission lines is determined by its root node OSS, ω. As no meshed topologies are allowed, a maximum of one transmission line is permitted to leave an OSS. The maximum capacity of a high voltage transmission line is therefore $P_{mn}^{\ell,max} = P_{\omega:m}^{\mathrm{o,max}}$ and the power flow at time t is $P_{mn,t}^{\ell} = P_{\omega:m,t}^{\mathrm{o}}$. In practise, due to finite availability of sizes,

particularly for cables, the actual thermal capacity of specified infrastructure may exceed the values of $P_{mn}^{\ell,max}$ and $P_{\omega:n}^{o,\max}$.

4.2.3 Combinatorial Super Set

For an offshore wind region with n OWPPs, g_i, is indexed by the set of positive integers from zero to $n-1$ as in:

$$\boldsymbol{A} = \{g_i, i \in \mathbb{Z}_{\geq 0} : i < n\}. \tag{4.1}$$

All possible combinations of OWPPs found on a radial feeder can then be represented by the set of length n binary strings j, ranging from one to $2^n - 1$ as in:

$$\boldsymbol{B} = \{j \in \mathbb{N}_2^n : 0 < j \leq 2^n - 1\}. \tag{4.2}$$

A binary string j, has its bit positions indexed by i, ranging from zero to $n-1$. The status of bit position i, $b_i \in \{0,1\}$, dictates the inclusion or exclusion of OWPP g_i within a radial feeder, i.e. if $b_i = 1$ within j, g_i is included in the associated feeder, if $b_i = 0$ within j, g_i is excluded from the associated feeder.

In discussing a binary string j, it is helpful to reference specific bit positions throughout the string. The terminology used within is outlined in Fig. 4.3. The least significant bit of value one is called α. The most significant bit of value one is γ. Addition and subtraction operations are used to reference neighbouring bits of α and γ, but the only bits of concern are of value one, hence positions of value zero are ignored. Bit position β refers to any position of value one between α and γ inclusive.

$$\begin{array}{ccccccccc} & \gamma & & \gamma-1 & & & \alpha+1 & \alpha & \\ \Big[\underset{\text{n-1}}{0} & \underset{\text{n-2}}{1} & \underset{\text{n-3}}{0} & \underset{\text{n-4}}{1} & ... & \underset{\text{3}}{0} & \underset{\text{2}}{1} & \underset{\text{1}}{1} & \underset{\text{0}}{0} \Big] \end{array}$$
$$\overleftarrow{\qquad \beta \qquad}\overrightarrow{\qquad}$$

Figure 4.3: Notation used for binary representation of OWPPs.

Considering only bit positions of value one are of interest, at times a string j is written with a superscript $(+)$. This notation refers to the subset $j^+ := \{i \in j : b_i = 1\}$. It is important to understand however, that bit positions remain constant between j and j^+. For example if $j = [01010]$, then $j^+ = [11]$ but the bit positions of status one in both j and j^+ are the same (i.e. $i \in 1,3$).

If a j contains more than one bit position of status equal to one (i.e. $b_i = 1$), it can be split at bit position β and rewritten as the sum of two smaller binary strings as in:

$$j = j_\beta + j_\beta^c, \tag{4.3}$$

such that:

$$(i \in j_\beta^+) \bigcap (i \in j_\beta^{c+}) = \emptyset \text{ and}$$

$$(i \in j_\beta^+) \bigcup (i \in j_\beta^{c+}) = (i \in j^+). \tag{4.4}$$

Here j_β^c is the complement of j_β. Advancing the bit position β from position α to $\gamma - 1$ results in the following sets:

$$\boldsymbol{C}_j = \{j_\beta, \ \beta \in j^+ : \beta < \gamma\}.$$

$$\boldsymbol{C}_j^c = \{j_\beta^c, \ \beta \in j^+ : \beta < \gamma\}. \tag{4.5}$$

Now, for each element $j_\beta^c \in \boldsymbol{C}_j^c$ that consists of more than one bit position of status equal to one (i.e. $b_i = 1$) we can apply the same splitting operation to obtain sets equivalent to (4.5) for j_β^c rather than the original j. In fact, this can be done iteratively for all resulting j_β^c with more than a single b_i equal to one. What we are therefore interested in, is finding for a given j and β, the set of all unique combinations of binary strings j that satisfy generalized versions of (4.3) and (4.4) for two to n binary strings j. This set is found by taking all k-combinations of $j \in \boldsymbol{B}$ as in:

$$\boldsymbol{E}_\beta = \binom{\boldsymbol{B}}{k} \tag{4.6}$$

such that:

$$\sum_{j \in k} j = j_\beta^c, j \neq j_\beta^c, \ \bigcap_{j \in k}(i \in j^+) = \emptyset, \ \bigcup_{j \in k}(i \in j^+) = (i \in j_\beta^{c+}). \tag{4.7}$$

Constraint (4.7) ensures that all the selected k-combinations sum to j_β^c without duplication of the trivial solution and that all OWPPs g_i that occur in j_β^c are also present in the k combination once and only once.

The exhaustive combinatorial search space is then calculated by taking the Cartesian product between j_β and $\boldsymbol{E}_\beta$ as in (4.8). Physically, $\boldsymbol{H}$ describes all the ways n OWPPs can be interconnected. Describing the combinations in this way provides a clear presentation of the indices of iteration. There are three nested loops: j, j_β and k.

$$\boldsymbol{H} = j_\beta \times \boldsymbol{E}_\beta : \forall j \in \boldsymbol{B}, \forall j_\beta \in \boldsymbol{C}_j \tag{4.8}$$

4.2.4 Greedy Search

Sets $\boldsymbol{A}$ to $\boldsymbol{H}$ serve as a purely mathematical model, providing an abstract representation of the combinatorial search space. They define the possible

combinations of OWPPs on a radial feeder. On the other hand, sets of physical topologies can also be established, encompassing an additional layer that incorporates the properties of the physical system, specifically the electrical infrastructure. To build these so called topological sets, the combinatorial sets are utilized as a mapping mechanism to ensure comprehensive coverage of the entire search space. The topological sets constitute the physical space that needs to be explored in order to discover the optimal transmission topology. To efficiently search this space, a greedy search algorithm has been devised. The output from the greedy search algorithm is the topological set $\boldsymbol{T}^{\text{H}}$, the set of lowest cost radial topologies, using a single export cable, for the combinations of OWPPs described by $\boldsymbol{B}$. The method for calculating $\boldsymbol{T}^{\text{H}}$ using the greedy search algorithm follows. For visual reference and guidance throughout the explanation, consult Algorithm 3, which includes a flow chart and pseudo code representation of the greedy search algorithm.

Algorithm 3: Greedy Search Algorithm.

1: **START**
2: $\boldsymbol{T}^{\text{H}} \leftarrow \boldsymbol{T}^{\text{B}}$
3: **for** $\boldsymbol{t_j^h} \in \boldsymbol{T}^{\text{H}}$ **do**
4:     **for** $t_j^{\text{h}} \in \{t_j^{\text{h,mv}}, t_j^{\text{h,hv}}\}$ **do**
5:         **for** $t_\beta \in \boldsymbol{T_j^c}$ **do**
6:             **if** MV cable removed? **then**
7:                 Re-solve (4.12)
8:             **end if**
9:             **for** $t_k^{\text{e}} \in \boldsymbol{T_\beta^{\text{E}}}$ **do**
10:                 $t_j' = t_\beta \cup j_k^{\text{e}}$
11:                 $\boldsymbol{T_{j_\beta}^{\text{H}}}.add(t_j')$
12:             **end for**
13:
            $\boldsymbol{T_j^{\text{H}}}.add(\min(\boldsymbol{T_{j_\beta}^{\text{H}}}))$
14:         **end for**
15:         $\boldsymbol{T}^{\text{H}}.add(\min(\boldsymbol{T_j^{\text{H}}}))$
16:     **end for**
17: **end for**
18: Return $\boldsymbol{T}^{\text{H}}$
19: **END**
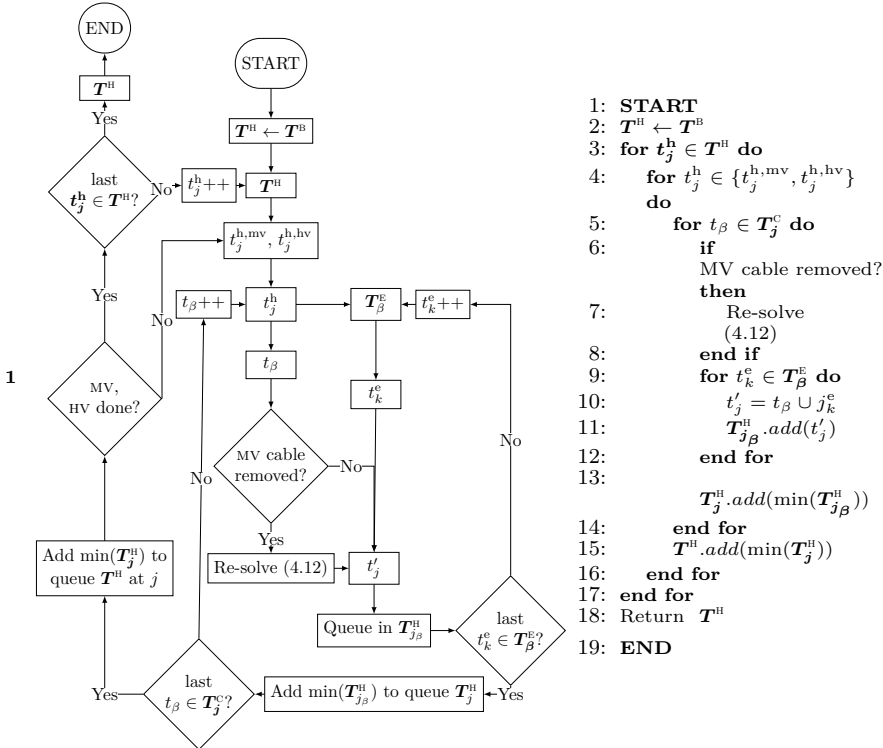
Topological basis set T^{B}. Pseudo code lines 1–4

The notation $\boldsymbol{T}^{\mathrm{B}}$ to $\boldsymbol{T}^{\mathrm{H}}$ is employed for topological sets, where the superscripts correspond to the associated combinatorial sets. A member of a topological set, such as $t_j^{\mathrm{b}} \in \boldsymbol{T}^{\mathrm{B}}$, represents a valid transmission topology that connects the combination of OWPPs defined by $j \in \boldsymbol{B}$ to the PCC. The rank of a topology refers to the number of OWPPs connected within it. A topology is considered full rank when it includes all OWPPs.

The topological set $\boldsymbol{T}^{\mathrm{B}}$ serves as the basis set of topologies, as it encompasses all combinations described in $\boldsymbol{B}$. $\boldsymbol{T}^{\mathrm{B}}$ will be the initial guess for the set $\boldsymbol{T}^{\mathrm{H}}$ (pseudo code line 2). All other topological sets will be derived by combining elements from $\boldsymbol{T}^{\mathrm{B}}$.

More specifically, $\boldsymbol{T}^{\mathrm{B}}$ consists of at least one topology for each $j \in \boldsymbol{B}$. The topology set $\boldsymbol{t_j^{b}}$ is formed through the union of $t_j^{\mathrm{b,mv}}$ and $t_j^{\mathrm{b,hv}}$ (pseudo code lines 3 and 4). The topology $t_j^{\mathrm{b,mv}}$ connects the OWPPs in combination j, giving priority to medium voltage connections. On the other hand, $t_j^{\mathrm{b,hv}}$ connects the OWPPs in combination j, prioritizing high voltage connections.

The distinction between medium voltage and high voltage topologies lies in the constraints imposed during the placement of the OSSs. The topologies in $\boldsymbol{T}^{\mathrm{B}}$ represent the simplest combinations of j OWPPs, where all OWPP feeders, whether medium voltage or high voltage transmission lines, are gathered at a single OSS. From there, a single export cable connects to the PCC. Examples of $t_j^{\mathrm{b,mv}}$ can be observed in Fig. 4.5 (in the subsequent section), labeled as t_{12}^{b} and t_{15}^{b}. The approach to OSS placement differentiating $t_j^{\mathrm{b,mv}}$ and $t_j^{\mathrm{b,hv}}$ is as follows.

The Cartesian coordinates $(x_\omega^{\mathrm{o}}, y_\omega^{\mathrm{o}})$ of the candidate OSS located at $\widetilde{n}_\omega^{\mathrm{o}}$, considering the combination of OWPPs specified by j, are determined by minimizing the non-linear objective associated with the edge length connected to the OSS as in (4.9). This is done using the interior point line search algorithm as implemented in the Ipopt solver [192].

$$\min \left(\sum_{(m,n)\in\mathcal{E}^{\mathrm{o}}} \|(m,n)\| \right), \text{ where } \mathcal{E}^{\mathrm{o}} = \{(m,n) \in \mathcal{E} : m = \widetilde{n}_\omega^{\mathrm{o}} \text{ or } n = \widetilde{n}_\omega^{\mathrm{o}}\}$$

$$(4.9)$$

In the case of a high voltage topology, $t_j^{\mathrm{b,hv}}$, (4.9) is subject to the constraints:

$$\min(x_\alpha^{\mathrm{g}}, x_d^{\mathrm{d}}) \leq x_\omega^{\mathrm{o}} \leq \max(x_\alpha^{\mathrm{g}}, x_d^{\mathrm{d}}) \text{ and}$$

$$\min(y_\alpha^{\mathrm{g}}, y_d^{\mathrm{d}}) \leq y_\omega^{\mathrm{o}} \leq \max(y_\alpha^{\mathrm{g}}, y_d^{\mathrm{d}}), \tag{4.10}$$

where the Cartesian coordinates $(x_\alpha^{\mathrm{g}}, y_\alpha^{\mathrm{g}})$ and $(x_d^{\mathrm{d}}, y_d^{\mathrm{d}})$ represent the geographical locations of OWPP α and PCC d respectively. It is important to recall that α corresponds to the first bit position with a value of one, which directly corresponds to an OWPP. Therefore, OWPP α refers to the geographically closest OWPP to the PCC that is included in the combination j. Constraint (4.10) is visualized as Region A of Fig. 4.4.
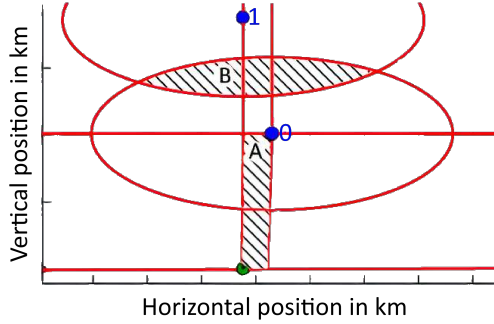
Figure 4.4: HV (A) and MV (B) OSS placement constraints.

In the case of an medium voltage topology, $t_j^{\mathrm{b,mv}}$, (4.9) is subject to the constraint:

$$(x_\omega^{\mathrm{o}}, y_\omega^{\mathrm{o}}) \in A_\alpha^{\mathrm{mv}}(l_\alpha^{\mathrm{mv,max}}) \cap A_{\alpha+1}^{\mathrm{mv}}(l_{\alpha+1}^{\mathrm{mv,max}}). \tag{4.11}$$

In this context, A_α^{mv} and $A_{\alpha+1}^{\mathrm{mv}}$ represent the areas surrounding OWPP α and $\alpha + 1$ respectively, with a radius of $l_g^{\mathrm{mv,max}}$. The value of $l_g^{\mathrm{mv,max}}$ corresponds to the distance threshold where transmitting electricity in MVAC is more cost-effective than constructing an OSS and transmitting in HVAC. This threshold is defined as the distance at which the cost of $\ell_{m_g^{\mathrm{g}} n_1^{\mathrm{o}}}^{\mathrm{mv}}$ (a transmission line in MVAC) is equal to the sum of the costs of $\ell_{m_0^{\mathrm{o}} n_1^{\mathrm{o}}}^{\mathrm{hv}}$ (a transmission line in HVAC) and ω_0^{o} (an OSS). Visualization of this constraint can be found in Region B of Fig. 4.4. If the intersection of A_α^{mv} and $A_{\alpha+1}^{\mathrm{mv}}$ is an empty set, it implies that $t_j^{\mathrm{b,mv}}$ does not exist, and the only available topology at j is the high voltage variation.

The rationale behind defining $t_j^{\mathrm{b,hv}}$ and $t_j^{\mathrm{b,mv}}$ using constraints (4.10) and (4.11) is to ensure that the search space encompasses potential locations for the optimal

placement of the OSS to interconnect neighboring OWPPs using both medium and high voltage cables. The non-continuous, piecewise cost associated with transitioning from medium to high voltage cables (i.e., the need to construct an additional OSS) makes it unlikely for a single OSS position to satisfy both configurations simultaneously. Therefore, by considering separate topologies for high voltage and medium voltage connections, the search space is expanded to account for the different cost trade-offs and to provide flexibility in selecting the most suitable OSS configuration.

Once the candidate location for the OSS is determined as above, the calculation of the necessary transmission cables can be carried out. The objective is to identify the most cost-effective option among a medium voltage cable and a high voltage cable with an additional OSS located at the OWPP node. From this, a cost per unit length $c_{mn}^{\ell,pu}$ is assigned to each transmission cable. The final positions of the candidate OSSs are subsequently determined (again using the Ipopt solver [192]) by minimizing the total cost associated with the connected transmission lines, expressed as follows:

$$\min\left(\sum_{(m,n)\in\mathcal{E}^{\mathrm{o}}} c_{mn}^{\ell,pu}\,\|(m,n)\|\right),\ \text{where } \mathcal{E}^{\mathrm{o}} = \{(m,n)\in\mathcal{E} : m = \widetilde{n}_{\omega}^{\mathrm{o}} \text{ or } n = \widetilde{n}_{\omega}^{\mathrm{o}}\},$$

$$(4.12)$$

Crossing Topologies. Pseudo code lines 5–11
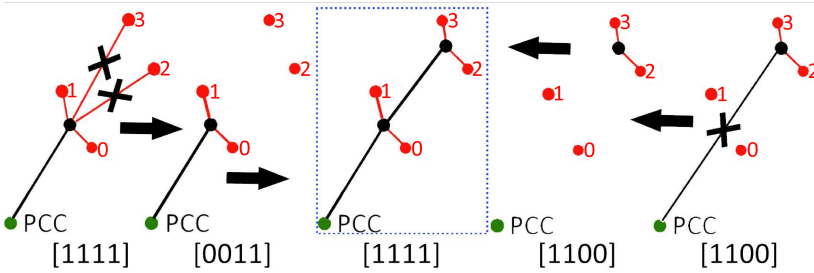
Figure 4.5: Crossing topologies for n=4 OWPPs. Moving from left to right the topologies are t_{15}^{b}, t_{β}, t_{15}', t_k^{e} and t_{12}^{b}.

The sets $\boldsymbol{T}_j^{\mathrm{C}}$, $\boldsymbol{T}_{\beta}^{\mathrm{E}}$ and $\boldsymbol{T}^{\mathrm{H}}$ are generated through a process of crossover involving the base topologies in $\boldsymbol{T}^{\mathrm{B}}$. This crossover operation is akin to the technique employed in a genetic algorithm, where two valid parent solutions are combined to produce a new valid descendant solution. However, unlike a genetic algorithm, the crossover procedure described here is entirely deterministic and follows the path of steepest descent.

If a topology t_j^h consists of multiple OWPPs, it can be divided at OWPP β into two or more partial topologies:

$$t_j^h = t_\beta + t_k^e, \tag{4.13}$$

The topology t_β is formed by including the OWPPs α to β from the original topology t_j^h (pseudo code line 5). On the other hand, the topologies t_k^e consist of OWPPs $\beta+1$ to γ (pseudo code line 9). To create t_β, all upstream infrastructure in t_j^h that serves OWPPs beyond β is removed. As a result, t_β represents a topology where OWPPs α to β are connected to an OSS via an oversized export cable with sufficient capacity for OWPPs α to γ. If a medium voltage cable connection is removed as part of this step, it is possible the chosen OSS location can be further optimized. As a consequence the location is re-calculated using (4.12) (pseudo code step 7)

The topology t_k^e is obtained by eliminating all infrastructure downstream of the OSS from k topologies in $\boldsymbol{T}^B$. This removal is carried out in such a way that condition (4.4) is met. Consequently, t_k^e represents a topology comprising of OWPPs $\beta+1$ to γ, where the OSS(s) serve as the most downstream component, implying that there is no connection to the PCC. The set $\boldsymbol{T}_\beta^E$ encompasses all k combinations in $\boldsymbol{T}^B$ that satisfy condition (4.7).

The creation of t_β and t_k^e is demonstrated in Fig. 4.5 for a simple four OWPP example, with $j = [1111]$ and $\beta = 1$. The derivation of t_β starts from t_{15}^h, as shown on the left side of the figure. Conversely, t_k^e is derived from t_{12}^h, starting from the right side. In the center of the figure, a novel topological variation on t_{15}^h is formed by connecting the OSS of t_β and t_k^e using a new high-voltage cable. In the general case, this newly created topology is referred to as t_j' (pseudo code line 10).

Iterating through the indices j, β, and k according to (4.8) enables the identification of all t_j' topologies (pseudo code lines 3, 5, 9). This process leads to the creation of sets $\boldsymbol{T}_j^C$, $\boldsymbol{T}_\beta^E$, and the exhaustive search space denoted by $\boldsymbol{T}^H$. Exhaustively exploring this search space using a brute force approach would yield the globally optimal solution. Unfortunately, this approach becomes infeasible for practical purposes as the number of OWPPs grows, resulting in a combinatorial increase in the problem size.

To overcome this limitation, the greedy search algorithm aims to find high-quality solutions while exploring only a fraction of the search space, providing a more feasible and efficient approach for larger OWPP configurations.

Instead of traversing the entire combinatorial space, the algorithm maintains ordered queues $\boldsymbol{T}_{j\beta}^H$ and $\boldsymbol{T}_j^H$ (pseudo code lines 13, 15), which store only the topologies with the lowest costs (as outlined in section 4.2.5).

4.2.5 Optimal radial topology

Having found $\boldsymbol{T}^{\text{H}}$ using the greedy algorithm, the next step is to calculate the optimal radial topology. To do so we begin by understanding the elements of $\boldsymbol{T}^{\text{H}}$. $\boldsymbol{T}^{\text{H}}$ is a set of ordered queues. One queue, $\boldsymbol{T}^{\text{H}}_j$, for each value of $j \in \boldsymbol{B}$. The first element of $\boldsymbol{T}^{\text{H}}_j$ is the optimal radial connection topology for j OWPPs to the PCC via a **single** export cable. We call this topology $t^{\text{h}*}_j$ and the subset of all $t^{\text{h}*}_j \in \boldsymbol{T}^{\text{H}}$, $\boldsymbol{T}^{\text{H}*}$.

We are looking for the optimal topology for $j = 2^n - 1$ OWPPs using $1 \leq k \leq n$ export cables. To do this we calculate a set of full rank topologies, $\boldsymbol{T}^{\text{FR}}$, from $\boldsymbol{T}^{\text{H}*}$ as in:

$$\boldsymbol{T}^{\text{FR}} = \binom{\boldsymbol{T}^{\text{H}*}}{k} \text{ such that: } \sum_{t_j \in k} j = 2^n - 1 \tag{4.14}$$

The lowest cost topology in $\boldsymbol{T}^{\text{FR}}$, $t^{\text{fr}*}$, is the optimal radial topology with $1 \leq k \leq n$ export cables, connecting n OWPPs to the PCC. The proof of this is simple and as follows. Since no meshed topologies are permitted, we can say in general that the optimal radial topology of $1 \leq k \leq n$ export cables must be the union of k independent radial topologies t_j such that $\sum_{t_j \in k} j = 2^n - 1$. The cost of such a topology would be the sum of the costs of the individual topologies and the lowest possible sum of individual topology costs occurs when each independent topology is the optimal, i.e. $t^{\text{h}*}_j \in \boldsymbol{T}^{\text{H}*}$.

4.3 Results

4.3.1 Test cases

To validate the greedy search algorithm, four test cases of increasing size are solved with the presented greedy search algorithm and an MILP benchmark. The benchmark MILP is built using the TNEP formulation of PowerModels.jl [193]. The Gurobi solver version 0.9.14 [194] is used to solve the MILP problem. All results were obtained on a standard Dell lap-top with an intel core-7 1.9 GHz processor and 16 GB of RAM.

Each of the four test cases are modelled considering a single PCC, a 66 kV MVAC candidate network, a 220 kV candidate HVAC network and a 400 kV candidate HVAC network. The smallest test case has only two OWPPs and is used for demonstrating the structure of the problem. The four and six OWPP

cases are of arbitrary regions, but the final test case with 8 OWPPs is based on the Belgian offshore wind development zone one.

Infrastructure sizing is calculated using the cost model presented in section A. CAPEX, losses and reliability via corrective maintenance and EENT are considered. It must be noted that at the time of the research, the cost of installation of 400 kV cables was considered similar to that of 220 kV. Unfortunately this assumption was wrong due to the requirement of using three single core cables versus a single three core cable. As such, the 400 kV topologies presented below are cheaper than they would be in reality. This, however, does not impact the methodology or conclusions drawn.

Benchmark model

The computation time of the TNEP increases exponentially with the number of binary variables (candidate equipment) modelled. As previously discussed, in green field problems such as the OW-TNEP, the number of binary decision variables increases rapidly. This is particularly true in the case where multiple candidate OSS locations are desirable. To evaluate the computational scalability of the benchmark TNEP we compare it to several implementations found in the literature with a similar number of binary variables. To this end, Fig. 4.6 shows the timing of the benchmark TNEP along side reported computation times of comparable problem formulations (medium voltage collection circuit formulations) that have a similar number of binary decision variables. As can be seen, our implementation is computationally representative of the problem class as a whole.

Ref	Binaries	Hours
[195]	3000-4000	23.3*
[195]	2000-3000	3.5
[196]	1500-2500	0.75
[196]	1500-2500	0.3

*Author cites memory constraints for high computation time.
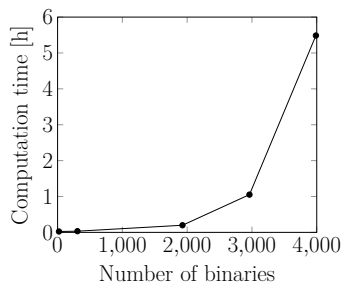
Figure 4.6: Typical computation times in state of the art MILP implementations in medium voltage collection circuit optimization for a similar number of binaries (left). Computation times of the TNEP MILP benchmark (right).

Test cases 1, 2 and 3

Table 4.3: Case 1: Summary of OWPP capacities (top) and candidate cables (bottom).

OWPPs [MW]	
g_0	350
g_1	250

Candidates	
kV	Amount
66	16
220	8
400	8
Total	32
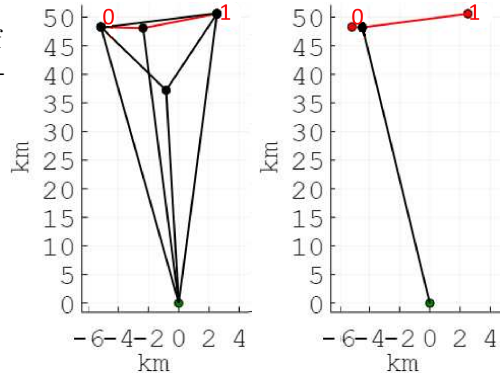
Figure 4.7: Case 1 Possible 220 kV connections for 2 OWPPs (left). Optimal Topology (right).

Case one with two OWPPs is described in detail here to provide a simple example of how the problem is structured for the benchmark TNEP. The 220 kV TNEP candidate grid for case one is shown on the left side of Fig. 4.7 with the capacities of modelled OWPPs listed in the top of Table 4.3. In the figure, medium voltage connections are shown in red and high voltage connections in black. OSSs are black dots. There are three possible candidate connection topologies considered:

- The first connects both OWPPs using medium voltage cable to a single OSS before connecting to the PCC.

- The second connects the second OWPP at 220 kV to the first at an OSS located at the first OWPP concession, before connecting to the PCC. This topology requires two OSSs.

- The final topology uses three OSSs, one at each OWPP to step up to 220 kV and then a third collection point prior to transmission to shore.

The three candidate grid topologies reflect the connection options consisting of one, two or three OSSs. In all cases the OSSs are optimally placed using (4.12). The option to connect each OWPP directly to the PCC is also included. If considering these candidate connection options for both 220 kV and 400 kV the total candidate lines required are as in Table 4.3. This corresponds to the candidates present in the set $\boldsymbol{T}^{\mathrm{H}}$ found by the greedy search algorithm. For

the remaining cases, candidates are modelled in a similar way to match the candidates in the TNEP with those present in $\boldsymbol{T}^{\mathrm{H}}$.

The optimal solution topology for case 1 is shown on the right side of Fig. 4.7. Both the TNEP and greedy search find the same solution topology with objective functions and computation times as in Table 4.6. The main characteristics

Table 4.4: Cases 1-3 Summary of Results.

Case	Number of OWPPs	Candidate Lines	TNEP [M€]	Greedy [M€]	TNEP [s]*	Greedy [s]*
1	2	32	358.1	357.9	36.1	36.4
2	4	307	1102.4	1103.0	50.2	48.7
3	6	1924	1974.1	1973.6	672.5	67.9

*Note: computation times include problem set up and solve time

for the four and six OWPP cases, including concession capacity and average distance from shore, is provided in Table 4.5. The number of candidate lines, objective function and computation times are listed in Table 4.6. For both test cases the TNEP and greedy search find the same optimal topology. Additionally, there is very little difference computationally in the four OWPPs case. In the six OWPPs case, however, the greedy search arrives at the optimal solution in about 10 % of the time.

Table 4.5: Cases 2-3 Summary of OWPP capacities [MVA].

Case	g_1	g_2	g_3	g_4	g_5	g_6	km*
2	500	600	450	400	-	-	61.6
3	500	600	450	550	400	600	69.2

*Note: Mean OWPP to PCC distance specified.

Test Case 4 - Belgian North Sea

The Belgian offshore development region one has an area of $238\,\mathrm{km}^2$ and installed capacity of $2.3\,\mathrm{GW}$. This test case is based on this region considered as a green field development area. As in the introduction we approximate it by 8-250 MW OWPPs placed at the coordinates of the existing concessions. A 220 kV substation at Zeebrugge is the PCC. The same coordinates of the OWPPs and PCC as summarized in Table 4.1 are used.

Unfortunately, it was found that modelling all the candidates considered within $\boldsymbol{T}^{\mathrm{H}}$ with the benchmark TNEP was computationally intractable. An attempt

to solve the problem directly using the TNEP model resulted in an optimality gap of 21.7% after 15 hours of computation. The best solution at that time was 1129.5 M€.

As no solution topology was found directly using the TNEP an alternative benchmark is the used. The solution from the sequentially cascading MILP found in [190] is used. Recall that transmission voltage options in that problem formulation include 33 kV and 132 kV in addition to the 66 kV, 220 kV and 400 kV considered by the greedy search. It is therefore a larger problem size than that solved by the greedy search. This is important to remember when comparing computation times.

In Fig. 4.8 the optimal topologies found by the greedy search algorithm and the cascading MILP are shown. Moving from left to right we see the optimal 400 kV and 220 kV topologies found by the greedy search algorithm. On the right side is the optimal topology found in [190]. The associated costs and computation times are summarized in Table 4.6. A detailed breakdown of infrastructure capacity, location and costs is provided in Tables 4.7, 4.8 and 4.9. In Table 4.7, CM and EENT are corrective maintenance and expected energy not transmitted respectively. For details on how these quantities are calculated refer to the economic model provided in Appendix A.
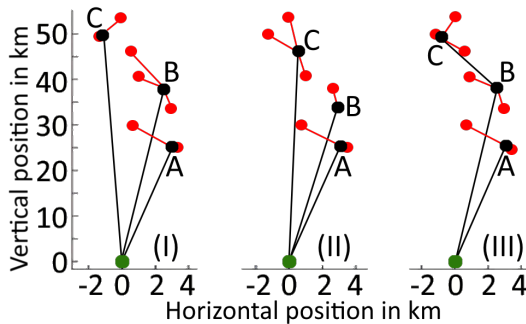
Figure 4.8: Optimal topologies for belgian offshore. (I) Optimal 400 kV topology. (II) Optimal 220 kV topology. (III) Topology found in [190].

In the table, four cases are listed. The first two refer to the best 400 kV and 220 kV topologies that were found using the greedy search. The last entry refers to the best topology found in [190]. The entry marked Greedy III is a topology returned as part of the ordered queue in $\boldsymbol{T}^{\mathrm{FR}}$ that matches identically that found in [190] allowing a direct comparison between the two methods. We can see that not only was the greedy algorithm able to find an overall better 220 kV solution but it was also able to find a better version of the best solution

Table 4.6: Case 4 Summary of Belgian Offshore Results.

Case	kV	HV cable[M€]	MV cable [M€]	Total [M€]	Time [s]
Greedy I	400	392	192.6	1049.3	344*
Greedy II	220	514.6	205.2	1131.2	349*
Greedy III	220	519.1	169.7	1142.7	349
[190]	220	492.5	200.5	1146.7	≈9 days

*Total greedy search time is 693s the sum of the 400 kV and 220 kV runs.

found in [190]. Notice that Greedy III is actually 4M€ less than the same topology in [190]. Comparing the cable costs in Table 4.6 we see that Greedy III positioned the substations to reduce to required medium voltage cable, making up the difference instead by extending the high voltage connections. This results in an overall lower cost topology. Better positioning of the OSS is a major advantage of greedy search and a draw back of the MILP formulation. With integer placement of candidate OSSs as is necessary in an MILP the optimal location may be missed and the truly optimal topology overlooked.

Table 4.7: Belgian Offshore Topology Cost Comparison in M€.

Topology	Materials	Labour	CM	Losses	EENT	Total
I	518.5	251.0	147.6	74.0	58.2	1049.3
II	533.2	335.2	167.1	51.6	44.1	1131.2
III	552.8	321.0	172.0	54.4	42.6	1142.7

4.4 Conclusions

In this chapter, a novel OW-TNEP model has been developed to address the gap in the literature for intermediate capacity networks, bridging the existing high and low-level models. In the process, several significant conclusions and observations have been made. The study has revealed that while mathematical programming approaches can provide a mathematically global optimal solution for offshore wind transmission systems, the strict requirements on the search space or on the problem formulation can eliminate a priori desirable solutions. Algorithmic approaches, on the other hand, such as the greedy algorithm presented in this chapter, may present the opportunity to search an expanded search space and a more elaborate problem formulation resulting in a superior solution despite not providing a guarantee on global optimality. It is important to remember that the mathematically optimal solution is for the mathematically

Table 4.8: Belgian Offshore Topologies - HVAC Cables.

Topology	Start	End	km	kV	cables	mm^2	M€
I	A	PCC	25.5	400	1	500	71.6
I	B	PCC	38.01	400	2	500	188.1
I	C	PCC	50.07	400	1	500	132.3
I	1-8	A,B,C	25.1	66	6	150	192.6
II	A	PCC	25.41	220	2	400	91.8
II	B	PCC	34.05	220	2	400	121.6
II	C	PCC	45.95	220	3	1000	301.2
II	1-8	A,B,C	27.04	66	6	150	205.2
III	A	PCC	25.41	220	2	400	91.8
III	B	PCC	38.01	220	5	630	361.5
III	C	B	11.75	220	3	400	65.8
III	1-8	A,B,C	21.57	66	6	150	169.7

Note: Specified MV cable is that required in addition to the
MV cable within the collection circuit proper.

Table 4.9: Belgian Offshore Topologies - OSS.

OSS	Transformers MVA	Reactors MVAR	Latitude	Longitude	M€
I-A	2-250	75	51.52869	3.01098	110.9
I-B	2-500	250	51.61862	2.90056	189.1
I-C	2-250	150	51.68853	2.75639	111.4
II-A	2-250	50	51.52814	3.01196	110.9
II-B	2-250	75	51.59112	2.93795	111.1
II-C	2-500	200	51.66676	2.80965	189.4
III-A	2-250	50	51.52814	3.01196	110.9
III-B	2-380	300	51.61862	2.90056	192.6
III-C	2-380	50	51.68392	2.76749	150.5

Note: Reactor cost is included in the cable cost.

defined search space, which can be an oversimplification of the physical problem at hand. Unfortunately, this is often overlooked in current state of the art models. In some cases, the most desirable solution may be excluded a priori in mathematical programming due to structural requirements on the search space, such as convexity or linearity. In the case of mixed-integer expansion planning problems, the heuristics used to define candidate equipment may also exclude this solution.

In this chapter, the proposed OW-TNEP formulation has been presented. First, it has been demonstrated that using a traditional approach based on integer positions of candidate OSSs can be problematic due to the combinatorial explosion of the number of binaries required for the candidate infrastructure. An alternative formulation using a greedy algorithm has been proposed. Underlying the greedy search approach is a multi-layer, set-based description of the search space. The sets describing the underlying combinatorial layer form the first layer, and a topological layer containing the physical characteristics of the problem is mapped over the top. The greedy search can efficiently search the topological search space for high-quality solutions, returning a priority queue of optimal topologies for all possible connection combinations of the OWPPs passing through a single export cable. From the greedy search result, a simple method to determine the optimal topology with $1 \le k \le n$ export cable connections to the PCC has been presented.

The greedy search has been benchmarked against a MILP formulation of the TNEP problem for four test cases of two, four, six, and eight OWPPs. In all cases, the greedy search has found either the same quality solution or better. Computation time was also similar for problems up to four OWPPs and an order of magnitude faster for the larger problem sizes. In the case of the eight OWPPs zone, which was based on the Belgian offshore, the greedy search not only found a better solution than the benchmark but also found a better version of the optimal solution returned by the benchmark. The improvement on the benchmark topology was due to the ability of the greedy search to optimally place OSSs in a continuum, rather than the integer placement within an MILP.

Chapter 5

Very large offshore wind development zones

5.1   Introduction

In this chapter[1] a novel approach using the machine learning technique of Association Rule Mining (ARM) is proposed as a method of reducing the size of the combinatorial search space in greedy search algorithm via dynamically generated constraints. As the size of wind development zones grow larger and the number of concessions climb, the combinatorial explosion rapidly grows beyond what is feasible using the greedy search algorithm. This point occurs after about twelve OWPPs.

Within the literature very few applications of machine learning in relation to the field of power system planning can be found. In terms of power system optimization the attention has focused mostly on operation and control, power flow calculations, optimal dispatch and the data rich areas of energy management, energy forecasting and electricity markets [37,47,197–199]. The proposed hybrid greedy-ARM optimization approach is an attempt to demonstrate that power system planning too, can benefit from the optimization techniques developed as

---

[1]The work of this chapter has been published as: *Stephen Hardy, Hakan Ergun and Dirk Van Hertem, 'Application of Association Rule Mining in Offshore HVAC Transmission Topology Optimization.', in the Journal Electric Power Systems Research.* The content of the paper has been modified here to make it consistent with the other chapters of this dissertation. The first author is the main author of the paper.

part of machine learning. To the best knowledge of the authors this is the first time ARM has been applied in such a manner.

In the following section the developed technique is presented. This includes how a representative synthetic data set of OWPPs is generated as well the data mining procedure used to discover patterns within the synthetic data which are then used to generate constraints to shrink the search space of the greedy search algorithm. The developed approach is applied to 18 case studies ranging in size from eight to 21 OWPPs. The results of the hybrid algorithm are compared to the basic greedy search algorithm when possible. When not possible, due to tractability, the predicted error is calculated and kept small. A sensitivity analysis on model parameters is also performed.

5.2 Clustering large scale OWPP regions

5.2.1 OWPP Clusters
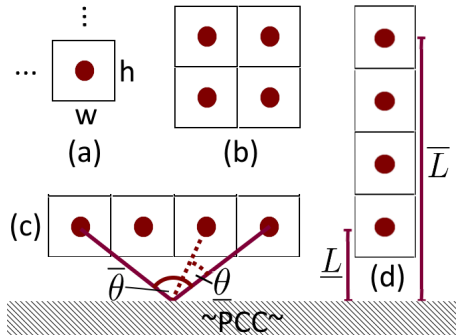
Figure 5.1: Structure of OWPP Clusters. (a) A single concession. (b) A block (#) cluster. (c) A parallel ($\parallel$) cluster. (d) A perpendicular ($\perp$) cluster.

As in section 4.2.2 an OWPP is modelled as an area of size $A_g^{\mathrm{g}} = P_g^{\mathrm{g}}/\rho_g$, where P_g^{g} and ρ_g are the capacity of the OWPP and the wind energy density of the region respectively. Rather than assuming a circular concession, however, for the purpose of the ARM-greedy hybrid search, each concession is modelled as a square of height, h and width, w as in Fig. 5.1(a). The connection point for medium voltage cable is the centroid of the square. Clusters of OWPPs are then formed by positioning OWPPs side by side with each other either horizontally or vertically as in Fig. 5.1(b)-(d). Three representative cluster shapes are considered. The first, stacks the OWPPs both vertically and

horizontally relative to each other forming a block of OWPPs. This type of cluster is illustrated in 5.1(b) and is referred to as a block cluster (#). The second cluster type, termed a parallel cluster (||) is constructed by positioning OWPPs in a strip along the shore line as in 5.1(c). The last cluster type, termed a perpendicular ($\perp$) cluster, is created by stacking OWPPs vertically while moving in a line away from shore as in 5.1(d).

The three cluster types are meant to model the extremes one could find, in terms of relative position of OWPPs to one another. In practise, most offshore regions would likely be classified as a block cluster but may have a principle axis lying more in the parallel or perpendicular direction relative to shore and the PCC.

A cluster is described by six parameters. The capacities of the concessions $G = \{g_1, g_2, ..., g_n\}$, the total number of concessions in the cluster, n, the Euclidean distances of the of the closest and furthest OWPPs to the PCC, $\underline{L}$ and $\overline{L}$ respectively, and the minimum and maximum angles created by any two OWPPs connected to the PCC, $\underline{\theta}$ and $\overline{\theta}$ respectively. These parameters are illustrated in Fig. 5.1.

5.2.2 Generating synthetic OWPP data

ARM is a machine learning technique that is applied to large data sets in order to identify useful patterns which can inform decision making. Currently, no such data sets exist for OWPP connections. As such an alternative approach, of generating a synthetic data set of representative OWPP connections is proposed. A rule making population K is generated with member κ defined by the following six descriptive variables:

$$\kappa = f(P_i^{\mathrm{g}}, P_j^{\mathrm{g}}, l_i, l_j, \theta_{ij}, \mathbb{B}). \tag{5.1}$$

The variables P_i^{g} and P_j^{g} are the capacities in MVA of two OWPPs, i and j, to be radially connected to a PCC. OWPPs i and j are a Euclidean distance of l_i and l_j kilometers from the PCC respectively and their Eucliean distances form an angle of θ_{ij} with each other when measured at the PCC. The final variable, $\mathbb{B} \in \{0, 1\}$, defines the optimal connection method. It is equal to one when the lowest cost connection is to group the OWPPs described by the first 5 variables into a single common export cable connection to the PCC and zero if it is cheaper to connect the OWPPs in isolation of each other. Each member

κ is drawn from a domain defined by the constraints:

$$P_i^{\mathrm{g}}, P_j^{\mathrm{g}} \in P_g^{\mathrm{g}};\ l_i, l_j \in L;\ \theta_{ij} \in \measuredangle$$

$$P_g^{\mathrm{g}} = \{P_i^{\mathrm{g}} = \sum_{\substack{k \in \binom{G}{k}, \\ g_i \in k}} g_i : P_i^{\mathrm{g}} \leq \overline{G} - \min(G)\}$$

$$L = \{l_i = \underline{L} + \Delta l : l_i \leq \overline{L} \text{ and } \Delta l \in \mathbb{Z}_0^+\}$$

$$\measuredangle = \{\theta_{ij} = \underline{\theta} + \Delta \theta : \theta_i \leq \overline{\theta} \text{ and } \Delta \theta \in \mathbb{Z}_0^+\},$$

(5.2)

where G, $\underline{L}$, $\overline{L}$, $\underline{\theta}$ and $\overline{\theta}$ are the variables described above for an OWPP cluster under consideration. $\overline{G}$ is a parameter that is set to the maximum desirable OSS size. Notice that P_i^{g} is the sum of capacities for k OWPPs g_i and that whether k is equal to one or to n, a member κ does not differentiate. Δl and $\Delta \theta$ are both step sizes that discretize the search space. They can be adjusted based on computational requirements.

5.2.3   Association Rule Mining (ARM)

The first instance of ARM was presented in [200] where it was used to search for useful relationships in point of sale transactions at supermarkets in order to improve sales. It has since been applied to a wide variety of problems as diverse as medical diagnosis [201] and power system restoration [202]. The principle advantage of using ARM over other supervised learning classification approaches, such as an Artificial Neural Network (ANN) or a Support Vector Machine (SVM) are the human interpretable rules that are obtained. While ANNs can be a black box of sorts, the output of an SVM is also difficult to comprehend due to the large number of numerical parameters, i.e. the support vectors [203]. ARM on the other hand, finds association rules in the human readable form of a logic statement as in:

$$X \Rightarrow Y \mid X \cap Y = \varnothing$$

(5.3)

where X and Y are sets of items within a database $\mathcal{D}$. Having human readable output has the advantage of easing integration with other optimization methods such as the greedy search algorithm. ARM depends on two properties of $\mathcal{D}$: the support p and the confidence P. Support is the frequency at which X occurs in the N entries of $\mathcal{D}$ as in:

$$p = |X|/N.$$

(5.4)

The vertical bars are used to indicate the cardinality of the enclosed item set. Confidence is the conditional probability that an entry which contains X also

contains Y. It is expressed as:

$$P(X \Rightarrow Y) = |XY|/|X|. \tag{5.5}$$

The rule mining is divided into two steps. In the first step, a list of all the item sets in $\mathcal{D}$ with a minimum threshold of support, p^{t}, is found. These item sets are referred to as the "frequent item sets". In the second step, the frequent item sets are reduced to include only those having a minimum level of confidence in reference to a different frequent item set. Computationally, the difficult part of this process is listing the frequent item sets, as the possible combinations increase exponentially with the number of items in $\mathcal{D}$. As such, there has been much research devoted to developing algorithms which can mine frequent item sets efficiently.

The apriori algorithm is the most widely known algorithm for mining frequent item sets. It uses a breadth first search. Other algorithms employ different search strategies such as depth first (the eclat algorithm [204]) or a pre-fix tree (the fp-growth algorithm [205]). Determining if a certain algorithm is better suited for this particular application is out of scope. In this work we mine frequent item sets using the apriori algorithm as in [206]. The pseudo code is presented in algorithm 4. The apriori algorithm is efficient at mining frequent item sets as it takes advantage of the downward closer principle. According to the downward closer principle an item set of length k can only be a frequent item set if all of its subsets of length $k-1$ are also frequent item sets. The downward closer principle can be seen in the Pseudo code on line 14.

The apriori algorithm cannot be directly applied to the population K. First we must condition the data into an apriori appropriate format. To do this, we begin by defining a set of unique items $I = \{I_1, I_2, ..., I_m\}$, where each item I_i is either a member of the set $\{0, 1\}$ or satisfies at least one of the following inequalities:

$$I_i \leq P_i^{\mathrm{g}},\ I_i > P_i^{\mathrm{g}}\ \forall P_i^{\mathrm{g}} \in P_g^{\mathrm{g}},$$

$$I_i \leq \theta_{ij},\ I_i > \theta_{ij}\ \forall \theta_{ij} \in \measuredangle, \tag{5.6}$$

$$I_i \leq l_{ij},\ I_i > l_{ij}\ \forall l_{ij} \in L_{ij}$$

Here P_g^{g} and $\measuredangle$ are as in (5.2) and L_{ij} is the set of Euclean distances from OWPP i to j. We then create length five subsets of I, $T = \{I_1, ..., I_5\}$ called transactions. A transaction is derived from a member $\kappa \in K$. Four of the items in a transaction are inequalities satisfying (5.6), one for each of the variables $(P_i^{\mathrm{g}}, P_j^{\mathrm{g}}, \theta_{ij}) \in \kappa$ and one considering the inter-OWPP distance l_{ij}. The fifth

---

Algorithm 4: Apriori Algorithm

Input: $\mathcal{D}$, p^{t}
Output: frequent item sets: $\cup(F_k)$

1 **Function** Apriori($\mathcal{D}$, p^{t}):
2      $F_1 \leftarrow \{\forall I_i \in D \mid : p_i \geq p^{\text{t}}\}$
3      $k = 2$
4   **while** $(F_{k-1} \neq \varnothing)$ **do**
5          $C_k = Generate(F_{k-1}, k)$
6          $F_k = Prune(C_k, p_t)$
7          $k = k + 1$
8   **return** $\cup(F_k)$

9

10 **Function** Generate(F_{k-1}, k):
11   **for** (X_i, X_j) *in* F_{k-1} **do**
12          $X_{ij} = (X_i \cup X_j)$
13   **if** $(length(X_{ij}) == k)$ **then**
14   **if** $(X_i \subseteq F_{k-1}, \forall X_i \in X_{ij} \mid : length(X_i) == k - 1)$ **then**
15                  $C_k.add(X_{ij})$
16   **return** C_k

17

18 **Function** Prune(C_k, p^{t}):
19   **for** X_i *in* C_k **do**
20   **if** $(support(X_i) \geq p^{\text{t}})$ **then**
21              $F_k.add(X_i)$
22   **return** F_k

---

item in a transaction is $\mathbb{B} \in \kappa$. There is at minimum one unique transaction per population member κ. The set of all transactions is the database $\mathcal{D}$.

The apriori algorithm can then be applied to $\mathcal{D}$ to find all frequent item sets $X_k \in \cup(F_k)$. Association rules of the form $S_k \Rightarrow (X_k \backslash S_k)$ are then calculated for all the subsets $S_k \in X_k$ for all $X_k \in \cup(F_k)$. If an association rule has a confidence above the desired threshold, it is a valid rule and is kept.

In our case we go further when defining a valid association rule. We require a confidence of one and the additional requirement that the right hand side is $\mathbb{B} = 0$ (Y of (5.3)). These requirements retain only the rules that are found to be correct 100% of the time in predicting connections that are not cost effective, thus eliminating part of the search space. It has been suggested that rules

with a right hand side of $\mathbb{B} = 1$ could also be used to reinforce the selection of candidates. Although this is technically true, in practise, this would require generating a much larger sample population to be a reliable indicator as any part of the search space that is missed during sampling would be eliminated without evidence. The underlying logic for this is that a rule with a right hand side of zero is direct evidence the tested connection is not economic, whereas, a right hand side of one says nothing about connections to eliminate, rather what connections should be maintained.

5.2.4   Greedy - ARM Hybridization

To easily understand the output of the ARM and how it is applied to reduce the required search space, a simple example follows. In (5.7), two possible rules are presented, one with a left hand side with the minimum possible number of items; one, $(\boldsymbol{X_1} \Rightarrow \boldsymbol{Y_1})$ and the other with a left hand side of the maximum possible number of items; four, $(\boldsymbol{X_2} \Rightarrow \boldsymbol{Y_2})$. Of course a rule can comprise any number of items between these two extremes.

$$\boldsymbol{X_1} = \{P_0^{\mathrm{g}} \geq 750\},$$

$$\boldsymbol{X_2} = \{P_0^{\mathrm{g}} \leq 250, P_1^{\mathrm{g}} > 500, l_{0,1} > 10, \theta_{0,1} > 10\}, \tag{5.7}$$

$$\boldsymbol{Y_1} = \boldsymbol{Y_2} = \{\mathbb{B} = 0\}.$$

The first rule $(\boldsymbol{X_1} \Rightarrow \boldsymbol{Y_1})$ states that if the closest of two OWPPs to the PCC has a capacity greater than or equal 750 MVA, then it is never economic to connect a second OWPP via a common export cable. The second rule $(\boldsymbol{X_2} \Rightarrow \boldsymbol{Y_2})$ states that should two OWPPs be separated by a distance greater than 10 km and the closest of the two OWPPs to the PCC has a capacity less than 250 MVA while the furthest has a capacity greater than 500 MVA, then a common export cable will never be the lowest cost option if the angle formed at the PCC by the Eucliean distances connecting each OWPP to the PCC is larger than 10°.

Combining ARM with the greedy search permits larger problem sizes to be solved as the constraints found by ARM can be used to eliminate candidate topologies within the sets $\boldsymbol{T}^{\mathrm{B}}$ and $\boldsymbol{T}^{\mathrm{H}}$. Due to the combinatorial nature of the problem, topologies eliminated from set $\boldsymbol{T}^{\mathrm{B}}$ have a much larger impact than those from $\boldsymbol{T}^{\mathrm{H}}$. To understand how constraints can reduce the size of these sets, consider the following example. picture an offshore region with four OWPPs, each having a capacity of 250 MVA. Within the set $\boldsymbol{T}^{\mathrm{B}}$ are candidate topologies based on the binary string combinations of [1110] and [1111]. If association

rule $X_1 \Rightarrow Y_1$ in (5.7) is a valid rule, then all variations of topology t_{15} where $t' = t_\beta \cup t_k^e = t_{14} \cup t_1$ can be immediately eliminated as the total capacity, P_i^g, of the three OWPPs in any topology $t_\beta = t_{14}$ is 750 MVA which satisfies the condition of X_1.

5.3   Results

5.3.1   ARM Sensitivity Analysis

Prior to testing the proposed algorithm, a sensitivity analysis on the size of the rule making population and minimum threshold of support is performed. Clusters of eight OWPPs are arranged in parallel, block and perpendicular formations. The algorithm is applied considering rule making population sizes varying from 1000 up to 5000 in steps of 1000 and minimum support thresholds varying from 1% up to 5% in steps of 1%. Two metrics of algorithmic quality, namely the percentage of eliminated connections (ϱ) and the associated error (ϵ), are recorded in this study. Both ϱ and ϵ are computed based on a control population K^C, which is independent from the population used for rule generation (K). The calculation of ϱ involves determining the ratio of eliminated connections to the total number of connections, as in:

$$\varrho = \frac{\left| \bigcup\limits_{i \in R} K_i^\text{C} \right|}{\left| K^\text{C} \right|}. \tag{5.8}$$

Here, R represents the set of valid association rules discovered, and K_i^C refers to the subset of K^C where rule $i \in R$ is applicable. The symbols $|\cdot|$ denote the cardinality of a set, indicating the number of elements within the set. On the other hand, ϵ measures the ratio of wrongly eliminated connections in K^C to the total number of connections, as in:

$$\epsilon = \frac{\left| \bigcup\limits_{i \in R} K_i^{\text{C},\mathbb{B}} \right|}{\left| K^\text{C} \right|}, \text{ where: } K_i^{\text{C},\mathbb{B}} = \{\kappa \in K_i^\text{C}, \mathbb{B} \in \kappa : \mathbb{B} = 1\} \tag{5.9}$$

In this equation, $K_i^{\text{C},\mathbb{B}}$ represents the subset of K_i^C where the associated binary variable $\mathbb{B}$ equals 1. Again, $|\cdot|$ denotes the cardinality of a set. A high value of ϱ indicates a significant reduction in the search space, which is desirable. Conversely, a low value of ϵ (ideally zero) suggests that the selected rules only eliminate undesirable connections. Fig. 5.2 presents the results of the sensitivity analysis. Looking at the percentage of connections that can be removed, we can see that it varies greatly depending on the layout of the cluster with the highest

percentage of connections eliminated occurring in the parallel layout (59.7%) and the least in the perpendicular layout (22.5%). This is a logical result as in the perpendicular layout the furthest OWPPs must pass very closely to the OWPPs situated nearer to shore, creating the opportunity to supply multiple OWPPs with a single export cable without significant rerouting away from the Euclean distance. By contrast in a cluster with a parallel layout, any OWPPs that are joined into a common feeder will have to have at least a small deviation away from straight line connections.

Adjusting the minimum support level also varies in its impact on the number of connections eliminated by cluster layout considered. Once again it is the perpendicular cluster that is impacted the most by a change in the minimum support. Similar logic as above also justifies this result. It is more difficult to eliminate connections with certainty when the OWPPs are in a line with each other moving away from the PCC as in the perpendicular case. As the parallel and block formations are mostly unaffected by changing the support level between 1% and 5%, it can be inferred that most applied rules enjoy a level of support above 5%.

The affect of varying the rule making population size has little effect on the number of connections that can be eliminated implying that similar rules are discovered with both the smaller and larger populations. As would be expected, however, increasing the population does have a positive impact on reducing the error. This of course comes at the trade off of increased computation time (τ) though. Since the error is quite low even in the worst case at 1.2%, it is difficult to justify a large rule making population. In the remainder of the cases, unless explicitly stated, a rule making population of 2000 and a minimum support of 2% are used.

5.3.2 Test Cases

The results from eighteen test cases ranging in size from eight to 21 OWPPs are presented in this section. The results are summarized in table 5.1. The results were obtained on a standard Dell lap-top with an intel core-7 1.9 GHz processor and 16 GB of RAM. In the table the test cases are sorted by cluster shape and then ordered by the number of OWPPs in a cluster. In terms of descriptive information about the test cases, the table lists the number and capacity of OWPPs within a cluster and the average distance the cluster is from the PCC (cyan columns). All clusters are assumed to have a common capacity among the OWPPs in the cluster with the exception of the last two test cases listed, that are made up of 13 and 21 OWPPs respectively.
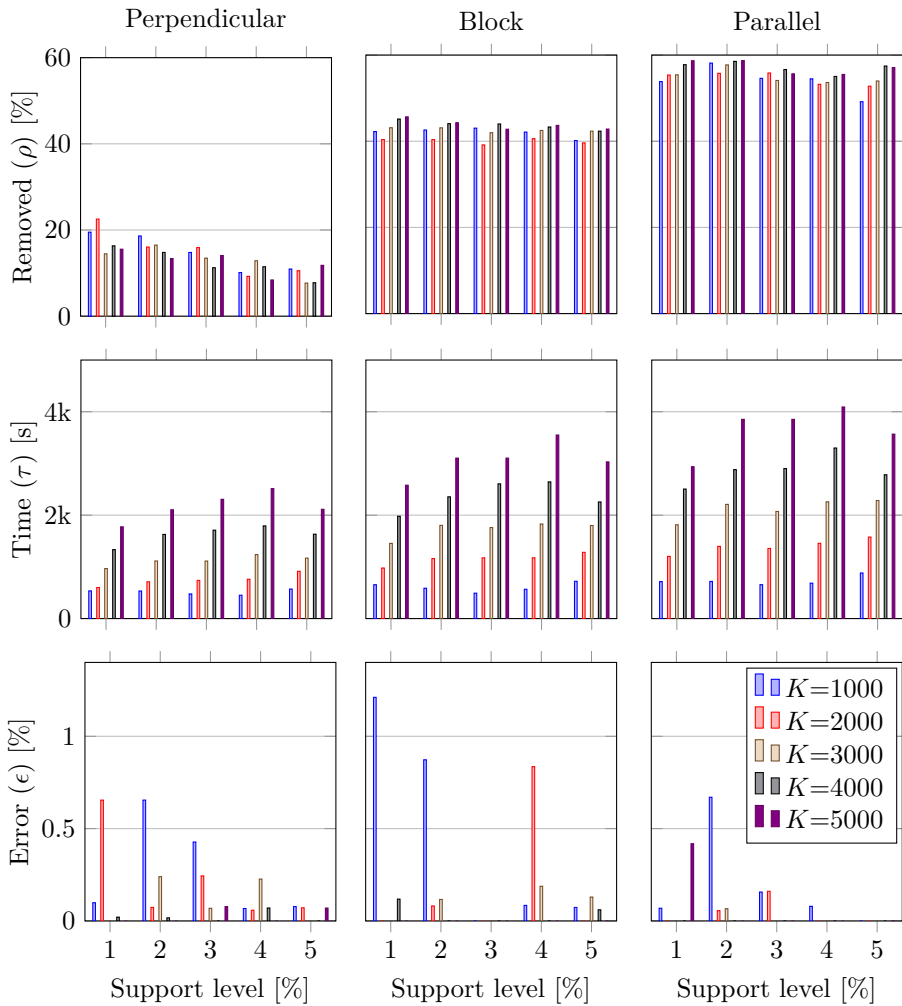
Figure 5.2: The variation in the achieved size reduction of the control population (ϱ), computational time (τ) and error (ϵ) in the control population for the perpendicular, block and parallel 8 OWPPs cases, considering multiple rule making population sizes (K) and minimum support levels.

Table 5.1: Comparison of the unmodified greedy algorithm to the ARM approach.

[MW]	[km]	OWPPs	[M€]	τ_g [s]	τ_{arm} [s]	ε [%]
Perpendicular						
250	65	8	1480	226	711	0.07
250	47	9	1434	814	982	1.05
250	65	10	1743	4042	2548	0.42
250	61	12	2199	84580	11862	0.36
Parallel						
250	35	8	1081	283	1397	0.06
250	60	9	1603	1593	2439	0.11
250	75	10	2169	6386	2697	0.08
250	54	12	*1807	161906	14050	0.27
Block K=2000						
250	85	8	1678	264	1160	0.08
250	59	9	1609	1313	1774	0.89
250	70	10	1953	6567	2577	0.88
250	40	12	1681	112463	2201	0.37
250	75	15	3069	-	176197	1.41
300	47	16	2933	-	18131	0.51
300	65	18	2833	-	1536	0.15
350	65	20	3492	-	6105	0.42
Fig.5.4	55	13	2946	-	4765	3.96
Fig.5.4	31	21	3546	-	25772	4.26
Block K=5000						
Fig.5.4	55	13	2946	-	7207	1.16
Fig.5.4	31	21	3545	-	74449	1.06

*hybrid greedy-ARM algorithm solution topology: 1809 M€.

Four results columns are presented (grey columns). The cost column is the cost of the optimal topology. Identical topologies were found in all cases for both the original greedy search and the hybrid approach with the exception of the one highlighted case involving twelve OWPPs in a parallel formation. In this case, the hybrid approach found a topology that costs slightly more (+0.1%). In the timing columns, the time required to find the solution for both the original greedy search algorithm (τ_g) and the hybrid-ARM algorithm (τ_{arm}) are provided. In the final column the error as defined in (5.9) is provided.

For perpendicular and parallel cluster layouts only clusters up to twelve OWPPs are simulated. This is the maximum number of OWPPs that can be compared directly to the basic greedy search solution. The larger test cases are all modelled

considering a block shaped cluster. As the original greedy search algorithm is unable to solve this problem size, the measure of solution quality is from the error alone. A control population (K^{c}) of 5000 is used for the calculation.

The main goal of developing the hybrid algorithm was to increase the feasible problem size that could be solved. This is successfully accomplished as demonstrated by all cluster sizes presented beyond twelve. Comparing the required computational times for cluster sizes that can be solved by both methods as in Fig. 5.3, it can be seen that it is at a cluster size of ten or more that the hybrid approach begins to out-perform the original algorithm. As is demonstrated by the difference in the solutions for the parallel cluster of twelve OWPPs, however, it makes the most sense to use the original algorithm up to twelve OWPPs and the hybrid approach for anything beyond this point.

While a definitive limit on the feasible problem size for the hybrid approach has not been established, we can make a reasonable estimate based on the 21 OWPPs problem. Memory constraints, in this case, were at their limit and would serve as the primary limiting factor when dealing with larger problem sizes. Although it is feasible to increase memory resources, such an action is likely unnecessary due to the presence of other limiting factors that impede significant expansion beyond this level. Factors such as the maximum loss of in-feed or the maximum feasible OSS size act as deterrents against the development of excessively large regions. Therefore, with problems sizes beyond this threshold, it would be advisable to adopt a topological design that involves dividing the larger region into several smaller, independent ones, as this approach would be more practical.

For all test cases with a common capacity across the OWPPs, the error remains very low. There is, however, an increase in the error for the final two test cases, the only ones with varying sizes of OWPPs included in the cluster. Fig. 5.4 shows the layouts and capacities of each OWPP for these clusters.

The errors in these cases are $3.96\,\%$ and $4.26\,\%$ for the 13 and 21 OWPP cases respectively. As this is higher than desirable, the rule making population was increased from 2000 up to 5000 and the simulations were run once again. Running these cases with a rule making population of 5000 dropped the error to an acceptable level of $1.16\,\%$ and $1.06\,\%$ respectively. A very slight improvement on the solution to the 21 OWPP case is observed. Although the improvement of the solution is insignificant at 0.02%, it is good to see that as the error rises, increasing the rule making population size can have a countering effect on solution degradation. The solution topologies for $K = 5000$ are shown in Fig. 5.4.
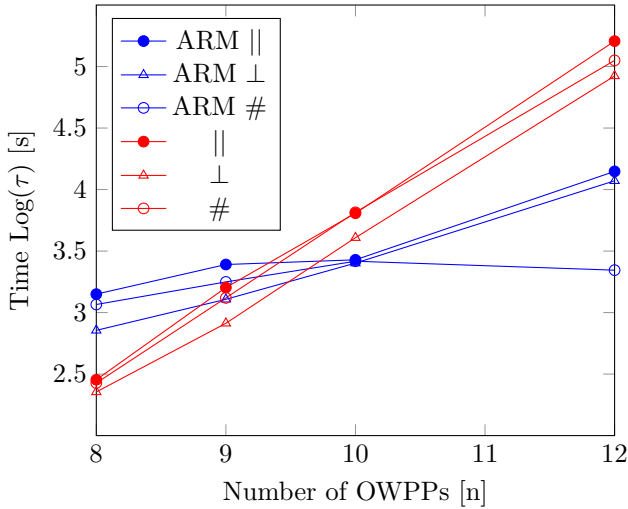
Figure 5.3: A log plot comparison of computation times for perpendicular, block and parallel clusters of 8 to 12 OWPPs.

5.4 Conclusions

This chapter presents an extension of the greedy search OW-TNEP algorithm, as described in the previous chapter, to allow for its application to very large offshore wind development zones. The proposed extension dynamically generates constraints using the machine learning technique of ARM. This significantly reduces the size of the search space traversed by the greedy algorithm. This approach addresses the need for robust rules for defining candidate equipment, as heuristics are often necessary and if improperly defined can lead to the exclusion of the optimal solution a priori.

The hybrid greedy-ARM algorithm is data-intensive, requiring a large data set to search for patterns. To address this issue, a method for effectively generating a synthetic population of OWPP pairs is proposed. Once an appropriately sized rule-making population is generated, the apriori algorithm is used to find all frequent item sets, from which association rules are extracted. Valid association rules are defined as those which predict with 100% confidence, an interconnection between a pair of OWPPs that will never be part of the lowest cost topology. These rules are then used to further constrain the search space traversed by the greedy algorithm.

The hybrid algorithm is tested against the original greedy search for clusters
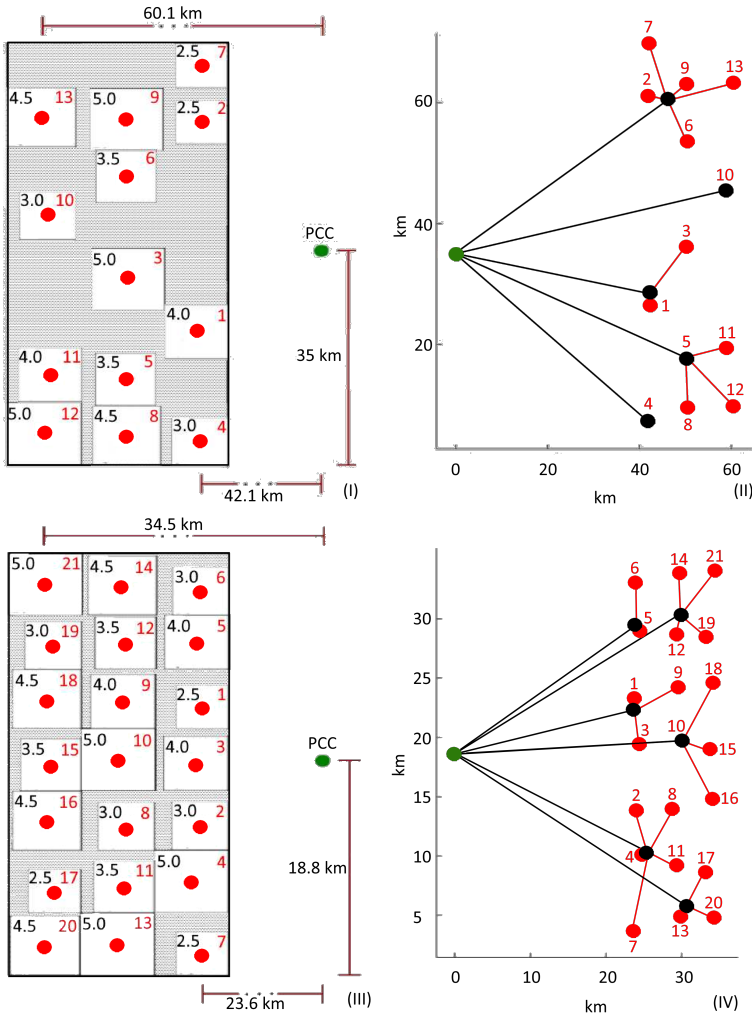
Figure 5.4: (I) Layout of 13 concessions-5.2 GW test case. (II) Solution topology of 13 concessions-5.2 GW test case. (III) Layout of 21 concessions-8 GW test case. (IV) Solution topology of 21 concessions-8 GW test case. In (I)/(III), the capacities of the OWPPs are displayed in the top left corner of each concession in units of 100 MW. In (II)/(IV), the black dots show the optimal location of OSSs, high voltage export cables in black are at 220 kV and medium voltage cables in red at 66 kV.

consisting of up to 12 OWPPs with different relative layouts. In all cases except one, the hybrid approach finds an identical solution to the original greedy search, with a degradation of solution quality of only 0.1% in the single exception. The hybrid algorithm is then applied to larger test cases that are intractable using the original greedy search algorithm alone, and high-quality solutions are found for clusters containing up to 21 OWPPs. Although a direct comparison with a benchmark is not possible for the larger test cases, a measurement of error in a control population demonstrates that the quality of the solution remains high. If an increase in error is detected, it can be mitigated effectively by increasing the size of the rule-making population.

To enhance the scope of the proposed approach, an intriguing expansion would involve refining the synthetic data generation method to incorporate specific engineering knowledge, which may not be easily expressed as a formal constraint. This modification would allow for the injection of domain expertise into the process. Subsequently, the ARM algorithm can be employed as a pre-optimization step to extract robust rules from the synthetic data, effectively reducing the candidate search space before applying traditional optimization methods.

Chapter 6

Transmission planning considering spatial constraints

6.1   Introduction

In this chapter[1] the methodology presented in the previous chapters is extended to account for multiple PCCs as well as further physical constraints associated with building at sea. The objective is better thought of as using the rules of optimization to search for an engineering optimal rather than a mathematical one as the additional physical constraints considered here are highly non-linear and vary unpredictably between different offshore regions. More specifically, we will adapt the greedy search OW-TNEP methodology to consider the bathymetry of the seabed as well as the no-go zones stemming from marine spatial planning requirements. Marine spatial planning in the North Sea is very complex as demonstrated by the Belgian offshore region shown in Fig. 6.1.

Considering this, a generalized mathematical planning model that can deal with this level of complexity and unpredictability is difficult if not impossible to develop. The methods of this section therefore attempt to address this complexity by proposing ad-hoc modifications to the methods discussed in previous chapters.

---

[1]The work of this chapter has been published as: *Stephen Hardy, Hakan Ergun and Dirk Van Hertem, 'A Methodology for Offshore Transmission System Optimization Considering Spatial Constraints'*, in the 2023 IEEE Belgrade PowerTech conference – under review. The content of the paper has been modified here to make it consistent with the other chapters of this dissertation. The first author is the main author of the paper.
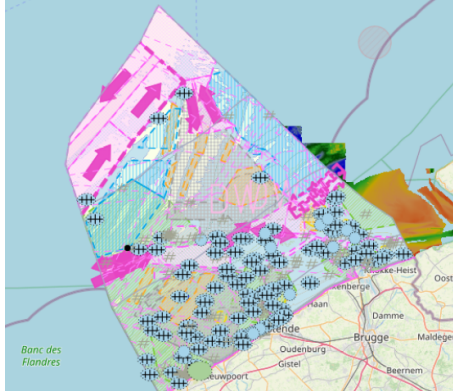
Figure 6.1: Hydrography and marine spatial plan of the Belgian continental shelf [176]. For markup details please refer to the source map in the reference.

6.2 Model

6.2.1 Methodology Overview

There are four main steps in the methodology. First, the domain is described in detail by including bathymetry data, marine spatial planning information and meterological data. Next, a set of candidate OSS locations are determined using a purpose built heuristic that considers both sea depth and shortest cable routing paths. Third, the greedy search presented in the previous chapters is adapted to consider the candidate OSS locations and optimal cable routing. Four, for each voltage level and PCC, the resulting set of topologies $\boldsymbol{T}^{\mathrm{H}}$ found by greedy search, is input into an MIP and the optimal topology considering multiple PCCs determined. These steps are summarized in Fig. 6.2.

6.2.2 Domain and boundary conditions

The optimization domain as in the previous chapters consists of existing network nodes ($n \in \mathcal{N}$), candidate network nodes ($\widetilde{n} \in \widetilde{\mathcal{N}}$), edges between nodes ($e \in \mathcal{E}$), OWPPs ($g \in G$), their associated wind power time series (Ψ_g^{g}) and PCCs ($d \in D$). Unlike in the previous chapters however, existing nodes and edges are tied to points in a three dimensional grid of bathymetry data. Nodes are therefore defined by a set of three coordinates (x_n, y_n, z_n) rather than only two. Additionally, nodes are spatially restricted by no-go zones. No-go zones are regions where no electrical infrastructure can be placed. No-go zones include

Define bathymetry, no-go zones, concessions, turbines, wind-power time series.
Find the set of candidate OSS locations.
For each PCC and kV find a set of candidate topologies: $\boldsymbol{T}^{\mathrm{H}^*}$ with modified greedy search.
Combine resulting $\boldsymbol{T}^{\mathrm{H}^*}$ and find final topology with topological MIP.
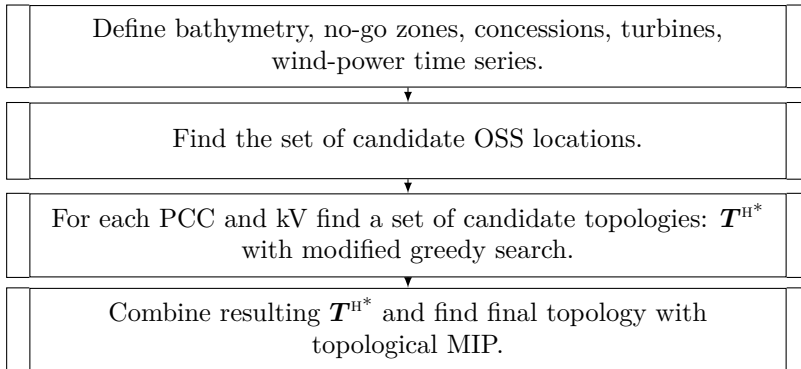
Figure 6.2: Overview of Optimization Process.

military zones, dedicated shipping routes or nature protection zones to name a few. A node in a no-go zone has a z coordinate equal to infinity. Edges connect nodes and have associated weights that are given by:

$$\|e_{mn}\| = \sqrt{(x_n - x_m)^2 + (y_n - y_m)^2 + (z_n - z_m)^2}. \tag{6.1}$$

When the approximate location of a candidate node is determined, its final location is the set of coordinates of the nearest existing node. For the purposes of this methodology, the turbine locations within a concession as well as the outer boundary of the concessions are assumed to be known a priori, i.e. both macro and micro sitting of OWPPs has already been done.

6.2.3 Locating OSS

Candidate OSS Algorithm

In the previous chapter the optimal location of OSSs was based solely on the minimization of cable cost connected to an OSS. In practice, however, it is desirable to locate the OSS based on both cable cost and OSS foundation cost minimization. The cost of an OSS foundation varies with the depth of the sea as well as other factors, such as soil type. Establishing a soil type to cost relationship based on available data was not possible and so this work only considers the variation in depth. If a relationship can be established, however, the weighted edge method presented below can be easily applied by modelling soil type as an equivalent depth. The cost of both materials and installation for the foundation increases as the depth increases. To approximate this relationship a set of scale factors for water depths between $10\,\mathrm{m}$ and $50\,\mathrm{m}$ first presented

in [177] are used. The original scale factors describe a discontinuous stair-case function. The function is poorly defined at the steps (2 scale factors for a single depth). As such, a linear approximation of these values resulting in a continuous water depth dependent scale factor for an OSS is calculated as in:

$$\sigma(\zeta) = 0.0136 \cdot (\zeta - 17) + 0.7676 \qquad (6.2)$$

where ζ is the water depth in meters measured from the seafloor to the surface. The maximum deviation from the original scale factors using this approximation is +/-10%.

To account for both seafloor depth and cable cost minimization an algorithm is proposed that searches for candidate OSS locations at the most elevated seafloor points in the vicinity of the shortest cable routing paths. These candidate locations are then compared to the location calculated using cable cost minimization alone and the best alternative is selected. The proposed algorithm is outlined in steps 1 to 11 below.

1. For each OWPP g, find its centroid node $n_g^{\mathrm{g}} \in \mathcal{N}^{\mathrm{G}}$. $\mathcal{N}^{\mathrm{G}}$ is a subset of $\mathcal{N}$ such that its members n_g^{g} are the nodes in $\mathcal{N}$ which minimize the Euclidean distance to the average $(\bar{x}, \bar{y})$ coordinates of the turbines within a concession g as in:

$$n_g^{\mathrm{g}} = argmin(\|(n, \bar{n})\|) : n \in \mathcal{N}, \qquad (6.3)$$

where the coordinates of $\bar{n}$ (the centroid) are calculated as in:

$$(\bar{x}, \bar{y}) = \frac{\displaystyle\sum_{n_g^{\mathrm{t}} \in \mathcal{N}_g^{\mathrm{T}}} (x_{n_g^{\mathrm{t}}}, y_{n_g^{\mathrm{t}}})}{k}. \qquad (6.4)$$

Here $\mathcal{N}_g^{\mathrm{T}}$ are the nodal locations of the k turbines in OWPP g.

2. Using the A* algorithm [29], assuming a 2D Euclidean heuristic (guaranteeing admissibility), find the set of shortest paths R^{GD} connecting each centroid node n_g^{g} to each PCC node, n_d^{d}. A route $r_{g,d} \in R^{\mathrm{GD}}$ is a set of weighted edges e_{mn}.

3. From R^{GD} find the set of nodes $\mathcal{N}^{\mathrm{GD}}$. Node $n_g^{\mathrm{gd}} \in \mathcal{N}^{\mathrm{GD}}$ is the node that is both within the path specified by $r_{g,d}$ and lies on the perimeter of OWPP concession g.

4. Find the set of subset paths $r'_{g,d} \in R^{\mathrm{GD'}}$ such that $r'_{g,d}$ contains all edges in $r_{g,d}$ between nodes n_g^{gd} and n_d^{d}.
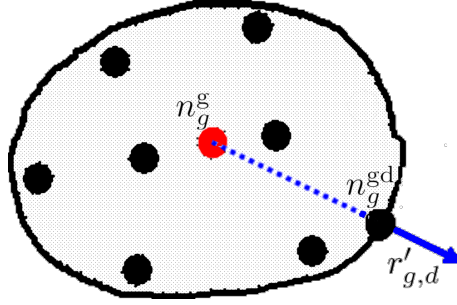
Figure 6.3: Generic OWPP concession showing n_g^{gd}, n_g^{g} and $r'_{g,d}$. Unlabelled nodes are $n_g^{\mathrm{t}} \in \mathcal{N}_g^{\mathrm{T}}$.

Fig. 6.3 shows a generic concession, identifying nodes n_g^{gd}, n_g^{g}, n_g^{t} and route $r'_{g,d}$. The discarded portion of path $r_{g,d}$ when making $r'_{g,d}$ is shown as a dotted line. The resultant end point of the shortest path, n_g^{gd}, is a good approximation of where the collection point of the MV grid should occur as it is the point of the OWPP that minimizes the required cable on route to the PCC. In steps 5 through 7 an analogous procedure to steps 2 through 4 is executed, however, it is applied to the paths between two OWPPs rather than OWPPs and the PCC.

5. Using the A* algorithm, find the set of shortest paths $r_{g,g'} \in R^{\mathrm{GG'}}$ connecting each pair of nodes $n_g^{\mathrm{g}} \in \mathcal{N}^{\mathrm{G}}$. Paths are undirected, i.e. $r_{g,g'} = r_{g',g}$.

6. From R^{GG} find the set of nodes $\mathcal{N}^{\mathrm{GG}}$. Node $n_g^{\mathrm{gg}} \in \mathcal{N}^{\mathrm{GG}}$ is the node that is both within the path specified by $r_{g,g'}$ and lies on the perimeter of OWPP concession g. Due to symmetry both ends of $r_{g,g'}$ have a node n_g^{gg}, i.e. the node $n_{g'}^{\mathrm{gg}}$ that is on the path specified by $r_{g,g'}$ and lies on the perimeter of OWPP concession g' is also a member of set $\mathcal{N}^{\mathrm{GG}}$.

7. Find the set of subset paths $r'_{g,g'} \in R^{\mathrm{GG'}}$ such that $r'_{g,g'}$ contains all edges in $r_{g,g'}$ between nodes n_g^{gg} and $n_{g'}^{\mathrm{gg}}$.

8. Define the set of all shortest paths as $R = R^{\mathrm{GD'}} \cup R^{\mathrm{GG'}}$.

In steps 9 through 11 the shallowest nodes situated in the vicinity of the shortest paths in R are located.

9. For each $r \in R$ find set $\widetilde{\mathcal{N}}_r^{\wedge}$ where $\widetilde{n}_r^{\wedge} \in \widetilde{\mathcal{N}}_r^{\wedge}$ is the shallowest node contained within a route section of length δr. δr is an adjustable parameter. Smaller values of δr result in a higher number of candidate node locations that are closely spaced. The set of all $\widetilde{\mathcal{N}}_r^{\wedge}$ is denoted by $\widetilde{\mathcal{N}}^{\wedge}$.

10. For each node $\widetilde{n}^\wedge \in \widetilde{\mathcal{N}}^\wedge$ search the surrounding area of radius δr for nodes $\widetilde{n}^{\wedge'}$ that satisfy the condition:

$$\frac{z_{\widetilde{n}^\wedge} - z_{\widetilde{n}^{\wedge'}}}{\sqrt{(x_{\widetilde{n}^\wedge} - x_{\widetilde{n}^{\wedge'}})^2 + (y_{\widetilde{n}^\wedge} - y_{\widetilde{n}^{\wedge'}})^2}} \geq \Delta s, \tag{6.5}$$

where Δs is a parameter defining the minimum seafloor rise per unit horizontal distance required to justify moving the OSS location away from the shortest path. The choice of an appropriate Δs is situation dependant. An example of selecting an appropriate Δs is provided in the results section. For each $\widetilde{n}^{\wedge'}$ satisfying (6.5), $\widetilde{n}^{\wedge'}$ replaces the incumbent $\widetilde{n}^\wedge \in \widetilde{\mathcal{N}}^\wedge$. Only unique points are maintained in $\widetilde{\mathcal{N}}^\wedge$.

11. Step 10 is repeated until no further nodes $\widetilde{n}^{\wedge'}$ satisfying condition (6.5) are found. The resulting set $\widetilde{\mathcal{N}}^{\wedge *}$ is the set of all candidate OSS locations.

A* route finding and penalty function

As stated earlier, the z component of a node lying on the boundary of a no-go zone is set to infinity making the weight of an edge attached to it also infinity and ensuring it can never be part of any shortest path. In addition to no-go zones, it may be beneficial to define regions where it is undesirable to run high voltage cabling. For example crossing a neighbouring OWPP concession's medium voltage collection grid with a high voltage cable should typically be avoided. To that end, the A* route finding algorithm is equipped with a penalty function. The penalty function increases the weight of any edge, e_{mn}, that lies in a region where it is undesirable to route cable, by a factor λ^*. In this work, the λ^* defined for neighboring concessions is set as the ratio of the concessions perimeter over the longest straight line cut through the concession. When source or destination nodes lie in an OWPP the λ^* for these concessions is equal to one i.e. there is no penalty. A λ^* of one for $n \in \mathcal{N}$ results in a standard implementation of the A* algorithm.

6.2.4 Greedy Search

Adapting the greedy search algorithm presented in chapter 4 to include the bathymetry data is straightforward. The algortithm remains unchanged until a candidate OSS location $\widetilde{n}_\omega^o$ is determined using (4.12). The nearest node $n \in \mathcal{N}$ to $\widetilde{n}_\omega^o$ is determined and defined as the incumbent $\widetilde{n}^{\wedge *'}$ location for the OSS. A subset of nodes $\widetilde{\mathcal{N}}^{\wedge *'} \subset \widetilde{\mathcal{N}}^{\wedge *}$ that satisfy (6.5) measured from $\widetilde{n}^{\wedge *'}$ is calculated. Cable lengths are then calculated as the shortest paths using A*

for all candidate OSS locations in $\widetilde{\mathcal{N}}^{\wedge *\prime}$. The lowest cost topology among the options is maintained.

Approximating the 3rd dimension in large systems

Solving the route finding problem for each candidate cable is computationally expensive as the graph size required to effectively capture bathymetry is large. For example with a 20m by 20m resolution, the required graph size for a small offshore region such as Belgium contains over 2^{14} nodes. Deducting no-go zones does reduce the problem size, but still network graphs of tens of millions of edges (over 32 million in the case of Belgium) remain. This results in computation times in the order of 10 to 15 seconds per shortest path calculation using the light graphs [207] implementation of A^* in julia [208], making some larger problem sizes intractable.

For large offshore regions two approximations of the full 3D implementation termed (A1) and (A2) are proposed.

- (A1) approximates the 3D path from the 2D Euclidean distance via a look up table as in Table 6.1 where $l_{mn}^{3\mathrm{d}} = \sum\limits_{e \in r_{m,n}} \|e\|$ and $l_{mn}^{2\mathrm{d}} = \sqrt{(x_n - x_m)^2 + (y_n - y_m)^2)}$. The appropriate multiplier in Table 6.1 is located by finding the start (column) and end (row) nodes with (x, y) coordinates that are closest to the start and end points of the route under consideration. Calculating Table 6.1 has a negligible impact on computation time as all the shortest paths are calculated as part of the OSS candidate locating algorithm of section 6.2.3.

Table 6.1: Multipliers for 3D approximation.

	g_1	...	g_n	$d_{1'}$	...	d_m
g_1	1	...	$\frac{l_{1n}^{3\mathrm{d}}}{l_{1n}^{2\mathrm{d}}}$	$\frac{l_{11'}^{3\mathrm{d}}}{l_{11'}^{2\mathrm{d}}}$	...	$\frac{l_{1m}^{3\mathrm{d}}}{l_{1m}^{2\mathrm{d}}}$
...	...	...	...	...	...	...
g_n	$\frac{l_{n1}^{3\mathrm{d}}}{l_{n1}^{2\mathrm{d}}}$	...	1	$\frac{l_{n1'}^{3\mathrm{d}}}{l_{n1'}^{2\mathrm{d}}}$	...	$\frac{l_{nm}^{3\mathrm{d}}}{l_{nm}^{2\mathrm{d}}}$
$d_{1'}$	$\frac{l_{1'1}^{3\mathrm{d}}}{l_{1'1}^{2\mathrm{d}}}$	...	$\frac{l_{1'n}^{3\mathrm{d}}}{l_{1'n}^{2\mathrm{d}}}$	1	...	n/a
...	...	...	...	...	...	...
d_m	$\frac{l_{m1}^{3\mathrm{d}}}{l_{m1}^{2\mathrm{d}}}$	...	$\frac{l_{mn}^{3\mathrm{d}}}{l_{mn}^{2\mathrm{d}}}$	n/a	...	1

- (A2) The second approximation is of the nodes where the medium voltage circuit collection point occurs. Recall that these nodes are calculated explicitly when solving the route finding problem as $\mathcal{N}^{\text{GD}}$ and $\mathcal{N}^{\text{GG}}$. During greedy search, however, as new candidate medium voltage connections are analyzed these nodes are unknown without solving for the shortest path. Not accounting for the length of the collection circuit results in an overestimate of the required medium voltage cable. The proposed approximation is to deduct the radius of the target concession from the total length of medium voltage cable. As concessions are not perfect circles, however, the radius is defined as the average Euclidean distance between a cluster's centroid ($\bar{n}_g$) and the nodes lying on its perimeter.

6.2.5 Topological MIP

The mixed integer program presented in this section is structured to fulfill two principle objectives. First, as discussed earlier in this work, a principal difference between traditional TNEP and OW-TNEP is the green field nature of the problem. This feature, coupled with the poor scalability of large numbers of binary decision variables, means the typical formulation for the TNEP, where each piece of candidate equipment has a binary decision variable assigned to it, can rapidly experience intractability as the problem size increases. The following formulation attempts to solve this issue and increase scalability by assigning a single binary variable to a radial topology rather than the component equipment of the topology. Secondly, when multiple voltage levels, or more than one PCC are considered, the greedy search algorithm results in a set of topologies $\boldsymbol{T}^{\text{H}*}_{d,v}$ for each voltage–PCC combination, where d and v subscripts refer to a PCC $d \in \boldsymbol{D}$ and transmission voltage $v \in \boldsymbol{V}$ respectively. There is an optimal combination of radial topologies within these various $\boldsymbol{T}^{\text{H}*}_{d,v}$ which form the lowest cost network. Finding the optimal combination of radial topologies when considering more than a single voltage level or PCC is the second objective of the formulation.

For the purpose of the following formulation $\boldsymbol{T}^{\text{H}*}$ is considered the union of all $\boldsymbol{T}^{\text{H}*}_{d,v}$ over all PCCs and voltage levels, i.e.

$$\boldsymbol{T}^{\text{H}*} = \bigcup_{d \in D, v \in V} \boldsymbol{T}^{\text{H}*}_{d,v}. \tag{6.6}$$

G is a set of n OWPPs g, each with a maximum generating capacity of $P_g^{\mathrm{g,max}}$ and D is a set of m PCCs with a demand less than or equal to $P_d^{\mathrm{d,max}}$ as in:

$$G = \{g_i, i \in \mathbb{Z}_{\geq 0} : i < n\}$$

$$D = \{d_k, k \in \mathbb{Z}_{\geq 0} : k < m\} \tag{6.7}$$

$$P_g^{\mathrm{g}} = P_g^{\mathrm{g,max}} \text{ and } P_d^{\mathrm{d}} \leq P_d^{\mathrm{d,max}}.$$

A set of auxiliary buses B are defined. The auxiliary buses j are represented by n-length binary strings such that the value b_i of bit position $i \in j$ is one if OWPP g_i is connected within the topology $t_j^{\mathrm{h}*}$:

$$B = \{j \in \mathbb{N}_2^n : 0 < j \leq 2^n - 1\}. \tag{6.8}$$

$\ell_{g_i,j} \in S^\ell$ are transmission lines connecting OWPP g_i to auxiliary bus j with maximum transmission capacity $P_{g_i,j}^{\ell,\mathrm{max}}$ equal to $P_{g_i}^{\mathrm{g,max}}$ as in:

$$S^\ell = \{\ell_{g_i,j} : b_i = 1, \ \ j \in B, \ \ i \in j\}$$

$$0 \leq P_{g_i,j}^\ell \leq P_{g_i,j}^{\ell,\mathrm{max}} = P_{g_i}^{\mathrm{g,max}}. \tag{6.9}$$

$\widetilde{\alpha}_{j,d,v} \in \widetilde{S}^\ell$ are candidate transmission lines connecting auxiliary bus j to PCC d with maximum transmission capacity $\widetilde{P}_{jd}^{\ell,\mathrm{max}}$ equal to the sum of OWPPs connected at bus j as in:

$$\widetilde{S}^\ell = \{\widetilde{\alpha}_{j,d,v} : j \in B, \ \ d \in D, \ \ v \in V\}, \ \ \widetilde{\alpha}_{j,d,v} = \{0,1\},$$

$$0 \leq \widetilde{P}_{j,d,v}^\ell \leq \sum_{i \in j^+} P_{g_i}^{\mathrm{g,max}}, \tag{6.10}$$

where $j^+ = \{i \in j : b_i = 1\}$. There is a single transmission line for each topology in $T^{\mathrm{H}*}$. Each candidate transmission line has a cost of construction $c_{j,d,v}$ that is equal to the cost of topology $t_{j,d,v}^{\mathrm{h}*}$. The optimization objective is to minimize the total cost of the transmission lines as in:

$$\min\Big(\sum_{\widetilde{\alpha}_{j,d,v} \in \widetilde{S}^\ell} \widetilde{\alpha}_{j,d,v} c_{j,d,v}\Big) \tag{6.11}$$

such that nodal power balance and PCC injection capacity limits are respected:

$$\sum_{j \in \boldsymbol{B}} P_{g,j}^{\ell} = P_g^{\mathrm{g,max}} \mid g \in \boldsymbol{G}$$

$$\sum_{\substack{d \in \boldsymbol{D}, \\ v \in \boldsymbol{V}}} \widetilde{\alpha}_{j,d,v} \widetilde{P}_{j,d,v}^{\ell} = \sum_{g \in \boldsymbol{G}} P_{g,j}^{\ell} \mid j \in \boldsymbol{B} \qquad (6.12)$$

$$\sum_{j \in \boldsymbol{B}} \widetilde{\alpha}_{j,d,v} \widetilde{P}_{j,d,v}^{\ell} \leq P_d^{\mathrm{d,max}} \mid d \in \boldsymbol{D}, \; v \in \boldsymbol{V}.$$

Costs of topologies are calculated as in Appendix A, including equipment procurement and installation as well as the net present value of losses, corrective maintenance and EENT considering a 25 year lifetime.

6.3 Case Study - Belgian Exclusive Economic Area

To test the proposed method designs for the Belgian EEA are calculated considering the full size problem as well as the proposed approximations (A1) and (A2). A 25 year lifespan and a discount rate of 4% is assumed. The resulting designs are compared based on overall cost and computation time. The assumed development timeline is that from the actual Belgian offshore. Zone 1 is developed first, followed by zones 2 and 3 simultaneously. In this way the maximum problem size in a single time step is 8-OWPPs, well within the feasible problem size of the unmodified greedy search algorithm. For larger problem sizes the proposed approach of chapter 5 may be necessary.

6.3.1 Domain and boundary conditions

The Belgian EEA including bathymetric data, PCCs, development zones, concessions, turbines and obstacles is shown in Fig. 6.4. The no-go zones are left white. The bathymetric and marine spatial planning data are sourced from [176]. This includes the outer boundaries of the zones but not the boundaries of the individual concessions or the turbine locations. In particular, for zones 2 and 3 this has yet to be finalized with an ongoing debate as to whether an extension of the module offshore grid 2 [209] should be implemented or an "energy island" [149] concept [1]. To deal with this deficiency the following approximations are made.

---

[1] This debate has since been settled in favour of an energy island [155].
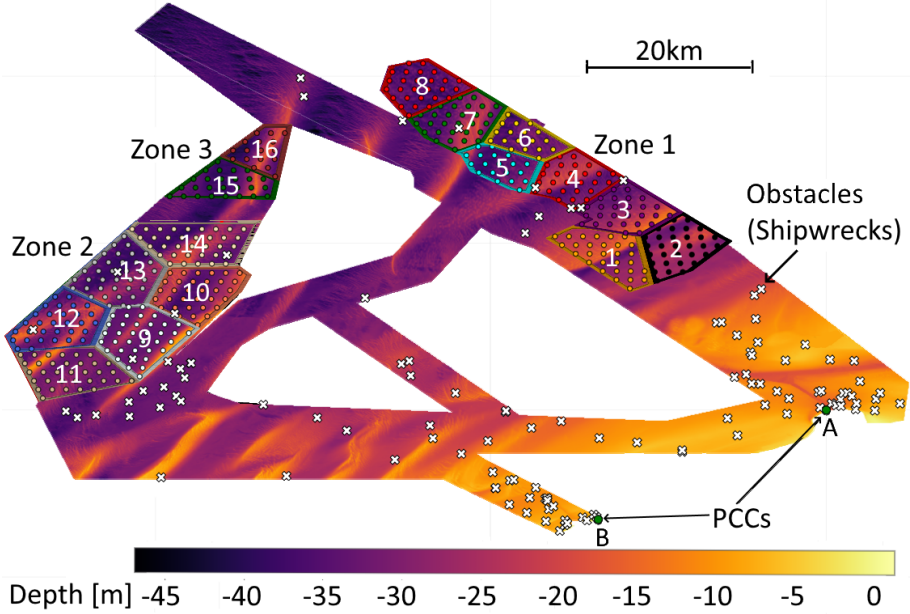
Figure 6.4: Belgian bathymetry, sea based renewables regions 1, 2 and 3, designated cable ways, PCCs and under water obstacles.

The boundaries of the OWPP concessions were determined using the k-means clustering method [210] on the (x, y) coordinates of nodes $n \in \mathcal{N}^z$ for $k = 16$ concessions, where $\mathcal{N}^z$ are the nodes within the boundaries of the three zones. 10 MW turbines were then laid out within each concession considering a wind energy density of 9.5 MW/km². The turbines are shown in the figure as points of the same colour as their parent concession. This spacing results in an overall peak generation capacity of 4.57 GW. A breakdown of capacity by individual concession is provided in Table 6.2. A service area between turbines of neighbouring concessions equal to two times the turbine spacing (≈ 2 km) is guaranteed. The two PCCs are in Zeebruges (A) and Oostende (B). A dimensioning incident of 3 GW is assumed, hence, this is the maximum that can be connected to a single PCC ($P_d^{d,\max}$). The white crosses in the figure are shipwrecks or unexploded ordinance that must be avoided.

Table 6.2: Capacities of individual concessions within zones 1, 2 and 3 of the Belgian offshore.

OWPP	1	2	3	4	5	6	7	8	9	10	11	12	13	14	15	16
MVA	290	310	270	270	190	180	290	270	330	380	370	360	320	310	260	170

6.3.2 OSS Candidates

With the domain defined, the set of all shortest paths, R, is calculated. In Fig. 6.5 these are shown in reference to PCC-A only as black lines. The candidate OSS locations, $\mathcal{N}^{\wedge *}$ are then found. Candidate OSS locations are shown as small crosses in Fig. 6.5 lying near to the shortest routes and clustered around the elevated regions. $\mathcal{N}^{\wedge *}$ was calculated assuming values of 1 km for δr and 1.4 m/km for Δs.

Both these parameters do require some case specific tuning. The number of candidate OSS selected is inversely proportional to their size. The value of δr was chosen to match approximately the spacing of the turbines. Δs was chosen by solving for topology t_j^{b} considering $j = [0000\ 0000\ 0000\ 1111]$ with no bathymetry, i.e. OWPPs 1, 2, 3 and 4. The location of the OSS was then shifted 1 km in the +/-x and +/-y directions and the average increase in cabling cost incurred from shifting the OSS away from the point of minimized cable cost calculated. The smaller these values are the more candidate locations are chosen and the higher the likelyhood the optimal location is not passed over.
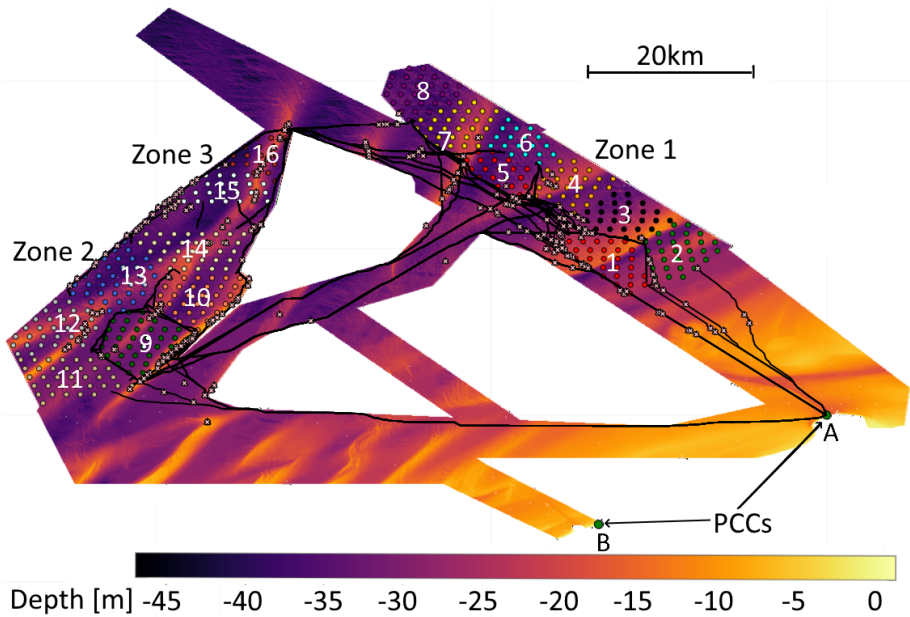
Figure 6.5: Belgian Offshore - Shortest paths and candidate OSS locations.

6.3.3   Results

When solving the full size spatial planning model with no approximations for the shortest paths, the hybrid greedy - MIP optimization finds a topology of cost 2285.6 M€, This is shown in Fig. 6.6. Four OSSs labelled A through D have been built, with capacities in alphabetical order of 540 MVA, 930 MVA, 1760 MVA and 740 MVA. Each substation is located in water of depth 12 m or less. The OSSs are connected to the PCCs by four 220 kV transmission corridors
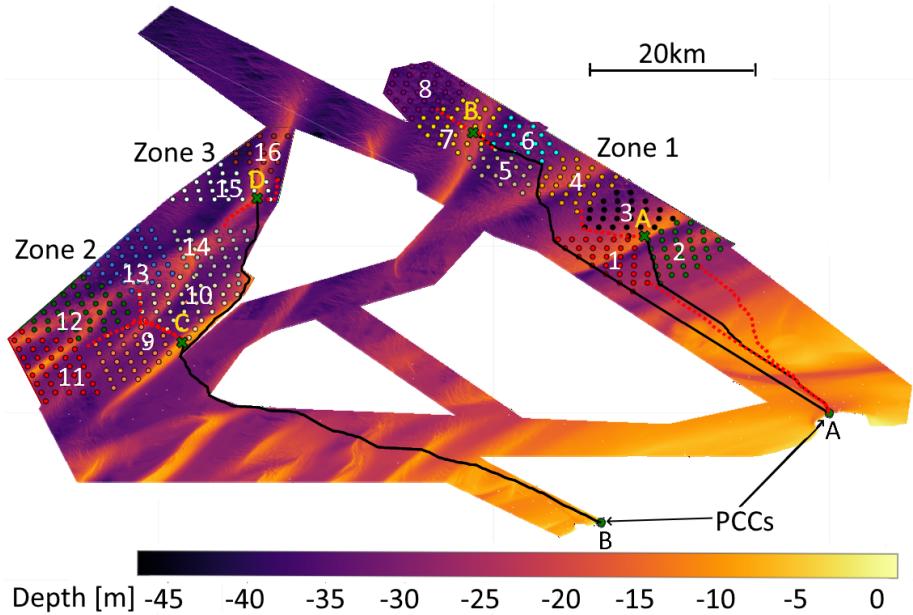
Figure 6.6: Optimal Solution for the Belgian offshore wind development zone. 220 kV cables are shown in black while 66 kV cables in red. OSSs are shown as green crosses and labelled A through D.

with cables as specified in Table 6.3. The dimentioning incidents of the PCCs are respected as PCC-A serves 2070 MVA exclusively from Zone 1 OWPPs and PCC-B serves 2500 MVA exclusively from zones 2 and 3 OWPPs. In Zone 1, OWPPs 1 and 2 are connected directly to the PCC at 66 kV. The connection points to the collection circuit are well defined, minimizing the required cable to reach the OSS (or PCC). The required CAPEX and OPEX is summarized in Table 6.4. CAPEX corresponds to slightly over three quarters of the total cost. All results were obtained on a standard Dell lap-top with an intel core-7 1.9 GHz processor and 16 GB of RAM.

Table 6.3: Selected 220 kV cables per solution topology.

Connection	km	n-mm^2	M€
Full			
OSSA-PCC1	27	2-500	79.3
OSSB-PCC1	46	4-400	216.7
OSSC-PCC2	43	6-630	358.9
OSSD-PCC2	70	3-500	251.2
(A1)+(A2)			
OSSA-PPC1	41	2-400	96.6
OSSB-PPC1	46	3-400	162.5
OSSC-PPC2	43	6-630	358.9
OSSD-PCC2	70	3-500	251.2

Table 6.4: Objective function values and computation times for the 3 optimizations.

	Full	(A1)	(A1)+(A2)
Objective [M€]			
CAPEX	1737.5	1737.5	1741.7
OPEX	548.1	548.1	569.8
Total	2285.6	2285.6	2311.5
Computation time [minutes]			
Domain	40.2	40.2	40.2
T^{H^*}	6720.1	3035.2	44.3
MIP	0.2	0.2	0.2
Post Process	3.7	3.7	3.7
Total	6764.2	3079.32	88.4

CAPEX: Procurement and Installation.
OPEX: Corrective Maintenance, EENT and Losses.

6.3.4 3D Approximations

Solving the route finding problem for all cable length calculations is computationally expensive taking approximately 4.7 days. A breakdown of the computation times of contributing calculations is provided in Table 6.4.

The vast majority of the computation time is consumed during the greedy search when calculating T^{H^*} as the route finding algorithm is run every time a cable length is calculated. While for a long term planning problem such high computation times are acceptable, for development zones larger than Belgium the problem may prove to be intractable. As such the proposed approximations

are tested as follows:

1. Approximation (A1) only: for route lengths the lookup table of 3D/2D ratios as in 6.1 is used but collection circuit connection points are calculated explicitly using route finding.

2. Both approximation (A1) and (A2): Route finding is only used to calculate $\mathcal{N}^{\wedge*}$ and on the final solution topology.

When using approximation (A1) the same solution topology results and the computation time is approximately cut in half. This is a good result, but computation times are still relatively high.

The results are summarized in Table 6.4. When both approximations are used, a different topology that is slightly more expensive results $(+1.1\%)$. This is below the uncertainty of the economic model. The gain in computation time is substantial though with a solution being found in less than 2 hours. About half of the computation time is now dedicated to the set up of the domain. This trade off of computational effort for solution quality is acceptable for large intractable problems. The resulting solution topology is shown in Fig. 6.7. We see that zones 2 and 3 are identical to Fig. 6.6. The difference arises in zone 1. Again two OSSs are built, but the location of OSS A is different and both OSSs are of a smaller capacity. OSS A is 460 MVA and OSS B, 740 MVA. 220 kV transmission is still the best option. The selected 220 kV cables are specified in Table 6.3. It is possible to have smaller OSSs as now OWPP 3 in addition to 1 and 2 is connected to shore at 66 kV.

It is important to point out that the computational times for T_H^*, although relatively lengthy for the full size problem, encompass various scenarios involving both 400 kV and 220 kV, along with potential connections to either PCC. These scenarios are entirely independent of each other. Consequently, the problem can be readily decomposed into parallel calculations along these lines. In the case of Belgium, this decomposition leads to a reduction in overall computation time by a factor of four.

6.4 Conclusions

Careful consideration is required when selecting constraints to improve the accuracy of the candidate infrastructure selection process. Chapter 6 provides an illustration of this concept by incorporating bathymetric data and marine spatial planning to narrow down the potential locations for OSS candidates.
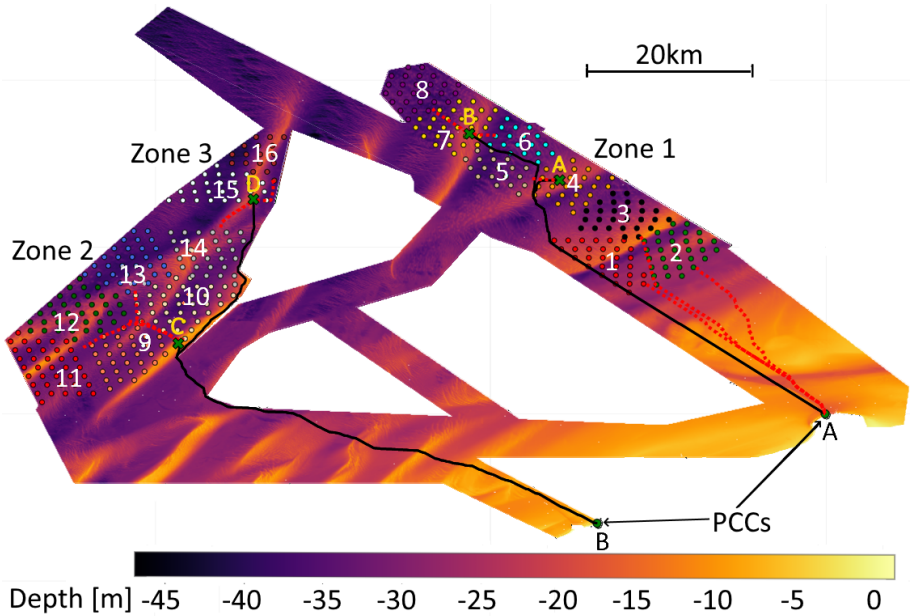
Figure 6.7: Optimal Solution for the Belgian offshore wind development zone using approximations (A1) and (A2). 220 kV cables are shown in black while 66 kV cables in red. OSSs are shown as green crosses and labelled A through D.

This chapter proposes an extension to the greedy search OW-TNEP formulation that allows for highly non-linear spatial constraints. When planning offshore transmission networks, it is crucial to consider complex marine spatial planning requirements imposed by authorities, which can include restrictions on areas reserved for military, ecological, and fishing purposes where electrical infrastructure cannot be located.

To address these challenges, ad-hoc methods are proposed that can be adapted to specific circumstances. First, a candidate OSS locating algorithm is proposed, which finds candidate locations for OSSs that balance optimal placement based on both minimal cable cost and minimized investment in OSS foundations. This is accomplished by identifying shallow locations that lie along the shortest paths between candidate connections.

To ensure cable routing is done while avoiding no-go zones and regions where it is undesirable, a penalty function in combination with the A* route finding algorithm is implemented. Since solving the route finding algorithm recursively is computationally demanding, two approximations of the full-size 3D spatial

planning model are proposed and compared to the full-size problem on the real-world test case of the Belgium EEA.

All three methods' resulting solution topologies are shown to be very close in quality, with the first approximation alone finding the identical solution to the full-size problem. Applying both approximations results in a topology with only a small (+1.1%) increase in total cost. However, the impact of the approximations on total computation time is significant, with using the first approximation alone resulting in a computation time half that of the full-size algorithm and applying both approximations simultaneously resulting in a reduction of 76 times.

Chapter 7

Generation and transmission planning in nodal and zonal market designs

7.1 Introduction

In this chapter[1], the proposed OW-GATE formulation of planning stages L.1 through L.4 is presented. The objective focuses on the grid level $\mathcal{G}^{\mathrm{L}}$ and the problem aims to determine the transmission topology, macro location and capacity of OWPPs as well as the timeline over which the network should be developed.

The highest portion of the offshore wind development takes place in the North Sea area bordered by many different countries. The expectation for the coming decades is the interconnection of the North Sea countries via a meshed transmission grid to further facilitate offshore wind development by providing flexible interconnection [16]. In the context of such a massive green field development the choice of the market design itself becomes a degree of freedom, i.e. a decision variable. Particularly for so-called Hybrid Offshore Assets (HOA), the

---

[1]The work of this chapter has been published as: *Stephen Hardy, Hakan Ergun and Dirk Van Hertem, 'Generation and transmission expansion planning under Zonal and Nodal market mechanisms,'*, in the Journal IEEE Transactions on Energy Markets, Policy and Regulation – under review. The content of the paper has been modified here to make it consistent with the other chapters of this dissertation. The first author is the main author of the paper.

choice of market design has become a topic of frequent debate. HOAs combine multiple assets that have been traditionally treated in isolation such as OW-PPs, interconnectors and storage into a single asset, leading to a more holistic planning approach.

In the liberalized energy markets of Europe and North America both nodal and zonal market designs are found. In Europe a zonal market clearing approach is adopted, whereas in North America a local marginal pricing approach, i.e. a nodal market design is implemented. At the macro scale of grid level $\mathcal{G}^{\mathrm{L}}$, the modelling of the market becomes crucial as it determines the future revenues of all actors involved.

There are three competing concepts for the market design of HOAs: a Home Market Design (HMD), a zonal Offshore Bidding Zone (zOBZ) and a nodal Offshore Bidding Zone (nOBZ). In a HMD, HOAs are included in the energy market of the Exclusive Economic Area (EEA) within which they are located. In a zOBZ, a new offshore market zone is defined and all HOAs within its boundary are within a common market. In a nOBZ each HOA is considered its own market and fully localized marginal pricing is employed.

The resulting formulation as is presented below is in the form of a stochastic, multi-level, step-wise, mixed integer linear program. The model is capable of handling both AC and DC transmission expansion planning as well as generation expansion planning and can do so under both nodal and zonal market designs.

7.2 Nodal versus zonal markets

The benefits of localized marginal pricing (nodal) are well known [211]. Localized pricing provides a high quality signal to identify the most beneficial investments. For TSOs not only can essential expansions or reinforcements to the transmission network be identified but they can also be funded via the collection of congestion rent. Private investment in generation is also more effectively allocated as developers are properly incentivized to build new generating facilities where energy prices are highest due to system congestion.

The use of zonal markets partially suppresses these signals making investment decisions more difficult to identify. Despite the well known benefits of nodal pricing it is possible to find practical examples where zonal markets provide an arguably more appealing market outcome for consumers. To illustrate this the pivotal supplier example is presented.

The pivotal supplier problem can be understood by considering a topology similar to that in Fig. 7.1 and comparing the result of a market cleared nodally

with one cleared zonally. The initial dispatch, redispatch and cost of meeting load for each market design is summarized in the associated table. In this example the market is day ahead pay as cleared (uniform pricing method) [212]. When in the zonal market, redispatch is necessary, then it is accomplished by regulatory redispatch with cost compensation (RDCC) [211].

In regulatory redispatch with cost compensation the balancing authority is considered an all knowing and all powerful entity. The balancing authority directs down and up regulation perfectly. Those required to up regulate are compensated at their marginal rate. Those required to down regulate are obligated to return the cost of any variable expenses avoided (e.g. fuel) but may keep any profits above this made from the initial auction. Participants are assumed to be honest and transparent and bid at their marginal rate. For the wind and solar generation, the marginal rate is assumed as 10 €/MWh. For natural gas it is 100 €/MWh.
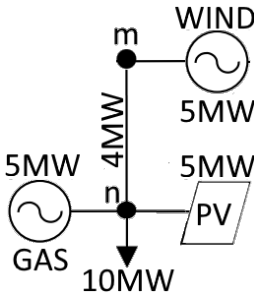
	P^g_{WIND} [MW]	P^g_{PV} [MW]	P^g_{GAS} [MW]	Cost [€]
Nodal				
ID	4.0	5.0	1.0	640
Zonal				
ID	5.0	5.0	0.0	100
RD	-1.0	0.0	1.0	100
			Zonal total:	200
ID: initial dispatch RD: redispatch				

Figure 7.1: Single line diagram of simple market clearing topology (left). Dispatch and redispatch amounts and costs in nodal and zonal market clearing mechanisms (right).

In the nodal market the transmission constraint of 4 MW between nodes m and n is considered when dispatching generation. As such the 10 MW demand at node n is met by 5 MW of solar, 4 MW of wind and 1 MW of gas. The resulting clearing prices are 10 €/MWh at node m and 100 €/MWh at node n. The total cost of meeting demand is therefore 640 €.

In the zonal market clearing design optimal dispatch is performed without the consideration of the intra-zonal congestion of 4 MW. This results in an initial dispatch of 5 MW of both wind and solar and a market clearing price of 10 €/MWh at each node. The cost after intial dispatch is 100 €. The initial dispatch, however, is not feasible due to the transmission constraint and redispatch must be performed. The balancing authority therefore directs the wind generator to down regulate 1 MW and the gas generator to up regulate

1 MW. No variable costs are avoided by the wind generator and the gas generator is compensated at its marginal rate. The cost of redispatch is 100 € and the total cost of meeting demand is 200 €.

It can be argued that an energy bill of 200 € rather than 640 € is a more desirable outcome. Of course, it can also be argued that the high energy price at node n is beneficial to either encourage further private investment in generation at node n or to fund increased transmission capacity via congestion rent. This should eventually result in lower prices at n, having actually solved the root problem causing the high energy price.

This perspective is correct, however, in a system with a high penetration of fluctuating RES, high clearing prices may in part be caused by unusually low wind or solar irradiation. Investments must therefore consider the root cause, or in this case, the expected frequency of the high energy prices.

7.3 Nodal market GATE planning model

The developed model is based on the one first presented in [26] with the principle additions being the consideration of benefits, rather than costs alone, the ability to expand generation and the inclusion of multiple market designs. The Gurobi solver version 0.9.14 [194] is used when solving the MILP.

7.3.1 Objective Function

Four agents participate in a centrally planned optimization. $\mathcal{A}_{\mathrm{w}}$, an OWPP developer is in charge of generation expansion (7.1). $\mathcal{A}_{\mathrm{o}}$, an offshore transmission system developer is in charge of network expansion (7.2). $\mathcal{A}_{\mathrm{j}}$, a storage developer is in charge of storage expansion (7.3). $\mathcal{A}_{\mathrm{e}}$, an existing grid operator manages existing infrastructure (7.4). $\mathcal{A}_{\mathrm{w}}$, $\mathcal{A}_{\mathrm{o}}$ and $\mathcal{A}_{\mathrm{j}}$ make yearly investments while $\mathcal{A}_{\mathrm{e}}$ manages hourly costs and benefits which are redistributed among the agents. The NPV equivalents of yearly and hourly quantities are obtained by scalars f_y^{Y} and f_y^{H} respectively. A discount rate of 4% is assumed. The optimization variables for each agent, following the notational convention of $(\sim)$ for candidate and $(-)$ for existing infrastructure, are as follows:

- $\mathcal{A}_{\mathrm{w}}$: the hourly power output ($\widetilde{\boldsymbol{P}}^{\mathrm{g}}$) and maximum capacity ($\Delta \widetilde{\boldsymbol{P}}^{\mathrm{g,max}}$) for candidate OWPPs.

- $\mathcal{A}_{\mathrm{o}}$: the voltage angles ($\boldsymbol{\theta}$), binary decision variables for candidate transmission lines ($\boldsymbol{\alpha}^{\ell}$) and maximum capacity of candidate converters ($\Delta \boldsymbol{P}^{\zeta,\mathrm{max}}$).

- $\mathcal{A}_j$: the hourly power injected ($\boldsymbol{P}^{j,inj}$) or absorbed ($\boldsymbol{P}^{j,abs}$) and the maximum energy capacity ($\Delta \boldsymbol{E}^{j,max}$) of storage devices. The maximum power rating of storage devices is a parameter defined as a fraction of the energy capacity.

- $\mathcal{A}_e$: the hourly output of existing generators ($\bar{\boldsymbol{P}}^g$) and hourly consumption ($\boldsymbol{P}^u$).

Developer $\mathcal{A}_w$ can make a strategic yearly investment in expanded generation capacity (7.1a) in order to accrue hourly benefits by selling energy produced ($\widetilde{P}_g^g$) at a market clearing price (λ_n) above its cost of production (C_g^g). The marginal cost of production for an OWPP is assumed to be zero.

$$\mathcal{U}_{y,s}^w = -f_y^Y \Big[(7.1a) \Big] \tag{7.1}$$

$$\sum_{n \in \mathcal{N}^{AC}} \sum_{\widetilde{g} \in \widetilde{\mathcal{S}}_{g:n}} \delta I_{\underset{\sim}{g:n,y}}^g \cdot \Delta P_{\underset{\sim}{g:n,y}}^{g,max} \tag{7.1a}$$

Developer $\mathcal{A}_o$ can make a strategic yearly investment in increased transmission capacity. This can come in the form of new transmission lines (7.2a) or expanded HVDC converter capacity (7.2b) or both. Benefits are accrued through arbitrage opportunities between markets with a delta in their energy prices. This is also called congestion rent.

$$\mathcal{U}_{y,s}^o = -f_y^Y \Big[(7.2a) + (7.2b) \Big] \tag{7.2}$$

$$\sum_{\substack{\{mn\} \subseteq \mathcal{N} \\ mn \in \mathcal{E}}} \sum_{\widetilde{l} \in \widetilde{\mathcal{S}}_{\ell:\{mn\}}} \alpha_{\underset{\sim}{l:\{mn\},y}}^\ell \cdot I_{\underset{\sim}{l:\{mn\},y}}^\ell \tag{7.2a}$$

$$\sum_{ne \in \mathcal{E}^{AC\text{-}DC}} \delta I_{ne,y}^\zeta \cdot \Delta P_{ne,y}^{\zeta,max} \tag{7.2b}$$

Developer $\mathcal{A}_j$ also gains via arbitrage opportunities, however, the delta is temporal rather than locational and is exploited by supplying ($P_j^{j,inj}$) and absorbing power ($P_{j:n,t,y,s}^{j,abs}$) at different times with different market prices. The marginal cost of charging and discharging is assumed to be zero. $\mathcal{A}_j$ can increase benefits accrued by making a strategic yearly investment in storage capacity ($E^{j,max}$) as in (7.3a).

$$\mathcal{U}_{y,s}^j = -f_y^Y \Big[(7.3a) \Big] \tag{7.3}$$

$$\sum_{n \in \mathcal{N}} \sum_{j \in \mathcal{S}_{j:n}} \delta I_{j:n,y}^{j} \cdot \Delta E_{j:n,y}^{j,\max} \tag{7.3a}$$

The existing network operator has hourly costs and benefits associated with existing generation (7.4a) and consumption (7.4b). Existing generators accrue hourly benefits through the sale of energy $(P_{\bar{g}}^{g})$ on the spot market at a price (λ_n) higher than their marginal production cost $(C_{\bar{g}}^{g})$. Consumers benefit when the spot price of energy λ_n is lower than the consumer's bid price (C_u^{u}) resulting in a surplus.

$$\mathcal{U}_{y,s}^{e} = f_y^{H} \sum_{t \in \mathcal{S}_t} \left[(7.4a) + (7.4b) \right] \tag{7.4}$$

$$\sum_{n \in \mathcal{N}^{\mathrm{AC}}} \sum_{\bar{g} \in \bar{\mathcal{S}}_{g:n}} \left(-C_{\bar{g}:n,t,y,s}^{g} \right) \cdot P_{\bar{g}:n,t,y,s}^{g} \tag{7.4a}$$

$$\sum_{n \in \mathcal{N}^{\mathrm{AC}}} \sum_{u \in \mathcal{S}_{u:n}} C_{u:n,t,y,s}^{u} \cdot P_{u:n,t,y,s}^{u} \tag{7.4b}$$

Combining all agent objectives into a single function we get the overall optimization objective to maximize the social welfare of the system, $\mathcal{U}$, where social welfare is defined as the sum of gross consumer surplus, gross producer surplus (including storage) and congestion rent, minus investment costs:

$$\max_{\mathcal{A}_{w},\mathcal{A}_{o},\mathcal{A}_{j},\mathcal{A}_{e}} \mathcal{U} := \sum_{s \in \mathcal{S}_s} \pi_s \sum_{y \in \mathcal{S}_y} \mathcal{U}_{y,s}^{w} + \mathcal{U}_{y,s}^{o} + \mathcal{U}_{y,s}^{j} + \mathcal{U}_{y,s}^{e} \tag{7.5}$$

where

$$\mathcal{A}_{w} = \left(\widetilde{\boldsymbol{P}}^{g}, \Delta\widetilde{\boldsymbol{P}}^{g,\max} \right), \quad \mathcal{A}_{o} = \left(\boldsymbol{\theta}, \boldsymbol{\alpha}^{\ell}, \Delta\boldsymbol{P}^{\zeta,\max} \right),$$

$$\mathcal{A}_{j} = \left(\boldsymbol{P}^{j,\mathrm{inj}}, \boldsymbol{P}^{j,\mathrm{abs}}, \Delta\boldsymbol{E}^{j,\max} \right), \quad \mathcal{A}_{e} = \left(\bar{\boldsymbol{P}}^{g}, \boldsymbol{P}^{u} \right)$$

The outer summations over sets $\mathcal{S}_s$ and $\mathcal{S}_y$ capture the uncertainty of long term planning as well as the multi-period nature respectively. $\mathcal{S}_s$ is a set of stochastic scenarios of probability π_s and $\mathcal{S}_y$ the modelling years.

The stated objective aims to achieve a balance between modeling simplicity and the incorporation of relevant problem features. However, it is important to note that the revenue mechanisms assigned to agents are mere approximations of real-world scenarios, and their simplified structure may influence the overall findings. Specifically, the role of transmission developers is represented as

merchants who derive revenues from congestion rent, rather than through energy tariffs. Additionally, the UK is treated on par with other market zones and is considered part of the European internal energy market. Finally, it is worth mentioning that the distinction that offshore transmission development in the UK is carried out by a private entity, the offshore transmission owner, rather than the transmission system operator (TSO), is overlooked [179].

7.3.2 Constraints

Generation

The technical limits of RESs and conventional generation are enforced by:

$$0 \leq P^{\mathrm{g}}_{g:n,t,y,s} \leq \Psi^{\mathrm{g}}_{g:n,t,y,s} \cdot P^{\mathrm{g,max}}_{g:n,y}$$
$$n \in \mathcal{N}^{\mathrm{AC}}, \quad g \in \mathcal{S}_{\mathrm{g}:n}, \quad t \in \mathcal{S}_{\mathrm{t}}, \quad y \in \mathcal{S}_{\mathrm{y}}, \quad s \in \mathcal{S}_{\mathrm{s}} \tag{7.6}$$

Parameter Ψ^{g}_{g} is the per-unit generation time series for RESs. For conventional generators its value is always one. When considering candidate OWPPs, an upper limit on expansion is specified by $\widehat{P^{\mathrm{g,max}}_{\underset{\sim}{g}}}$. Additionally $P^{\mathrm{g,max}}_{\underset{\sim}{g}}$ may only increase or remain constant year over year as in:

$$P^{\mathrm{g,max}}_{\underset{\sim}{g}:n,y} \leq \widehat{P^{\mathrm{g,max}}_{\underset{\sim}{g}:n}}, \quad P^{\mathrm{g,max}}_{\underset{\sim}{g}:n,y-\Delta y} \leq P^{\mathrm{g,max}}_{\underset{\sim}{g}:n,y}$$
$$\widetilde{g} \in \widetilde{\mathcal{S}}_{\mathrm{g}:n}, \quad n \in \mathcal{N}^{\mathrm{AC}}, \quad y \in \mathcal{S}_{\mathrm{y}}. \tag{7.7}$$

Here Δy is the number of years between modelling years. It is enforced that in the first year $P^{\mathrm{g,max}}_{\underset{\sim}{g}:n,y-\Delta y}$ is zero.

Demand

Demand, too, must remain within its technical limitations. The upper limit of demand is set by the demand time series, Ψ^{u}_{u} as in:

$$0 \leq P^{\mathrm{u}}_{u:n,t,y,s} \leq \Psi^{\mathrm{u}}_{u:n,t,y,s}$$
$$n \in \mathcal{N}^{\mathrm{AC}}, \quad u \in \mathcal{S}_{\mathrm{u}:n}, \quad t \in \mathcal{S}_{\mathrm{t}}, \quad y \in \mathcal{S}_{\mathrm{y}}, \quad s \in \mathcal{S}_{\mathrm{s}} \tag{7.8}$$

The cost of load shedding is set to a large value ensuring it is only a last resort option.

Storage

The state of charge (E_j^{j}) of a storage device at time step Δt is set by:

$$E_{j:n,t,y,s}^{\mathrm{j}} = (1 - \gamma_{j:n}^{\mathrm{j}})^{\Delta t} E_{j:n,t-\Delta t,y,s}^{\mathrm{j}} + \Delta t (\eta_{j:n}^{\mathrm{j,abs}} P_{j:n,t,y,s}^{\mathrm{j,abs}} - \frac{P_{j:n,t,y,s}^{\mathrm{j,inj}}}{\eta_{j:n}^{\mathrm{j,inj}}}) \quad (7.9)$$

$$j \in \mathcal{S}_{\mathrm{j}:n}, \quad n \in \mathcal{N}^{\mathrm{AC}}, \quad t \in \mathcal{S}_{\mathrm{t}}^{*}, \quad y \in \mathcal{S}_{\mathrm{y}}, \quad s \in \mathcal{S}_{\mathrm{s}}.$$

$\mathcal{S}_{\mathrm{t}}^{*}$ includes all time steps except the first. $\eta_j^{\mathrm{j,inj}}$ and $\eta_j^{\mathrm{j,abs}}$ are respectively the discharge and charge efficiencies. γ_j^{j} is the self discharge rate. The state of charge must remain between zero and the maximum rating of the device $E_j^{\mathrm{j,max}}$ as in:

$$0 \leq E_{j:n,t,y,s}^{\mathrm{j}} \leq E_{j:n,y}^{\mathrm{j,max}}$$

$$n \in \mathcal{N}^{\mathrm{AC}}, \quad j \in \mathcal{S}_{\mathrm{j}:n}\, t \in \mathcal{S}_{\mathrm{t}}, \quad y \in \mathcal{S}_{\mathrm{y}}, \quad s \in \mathcal{S}_{\mathrm{s}}. \quad (7.10)$$

The maximum rating of the storage device can be expanded up to $\widehat{E_j^{\mathrm{j,max}}}$ but may only increase or remain constant year over year as in:

$$E_{j:n,y-\Delta y}^{\mathrm{j,max}} \leq E_{j:n,y}^{\mathrm{j,max}} \leq \widehat{E_{j:n}^{\mathrm{j,max}}}$$

$$n \in \mathcal{N}^{\mathrm{AC}}, \quad j \in \mathcal{S}_{\mathrm{j}:n}, \quad t \in \mathcal{S}_{\mathrm{t}}, \quad y \in \mathcal{S}_{\mathrm{y}}, \quad s \in \mathcal{S}_{\mathrm{s}}. \quad (7.11)$$

In the first year, $E_{j:n,y-\Delta y}$ is set to zero. The maximum rates at which a storage device can charge and discharge are set by the normalized charge and discharge rates: $\xi_j^{\mathrm{j,c}}$ and $\xi_j^{\mathrm{j,d}}$ as in:

$$0 \leq P_{j:n,t,y,s}^{\mathrm{j,abs}} \leq \xi_{j:n}^{\mathrm{j,c}} \cdot E_{j:n,y}^{\mathrm{j,max}}$$

$$0 \leq P_{j:n,t,y,s}^{\mathrm{j,inj}} \leq \xi_{j:n}^{\mathrm{j,d}} \cdot E_{j:n,y}^{\mathrm{j,max}} \quad (7.12)$$

$$n \in \mathcal{N}^{\mathrm{AC}}, \quad j \in \mathcal{S}_{\mathrm{j}:n}, \quad t \in \mathcal{S}_{\mathrm{t}}, \quad y \in \mathcal{S}_{\mathrm{y}}, \quad s \in \mathcal{S}_{\mathrm{s}}$$

The initial and final states of charge for storage are set to half capacity as in:

$$E_{j:n,1,y,s}^{\mathrm{j}} = \frac{E_{j:n,y}^{\mathrm{j,max}}}{2} + \eta_{j:n}^{\mathrm{j,abs}} P_{j:n,1,y,s}^{\mathrm{j,abs}} - \frac{P_{j:n,1,y,s}^{\mathrm{j,inj}}}{\eta_{j:n}^{\mathrm{j,inj}}}$$

$$E_{j:n,T,y,s}^{\mathrm{j}} = \frac{E_{j:n,y}^{\mathrm{j,max}}}{2} \quad (7.13)$$

$$n \in \mathcal{N}^{\mathrm{AC}}, \quad j \in \mathcal{S}_{\mathrm{j}:n}, \quad y \in \mathcal{S}_{\mathrm{y}}, \quad s \in \mathcal{S}_{\mathrm{s}}$$

The final constraint on storage is the requirement to that charging and discharging cannot happen simultaneously. In this model this constraint is not explicitly enforced as this would require introducing additional binary variables or non-linearities. Rather, the constraint is implicitly guaranteed by charge and discharge efficiencies that are less than one.

Network

Both AC and DC networks are modelled. This is done using the PowerModels(ACDC).jl packages in the Julia programming language [208, 213]. On the AC side a bus injection model is considered with linear 'DC' power flow:

$$P^{\ell}_{\bar{l}:mn,t,y,s} = \frac{b_{\bar{l}:\{mn\}}}{\tau}[\theta_{m,t,y,s} - \theta_{n,t,y,s}]$$

$$P^{\ell}_{\widetilde{l}:mn,t,y,s} = \frac{b_{\widetilde{l}:\{mn\}}}{\tau}[\widetilde{\theta}_{\widetilde{l}:mn,t,y,s} - \widetilde{\theta}_{\widetilde{l}:nm,t,y,s}]$$

(7.14)

$$mn \in \mathcal{E}^{\text{AC}}, \quad \bar{l} \in \bar{\mathcal{S}}^{\text{AC}}_{\ell:\{mn\}}, \quad \widetilde{l} \in \widetilde{\mathcal{S}}^{\text{AC}}_{\ell:\{mn\}}, \quad t \in \mathcal{S}_{\text{t}}, \quad y \in \mathcal{S}_{\text{y}}, \quad s \in \mathcal{S}_{\text{s}}.$$

Here, τ is the transformer ratio (equal to one when no transformer is present), θ_m is the voltage angle at node m and b_l is the susceptance of line l. The power flowing in transmission line l must remain within the technical limitations of the line. This is enforced for existing and candidate lines by:

$$|P^{\ell}_{\bar{l}:mn,t,y,s}| \leq P^{\ell,\text{max}}_{\bar{l}:\{mn\}}$$

$$|P^{\ell}_{\widetilde{l}:mn,t,y,s}| \leq P^{\ell,\text{max}}_{\widetilde{l}:\{mn\}} \cdot \alpha^{\ell}_{\widetilde{l}:\{mn\},y}$$

(7.15)

$$mn \in \mathcal{E}^{\text{AC}}, \quad \bar{l} \in \bar{\mathcal{S}}^{\text{AC}}_{\ell:\{mn\}}, \quad \widetilde{l} \in \widetilde{\mathcal{S}}^{\text{AC}}_{\ell:\{mn\}}, \quad t \in \mathcal{S}_{\text{t}}, \quad y \in \mathcal{S}_{\text{y}}, \quad s \in \mathcal{S}_{\text{s}}.$$

The nodal voltage angle must remain within the minimum and maximum range set by θ^{min} and θ^{max}. Furthermore there is a maximum allowable divergence, $\Delta\theta^{\text{max}}$, that may occur between angles. This acts as a proxy for dynamic stability constraints. These constraints for existing lines are:

$$\theta^{\text{min}} \leq \theta_{n,t,y,s} \leq \theta^{\text{max}}$$

$$|\theta_{n,t,y,s} - \theta_{m,t,y,s}| \leq \Delta\theta^{\text{max}}$$

(7.16)

$$mn \in \mathcal{E}^{\text{AC}}, \quad \widetilde{l} \in \widetilde{\mathcal{S}}^{\text{AC}}_{\ell:\{mn\}}, \quad t \in \mathcal{S}_{\text{t}}, \quad y \in \mathcal{S}_{\text{y}}, \quad s \in \mathcal{S}_{\text{s}}.$$

The same constraints for candidate lines are:

$$\theta^{\min} \leq \widetilde{\theta}_{\widetilde{l}:mn,t,y,s} \leq \theta^{\max}$$

$$|\widetilde{\theta}_{\widetilde{l}:mn,t,y,s} - \widetilde{\theta}_{\widetilde{l}:nm,t,y,s}| \leq \Delta\theta^{\max}$$

$$|\widetilde{\theta}_{\widetilde{l}:mn,t,y,s} - \theta_{m,t,y,s}| \leq (1 - \alpha^{\ell}_{\widetilde{l}:\{mn\},y}) \cdot M$$

$$mn \in \mathcal{E}^{\mathrm{AC}} \ , \widetilde{l} \in \widetilde{\mathcal{S}}^{\mathrm{AC}}_{\ell:\{mn\}} \ , t \in \mathcal{S}_{\mathrm{t}}, \ \ y \in \mathcal{S}_{\mathrm{y}}, \ \ s \in \mathcal{S}_{\mathrm{s}}.$$

(7.17)

The additional constraint required for candidate lines is necessary as candidate angles are only considered when the line itself is active, i.e. $\alpha^{\ell} = 1$. M must be a sufficiently large angle to ensure the constraint is non-binding when $\alpha^{\ell} = 0$. It is set to π within the model.

HVDC converters link the AC and DC networks. The maximum AC side converter capacity, $P^{\zeta,\max}$, may be expanded up to a maximum of $\widehat{P^{\zeta,\max}}$. $P^{\zeta,\max}$ can only increase or remain constant year over year as in:

$$|P^{\zeta,\mathrm{AC}}_{ne,t,y,s}| \leq P^{\zeta,\max}_{ne,y}$$

$$P^{\zeta,\max}_{ne,y-\Delta y} \leq P^{\zeta,\max}_{ne,y} \leq \widehat{P^{\zeta,\max}_{ne}}$$

(7.18)

$$ne \in \mathcal{E}^{\mathrm{AC\text{-}DC}}, \ \ t \in \mathcal{S}_{\mathrm{t}}, \ \ y \in \mathcal{S}_{\mathrm{y}}, \ \ s \in \mathcal{S}_{\mathrm{s}}.$$

Converters have non negative losses, L^{ζ}, that link DC side power to the AC side. DC side power is constrained as in:

$$P^{\zeta,\mathrm{DC}}_{en,t,y,s} \leq (1 - L^{\zeta})P^{\zeta,\max}_{ne,y}$$

$$(L^{\zeta} - 1)P^{\zeta,\max}_{ne,y} \leq P^{\zeta,\mathrm{DC}}_{en,t,y,s}$$

$$P^{\zeta,\mathrm{loss}}_{ne,t,y,s} = L^{\zeta} P^{\zeta,\mathrm{AC}}_{ne,t,y,s} \geq 0$$

(7.19)

$$P^{\zeta,\mathrm{AC}}_{ne,t,y,s} + P^{\zeta,\mathrm{DC}}_{en,t,y,s} = P^{\zeta,\mathrm{loss}}_{ne,t,y,s}$$

$$ne \in \mathcal{E}^{\mathrm{AC\text{-}DC}}, \ \ t \in \mathcal{S}_{\mathrm{t}}, \ \ y \in \mathcal{S}_{\mathrm{y}}, \ \ s \in \mathcal{S}_{\mathrm{s}}.$$

Linearized power flow is also used for the DC network which reduces to a network flow model:

$$P^\ell_{\bar{l}:ef,t,y,s} = -P^\ell_{\bar{l}:fe,t,y,s}$$

$$P^\ell_{\widetilde{l}:ef,t,y,s} = -P^\ell_{\widetilde{l}:fe,t,y,s} \tag{7.20}$$

$$ef \in \mathcal{E}^{\text{DC}}, \quad \bar{l} \in \bar{\mathcal{S}}^{\text{DC}}_{\ell:\{ef\}}, \quad \widetilde{l} \in \widetilde{\mathcal{S}}^{\text{DC}}_{\ell:\{ef\}}, \quad t \in \mathcal{S}_{\text{t}}, \quad y \in \mathcal{S}_{\text{y}}, \quad s \in \mathcal{S}_{\text{s}}.$$

As with AC lines, the power flow through DC transmission lines is constrained to the thermal limit of the cable. For existing and candidate lines this is expressed as:

$$|P^\ell_{\bar{l}:ef,t,y,s}| \le P^{\ell,\max}_{\bar{l}:\{ef\}}$$

$$|P^\ell_{\widetilde{l}:ef,t,y,s}| \le P^{\ell,\max}_{\widetilde{l}:\{ef\}} \cdot \alpha^\ell_{\widetilde{l}:\{ef\},y} \tag{7.21}$$

$$ef \in \mathcal{E}^{\text{DC}}, \quad \bar{l} \in \bar{\mathcal{S}}^{\text{DC}}_{\ell:\{ef\}}, \quad \widetilde{l} \in \widetilde{\mathcal{S}}^{\text{DC}}_{\ell:\{ef\}}, \quad t \in \mathcal{S}_{\text{t}}, \quad y \in \mathcal{S}_{\text{y}}, \quad s \in \mathcal{S}_{\text{s}}$$

The final network constraints to discuss are the nodal power balance equations. On the AC side this equation is a complicating constraint as it links the optimization variables of all agents. The dual variable of the AC power balance constraint is λ_m, the marginal price of energy. AC power balance is enforced by:

$$\left.\begin{aligned} &\sum_{e \in \mathcal{N}^{\text{DC}}_m} P^{\zeta,\text{AC}}_{me,t,y,s} - \sum_{n \in \mathcal{N}^{\text{AC}}_m} \sum_{l \in \mathcal{S}^{\text{AC}}_{\ell:\{mn\}}} P^\ell_{l:mn,t,y,s} \\ &+ \sum_{g \in \mathcal{S}_{\text{g}:n}} P^{\text{g}}_{g:m,t,y,s} - \sum_{u \in \mathcal{S}_{\text{u}:n}} P^{\text{u}}_{u:m,t,y,s} \\ &+ \sum_{j \in \mathcal{S}_{\text{j}:n}} P^{\text{j,inj}}_{j:m,t,y,s} - \sum_{j \in \mathcal{S}_{\text{j}:n}} P^{\text{j,abs}}_{j:m,t,y,s} = 0 \end{aligned}\right\} \begin{aligned} &m \in \mathcal{N}^{\text{AC}} \\ &t \in \mathcal{S}_{\text{t}} \\ &y \in \mathcal{S}_{\text{y}} \\ &s \in \mathcal{S}_{\text{s}} \\ &(: \lambda_{m,t,y,s}) \end{aligned} \tag{7.22}$$

Here, $\mathcal{N}^{\text{AC}}_m := \{n \in \mathcal{N}^{\text{AC}} : mn \in \mathcal{E}^{\text{AC}}\}$ and $\mathcal{N}^{\text{DC}}_m := \{e \in \mathcal{N}^{\text{DC}} : me \in \mathcal{E}^{\text{AC-DC}}\}$ are the AC and DC neighbors of $m \in \mathcal{N}$ respectively. The DC network side equivalent is non-complicating. The dual variable of the DC nodal power balance equation indicates the marginal price of supplying energy to the DC side of the node, however, as there is no generation or consumption on the DC side it is not used within the model. The DC nodal power balance constraint is:

$$\sum_{m \in \mathcal{N}^{\text{AC}}_e} P^{\zeta,\text{DC}}_{em,t,y,s} + \sum_{f \in \mathcal{N}^{\text{DC}}_e} \sum_{l \in \mathcal{S}^{\text{DC}}_{\ell:\{ef\}}} P^\ell_{l:ef,t,y,s} = 0. \tag{7.23}$$

$$e \in \mathcal{N}^{\text{DC}}, \quad t \in \mathcal{S}_{\text{t}}, \quad y \in \mathcal{S}_{\text{y}}, \quad s \in \mathcal{S}_{\text{s}}.$$

7.4 Zonal market GATE planning model

The first step in modelling a zonal market is to define the zonal market boundaries. This is done by partitioning the nodes into $\mathcal{Z}$ disjoint market zones: $\mathcal{N} = \bigcup_{z \in \mathcal{Z}} z$. We can then define two sub-sets of edges, inter-zonal edges: $\mathcal{E}^{\mathrm{te}} \subseteq \{mn : z \in \mathcal{Z}, m \in z, n \notin z\}$ and intra-zonal edges: $\mathcal{E}^{\mathrm{br}} \subseteq \{mn : z \in \mathcal{Z}, m \in z, n \in z\}$. Similar sub-sets can be defined for candidate transmission lines, both inter-zonal: θ^{te}, $\alpha^{\ell,\mathrm{te}}$ and intra-zonal: θ^{br}, $\alpha^{\ell,\mathrm{br}}$. The superscripts refer to a new distribution of optimization variables among two newly created agents: the Transmission Expansion agent ($\mathcal{A}^{\mathrm{te}}$) and the Balancing Responsible agent ($\mathcal{A}^{\mathrm{br}}$). The variables are redistributed as:

$$\mathcal{A}^{\mathrm{te}} = (\mathcal{A}_{\mathrm{w}}, \mathcal{A}_{\mathrm{j}}, \mathcal{A}_{\mathrm{e}}, \mathcal{A}_{\mathrm{o}}^{\mathrm{te}}) \text{ and } \mathcal{A}^{\mathrm{br}} = (\mathcal{A}_{\mathrm{w}}, \mathcal{A}_{\mathrm{j}}, \mathcal{A}_{\mathrm{e}}, \mathcal{A}_{\mathrm{o}}^{\mathrm{br}}),$$

where $\mathcal{A}_{\mathrm{o}}^{\mathrm{te}}$ is identical to $\mathcal{A}_{\mathrm{o}}$ except that only candidate transmission lines within ($\boldsymbol{\alpha}^{\ell,\mathrm{te}}$) are considered. The compliment to this, is of course $\mathcal{A}_{\mathrm{o}}^{\mathrm{br}}$ which only considers transmission lines within ($\boldsymbol{\alpha}^{\ell,\mathrm{br}}$).

The vast majority of constraints on the system remain unchanged in a zonal market. The exceptions to this are the nodal power balance equations (7.22) and (7.23). In a zonal market intra-zonal congestion is ignored when solving initial dispatch and when calculating the inter-zonal power flows. As such power balance must only be satisfied around the boundary of each zone as in:

$$\left. \begin{aligned} &\sum_{m \in z} \left(\sum_{e \in \mathcal{N}_m^{\mathrm{DC}}} P_{me,t,y,s}^{\zeta,\mathrm{AC}} - \sum_{g \in \mathcal{S}_{g:n}} P_{g:m,t,y,s}^{\mathrm{g}} \right. \\ &+ \sum_{n \in \mathcal{N}_m^{\mathrm{AC}}} \sum_{l \in \mathcal{S}_{\ell:\{mn\}}^{\mathrm{te,AC}}} P_{l:mn,t,y,s}^{\ell} - \sum_{u \in \mathcal{S}_{u:n}} P_{u:m,t,y,s}^{\mathrm{u}} \\ &+ \sum_{j \in \mathcal{S}_{j:n}} P_{j:m,t,y,s}^{\mathrm{j,inj}} - \left. \sum_{j \in \mathcal{S}_{j:n}} P_{j:m,t,y,s}^{\mathrm{j,abs}} \right) = 0 \end{aligned} \right\} \begin{aligned} &z \in \mathcal{Z}, \\ &t \in \mathcal{S}_{\mathrm{t}}, \\ &y \in \mathcal{S}_{\mathrm{y}}, \\ &s \in \mathcal{S}_{\mathrm{s}}, \\ &(: \lambda_{z,t,y,s}^{\mathrm{z}}). \end{aligned} \qquad (7.24)$$

In a zonal market (7.24) is the market clearing condition and the dual variable λ_z^{z} the marginal price of energy for all nodes in z. Likewise on the DC network side power balance is only required along the market boundary as in:

$$\sum_{e \in z} \left(\sum_{m \in \mathcal{N}_e^{\mathrm{AC}}} P_{em,t,y,s}^{\zeta,\mathrm{DC}} + \sum_{f \in \mathcal{N}_e^{\mathrm{DC}}} \sum_{l \in \mathcal{S}_{\ell:\{ef\}}^{\mathrm{te,DC}}} P_{l:ef,t,y,s}^{\ell} \right) = 0 \qquad (7.25)$$

$$z \in \mathcal{Z}, \quad t \in \mathcal{S}_{\mathrm{t}}, \quad y \in \mathcal{S}_{\mathrm{y}}, \quad s \in \mathcal{S}_{\mathrm{s}}.$$

When only zonal power balance is considered, GATE planning intra-zonally becomes very difficult as no congestion signals are generated to indicate desirable

investments. To overcome this difficulty a multi-step approach is adopted to expansion planning. This multi-step approach involves first optimally expanding the inter-zonal transmission network assuming zero congestion intra-zonally (a copper plate). Then, after fixing the inter-zonal network, proceeding to solve a standard nodal based GATE problem for the intra-zonal network(s), considering the available inter-zonal congestion determined in the previous step. This approach is summarized in Fig. 7.2 and outlined in further detail below.
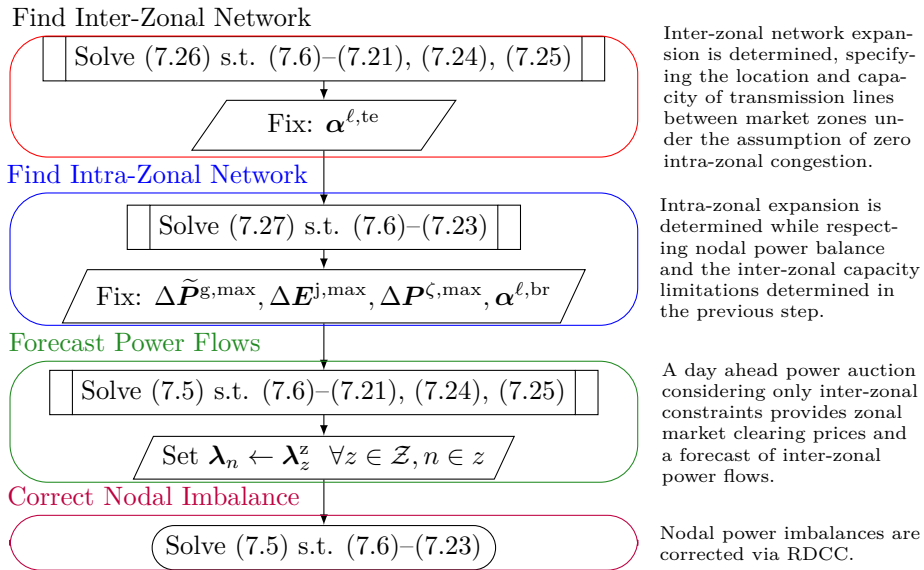
Figure 7.2: Flowchart of solution method for zonal market clearing formulation. "Solve" refers to the specified equations considering the fixed decision variables found previously.

Step one: considering only agent $\mathcal{A}^{\text{te}}$ variables solve (7.26) ((7.5) with (7.26a) substituted for (7.2a)) such that constraints (7.6) through (7.21) are satisfied. Power balance is only enforced zonally as in (7.24) and (7.25). The variables $\boldsymbol{\alpha}^{\ell,\text{te}}$ determining the inter-zonal transmission lines are fixed and passed to agent $\mathcal{A}^{\text{br}}$ for the next step.

$$\max_{\mathcal{A}^{\text{te}}} \mathcal{U} := \sum_{s \in \mathcal{S}_{\text{s}}} \pi_s \sum_{y \in \mathcal{S}_{\text{y}}} f_y^{\text{H}} \sum_{t \in \mathcal{S}_{\text{t}}} \Big[(7.4\text{a}) + (7.4\text{b}) \Big] \tag{7.26}$$
$$- f_y^{\text{Y}} \Big[(7.1\text{a}) + (7.2\text{b}) + (7.3\text{a}) + (7.26\text{a}) \Big]$$

$$\sum_{\substack{\{mn\}\subseteq\mathcal{N} \\ mn\in\mathcal{E}^{\mathrm{te}}}}\sum_{\widetilde{l}\in\widetilde{\mathcal{S}}_{\ell:\{mn\}}} \underset{\sim}{\alpha}_{\widetilde{l}:\{mn\},y}^{\ell,\mathrm{te}}\cdot I_{\widetilde{l},y} \tag{7.26a}$$

Step two: considering only $\mathcal{A}^{\mathrm{br}}$ variables solve (7.27) ((7.5) with (7.27a) substituted for (7.2a)) such that (7.6) through (7.21) are satisfied. Power balance is enforced nodally as in (7.22) and (7.23). Achieving nodal balance at the lowest cost can be accomplished via the construction of new lines $\alpha^{\ell,\mathrm{br}}$, expanding or reducing the capacity of newly constructed OWPPs and/or storage $(\widetilde{P}_{\underset{g}{\sim}}^{\mathrm{g,max}}, E_j^{\mathrm{j,max}})$ or curtailing and/or up regulating network generators (S_{g}). All remaining expansion related variables are set at this stage $(\Delta\widetilde{\boldsymbol{P}}^{\mathrm{g,max}},\Delta\boldsymbol{E}^{\mathrm{j,max}},\Delta\boldsymbol{P}^{\zeta,\mathrm{max}},\boldsymbol{\alpha}^{\ell,\mathrm{br}})$. No further expansion planning is needed. An existing topology is passed to step three to undergo a power auction.

$$\max_{\mathcal{A}^{\mathrm{br}}}\mathcal{U} := \sum_{s\in\mathcal{S}_{\mathrm{s}}}\pi_s\sum_{y\in\mathcal{S}_{\mathrm{y}}}f_y^{\mathrm{H}}\sum_{t\in\mathcal{S}_{\mathrm{t}}}\left[(7.4\mathrm{a})+(7.4\mathrm{b})\right] \tag{7.27}$$
$$-f_y^{\mathrm{Y}}\left[(7.1\mathrm{a})+(7.2\mathrm{b})+(7.3\mathrm{a})+(7.27\mathrm{a})\right]$$

$$\sum_{\substack{\{mn\}\subseteq\mathcal{N} \\ mn\in\mathcal{E}^{\mathrm{br}}}}\sum_{\widetilde{l}\in\widetilde{\mathcal{S}}_{\ell:\{mn\}}} \underset{\sim}{\alpha}_{\widetilde{l}:\{mn\},y}^{\ell,\mathrm{br}}\cdot I_{\widetilde{l}:\{mn\},y} \tag{7.27a}$$

Step three: considering the fixed topology variables selected in the previous two steps, power flows are forecast for a zonal market by solving (7.5) such that (7.6) through (7.23) are satisfied. Power balance is only enforced zonally as in (7.24) and (7.25). The market clearing price for each market zone $(\boldsymbol{\lambda}_z^{\mathrm{z}})$ is determined and fixed.

Step four: if the power flows from step three are feasible nothing remains to do. If by contrast intra-zonal congestion means the forecasted flows are not physically feasible then we again solve (7.5) such that (7.6) through (7.23) are satisfied, however, power balance is now enforced nodally as in (7.22) and (7.23). The cost of redispatch is then calculated considering initial dispatch and spot market prices from 3 with final dispatch and power flows from 4.

Redispatch

The mechanism used for calculating the cost of redispatch is regulatory redispatch with cost compensation (RDCC) [211] as described in section 7.2 above.
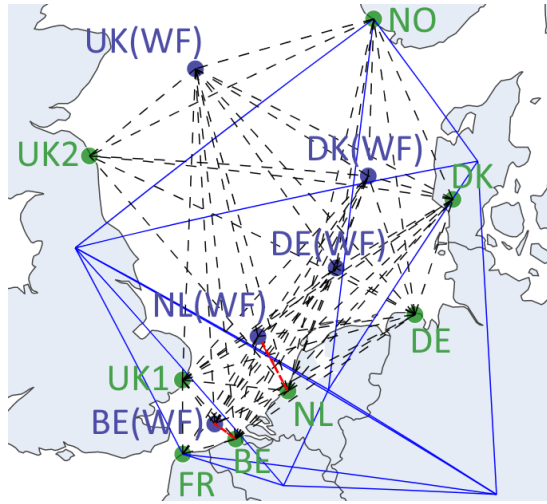
Figure 7.3: North Sea domain. Lines: NTCs of existing connections (solid blue), candidate HVDC connections (dashed black), candidate HVAC connections (dashed red).

As all players are contractually obligated to participate and we assume perfect transparency from generators regarding their variable cost and available capacity, we argue that regulatory redispatch with cost compensation forms an upper bound on the social welfare achievable under a zonal market design.

7.5 Test Case

7.5.1 Domain and boundary conditions

In this section the presented model is applied to a test grid ($\mathcal{G}^\mathrm{L}$) in the North Sea. A schematic of the test grid is shown in Fig. 7.3. The location of onshore and offshore nodes, candidate connection routes for HVAC and HVDC transmission lines and the existing onshore grid (NTCs) are illustrated. The exact locations of onshore and offshore nodes are listed in Table 7.1.

Table 7.1: Location of nodes in test grids and maximum capacity of candidate Infrastructure.

Point	Longitude	Latitude	$\widehat{P^{\zeta,\mathrm{max}}}$ [GW]	$\widehat{P^{\mathrm{g,max}}}$ [GW]	$\widehat{E^{\mathrm{j,max}}}$ [GWh]
UK1	52.21025	1.57374	3.0	-	1.0
FR	50.96332	1.82967	3.0	-	1.0
BE	51.32081	3.20768	3.0	-	1.0
NL	52.22215	4.49556	3.0	-	1.0
DE	53.67043	7.84620	3.0	-	1.0
DK	55.61420	8.72899	3.0	-	1.0
NO	58.43791	6.00292	3.0	-	1.0
UK2	55.68940	-1.91052	3.0	-	1.0
BE(WF)	51.53509	2.59644	4.0	4.0	0.02
NL(WF)	53.08300	3.51802	4.0	4.0	0.02
DE(WF)	54.34610	5.52400	4.0	4.0	0.02
DK(WF)	55.90115	6.22240	4.0	4.0	0.02
UK(WF)	57.33721	0.81425	4.0	4.0	0.02

*The coordinates specified are only estimates based on
proposed projects in [173, 214].

Candidate Expansion

GATE planning is carried out on test grid $\mathcal{G}^{\mathrm{L}}$ considering the maximum capacities for candidate OWPPs ($\widehat{P^{\mathrm{g,max}}}$), HVDC converters ($\widehat{P^{\zeta,\mathrm{max}}}$) and storage devices ($\widehat{E^{\mathrm{j,max}}}$) specified in Table 7.1. The costs of these components are listed in Table 7.3. The upper limits placed on onshore converters reflect a dimensioning incident of ±3 GW at all PCCs. Storage devices are assumed to be lithium ion battery energy storage systems with a four hour duration. A summary of type, capacity, length and cost for candidate cables is found in Table 7.2. Because reactive power considerations in HVAC cables depend on both distance and capacity, specific candidate cables are listed. By contrast, HVDC cables maintain their transmission capacity over distance, hence to be concise, only the capacities and per kilometer costs of the three candidate cable types used are provided. For the full list of candidate HVDC cables refer to Table C.1 of the Appendix.

Table 7.2: HVAC and HVDC candidate cables [215, 216].

	n·cm²	MVA	km	Cost
AC1	12·16	4213	61	1520
AC2	11·10	3319	61	1065
AC3	8·10	2414	61	785
AC4	11·16	3236	146	3345
AC5	12·6.3	2479	146	2338
DC1	4·15	4085	-	3.593
DC2	4·10	3288	-	3.194
DC3	2·20	2407	-	2.575

HVAC cable costs are in M€
HVDC cable costs are in M€/km

Table 7.3: Infrastructure costs [215, 217]

Component	Cost
OWPPs	2100
Onshore converters	192.5
Offshore converters	577.5
Onshore storage	183
Offshore storage	275

Costs are in €/kW
(€/kWh for storage)

Table 7.4: Marginal price of generators [173].

Generation Type	€/MWh
PV, Hydro	18
Onshore wind	25
Offshore wind	59
Other RES	60
Gas CCGT	89
Nuclear	110
Demand side response	119
Gas OCGT, Coal, Pump storage, P2G, Other non-RES	120
Light oil	140
Heavy oil, Shale oil	150

Existing Generation

The 2020 TYNDP by ENTSO-E [173, 218] provides current as well as 2030 and 2040 scenario based projections of the energy mixes per EU member state and the UK. More on the scenario modelling is provided below. The capacity of existing generation at onshore nodes (Ψ^g, $\bar{P}^{g,max}$) is taken directly from this resource and evolves through the simulation years based on the ENTSO-E forecast. The assumed marginal costs per generation type, based on the LCOE, are listed in Table 7.4.

Table 7.5: Net transfer capacities in GW [173][2].

	BE	FR	UK	NL	DE	NO	DK
BE		4.3	1	2.4	1		
FR	4.3		4		3		
UK	1	4		1	1.4	2.8	1.4
NL	2.4		1		5	0.7	0.7
DE	1	3	1.4	5			3.5
NO			2.8	0.7			1.64
DK			1.4	0.7	3.5	1.64	

Onshore grid

The 2020 TYNDP also provides the NTCs between EU member states plus the UK. These are specified for the modelled onshore nodes in Table 7.5. The existing onshore grid is modelled using point to point DC connections of capacity equal to the associated NTC. The NTCs listed are for the year 2025. Throughout the simulation years the onshore grid capacity remains static.

Demand

Similar to generation, the demand (Ψ^{u}) evolves over the simulation years following the scenario projections for 2030 and 2040 provided in the TYNDP. In the case that load cannot be fully met by available generation, demand side response at a cost of 119 €/MWh can be activated. Should available demand side response be exhausted and further load shedding still be required the Value Of Lost Load (VOLL) is 5000€/MWh. The cost of demand side response is considered in market price formation, the cost of VOLL on the other hand is not. In the event of extreme energy shortage when VOLL is activated, an energy price cap of 180 €/MWh as per EU regulation 2022/1854 [219] is enforced. A constant consumer bid price of 150 €/MWh is assumed for calculating gross consumer surplus.

Scenarios

The TYNDP scenarios of Distributed Generation, Global Ambition, and National Trends are utilized in the analysis. Each scenario presents projections regarding the evolution of demand and energy mix in EU member states and

---

[2]The NTC between DE and NO is 1.4 GW but was inadvertently excluded when calculating the presented results.

the UK, focusing on diverse pathways towards achieving a net-zero emissions target by 2050. The Distributed Generation scenario assumes that these targets will be accomplished through widespread adoption of distributed RES. In the Global Ambition scenario, the goals primarily rely on the commitments made under the Paris Agreement. In National Trends, current policy of member states is considered and a convergence with Paris agreement commitments assumed come 2040.

Scenario generation is based on an iterative approach, involving stakeholder consultation, scenario development and analysis, and further stakeholder engagement. This approach aims at identifying the most realistic pathways towards a low-carbon energy system of the future. Every two years, selected scenarios, along with pertinent datasets, are published in the TYNDP scenario report.

Stakeholder consultation starts by identifying the key drivers and sources of uncertainty that shape the future energy system. These factors, in combination with historical datasets, serve as the basis for creating a range of potential future scenarios. Subsequently, comprehensive analysis is performed on these scenarios, and the results are presented to stakeholders for further refinement, enabling the identification and improvement of any gaps within the modeling methodology. For detailed information on the scenario development, please refer to the TYNDP directly [218].

The three TYNDP scenarios discussed, are combined with normalized historical RES generation profiles from the years 2014 and 2015, resulting in a total of six scenarios within $\mathcal{S}_s$. In this work each scenario is assumed to have an equally likely probability of occurrence denoted as $\pi_s = 1/6$, $s \in \mathcal{S}_s$.

Temporal resolution

Hourly data is utilized for the demand and RES time series; however, to obtain computational tractability, the problem size needed to be reduced. Each simulation year was, therefore, represented by four selected 24-hour days. These representative days were obtained by focusing on the offshore wind time series' alone, as they hold primary importance in the model.

The clustering approach involves initially dividing the yearly time series' into four seasonal time series, spring, summer, fall and winter. Following this, the k-medoids clustering method [220] is used on the normalized average of all the considered offshore development zones, in order to identify a single representative day for each season. Subsequently, the same identified time steps are used for all other time series to ensure any temporal correlation is preserved among them.

For the modeling of the 30-year time horizon up to 2050, three representative simulation years are used: 2020, 2030, and 2040. The data from the year 2020 is applied for the period 2020-2029, the data from 2030 is used for the period 2030-2039, and the data from 2040 is employed for the period 2040-2049. All results presented below were obtained on a standard Dell lap-top with an intel core-7 1.9 GHz processor and 16 GB of RAM.

7.5.2   Results

In this section the results of the proposed expansion planning model applied to $\mathcal{G}^{\mathrm{L}}$ are presented. Three market design case studies are examined to assess the impact of the market on the GATE planning problem. The case studies are as follows:

- nOBZ: each node is its own market zone.

- HMD: each OWPP is part of its home market zone.

- zOBZ: all OWPPs form a common offshore market.

In each test case a different offshore topology is obtained. The topology for the nOBZ is shown in Fig. 7.4, that for the HMD in Fig. 7.5 and the zOBZ topology is in Fig. 7.6. Please note, it is not the intent of this work to claim with any certainty these are the best offshore networks possible, rather, they are the optimal solutions found by our model under the many simplifying assumptions we have discussed. This is not investment advice.

In the figures, the selected transmission line capacities as well as the build schedule is shown. The capacities and build schedule for the HVDC converters are shown adjacent to the respective figures in Tables 7.6, 7.7 and 7.8. In terms of generation expansion, all OWPPs are expanded to the maximum 4 GW immediately in the nOBZ and HMD. In the zOBZ, Belgian, German and Dutch OWPPs are expanded to the maximum 4 GW in 2020 while in the UK 3.9 GW are added in 2020, then the remainder in 2030 (essentially the same). In terms of storage, 1 GWh of storage is scheduled for the Netherlands in 2040 regardless of market design. A dominant feature of all topologies is the presence of HOAs. Only a single radial OWPP connection is chosen across the case studies. This is found in the HMD topology for the Belgian OWPP. This is reasonable as it is the closest OWPP to shore.

Table 7.9 presents a ranking based on social welfare of gross consumer surplus, redispatch cost, and combined net benefits for all agents for each case study. To provide a more detailed analysis of the net benefits, Table 7.10 breaks them
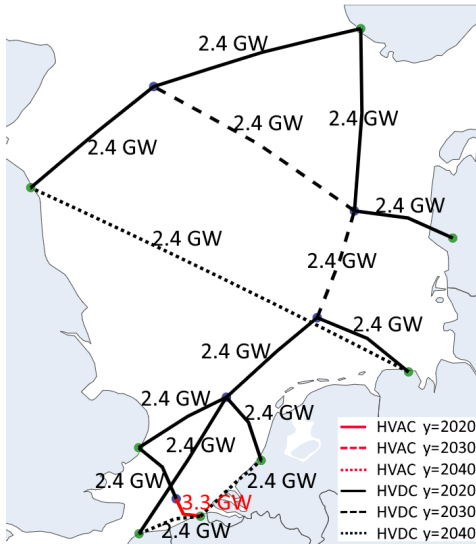
Figure 7.4: nOBZ $\mathcal{G}^{\text{L}}$ topology.

Table 7.6: HVDC converter expansion planning schedule for nOBZ grid $\mathcal{G}^{\text{L}}$.

Year	'20	'30	'40
	$P_{ne,y}^{\zeta,\max}$ [GW]		
UK1	2.9	3	3
FR	2.4	2.4	3
BE	0	0	1.8
NL	2.4	2.4	3
DE	2.4	2.4	3
DK	1.6	2.4	2.4
NO	3	3	3
UK2	1.9	2.4	3
BE(WF)	0.5	0.6	0.6
DE(WF)	3.7	3.7	3.7
NL(WF)	3.8	3.8	3.8
DK(WF)	3.7	3.7	3.8
UK(WF)	3.2	3.4	3.6

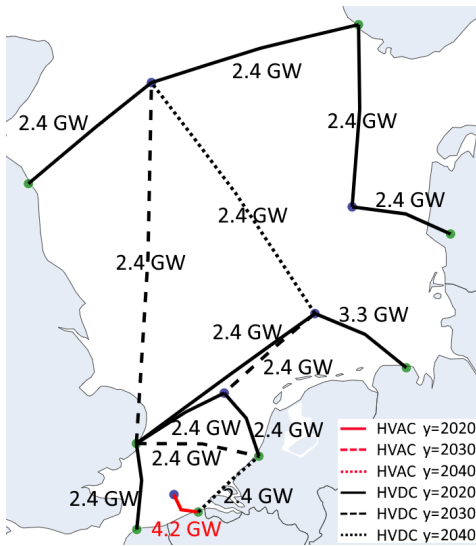Figure 7.5: HMD $\mathcal{G}^{\text{L}}$ topology.

Table 7.7: HVDC converter expansion planning schedule for HMD grid $\mathcal{G}^{\text{L}}$.

Year	'20	'30	'40
	$P_{ne,y}^{\zeta,\max}$ [GW]		
UK1	3	3	3
FR	2.4	2.4	2.4
BE	0	0	2.4
NL	2.4	3	3
DE	3	3	3
DK	1.7	1.9	1.9
NO	3	3	3
UK2	1.7	2.4	2.4
BE(WF)	0	0	0
DE(WF)	3.7	3.7	3.7
NL(WF)	3.8	3.8	3.8
DK(WF)	3.7	3.7	3.8
UK(WF)	3.2	3.4	3.6

down by agent. In this context, net benefits refer to the difference between gross producer surplus and investment costs for OWPP and storage developers,
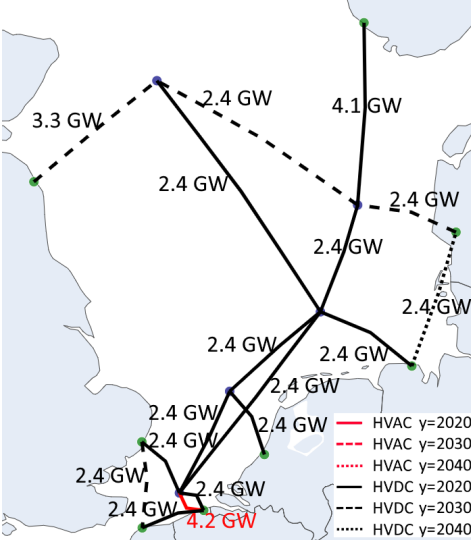
Figure 7.6: zOBZ $\mathcal{G}^{\mathrm{L}}$ topology.

Table 7.8: HVDC converter expansion planning schedule for zOBZ grid $\mathcal{G}^{\mathrm{L}}$.

Year	'20	'30	'40
	$P_{ne,y}^{\zeta,\max}$ [GW]		
UK1	2.4	3	3
FR	2.4	3	3
BE	0	0.6	1.5
NL	2.4	2.4	2.4
DE	2.4	2.4	3
DK	0	2.4	2.4
NO	3	3	3
UK2	0	3	3
BE(WF)	0	0	0
DE(WF)	3.6	3.7	3.7
NL(WF)	3.8	3.8	3.8
DK(WF)	3.7	3.7	3.8
UK(WF)	2.4	3.4	3.6

and congestion rent minus investment costs for TSOs. Four additional entries indicated by asterisks(*) are listed. These four entries indicate the results of operating either the HMD, zOBZ or nOBZ topology in a different market design from which it was initially intended and are as follows:

- HMD*: the HMD topology operating in an nOBZ market.

- zOBZ*: the zOBZ topology operating in an nOBZ market.

- nOBZ*: the nOBZ topology operating in an HMD market.

- nOBZ**: the nOBZ topology operating in a zOBZ market.

The highest social welfare is achieved with a nodal pricing scheme. This is not a surprising result. A result that is surprising, however, is that there is essentially no difference in social welfare between the three topologies provided they operate within a nodal based market design (nOBZ, zOBZ* and HMD*). This effectively demonstrates the flatness of the solution space around the optimal point(s), since the nOBZ topology is a proven globally optimal solution with a known continuous upper bound. This knowledge is useful for planners who need not invest large resources in guaranteeing global optimality as the associated uncertainty is far larger than the small difference between a good solution and the optimal solution.

Table 7.9: Summary of social welfare for $\mathcal{G}^{\mathrm{L}}$ in B€ over the 30 year time horizon.

	Net Benefit	GCS	Redispatch	Social Welfare	Difference [%]
nOBZ	134.527	1920.331	0.000	2054.858	-
HMD*	134.040	1920.299	0.000	2054.340	-0.03
zOBZ*	131.151	1922.617	0.000	2053.767	-0.05
zOBZ	128.073	1926.606	128.596	1926.083	-6.27
nOBZ**	129.561	1921.987	127.006	1924.543	-6.34
nOBZ*	128.707	1924.729	145.615	1907.821	-7.16
HMD	128.284	1916.556	155.168	1889.672	-8.04

Table 7.10: Summary of costs and benefits for $\mathcal{G}^{\mathrm{L}}$ in B€ over the 30 year time horizon.

	Transmission		OWPP		Storage	
	Costs	Benefits	Costs	Benefits	Costs	Benefits
nOBZ	21.754	64.147	42.000	134.135	0.059	0.058
HMD*	22.380	64.722	42.000	133.700	0.059	0.058
zOBZ*	22.984	70.453	41.885	125.568	0.059	0.057
zOBZ	22.984	57.703	41.885	135.241	0.059	0.056
nOBZ**	21.754	53.452	42.000	139.866	0.059	0.057
nOBZ*	21.754	49.015	42.000	143.459	0.059	0.047
HMD	22.380	48.526	42.000	144.152	0.059	0.046

Perhaps a more interesting aspect for planners to focus resources on is finding a topology that has high social welfare coupled with a desirable distribution of benefits among stakeholders. For example, the nOBZ has 6.8% higher benefits for OWPP developers compared to the zOBZ*. Of course, there is no free lunch as benefits decrease by 9% for the transmission developer between these two topologies. A favourable distribution of benefits may help attract more private investment and facilitate the approval process. Doing so without sacrificing overall social welfare is an obvious positive.

Upon comparing the initial three rows of Table 7.9 with the subsequent four rows, a noteworthy observation is made: the nodal market case studies outperform all zonal market case studies by 6–8% in terms of social welfare. Within the zonal market models, the HMD model exhibits the poorest performance. Our modeling results indicate that having prior knowledge of the market design was not essential, as the social welfare achieved when operating a topology designed for one market design in another is nearly equivalent to that achieved with the market-specific design. It is important, however, to exercise caution

when extrapolating this conclusion more broadly, as a single test grid does not provide sufficient evidence to do so.

Despite the poor performance of the topologies intended for use in a zonal market, their high level of social welfare in a nodal market makes them possible candidates as decomposition techniques. Unfortunately, the nOBZ approach does not scale well and is more computationally expensive when compared to the zonal approaches. Comparing computation times the zonal approaches each found a solution in ≈2.5 hours, while the nOBZ took twelve hours before timing out with a small optimallity gap of 0.04%. For large problem sizes where the nOBZ approach proves intractable, the proposed zonal may be a good alternative or starting point for the optimization process. The zonal approach is expected to scale better than the nOBZ as it naturally decomposes the problem into inter- and intra-zonal variables.

The return on investment is shown in Fig. 7.7. In this case study, all developers achieve a positive return on investment regardless of market design. Certain market designs are more appealing to certain developers however. Under a HMD the return on investment for OWPP developers is highest while transmission and storage developers have their highest return on investment in an nOBZ. The increased benefits to OWPPs in a HMD is explained by increased energy prices. The average energy price for onshore nodes is shown in Fig. 7.8 and for offshore nodes in 7.9. The HMD design boasts the highest average energy prices both offshore and onshore. While this equates to higher profits for OWPPs it also means lower gross consumer surplus hence the poor performance of this market design. In our model, the average European wide energy prices from lowest to highest were found in the nOBZ (90.86 €/MWh), zOBZ (91.21 €/MWh) and HMD (93.23 €/MWh). Of course, due to the simplicity of such a model, this cannot be reliably extrapolated to the real European energy market as a whole.

From a wind resource use perspective the topologies do not differentiate from each other. All designs result in very little wind curtailment as internal congestion of the offshore grid is not considered. This is shown in Fig. 7.10. The zOBZ does result in a higher amount than the other two but the total is still only about 0.5% of the total energy production.

Redispatch cost does vary substantially across zonal market models. The HMDs have higher redispatch costs than the zOBZs. In Fig. 7.11 a percent breakdown of redispatch costs by generator type is shown. In all cases the most commonly redispatched generator type is a CCGT. The value given for RES includes hydro sources. Observe that in the HMDs, almost 5% of the overall redispatch cost is attributed to VOLL. This is particularly interesting as there is no increase in lost load between the market designs. They all result in approximately 3.5 TWh of lost load, see Fig. 7.10. This can be attributed to the pivotal supplier effect
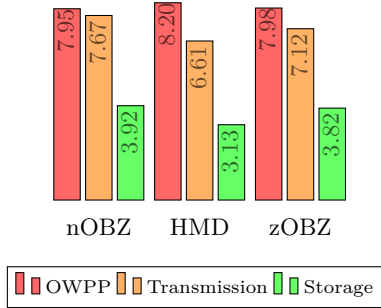
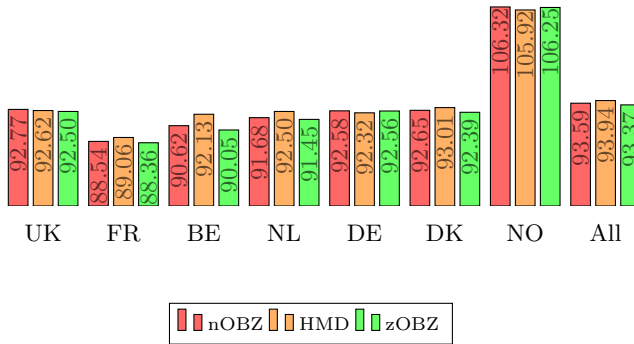Figure 7.7: Yearly percent return on investment for $\mathcal{G}^{\mathrm{L}}$.

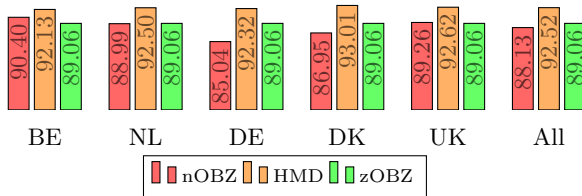Figure 7.8: Average onshore energy prices for $\mathcal{G}^{\mathrm{L}}$ [€/MWh].

Figure 7.9: Average offshore energy prices per country for $\mathcal{G}^{\mathrm{L}}$ [€/MWh].
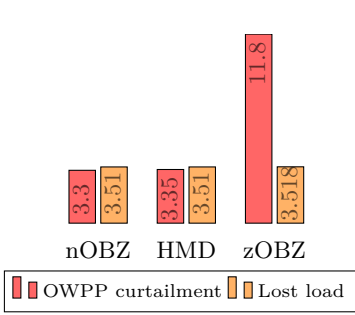
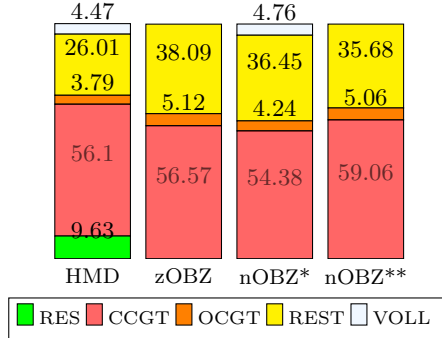Figure 7.10: OWPP curtailment and lost load in TWh.[3]

Figure 7.11: Percent breakdown of redispatch costs.

discussed in section 7.2. Since OWPP to home market congestion is ignored at initial dispatch the VOLL is shifted to the redispatch phase. Since VOLL has such a high cost (5k€/MWh), if it were considered as part of market price formation wind fall profits would result in the nodal pricing schemes and the overall social welfare of the market design would be reduced. This could lead to a misinterpretation of the results as HMDs would appear much better than in reality. In this case the energy cap of 180 €/MWh implemented when VOLL is activated avoids this scenario.

A final point worthy of mentioning is the noticeable lack of storage built across the test cases. This could be for many reasons related to the simplicity of the modelling approach. Some possible improvements that could be made to better model storage expansion are a two stage market, reserve market and unit commitment constraints.

7.6 Conclusions

In this chapter, we present the formulation of the OW-GATE planning model for grid level $\mathcal{G}^\mathrm{L}$. The goal of this planning model is to find the optimal transmission topology, the macro location and capacity of new OWPPs, and the timeline for constructing the network and generation. The implemented formulation is a stochastic, multi-level, step-wise, mixed-integer linear program.

_____

[3]Potential OWPP production: 2287 TWh (nOBZ/HMD), 2284 TWh (zOBZ). Total load: 50366 TWh.

We present two variations on the formulation based on different energy market designs: nodal pricing mechanism and zonal pricing mechanisms. The formulations allow OW-GATE planning to be performed under the assumption of a certain market design, or to investigate how an existing transmission network would perform given a change in the energy market design.

We test the OW-GATE formulation on a North Sea test grid, and investigate three offshore market designs: a nOBZ, a zOBZ, and a HMD. All three topologies incorporate HOAs. The nOBZ is shown to be the market design with the highest social welfare, while the HMD provided the lowest amount of social welfare and the highest average European-wide energy prices.

We find that social welfare is more market-dependent than topology-dependent, as all three topologies resulted in similar overall social welfare, provided they were operated in a nOBZ. As an upper bound on social welfare is calculated as part of the expansion plan obtained considering a nOBZ a priori, we can infer from the result that the solution space is fairly flat around the optimal point. Planners should therefore focus on finding a topology that distributes benefits among stakeholders in a desirable manner rather than overly stressing to design the optimal topology.

While zonal markets were shown to be undesirable from a social welfare perspective, a zonal planning model shows promise from a computational perspective. The nodal planning model is much more computationally expensive than the zonal models as zonal models naturally decompose the problem into inter- and intra-zonal networks. Using a zonal expansion strategy may prove a desirable starting point when modelling computationally intractable problems. This is not to say, however, that investigating more efficient structure exploiting decomposition strategies such as fast consensus ADMM [221] or Bender's [123] should be overlooked.

We identify potential shortcomings of the model due to the lack of storage built under any of the market designs. It is theorized that capturing the benefits of storage may require the implementation of some or all (and more) of the following: a two stage market, a reserve market and unit commitment constraints. Another shortcoming of the model is the lack of consideration of uncertainty within the operational time frame.

Chapter 8

Conclusions and future work

8.1 Overview

Europe is currently undergoing a significant energy transition towards distributed, carbon-free, renewable energy technologies, such as solar and wind, to mitigate the worst effects of climate change by limiting greenhouse gas emissions. In the North Sea, where vast offshore wind resources exist, offshore wind power plants are set to play a crucial role in this transition. However, efficiently harnessing the North Sea wind resources requires the development of an offshore transmission network to the best development regions for the power plants, due to the physical location of the resource. As the North Sea is surrounded by multiple countries, each with their own energy markets, interconnecting these regions would increase market integration and offset some of the inherent volatility in renewable energy sources. A meshed HVDC network is the most desirable technological solution due to the high capacity and length of the required transmission, as well as the high reactive power flows in subsea HVAC cables.

To efficiently develop the necessary offshore wind power plants and transmission infrastructure, a holistic expansion planning methodology and set of tools are required that can consider market design during the decision-making process. The goal of this thesis was to develop such a methodology and framework that integrates existing state-of-the-art planning approaches and newly proposed methods where gaps in the state of the art exist.

Two gaps in the state-of-the-art offshore wind expansion planning models were identified. First, the existing models focus either on high-level expansion plan-

ning for transnational grid development or on low-level models for planning collection circuits and simple transmission networks for isolated, radially connected offshore wind power plants. This gap is a result of the rapid development in the offshore wind industry over the last three decades, with significant increases in turbine and wind farm capacities and a shift towards far from shore locations. The research conducted in chapters 4, 5, and 6 address this gap by developing an intermediate capacity network expansion model that considers multiple neighboring offshore wind power plants.

Second, while state-of-the-art expansion planning models have been developed for energy market structures defined a priori, there is a lack of effective models that address the initial decision of what market structure should be implemented. This gap has led to the current situation where we are moving towards a meshed offshore HVDC grid without a clearly defined energy market structure, resulting in higher uncertainty and costs for developers. To address this, chapter 7 presents a market-aware generation and expansion planning model that considers the market structure as part of the decision-making process.

8.2   Summary of work performed

The principle objectives of the thesis were divided into smaller goals that are addressed as the chapters progress. Chapter 2 provides an in-depth presentation of the necessary background theory, including an introduction to the problem of expansion planning and the available solution methods that can be used to solve it. The chapter also discusses the drivers of complexity, with a focus on those specific to offshore expansion planning. These include the high reactive power in HVAC sub-sea cables compared to overhead lines, and the green field (or only slightly browned field) nature of the problem. Increased reactive power tends to favor HVDC, while the green field nature of the problem increases the number of binary decision variables needed for candidate equipment. The chapter then provides an overview of the state-of-the-art models available, highlighting the high and low-level models and the gap in between the two scales.

Chapter 3 presents a high-level overview of the proposed methodology. A divide and conquer approach is proposed. The problem is split into three grid capacity levels. These levels are then each sub-divided further into a collection of fourteen steps grouped into six sequential planning stages. Following the six planning stages, an offshore grid can be constructed in a top-down manner, where the higher capacity grids define the macro location and build schedule inputs of the lower capacity grids, and the lower capacity grids dictate the micro location of infrastructure such as offshore substations. The chapter also discusses the best

available data sources for describing the domain and boundary conditions of the problem. Five categories of data are identified, then, sorted by relevancy to each sub-problem. When multiple data sets are available for a given data type, the strengths and weaknesses of the sets are contrasted.

Chapter 4 presents the proposed offshore wind transmission network expansion planning problem formulation for multiple neighboring offshore wind power plants. The chapter highlights the challenges posed by the green field nature of the problem, which can make using a traditional approach based on integer positions of candidate offshore substations problematic. The number of binaries required for the candidate infrastructure experiences a combinatorial explosion, quickly creating a problem that is intractable. To address this, an alternative greedy search algorithm is proposed, which is able to efficiently search the topological search space for high-quality solutions, returning a priority queue of optimal topologies for all possible connection combinations of the offshore wind power plants passing through a single export cable.

From the greedy search result, a simple method to determine the optimal topology with one or more export cable connections to a point of common coupling is presented. The greedy search algorithm is bench-marked against an MILP formulation and shown to at least match the solution quality with much lower computation times. It is also shown to solve problem sizes that are intractable to the MILP. This problem size is bench-marked against a sequentially cascading MILP. Not only does the greedy search find a better solution than the benchmark in a quicker time, but it is also able to find a better version of the benchmark solution topology. The improved version of the solution topology is due to the ability of the greedy search algorithm to model the positions of candidate offshore substations as a continuous variable versus the integer positions necessary in the benchmark, thus locating the offshore substation optimally.

Chapter 5 presents an extension to the greedy search algorithm, which enhances its capacity to handle larger feasible problem sizes. This extension employs association rule mining, a machine learning approach, to generate dynamic constraints for the feasible search space of the algorithm. Since training data sets for wind farm transmission connections are limited, a synthetic data generation method is also proposed.

The hybrid ARM-greedy search algorithm is compared against the original greedy search algorithm for feasible problem sizes and is shown to find the identical result in all cases except one. The single exception resulted in a tiny degradation on the original solution of 0.1%, well within the error of the model. Subsequently, the hybrid algorithm is tested on problem sizes that are beyond the capability of the original greedy search algorithm. The solution quality is

assessed using the error in a control population of wind power plant connections, and it is found that the solutions generated by the hybrid algorithm remain of high quality effectively increasing the feasible range of problem sizes of the original greedy search algorithm up to 21 OWPPs from twelve.

In Chapter 6, a further addition to the greedy search algorithm is introduced that enables the incorporation of highly non-linear constraints, such as seafloor bathymetry and marine spatial planning. As these constraints vary significantly across different cases, ad-hoc approaches are proposed. An algorithm is presented that identifies candidate offshore substation locations by balancing the minimized cable length cost against the cost of the offshore substation foundation. The algorithm employs a penalty function and the A^* route finding algorithm to determine the shortest paths between connection points and then identifies the shallowest areas in the vicinity of these paths. Given the large size of the graphs used to represent sea bathymetry, the route finding algorithm can be computationally expensive. Therefore, two approximations of the full 3D spatial approach are proposed. The full method and the two approximations are compared using the Belgian offshore wind development region as a case study. All methods are capable of identifying high-quality solutions, with the approximations resulting in a considerable reduction in computation time at the cost of a minor degradation in solution quality.

In Chapter 7, an offshore wind generation and transmission expansion planning formulation is introduced. This formulation is designed to be market-aware and is presented in the form of a stochastic, step-wise, mixed integer linear program. Two variations of the formulation are presented, one based on a nodal pricing method and the other on a zonal pricing method. These formulations enable the user to design for a specific market structure and also compare different designs under varying market structures.

A test case is presented for the North Sea region to plan offshore generation and transmission infrastructure over a thirty-year horizon while considering three possible market structures: a nodal offshore bidding zone, a home market design, and a zonal offshore bidding zone. The resulting offshore network topologies suggest that the market structure has a more significant impact on social welfare than the network topology. It is observed that operating within a nodal offshore bidding zone leads to higher social welfare regardless of the solution topology chosen. Furthermore, the study finds little difference in social welfare between the three solution topologies provided they all operate within a nodal offshore bidding zone market structure.

8.3   Overall conclusions

Several important conclusions have been drawn from this research. It is useful to partition these into those relevant for modelers and those relevant to grid planners such as TSOs. Those relevant to modelers will be discussed first, followed by those relevant to planners.

At the scale of offshore wind power plant transmission systems, it has been found that while mathematical programming approaches can provide a mathematically global optimal solution, the strict requirements on the search space can eliminate a priori desirable solutions. Algorithmic approaches, on the other hand, such as the greedy algorithm presented in chapter 4, may provide the opportunity to define an expanded search space resulting in a superior solution despite not providing a guarantee on global optimality.

The exclusion of an optimal solution can occur a priori in mathematical programming due to structural constraints on the search space, such as convexity or linearity, or in the case of mixed integer expansion planning problems, due to heuristics introduced when defining the candidate equipment in the first place. This underscores the importance of having robust rules for defining candidates, and approaches such as that presented in Chapter 5 using association rule mining can greatly improve performance of a particular method.

Additionally, much consideration should be given to what constraints can be used to better define candidate infrastructure and restrict the search space. As demonstrated in Chapter 6, including bathymetric data and marine spatial planning can actually narrow down the possible locations for candidate offshore substations, simplifying the problem.

For planners, at the macro grid scale, while considering market-aware planning, our model presented in chapter 7 indicated that the social welfare of the system is more dependent on the market design than the technological design. Multiple topologies with very similar levels of social welfare, including one with a guarantee of global optimality, could be built in a nodally priced market structure, indicating that the search space around the optimal solution topology is relatively flat. This implies that planners should be less focused on designing the singular optimal topology and more focused on finding a topology that distributes the benefits among stakeholders in a desirable manner under the chosen market structure. To this end, our model indicated a nodal offshore bidding zone provides the highest social welfare, while the home market design provided the least.

8.4   Limitations

First, it is important to stress that the work performed as part of this thesis is not investment advice. I am not a financial advisor. The topologies presented and infrastructure investments discussed are the product of (often simple) test cases developed to investigate various planning and optimization strategies. In each case, there was an honest effort to choose the best available input data and make the most logical assumptions when needed. This does not imply, however, they are without error. I have done my best to be transparent with the assumptions and input data and leave it to the reader to decide for themselves when and where these were valid. And to do their own research. Hopefully research based on something interesting or novel that they learned while reading this thesis, that is related to the overall methodology or a particular approach adopted and not based on the specifics of the resulting infrastructure designs. In short, if anyone reading this gets the urge to invest billions of euros into infrastructure presented in this work, my recommendation is to please take a cold shower, then contact your financial advisor.

In an effort to enhance transparency, the author presents a list of assumptions made for the optimization models presented in this work. It is important to note that while these assumptions were deemed acceptable by the author, they may not be considered as such under certain conditions by readers.

- For Chapters 4, 5, and 6, the following assumptions were made:
  - The calculation of OPEX (losses, expected energy not transmitted, and corrective maintenance) for a radial topology is assumed to be possible a priori.
  - The aforementioned quantities are assumed to be reasonably estimated based on a historical generation time series.
  - CAPEX is assumed to be reasonably estimated based on historical prices.
  - The greedy algorithm assumes that the optimal topology can be obtained through cost minimization alone, i.e., the sum of CAPEX and OPEX.
  - The greedy algorithm models a single OWPP as a point located at the geographic center of the proposed concession, and the concession is modeled as a perfect circle.
  - The greedy algorithm TNEP formulation assumes that the optimal topology is radial.
- For Chapter 5, the following additional assumptions were made:

– The ARM-greedy algorithm assumes that a sufficient description of the search space is obtained by modeling the relative extremes and the mean in terms of possible wind development region layouts, i.e., parallel, perpendicular, and block formations.

– The ARM-greedy algorithm assumes that the proposed method of synthetic data generation provides a "rule-making" and a "control" population that are sufficiently independent to permit cross-validation.

- For Chapter 6, the following additional assumption was made:

  – The 3D candidate OSS placement algorithm assumes that an increase in depth alone is sufficient to approximate the additional OSS foundation cost.

- For Chapter 7, the following assumptions were made:

  – Transmission developers are modeled as merchants obtaining revenues from congestion rent rather than via energy tariffs.

  – Uncertainty within the operational time frame is ignored, as are unit commitment constraints.

  – The regulatory environment is considered uniform across European synchronous zones and the UK.

  – The UK is modeled as a member of the European internal energy market.

8.5   Future work

To conclude, I would really like to thank anyone who has made it this far and award them with some recommendations for interesting future work that have come out of this research.

1. Establish benchmarks for the offshore wind transmission expansion planning problem to allow for more meaningful testing and comparison of algorithms.

2. Develop algorithms for pre-processing candidate lines to reduce the number of binary decision variables required in simulations.

3. Revisit collection circuit optimization to consider advancements in technology, such as the soon-to-be reality of 132 kV technology for collection circuits, and investigate the most effective state-of-the-art approaches for this voltage level in combination with an HVDC transmission network.

4. Model and compare different kinds of flexible devices, such as lithium-ion storage systems, electrolyzers, data centers and even crypto currency mining rigs in the context of the offshore wind generation and expansion planning problem to capture the benefits of flexible devices on the system.

5. Address the lack of consideration of the uncertainty within the operational time frame in the GATE planning model of chapter 7. Consider modelling a two stage energy market, a reserve market and unit commitment.

6. Optimize the sizing of transmission cables for renewable energy sources by considering seasonality and exploring the possibility of combining floating solar with offshore wind.

7. Develop decomposition strategies for the offshore wind GATE planning problem to account for localized marginal (nodal) pricing, such as fast consensus ADMM or Bender's, and consider whether zonal decomposition is an effective approach.

Finally, bridging the gap between academic research models, as presented in this thesis, and those adopted by industry remains an essential task. Optimization models developed in academia often focus on generating a single global optimal solution based on a specific problem definition. However, industry requirements are often more complex, and the problem definition may change from one situation to another. As a result, solutions generated by academic models may not fully meet industry use cases, and adapting them to do so can be costly and time-consuming.

To address this challenge, it is important to prioritize models that offer flexibility, allowing for the generation of multiple options that can be iteratively dissected, recombined, and improved upon by design engineers. These hybrid tools should leverage both cutting-edge algorithms and human intuition and experience. Sacrificing the proof of global optimality for usability and flexibility may be necessary in some cases, and finding the right balance between the two is a challenging optimization problem in its own right.

Appendix A

Offshore transmission

A.1 Introduction

Onshore, HVAC transmission makes up the bulk of the existing transmission network. HVDC is present but is generally reserved for high capacity point to point connections. Offshore, this is unlikely to be the case as reactive power in subsea HVAC cables makes long distance, high capacity transmission inefficient and costly. The high reactive power in subsea HVAC transmission is perhaps the single most influential factor when determining the choice of transmission technology offshore. This important effect is visualized in Fig. A.1 for various AC transmission voltages.

Two important conclusions can be drawn from the figure. First, the traditional onshore approach of increasing the transmission voltage in order to increase capacity while reducing transmission losses has its limitations, since reactive power flows are proportional to the square of the voltage. Second, the impact can be mitigated or eliminated by lowering the frequency. The infrastructure required to alter the frequency, however, is expensive. Hence the choice of transmission technology from an economics perspective comes down to whether it is cheaper to compensate for the reactive power in an HVAC system or convert to a different network frequency.

---

[1]The work of this chapter has been published as: *Stephen Hardy, Hakan Ergun, Dirk Van Hertem, Stijn Hendrix, Kristof Van Brusselen, 'Techno-Economic Analysis of HVAC, HVDC and OFAC Offshore Wind Power Connections,'* in the conference proceedings of the 2019 IEEE Milan PowerTech. The content of the paper has been modified here to make it consistent with the other chapters of this dissertation. The first author is the main author of the paper.
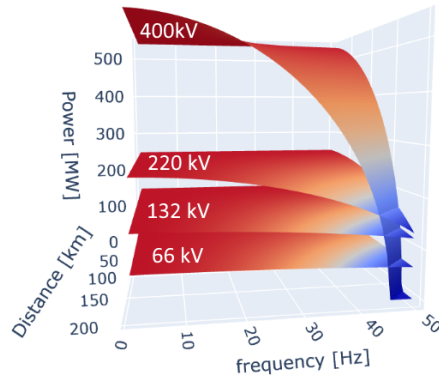
Figure A.1: 500mm^2 AC cable capacity dependence on voltage, frequency and distance.

A.2 Transmission options

The purpose of an offshore electrical power system is to efficiently and reliably collect and transmit the power generated at an offshore wind turbine to an onshore PCC. The power system can be effectively divided into three sub-systems. The collection circuit, the collection platform or OSS and the transmission system. Within each sub-system decisions such as technology e.g. alternating current or direct current, voltage level, frequency, topology and redundancy must be assessed.

The simplest transmission system consists of a radial connection to shore. A majority of OWPPs to date are connected in this manner. Transmission can be done in either HVAC or HVDC. There are several variations on HVAC transmission. The transmission options available are summarized in Fig. A.2.

Option (A): MVAC. A connection is made directly to shore at the voltage level of the collection circuit. This is only feasible when OWPPs are very close to shore.

Option (B): HVAC. As an OWPP moves further from shore, there comes a point where it is cheaper to build an OSS and step up the transmission voltage from MVAC to HVAC [222]. Lengthening HVAC submarine cables suffer from ever increasing capacitive reactance. The reactive currents eventually become so large that the entire thermal capacity of the transmission line is consumed by reactive power. This cut-off point is
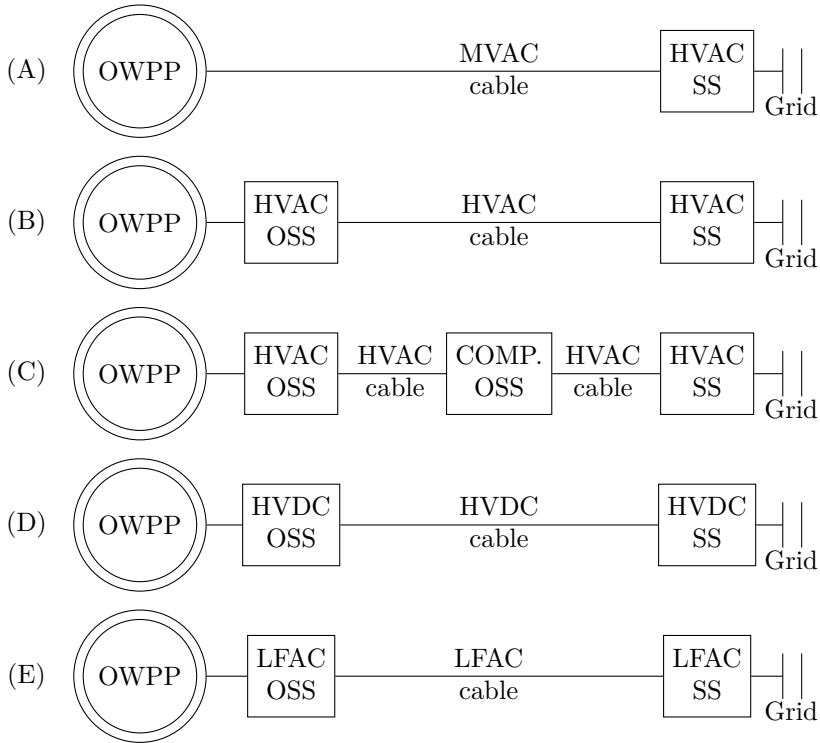
Figure A.2: Single line diagrams of (A) MVAC. (B) HVAC. (C) Mid-point compensated HVAC. (D) HVDC. (E) LFAC.

calculated as in:

$$L = \frac{I}{2\pi f C' \cdot V},$$ (A.1)

where I is the rated current, V is the rated voltage, f is the system frequency and C' is the cable capacitance.

Option (C):MPC-AC. Over a certain range, it is economic to compensate the reactive power in the cable by using shunt reactors at each end. When this range is exceeded, there is the option to build a platform at the mid-point of the cable and provide compensation in three spots rather than two.

Option (D): HVDC. As capacity and distance increase past a certain point, compensating for reactive power becomes too costly and HVDC transmission is the economic choice. MVAC is brought to an HVDC OSS where the voltage level is increased and it is rectified for transmission to

shore. Onshore a second HVDC station inverts the DC back to AC for connection with the existing grid.

Option (E): LFAC. There is a further option for dealing with the excessive reactive power buildup, transmitting at a frequency lower than standard 50 Hz but above 0 Hz (HVDC). Typical low frequency systems such as those used in railway traction operate at 1/3 mains frequency or 16.7 Hz. Theoretically, however, we can chose any frequency we like from direct current up to 50Hz.

A.3   Cost modelling

The cost model developed for this work attempts to capture the non-linear effects associated with reactive power and the discontinuities due to integer quantities of infrastructure investment. A trade-off between an investment in redundant paths (reliability) and upfront CAPEX is sought. The cost functions are adapted from those first proposed in [139]. Costs reported in commercial projects [183–188] are then relied on to calibrate the costs of contributing components. Cable data is taken from [216, 223, 224]. The included cable cross sections at each voltage level are listed in tables A.1 and A.2. The data structure of the model is displayed in Fig. A.3. As the original cost model was developed four years ago, the results presented in this chapter have been updated to reflect the most recently available data.

Transmission systems are broken down into several contributing costs. First, TCs and RCs are differentiated. TCs are distance independent costs associated to a node, for example an OSS and its components. RCs are costs tied to the cabling and depend on distance. TCs and RCs are then further subdivided into CAPEXs and OPEXs. All up front costs for equipment and installation are grouped into CAPEXs. All lifetime costs for corrective maintenance, losses and EENT are grouped into OPEX. The terms TCCs and RCCs are used for CAPEXs while TLCs and RLCs are used for OPEXs.

A.3.1   CAPEX

The non-linear features of the RCCs and TCCs are discussed in this section. The functions presented below use a superscript notation to avoid unnecessary repetition of equations. The xx notation is a place holder identifier that varies based on the transmission technology chosen. The cost of a specific technological solution can be determined by replacing xx with *AC* for HVAC, *DC* for HVDC or *LF* for LFAC and choosing the relevant cost parameter from table A.3.

Table A.1: HVAC cable sizes.

kV	mm^2	Amps	€/m
66	95	300	187.9
66	120	340	199.5
66	150	375	211.1
66	185	420	227.4
66	240	480	251.7
66	300	530	274.9
66	400	590	306.2
66	500	655	345.7
66	630	715	387.4
66	800	775	436.2
66	1000	825	482.6
132	300	468	313.4
132	400	523	401.4
132	500	581	471.5
132	630	642	512.7
132	800	702	609.6
132	1000	1007	647.3
132	1200	1081	680
132	1600	1227	740
220	400	590	496.5
220	500	655	597.4
220	630	715	638
220	800	775	783
220	1000	825	812
220	1600	950	1162
400	630	594	1374.6
400	800	636	1496.4
400	1000	671	1731.3
400	1600	779	2436
400	2000	840	2670.9
400	2500	893	3000

Table A.2: HVDC cable sizes.

kV	mm^2	Amps	€/km
500	95	404	277.2
500	120	387	294.4
500	150	463	311.5
500	185	496	335.4
500	240	580	371.4
500	300	662	405.6
500	500	1072	510
500	630	1246	516.5
500	800	1438	525
500	1000	1644	535
500	1200	1791	545
500	1400	1962	555
500	1500	2043	560
500	1600	2123	565
500	1800	2265	575
500	2000	2407	604
500	2200	2540	633
500	2400	2678	662
500	2500	2746	719
500	2600	2814	776
500	2800	2937	890
500	3000	3066	1004

RCC

Subsea transmission is complicated by high reactive power flows within alternating current cables that increase with network frequency, transmission voltage and distance as in:

$$Q^{\text{xx}} = 2\pi \cdot f^{\text{xx}} \cdot q_{cbl}^{\text{xx}} \cdot (V^{\text{xx}})^2 \cdot l_{cbl}^{\text{xx}} \cdot n_{cbl}^{\text{xx}}, \tag{A.2}$$

where, f is the network frequency in Hz, V the transmission voltage in kV, q_{cbl} the capacitance of the cable in F/km, l_{cbl} is the cable length in km and n_{cbl} is the number of cables in parallel.

It is typical to distribute reactive power compensation 50% onshore and 50% offshore. With this distribution the remaining cable capacity available for real
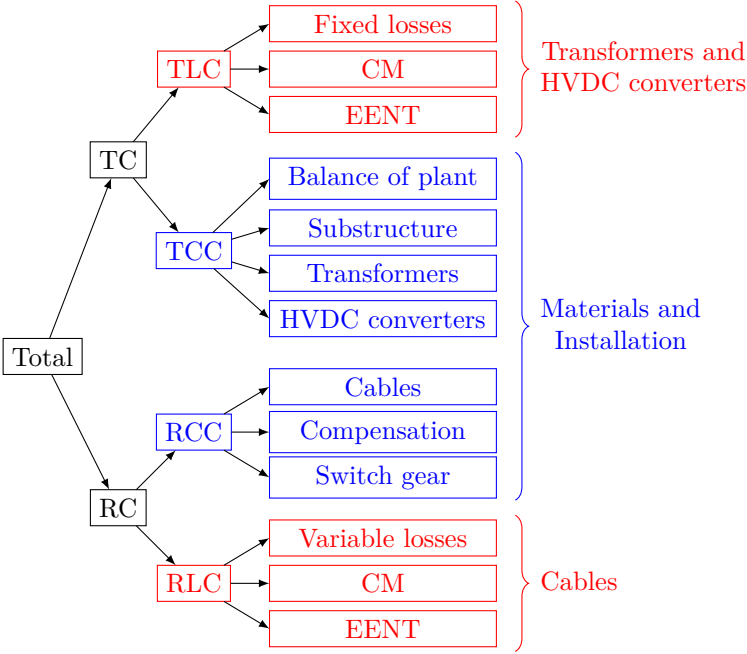
Figure A.3: Hierarchy of the cost model. CAPEX is in blue. OPEX is in red.

power transfer is calculated as in:

$$P_{cbl}^{\text{xx}} = \sqrt{(S_{cbl}^{\text{xx}})^2 - \left(\frac{Q^{\text{xx}}}{2}\right)^2}. \tag{A.3}$$

The cost of supplying this compensation is estimated as:

$$C_q^{\text{xx}} = \frac{c_{oss}^{\text{xx}} Q^{\text{xx}}}{2} + \frac{c_{ss}^{\text{xx}} Q^{\text{xx}}}{2}, \tag{A.4}$$

where c_{oss} and c_{ss} are the per unit costs specified in table A.3 for offshore and onshore reactive compensation respectively. The cost of supplying the cable is given by:

$$C_{cbl}^{\text{xx}} = n_{cbl}^{\text{xx}} \cdot c_{cbl}^{\text{xx}} \cdot l_{cbl}^{\text{xx}} \tag{A.5}$$

where c_{cbl}^{xx} is the per unit length cost in €/km. The total RCC is the sum of the cable and reactive power compensation as in:

$$RCC^{\text{xx}} = C_q^{\text{xx}} + C_{cbl}^{\text{xx}}. \tag{A.6}$$

Table A.3: Summary of cost parameters used in the economic model.

XX:	AC	DC	LF	Units	Description
c_{oss}^{XX}	0.10	0.00	0.10	€/W	cost of reactive compensation offshore
c_{ss}^{XX}	0.17	0.00	0.17	€/W	cost of reactive compensation onshore
$\overline{c_{oss}^{\text{XX}}}$	19.60	110.25	19.60	M€	fixed cost of OSS
$\widetilde{c_{oss}^{\text{XX}}}$	0.08	0.24	0.08	€/W	OSS substructure variable cost
$\widetilde{c_{oss}^{\text{XX}'}}$	0.10	0.24	0.10	€/W	OSS balance of plant variable cost
β_{oss}^{XX}	0.10	0.10	0.10	€/W	OSS penalization factor for parallel paths
β_{ss}^{XX}	0.33	0.15	0.15	€/W	Onshore substation variable linear cost
γ_{ss}^{XX}	0.75	1	1	-	Onshore substation variable exponential cost
η_{oss}^{XX}	99	98	98	%	OSS conversion efficiency
η_{ss}^{XX}	99	98	98	%	Onshore substation conversion efficiency

The non-continuous, exponentially increasing cost of (A.6) for a 220 kV, 50 Hz HVAC transmission up to a capacity of 1 GW and length of 100 km is shown in Fig. A.4. The non-continuous step-wise nature of the function is a product of the finite set of available cable cross sections.

TCC

TCC is the sum of the costs for the offshore and onshore substations. The cost of an OSS varies over the multi-dimensional axes of capacity, redundancy, and ocean depth as in Fig. A.5. The discontinuous plots of one to four illustrate the number of parallel paths within the OSS (redundancy). This relationship is expressed as:

$$C_{oss}^{\text{XX}} = \sigma(\zeta)(\overline{c_{oss}^{\text{XX}}} + (1 + \beta_{oss}^{\text{XX}} \cdot (n_{oss}^{\text{XX}} - 2))(\widetilde{c_{oss}^{\text{XX}}} + \widetilde{c_{oss}^{\text{XX}'}}) \cdot P_{oss}^{\text{XX}} \cdot \alpha^{\text{XX}}),$$

$$\text{where } \sigma(\zeta) = 0.0136 \cdot (\zeta - 17) + 0.7676 \tag{A.7}$$

where n_{oss} is the number of parallel paths, β_{oss} is the penalization factor for greater than two parallel paths, $\overline{c_{oss}}$ is the fixed OSS cost, $\widetilde{c_{oss}}$ is the variable
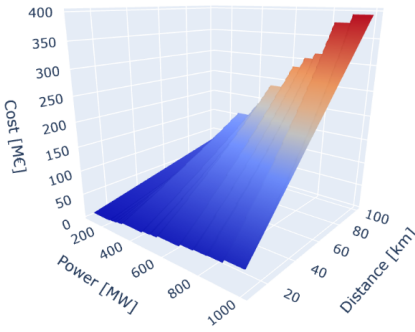
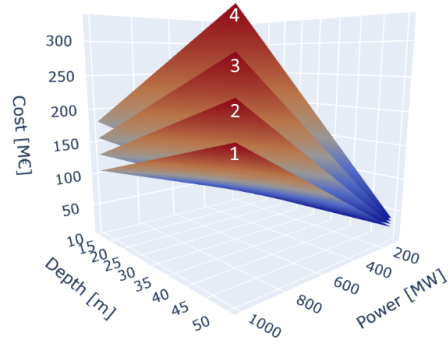Figure A.4: 220 kV, 50 Hz cable cost as a function of power and distance.

Figure A.5: Cost of an OSS as a function of sea depth, capacity and redundancy.

substructure cost, $\widetilde{c'_{oss}}$ is the variable balance of plant cost, P_{oss} is the substation capacity and ζ is the sea floor depth. α is a scaling factor for LFAC discussed in further detail below. For HVAC and HVDC networks it is always equal to one.

In an onshore substation, no substructure is required therefore increased reliability does not result in a substantial increase in steel and concrete as it does offshore. As such, n-1 reliability is assumed and the simpler cost function:

$$C_{ss}^{\text{XX}} = \beta_{ss}^{\text{XX}} \cdot (P_{ss}^{\text{XX}})^{\gamma^{\text{XX}}}. \tag{A.8}$$

is considered.

LFAC

Estimating the cost of an LFAC system is difficult as no commercial projects have been built. In this work it is assumed that the lower frequency would be generated at the output of each turbine. As such the collection circuit as well as the transmission system benefit from the lower frequency. It is assumed that no additional cost is incurred to supply a sub 50 Hz frequency turbine mounted inverter. The cable costs are also assumed to be the same as a 50 Hz system despite an expected decrease in the skin effect, potentially allowing the cross section to be reduced. These two neglected costs are assumed to be small and to operate in opposite directions, i.e. reducing converter frequency to non standard will increase cost while reducing skin effect will reduce it.

The main cost associated with a lower frequency is assumed to be at the OSS as transformers and reactors are the components most affected by a drop in frequency. Since the magnetic flux density is not significantly altered with changing frequency, the desired voltage must be maintained by either changing the number of turns or the area of the core [225]. This will result in an increase in the size and cost of the components, which in turn will translate to an overall increase in the size and cost of the OSS.

As frequency decreases from 50 Hz, it is assumed the cost of an LFAC OSS will range from that of a standard HVAC OSS of the same capacity up to that of an HVDC OSS as the frequency approaches 0 Hz. It is also assumed that cost will increase proportionately with the size of a transformer. Therefore to size α in (A.7), studies estimating the increase in size required for 1/3 frequency transformers were consulted. In [225] the overall increase in the mass of transformers is shown to be approximately 77 %. In [226] however, a doubling in mass is projected. Using these two bounds, an expected range for the OSS cost is defined as:

$$(\frac{f^{\text{AC}}}{f^{\text{XX}}} + 1.6)/2.6 \leq \alpha^{\text{XX}} \leq (\frac{f^{\text{AC}}}{f^{\text{XX}}} + 1)/2 \; : \; f^{\text{XX}} > 0. \;\; \alpha^{\text{XX}} = 1 \; : \; f^{\text{XX}} = 0. \;\; \text{(A.9)}$$

The onshore LFAC substation is assumed to cost the same as an equivalently sized voltage source converter HVDC substation. On one hand this may be an underestimate as according to [227], the number of active switches and reactive components for an AC/AC converter is greater than for an AC/DC. Particularly, if back to back converters are required. On the other hand, the use of lower cost line commutated converter technology rather than voltage source converters should be possible.

A.3.2 OPEX

Losses

Equipment losses are modelled as the sum of variable losses in the cables (RLC) and fixed losses in the transformers and converters (TLC). Variable losses capture the I^2R losses in cables. Both alternating current and direct current cables are modelled with the same equation:

$$RLC^{\text{XX}} = \left(\frac{P_{oss}^{\text{XX}} \cdot \eta_{oss}^{\text{XX}}}{n_{cbl}^{\text{XX}} \cdot V^{\text{XX}}} \right)^2 \cdot r_{cbl}^{\text{XX}} \cdot l_{cbl}^{\text{XX}} \cdot n_{cbl}^{\text{XX}} \cdot T \cdot E \cdot \delta, \qquad \text{(A.10)}$$

where r_{cbl} is the cable resistance in Ω/km and η_{oss} is the conversion efficiency of the OSS in percent. The alternating current resistance is used for alternating

current cables and direct current resistance for direct current cables. T, E and δ are the operational lifetime (25 years), energy price (90€/MWh) and load loss factor.

The load loss factor is a function of the square of the per unit power generation profile as in:

$$\delta = \frac{\sum\limits_{t=0}^{T}(S_{g,t}^{\mathrm{pu}})^2}{T}. \tag{A.11}$$

Fixed losses occur in the transformers and converters. They are the magnetic core losses in the transformers and the switching losses in the converters. The fixed losses for offshore and onshore components are given by equations A.12 and A.13. η_{ss} is the onshore substation conversion efficiency.

$$TLC_{oss}^{\mathrm{XX}} = P_{pcc}^{\mathrm{XX}} \cdot (1 - \eta_{oss}^{\mathrm{XX}}) \cdot T \cdot E \cdot \delta \tag{A.12}$$

$$TLC_{ss}^{\mathrm{XX}} = (P_{pcc}^{\mathrm{XX}} \cdot T \cdot E \cdot \delta - RLC^{\mathrm{XX}})(1 - \eta_{ss}^{\mathrm{XX}}) \tag{A.13}$$

Reliability

System reliability is considered in terms of corrective maintenance and EENT. corrective maintenance is considered post fault, meaning it is the cost of replacing or repairing faulty equipment. Preventative maintenance is not considered within the scope. Yearly corrective maintenance is calculated using the mean time to repair(μ), failure rate(λ) and mean cost per repair(ξ) as in (A.14) [139]. The parameters for transformers, converters and cables are given in table A.4. corrective maintenance for the remaining components is not considered. The total corrective maintenance is obtained by summing over the NPV of all years within the lifetime of the project. An intuitive understanding of (A.14) is as the product of the availability (A), failure rate (λ) and mean cost of repair (ξ) for each piece of equipment.

$$CM_y = \left[\frac{n_{oss}^{\mathrm{XX}} \cdot \xi_{oss}^{\mathrm{XX}}}{\frac{1}{\lambda_{oss}^{\mathrm{XX}}} + \frac{\mu_{oss}^{\mathrm{XX}}}{8760}} + \frac{n_{cbl}^{\mathrm{XX}} \cdot \xi_{cbl}^{\mathrm{XX}}}{\frac{1}{\lambda_{cbl}^{\mathrm{XX}}} + \frac{\mu_{cbl}^{\mathrm{XX}}}{8760}} + \frac{n_{ss}^{\mathrm{XX}} \cdot \xi_{ss}^{\mathrm{XX}}}{\frac{1}{\lambda_{ss}^{\mathrm{XX}}} + \frac{\mu_{ss}^{\mathrm{XX}}}{8760}} \right] \tag{A.14}$$

The second component of reliability considered is EENT. Additional EENT is available wind energy that must be curtailed due to system capacity constraints. The system capacity may be constrained intentionally through under sizing of equipment or due to component failure. ΔEENT is calculated as follows: consider contingency i with constrained capacity, P_i^{cons}, and probability of occurrence, π_i^{cons}, the per unit ΔEENT is given by:

Table A.4: Reliability Parameters [139]

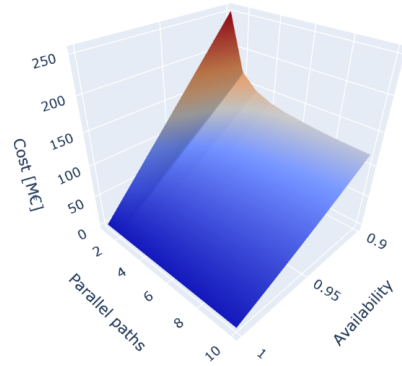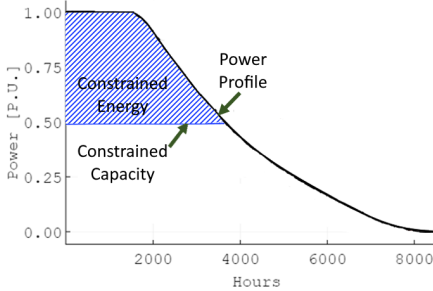| Equipment	λ $[1/yr]$	μ $[hours]$	ξ $[M\text{\euro}]$
Transformers	0.03	1440(PCC) 4320(OSS)	2.75
Converters	0.12	720	0.56
Cables	0.08/100km	1440	0.56

Figure A.6: The constrained energy is equal to the area under the power profile and above the constrained capacity.

Figure A.7: The cost of EENT for an arbitrary 1 GW piece of equipment as a function of parallel paths and availability.

$$\Delta EENT_i^{\text{PU}} = \text{A}_i^{\text{cons}} \cdot \pi_i^{\text{cons}}. \tag{A.15}$$

Where A_i^{cons} is the area under the OWPP generation power curve and above the line y=P_i^{cons} shown in Fig. A.6. The power generation profile is obtained using meteorological data and the CorWind software [168]. Summing over all contingencies and multiplying by the OWPP peak capacity gives the yearly EENT. The cost of EENT is then obtained by summing the NPV of each year within the lifetime.

Constrained capacities and their probabilities are calculated from capacity outage probability tables for all considered contingencies. The capacity outage probability table of a single piece of equipment is calculated as follows. A piece of equipment x has capacity, P_x. The number of possible states N_x of the equipment is modelled as binary (1: functional, 0: broken). The availability of

the piece of equipment A_x, is given by:

$$A_x = \frac{1}{1 + \lambda_x \cdot \frac{\mu_x}{8760}}.$$ (A.16)

The resulting capacity outage probability table is as in table A.5. To construct

Table A.5: Example capacity outage probability table.

State (i)	Capacity ($P_{x,i}^{\mathrm{cons}}$)	Probability ($\pi_{x,i}^{\mathrm{cons}}$)
1	P_x	A_x
0	0	1-A_x

a capacity outage probability table for an entire system, convolution of all component capacity outage probability tables is done as in:

$$P_k =: \begin{cases} P_{x,i} + P_{y,j} & \text{Parallel} \\ min(P_{x,i}, P_{y,j}) & \text{Series} \end{cases}$$

$$\pi_k = \pi_{x,i} \cdot \pi_{y,j}$$ (A.17)

$$\text{where } i = \{1,..,N_x\}, j = \{1,..,N_y\}, k = \{1,...,N_x \cdot N_y\}$$

If after combining two tables, two rows k have identical capacities, they are combined into a single row with a common capacity and a probability equal to the sum of the individual probabilities.

To illustrate the relationship between the redundancy of equipment, availability and EENT, Fig. A.7 shows the cost of EENT for a fictitious transmission system component connecting a 1 GW OWPP. The availability of the component is varied between 0.9 and 1 while simultaneously varying the number of parallel paths from one to ten. The net transmission capacity of the component is maintained constant at 1 GW no matter the number of parallel paths. It is an important observation that the marginal decrease in EENT is small after the number of parallel paths exceeds two.

A.4 Results

What follows are the resulting estimates for the ranges of the analyzed transmission technology options. Please note, the proposed model is simple and the exact range for the technologies is highly dependant on available data thus the presented ranges should be understood as only very rough estimates. When considering a radial connection with the options of 66 kV MVAC, 132 kV, 220 kV

and 400 kV HVAC, 220 kV MPC-AC and 500 kV HVDC the technological solution space is shown in Fig. A.8. Above 500 MW a relatively stable relation appears where a connection made at 66 kV is the lowest cost option up to about 60 km, between 60 and 125 km it is better to transmit at 220 kV and once 125 km has been surpassed, HVDC becomes the best option. Below 500 MW the relationship complicates.

At very low power levels the 66 kV range increases to a maximum of 125 km at 100 MW. The range of 220 kV HVAC also increases. The highest viable distance is at 225 km at 100 MW. In very few instances 132 kV becomes the optimal choice. The range of MPC-AC starts around 150 km and reaches it's
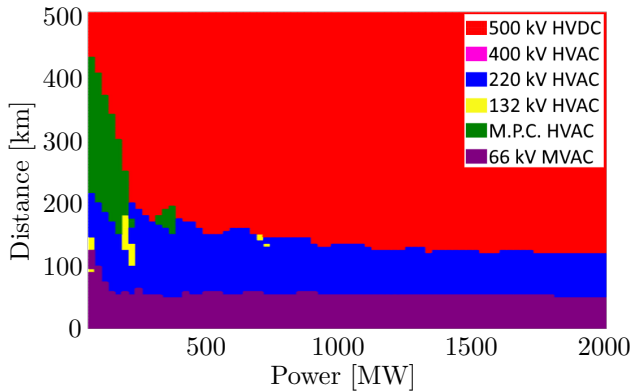

Figure A.8: Range of optimal technology for a point to point connection considering: 66 kV collection circuit, 132 kV/220 kV/400 kV HVAC, 220 kV mid-point compensated HVAC, 500 kV HVDC.

maximum feasible range near 425 km. The optimal choice of technology in the lower range of OWPP capacity appears complicated, however, it is likely that this complicated technological solution space is more of a product of poor data availability than a truly varied technological optimal. At low capacities, the relative jump between single cable sizes can have a substantial impact on the cost, e.g. choosing between a cable of 100 MW and 150 MW to transmit 110 MW. At higher capacities as cables start to be placed in parallel to meet the load, the relative jump between available options decreases. This jump between available sizes can be reduced by considering an exhaustive list of available conductor sizes from multiple manufacturers as well as both aluminium and copper options.

A surprising result is perhaps the complete lack of an optimal range for 400 kV HVAC transmission. In reality, however, this result is expected. First, as was

demonstrated in Fig. A.1 the available capacity of an HVAC cable for real power drops with the square of the voltage as distance increases. This means that the advantages gained of higher capacity and lower losses that make a higher transmission voltage appealing for over-head lines are offset at higher distances by reactive power flows. This fact alone would perhaps not completely eliminate 400 kV from the technological solution space but there is also the fact that due to higher insulating requirements 3-core 400 kV cables are not available, making the cost of installation significantly higher than at lower transmission voltages.

Considering the high value associated with standardization the results support the idea that only three transmission technologies need be considered offshore: 66 kV collection circuits, 220 kV HVAC transmission and 500 kV HVDC. In certain edge cases mid-point compensated HVAC may prove useful. It is strongly believed, however, that in practice when cable manufacturers can be consulted directly and an exhaustive selection of cross sections in both aluminium and copper conductors can be considered any alternatives to these voltage levels and technologies would only be marginally cheaper at the very best.

Having examined the technological solution space considering the current state of available technologies, it is important to think in terms of future technological solutions. In the near future 132 kV collection circuits will be available. If we again calculate the optimal range considering currently available technologies plus 132 kV collection circuits, the picture simplifies further as can be seen in Fig. A.9. The need for anything beyond 132 kV collection circuits with 500 kV HVDC seems unlikely. 132 kV collection circuits are the lowest cost option up to about 175 km. From this point 500 kV takes over as the cheapest solution. This technological arrangement results in a network that is simple and highly standardized, simplifying long term planning significantly.

LFAC

If one is to consider the option of LFAC, the optimal choice of technology in the 100–500 MW range is affected. This is shown in Fig. A.10. Almost the entire range of mid point compensated HVAC would be better served by LFAC, even if considering the high end cost estimate for LFAC (right side of the figure). Despite having an applicable range, it seems difficult to justify the development of such a technology for such a limited application. Using LFAC would severely complicate standardization and supply chains. Furthermore, as previously discussed, it is likely that sourcing more cable cross sections would permit 500 kV HVDC to operate more cheaply within this range.

Comparing the various technological options available in greater detail for 225 MW as in Fig. A.11, we can see several transitions between different
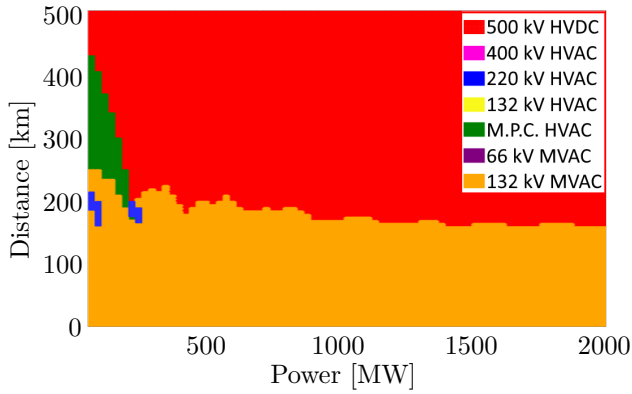
Figure A.9: Range of optimal technology considering: 132 kV collection circuit, 132 kV/220 kV/400 kV HVAC, 220 kV mid-point compensated HVAC, 500 kV HVDC.
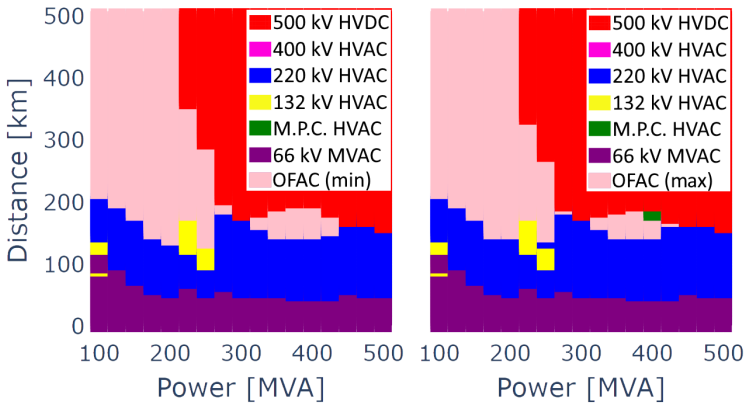

Figure A.10: Optimal range for LFAC technology when considering 66 kV collection circuit, 220 kV HVAC, 220 kV mid-point compensated HVAC, 500 kV HVDC up to 500 MW.

technologies as the OWPP moves away from shore. The interplay of each technological cost function is interesting. We can see that the alternating current technologies start out much cheaper than the alternatives but their cost starts to rapidly increase eventually turning parabolic. The increase affects higher voltage levels quicker, first 220 kV moves to parabolic, then 132 kV and 66 kV. Using MPC-AC reduces this effect on 220 kV for a while but eventually it too succumbs to the high cost associated with reactive power. Reactive power is dealt with well by LFAC. Along the base of the figure, the slowly dropping optimal frequency of transmission is shown allowing the cost function to remain linear. The optimal frequency first starts to drop below 50 Hz around 100 km from shore. Once 185 km is reached the frequency is 27 Hz and LFAC is the lowest cost option. This continues up to 375 km. From 375 km on, there is but one option, HVDC. When comparing the cost of LFAC and HVDC, both are essentially linear, as reactive power does not play a significant role. HVDC, though, has a higher fixed cost and LFAC a higher variable cost.
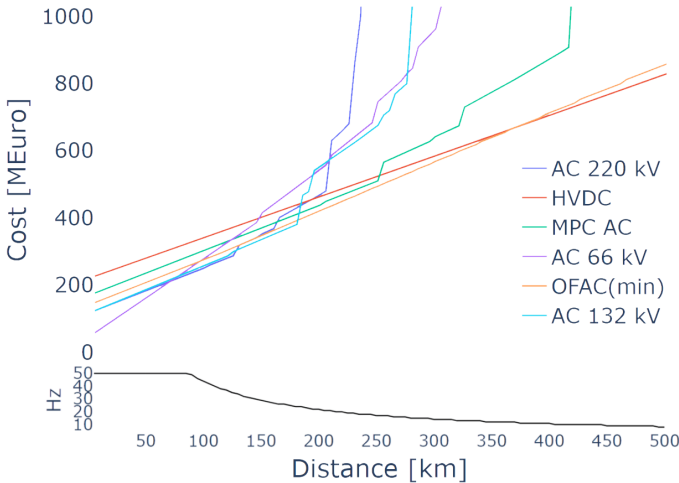

Figure A.11: Cost functions for different technologies at 225 MW.

A.5 Conclusions

In this section a techno-economic model for OWPP connections is developed. Connection technologies considered are MVAC, HVAC, MPC-AC, HVDC and LFAC. The model accounts for CAPEX, electrical losses, corrective maintenance

and EENT. System reliability is considered by balancing upfront investment in redundant paths (parallel equipment) with EENT and corrective maintenance.

The model is used to predict an optimal technological solution space under varying OWPP capacities and distances from shore. It is shown that the entire solution space can be effectively covered by only considering 66 kV collection circuits with 220 kV HVAC and 500 kV HVDC. Both MPC-AC and LFAC are found to have a useful range below 500 MW however, it is theorized that this range would shrink and possibly disappear if a larger selection of cable cross sections are considered as well as both copper and alluminium conductors. It is also concluded that developing an LFAC system for such a limited range is not desirable, especially when considering the benefits of standardization and efficiency in supply chains.

When considering future technologies, 132 kV collection circuits can be included. Doing so has a dramatic and positive impact on the solution space. If 132 kV collection circuits are adopted, the 220 kV transmission level can be completely eliminated. 132 kV becomes the best option for transmission up to about 175 km, after which 500 kV HVDC takes over. Having a single, standardized HVAC and HVDC transmission voltage for all offshore transmission is certainly a desirable outcome.

Appendix B

Meshed connections

B.1 Introduction

Until now, only radial connections for single OWPPs have been considered. In this section the possibility of meshed connections between neighbouring OWPPs are considered. As there is a growing consensus that an HVDC grid would be meshed [16, 228], the focus of this study is the HVAC network. To investigate the question of whether offshore HVAC transmission networks should be meshed, the following study is performed.

1. A random population of pairs of OWPPs is generated as described in section B.1.1.

2. For each pair of OWPPs within the population two connection topologies are calculated:

   - The lowest cost radial connection.
   - The lowest cost meshed connection.

   Topologies are determined using the brute force method as described in section section B.1.2.

[1]The work of this chapter has been published as: *Stephen Hardy, Hakan Ergun, Dirk Van Hertem, 'A Techno-Economic Analysis of meshed Topologies of Offshore Wind HVAC Transmission'*, in the conference proceedings of the 2021 IEEE Madrid PowerTech. The content of the paper has been modified here to make it consistent with the other chapters of this dissertation. The first author is the main author of the paper.

3. A statistical analysis is performed on the results to provide insight into the frequency meshed topologies are the lowest cost option as well as the characteristics of the OWPP layouts where this is most likely to be the case.

B.1.1   OWPP population

A random population K of pairs of OWPPs is generated from the search space described in Fig. B.1.
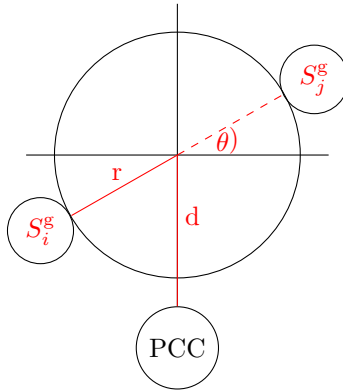

Figure B.1: Sampling domain.

A member $\kappa \in K$ is described by a set of five variables:

$$\kappa = (S_i^{\mathrm{g}}, S_j^{\mathrm{g}}, r, d, \theta). \tag{B.1}$$

S_i^{g} and S_j^{g} are the maximum capacities of OWPPs i and j respectively. r is the radius of the circle with both OWPPs laying on its perimeter. d is the distance to the centre of the the circle measured from the PCC. And θ is the angle formed by the line connecting the centre of the circle with OWPP j and a perpendicular line to d that emanates from the centre of the circle. The values of decision variables are restricted to the following ranges:

$$S_i^{\mathrm{g}} \text{ and } S_j^{\mathrm{g}} \in \{200, 210, ...990, 1000\} \text{ [MVA]},$$

$$0.5 \le r \le 15\,km,\ 20 \le d \le 100\,km,\ 0 \le \theta \le \pi/2 \tag{B.2}$$

The inherent symmetry of the search space is leveraged to restrict θ between 0 and $\pi/2$ without loss of information. Sampling with replacement as in [229] is

used to build a total population K of size $N = 16513$. The population size was selected to provide a $(1 - \alpha)$ confidence interval of 99%, implying a sampling error, e, of less than 1% as in:

$$N \geq \frac{z_{\alpha/2}^2}{4e^2}, \tag{B.3}$$

where $z_{\alpha/2}$ is the Z-statistic.
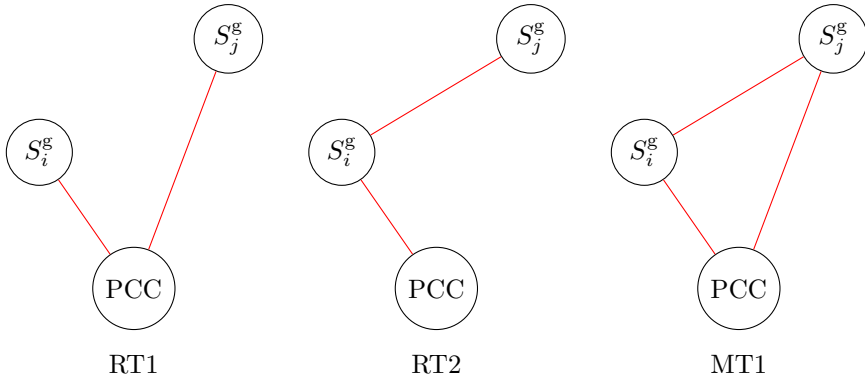
B.1.2 Connection topologies

Figure B.2: Connection options.

For each OWPP pair, κ, three topological variations of connections to the PCC: radial connection 1 (RT1), radial connection 2 (RT2) and a meshed connection (MT1) as shown in Fig. B.2 are calculated. The brute force approach is used in each case to find the lowest cost component infrastructure. On the medium voltage side 66 kV is considered and on the high voltage side, both 220 kV and 400 kV options are considered.

EENT

The cost of topologies RT1 and RT2 are calculated in the manner presented in section A.3 of this chapter and require no further explanation. In the case of topology MT1, however, a reduction in EENT is expected due to the increased reliability inherent in a meshed topology. A modification in the calculation of EENT is therefore required and is done as follows.

Two variations of topology MT1 are defined: $MT1^{\#}$ and $MT1^{-}$. $MT1^{\#}$ is identical to MT1 in every way while $MT1^{-}$ is MT1 with the meshed connection removed. For each of these variations we solve a linear program to maximize the consumption at the PCC as in:

$$\max_{\mathbf{S}^{\mathrm{g}}, \mathbf{S}^{\mathrm{d}}, \theta} S^{\mathrm{d}}_{pcc} \tag{B.4}$$

subject to constraints (B.5) for each considered contingency, c, i.e. failure of a cable or transformer. This is done considering OWPP generation levels g of 20, 40, 60, 80 and 100% of full capacity. Due to the geographic proximity of the OWPPs, the wind speeds are assumed highly correlated therefore $S^{\mathrm{g,max}}_i$ and $S^{\mathrm{g,max}}_j$ are varied in unison.

In (B.5) $\mathcal{N}$ is the set of nodes in the topology and $\mathcal{E}$ the edges connecting the nodes. S^{g}_i and S^{d}_i are the generation and demand at node i respectively, S_{ij} the power flow from node i to j, b_{ij} the susceptance between node i and j and θ_i the voltage angle at node i.

$$
\left.
\begin{aligned}
S^{\mathrm{g}}_i - S^{\mathrm{d}}_i &= \sum_{(i,j) \in \mathcal{E}} S_{ij} - \sum_{(j,i) \in \mathcal{E}} S_{ji} \\[2mm]
S_{ij} &= \sum_{(i,j) \in \mathcal{E}} b_{ij}(\theta_i - \theta_j) \\[2mm]
S_{ij} &= -S_{ji} \\[2mm]
0 &\leq S^{\mathrm{g}}_i \leq S^{\mathrm{g, max}}_i \\[2mm]
-S^{\mathrm{max}}_{ij} &\leq S_{ij} \leq S^{\mathrm{max}}_{ij} \\[2mm]
\theta^{\mathrm{min}}_i &\leq \Delta\theta_i \leq \theta^{\mathrm{max}}_i
\end{aligned}
\right\}
\quad
\begin{aligned}
&\forall i \in \mathcal{N} \\[4mm]
&\forall (i,j) \in \mathcal{E}
\end{aligned}
\tag{B.5}
$$

For each contingency c and generation level g the additional power delivered to the PCC via the meshed connection as in:

$$\Delta S_d(g, c) = S^{\mathrm{d,\#}}_{pcc}(g, c) - S^{\mathrm{d,-}}_{pcc}(g, c) \tag{B.6}$$

is calculated. By subtracting ΔS_d from the radial generation profile a new power generation profile as seen by the component under contingency operation in MT1 can now be constructed as in Fig. B.3. The adjusted EENT for MT1 is then calculated in the same manner as for a radial connection but with the constrained energy defined by the area under curve $S^{\#}_{ij}$ rather than S^{-}_{ij}.
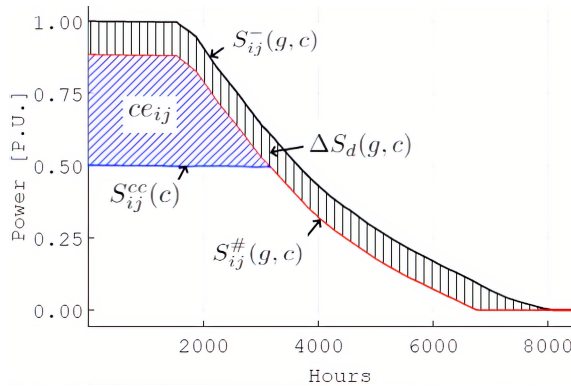
Figure B.3: Adjusted power injection profile in meshed topology.

B.2   Statistical Analysis

Considering RT1, RT2 and MT1 topologies as options results in a very low percentage of MT1 topologies being chosen. At 220 kV this amounts to 0.6 % of the time and at 400 kV, 1.4 %. A summary of the percent composition of lowest cost topology over the sample population is provided in table B.1.

Table B.1: Percent composition of lowest cost connection topology for the sample population considering RT1, RT2 and MT1 options.

220 kV			400 kV		
RT1	RT2	MT1	RT1	RT2	MT1
61.4	38.0	0.6	47.6	51.0	1.4

To better understand this result it is insightful to exclude the RT2 topology and make a comparison when considering only RT1 and MT1 topologies, as these two variations only differ by the inclusion or exclusion of the meshed connection. When doing so, the percentage of MT1 topologies selected increases to 4.2 % at 220 kV and 9.6 % at 400 kV. Of these connections a majority of meshing is on the HV bus side (69.4 %) versus MV bus side (18.1 %).

The average savings achieved when a meshed connection is selected is small, 2.6 % at 220 kV and 6.5 % for 400 kV. Under the best conditions, however, the savings can be much higher with the maximum savings at 220 kV found to be 14.7 % and 21.1 % for 400 kV. After isolating only the most beneficial meshed connections, those that result in a savings of at least 10 %, they are found to be concentrated around two regions in the solution space. For 220 kV this is

found when OWPPs capacities are in the 300-400 MVA range and for 400 kV
in the 500-800 MVA range. These regions are illustrated by holding θ at zero
while plotting the savings of MT1 over RT1 in Fig. B.4.

In figures (A) and (C) the OWPP capacities are held constant while the distance
to shore (d) versus OSS to OSS distance ($2r$) is varied. In (B) and (D) the
distance to shore (d) versus OWPP capacity ($S_i^{g,max}$, $S_j^{g,max}$) is varied, while
holding $r = 1$ km constant.
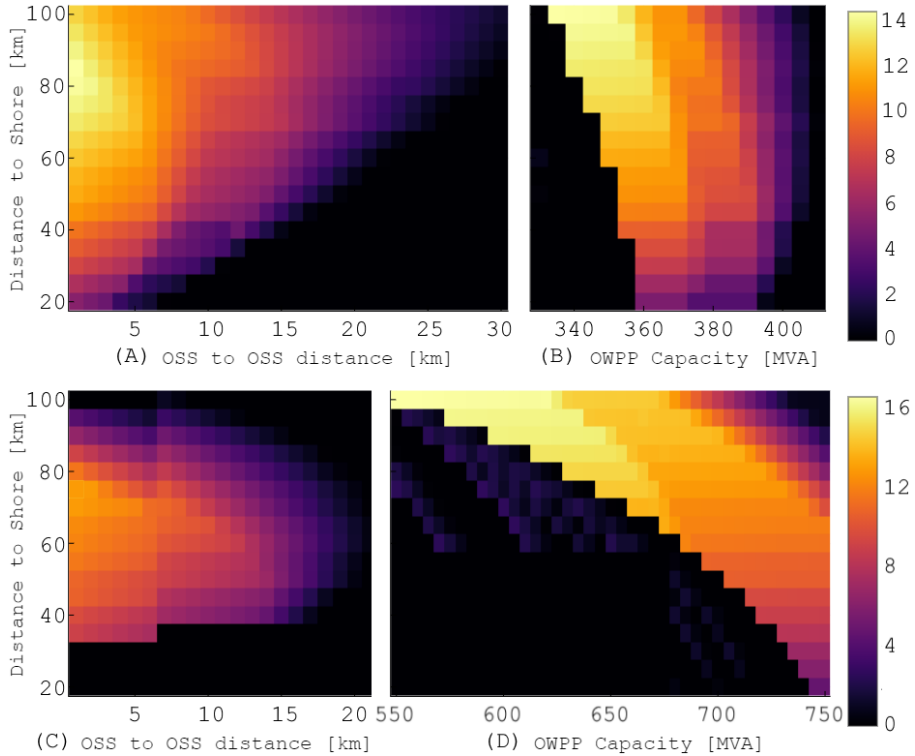
Figure B.4: Heatmap of percent savings of MT1 over RT1 for θ=0. Top: 220 kV.
Bottom: 400 kV. (A) $S_i^{g,max} = S_j^{g,max} = 360$ MVA. (C) $S_i^{g,max} = S_j^{g,max} =$
720 MVA. (B), (D) The OSS to OSS distance is fixed at 1 km.

A first observation, from (A) and (C), is that as the distance between OSSs
shrinks, the benefit of a meshed connection increases. This is a very logical result
as the cost of connecting the OSSs drops the closer they are. This also explains
why so many fewer MT1 topologies are selected when including the option of
an RT2 topology, as at short OSS to OSS distances the best alternative is to
eliminate an OSS entirely and connect both OWPPs at 66 kV to a single OSS

and export cable. This observation is reinforced by the fact that the median distance between OWPPs for selected MT1 topologies increases from 14 km to 20 km at 220 kV and 12 km to 19 km at 400 kV if RT2 is considered.

A second observation, from (B) and (D) is that there is an abrupt transition (black to yellow) where MT1 topologies are most beneficial. Investigating these regions in detail we find that this transition at 220 kV is at the point where the RT1 export cable changes from a single 1000 mm^2 3-core cable to two parallel 400 mm^2 3-core cables. At 400 kV a similar finding, where three single core 2000 mm^2 cables are no longer of sufficient capacity and are replaced by two parallel sets of single core 630 mm^2 cables. At both of these transitions the new cable sets have low loading to max capacity ratios of around 70 %. In other words, there is a poor match between available cable capacities and desired transmission capacity.

This observation is further evidence towards the conclusion that radial offshore HVAC network topologies are the best choice, since those found to benefit most from meshed connections are due to the large step sizes between the cable cross sections. This implies the very small percentage of MT1 topologies selected would be even further reduced if an exhaustive list of available cable cross sections and conductor materials were considered.

A final observation is that beyond the capacities discussed above, it becomes necessary to start using parallel feeders for radial connections. As it was demonstrated earlier in Fig. A.7, the benefit beyond two parallel paths from increased reliability drops off rapidly making the need for meshing less likely. Hence the lack of selected MT1 topologies in the higher capacity regions is in line with expectations. Extending this thinking, we would not expect this to change with an increase in OWPP capacities beyond the modelled 1 GW range or 100 km distance from shore.

B.3   Conclusions

Having established a techno-economic solution space for radial OWPP connections, a method to investigate the benefits of increased reliability through meshed topologies is presented. The method looks at a representative sample of pairs of OWPPs to see when the lowest cost connection involves a meshed connection between the OSSs. Meshed connections are found to be rarely cheaper than the simple radial connections.

Those that are cost effective tend to be concentrated around regions where there is a poor match between available export cable cross sections and desired

transmission capacity. As with the range for MPC-AC and LFAC it is believed that in practice manufacturers would be able to provide a large enough selection of cable cross sections and conductor materials to effectively reduce the higher cost radial connections and make them competitive or even cheaper than the few meshed topologies that were found to be cost efficient. An important observation as to why meshing is not so effective is that many high capacity radial connections already have built in redundancy as parallel cables are needed to carry the required capacity (particularly at 220 kV). The marginal increase in reliability gained from parallel paths above two can rarely be justified.

Appendix C

Candidate transmission lines

Table C.1: HVAC and HVDC Candidate transmission lines for North Sea GATE test case.

Routes			Candidate Cables (S_ℓ)
start	end	km	$\mathcal{G}$
UK1	FR	175	DC1-DC3
UK1	BE	188	DC1-DC3
UK1	NL	250	DC1-DC3
UK1	DE	565	DC1-DC3
UK1	DK	754	DC1-DC3
UK1	BE(WF)	129	DC1-DC3
UK1	DE(WF)	443	DC1-DC3
UK1	NL(WF)	204	DC1-DC3
UK1	DK(WF)	639	DC1-DC3
UK1	UK(WF)	716	DC1-DC3
FR	BE	130	DC1-DC3
FR	DE(WF)	565	DC1-DC3
FR	NL(WF)	328	DC1-DC3
BE	NL	168	DC1-DC3
BE	DE	511	DC1-DC3
BE	DK	752	DC1-DC3
BE	BE(WF)	61	DC1-DC3, AC1-AC3
BE	DE(WF)	464	DC1-DC3
BE	NL(WF)	247	DC1-DC3
BE	DK(WF)	684	DC1-DC3
BE	UK(WF)	859	DC1-DC3

NL	DE	346	DC1-DC3
NL	DK	586	DC1-DC3
NL	NO	873	DC1-DC3
NL	UK2	713	DC1-DC3
NL	BE(WF)	189	DC1-DC3
NL	DE(WF)	308	DC1-DC3
NL	NL(WF)	146	DC1-DC3, AC4, AC5
NL	DK(WF)	531	DC1-DC3
NL	UK(WF)	770	DC1-DC3
DE	DK	280	DC1-DC3
DE	NO	679	DC1-DC3
DE	UK2	834	DC1-DC3
DE	BE(WF)	534	DC1-DC3
DE	DE(WF)	212	DC1-DC3
DE	NL(WF)	369	DC1-DC3
DE	DK(WF)	337	DC1-DC3
DE	UK(WF)	753	DC1-DC3
DK	NO	444	DC1-DC3
DK	UK2	836	DC1-DC3
DK	BE(WF)	761	DC1-DC3
DK	DE(WF)	311	DC1-DC3
DK	NL(WF)	550	DC1-DC3
DK	DK(WF)	201	DC1-DC3
DK	UK(WF)	654	DC1-DC3
NO	UK2	711	DC1-DC3
NO	DE(WF)	571	DC1-DC3
NO	DK(WF)	353	DC1-DC3
NO	UK(WF)	414	DC1-DC3
UK2	DK(WF)	638	DC1-DC3
UK2	UK(WF)	311	DC1-DC3
BE(WF)	DE(WF)	462	DC1-DC3
BE(WF)	NL(WF)	229	DC1-DC3
BE(WF)	DK(WF)	677	DC1-DC3
BE(WF)	UK(WF)	820	DC1-DC3
DE(WF)	NL(WF)	241	DC1-DC3
DE(WF)	DK(WF)	223	DC1-DC3
DE(WF)	UK(WF)	556	DC1-DC3
NL(WF)	DK(WF)	449	DC1-DC3
NL(WF)	UK(WF)	630	DC1-DC3
DK(WF)	UK(WF)	460	DC1-DC3

Note: The specified lengths are 125% of the Euclidean
distances to account for obstructions in the shortest path.

Bibliography

[1] Masson-Delmotte et al., "IPCC, 2021: Climate Change 2021: The Physical Science Basis. Contribution of Working Group I to the Sixth Assessment Report of the Intergovernmental Panel on Climate Change," UN IPCC Intergovernmental Panel on Climate Change, Tech. Rep., 2021.

[2] IRENA, "World Energy Transitions Outlook 2022: 1.5°C Pathway," International Renewable Energy Agency, Tech. Rep., 2022.

[3] Dr Fatih Birol et al, "World Energy Outlook 2022," IEA International Energy Agency, Tech. Rep., 2022.

[4] J. Hansen, D. Johnson, A. Lacis, S. Lebedeff, P. Lee, D. Rind, and G. Russell, "Climate impact of increasing atmospheric carbon dioxide," *Science*, vol. 213, pp. 957–966, 1981.

[5] "The Paris Agreement," United Nations Treaty Collection XXVII 7.d.

[6] European Commission, "Re power EU with clean energy," 2022.

[7] Orsted. The world's first offshore wind farm is retiring. [Online]. Available: https://orsted.com/en/media/newsroom/news/2017/03/the-worlds-first-offshore-wind-farm-is-retiring

[8] Electrek. Vestas takes GE's 'world's largest offshore wind turbine' title. [Online]. Available: https://electrek.co/2021/02/10/vestas-gm-worlds-largest-offshore-wind-turbine/

[9] Orsted. Hornsea 2 powering well over 1.4 million homes with green electricity. [Online]. Available: https://hornseaprojects.co.uk/hornsea-project-two

[10] Department of Energy. Offshore wind market report: 2022 edition. [Online]. Available: https://www.energy.gov/eere/wind/articles/offshore-wind-market-report-2022-edition

[11] Jansen, M. et al., "Offshore wind competitiveness in mature markets without subsidy." *Nature Energy*, no. 5, p. 614–622, 2020.

[12] L. Ramírez, "Offshore wind energy 2022 mid-year statistics," Wind Europe, Tech. Rep., 2022.

[13] Rebecca Williams, Feng Zhao, Joyce Lee, "Global Offshore Wind Report 2022." World Forum Offshore Wind., Tech. Rep., 2022.

[14] ENTSO-E. (2018) Transparency platform. [Online]. Available: https://transparency.entsoe.eu/

[15] Wang et. al., "Review and outlook of HVDC grids as backbone of transmission system," *CSEE Journal of Power and Energy Systems*, vol. 7, no. 4, pp. 797–810, 2021.

[16] J.-B. Curis, J. Descloux, N. Grisey *et al.*, "Deliverable 1.3: Synthesis of available studies on offshore meshed HVDC grids," 2016.

[17] Van Hertem, Dirk and Ghandhari, Mehrdad, "Multi-terminal VSC HVDC for the European supergrid: Obstacles," 2010.

[18] *HVDC Grids: For Offshore and Supergrid of the Future.* Wiley, 2016.

[19] Haileselassie, Temesgen M and Uhlen, Kjetil, "Power system security in a meshed north sea HVDC grid," *Proceedings of the IEEE*, vol. 101, no. 4, pp. 978–990, 2013.

[20] Wang, Mian, "Multi-vendor Protection Systems for Meshed HVDC Grids," Leuven, 2020.

[21] X. Guo, Y. Zhou, N. Mei, and B. Zhao, "Construction and characteristic analysis of zhangbei flexible dc grid," *Dianwang Jishu/Power System Technology*, vol. 42, pp. 3698–3707, 11 2018.

[22] Tennet. Windstrom-booster-konzept. [Online]. Available: https://www.tennet.eu/de/ueber-uns/innovationen-und-partnerschaften/windstrom-booster-konzept

[23] "TYNDP 2022 Scenario Report." https://2022.entsos-tyndp-scenarios.eu/wp-content/uploads/2022/04/TYNDP2022_Joint_Scenario_Full-Report-April-2022.pdf, accessed: 2022-11-23.

[24] Horizon 2020 Research Program. Progress on meshed HVDC offshore transmission networks. [Online]. Available: https://www.promotion-offshore.net/

[25] Marie Curie Initial Training Network. Multi-terminal DC grid for offshore wind. [Online]. Available: https://sites.cardiff.ac.uk/medow/

[26] Ergun, Hakan, "Probabilistic optimization of T and D systems planning with high grid flexibility and its scalability Flexplan D1.2," KU Leuven, Tech. Rep., 2021.

[27] Horizon 2020 Research Program. Innovative tools for offshore wind and dc grids. [Online]. Available: https://innodc.org/

[28] VLAIO. Coordinated Planning of Hybrid Offshore Assets. [Online]. Available: https://www.blauwecluster.be/project/cordoba

[29] P. E. Hart, N. J. Nilsson, and B. Raphael, "A formal basis for the heuristic determination of minimum cost paths," *IEEE transactions on systems science and cybernetics*, vol. 4, no. 2, pp. 100–107, 1968.

[30] J.-A. Pérez-Rúa and N. A. Cutululis, "Electrical cable optimization in offshore wind farms—a review," *IEEE Access*, vol. 7, pp. 85 796–85 811, 2019.

[31] Georgilakis, Pavlos S. and Hatziargyriou, Nikos D., "A review of power distribution planning in the modern power systems era: Models, methods and future research," *Electric power systems research*, vol. 121, pp. 89–100, 2015.

[32] F. M. Gonzalez-Longatt, P. Wall, P. Regulski, and V. Terzija, "Optimal electric network design for a large offshore wind farm based on a modified genetic algorithm approach," *IEEE Systems Journal*, vol. 6, no. 1, pp. 164–172, 2012.

[33] Rajabdorri, Mohammad and Kazemtabrizi, Behzad and Troffaes, Matthias and Sigrist, Lukas and Lobato, Enrique, "Inclusion of Frequency Nadir constraint in the Unit Commitment Problem of Small Power Systems Using Machine Learning," *arXiv.org*, 2022.

[34] Somogyi, Zoltan, *The application of artificial intelligence : step-by-step guide from beginner to expert* . Cham, Switzerland: Springer, 2021 - 2021.

[35] Wikipedia. Machine learning. [Online]. Available: https://en.wikipedia.org/wiki/Machine_learning

[36] H. Teichgraeber and A. R. Brandt, "Clustering methods to find representative periods for the optimization of energy systems: An initial framework and comparison," *Applied Energy*, vol. 239, pp. 1283–1293,

2019. [Online]. Available: https://www.sciencedirect.com/science/article/pii/S0306261919303022

[37] M. S. Ibrahim, W. Dong, and Q. Yang, "Machine learning driven smart electric power systems: Current trends and new perspectives," *Applied energy*, vol. 272, p. 115237, 2020.

[38] S. Lumbreras and A. Ramos, "Offshore wind farm electrical design: a review," *Wind Energy*, vol. 16, no. 3, pp. 459–473, April 2013.

[39] A. J. Conejo, L. Baringo, S. J. Kazempour, and A. S. Siddiqui, *Investment in Electricity Generation and Transmission: Decision Making under Uncertainty.* Cham: Springer International Publishing AG, 2016.

[40] A. J. Conejo, E. Castillo, R. García-Bertrand, and R. Mínguez, *Decomposition Techniques in Mathematical Programming: Engineering and Science Applications*, 1st ed. Berlin, Heidelberg: Springer-Verlag, 2006.

[41] G. Oliveira, A. Costa, and S. Binato, "Large scale transmission network planning using optimization and heuristic techniques," *IEEE Transactions on Power Systems*, vol. 10, no. 4, pp. 1828–1834, 1995.

[42] G. Latorre-Bayona and I. Perez-Arriaga, "Chopin, a heuristic model for long term transmission expansion planning," *IEEE Transactions on Power Systems*, vol. 9, no. 4, pp. 1886–1894, 1994.

[43] R. Gallego, "Transmision system expansion planning by an extended genetic algorithm," *IEEE Proceedings - Generation, Transmission and Distribution*, vol. 145, pp. 329–335(6), May 1998. [Online]. Available: https://digital-library.theiet.org/content/journals/10.1049/ip-gtd_19981895

[44] R. Romero, R. Gallego, and A. Monticelli, "Transmission system expansion planning by simulated annealing," in *Proceedings of Power Industry Computer Applications Conference*, 1995, pp. 278–283.

[45] P. Sensarma, M. Rahmani, and A. Carvalho, "A comprehensive method for optimal expansion planning using particle swarm optimization," in *2002 IEEE Power Engineering Society Winter Meeting. Conference Proceedings (Cat. No.02CH37309)*, vol. 2. IEEE, 2002, pp. 1317–1322 vol.2.

[46] E. Da Silva, J. Ortiz, G. De Oliveira, and S. Binato, "Transmission network expansion planning under a tabu search approach," *IEEE Transactions on Power Systems*, vol. 16, no. 1, pp. 62–68, 2001.

[47] G. Ruan, H. Zhong, G. Zhang, Y. He, X. Wang, and T. Pu, "Review of Learning-Assisted Power System Optimization," 2020.

[48] L. L. Garver, "Transmission network estimation using linear programming," *IEEE Transactions on Power Apparatus and Systems*, vol. PAS-89, no. 7, pp. 1688–1697, 1970.

[49] Z. M. Al-Hamouz and A. S. Al-Faraj, "Transmission-expansion planning based on anon-linear programming algorithm," *Applied energy*, vol. 76, no. 1, pp. 169–177, 2003.

[50] V. A. Levi, "A new mixed-integer methodology for optimal transmission expansion planning," *Electric power systems research*, vol. 32, no. 3, pp. 227–238, 1995.

[51] J. Lopez, K. Ponnambalam, and V. Quintana, "Generation and transmission expansion under risk using stochastic programming," *IEEE Transactions on Power Systems*, vol. 22, no. 3, pp. 1369–1378, 2007.

[52] A. Botterud, M. Ilic, and I. Wangensteen, "Optimal investments in power generation under centralized and decentralized decision making," *IEEE Transactions on Power Systems*, vol. 20, no. 1, pp. 254–263, 2005.

[53] European Commission, "Council regulation EU 2019/942 of 5 June 2019 on establishing a european union agency for the cooperation of energy regulators," *Official Journal of the European Union*, 2019.

[54] D. K. Molzahn and I. A. Hiskens, *A Survey of Relaxations and Approximations of the Power Flow Equations*, 2019, vol. 4, no. 1-2.

[55] C. Coffrin, H. Hijazi, and P. Van Hentenryck, "The qc relaxation: A theoretical and computational study on optimal power flow," in *2017 IEEE Power and Energy Society General Meeting*, 2017, pp. 1–1.

[56] Jay Dave, Hakan Ergun, Ting An, Jingjing Lu, Dirk Van Hertem, "TNEP of meshed HVDC grids: 'AC', 'DC' and convex formulations," *IET Generation, Transmission and Distribution*, vol. 13, pp. 5523–5532(9), December 2019. [Online]. Available: https://digital-library.theiet.org/content/journals/10.1049/iet-gtd.2019.0383

[57] X. Bai, H. Wei, K. Fujisawa, and Y. Wang, "Semidefinite programming for optimal power flow problems," *International journal of electrical power and energy systems*, vol. 30, no. 6, pp. 383–392, 2008.

[58] R. Bent, C. Coffrin, R. R. E. Gumucio, and P. Van Hentenryck, "Transmission network expansion planning: Bridging the gap between ac heuristics and dc approximations," in *2014 Power Systems Computation Conference*, 2014, pp. 1–8.

[59] J. Dave, "Dc grid protection aware planning of offshore hvdc grids," Leuven, 2022.

[60] B. Stott, J. Jardim, and O. Alsac, "Dc power flow revisited," *IEEE transactions on power systems*, vol. 24, no. 3, pp. 1290–1300, 2009.

[61] S. Dutta and T. J. Overbye, "Optimal wind farm collector system topology design considering total trenching length," *IEEE Transactions on Sustainable Energy*, vol. 3, no. 3, pp. 339–348, 2012.

[62] S. Dutta and T. Overbye, "A graph-theoretic approach for addressing trenching constraints in wind farm collector system design," in *2013 IEEE Power and Energy Conference at Illinois (PECI)*, 2013, pp. 48–52.

[63] J. Bauer and J. Lysgaard, "The offshore wind farm array cable layout problem: a planar open vehicle routing problem," *Journal of the Operational Research Society*, vol. 66, no. 3, pp. 360–368, 2015. [Online]. Available: http://www.tandfonline.com/doi/abs/10.1057/jors.2013.188

[64] R. Srikakulapu and U. Vinatha, "Optimal design of collector topology for offshore wind farm based on ant colony optimization approach," in *2016 IEEE International Conference on Power Electronics, Drives and Energy Systems (PEDES)*, 2016, pp. 1–6.

[65] P. Hou, W. Hu, C. Chen, and Z. Chen, "Optimisation of offshore wind farm cable connection layout considering levelised production cost using dynamic minimum spanning tree algorithm," *IET renewable power generation*, vol. 10, no. 2, pp. 175–183, 2016.

[66] G. Quinonez-Varela, "Electrical collector system options for large offshore wind farms," *IET Renewable Power Generation*, vol. 1, pp. 107–114(7), June 2007. [Online]. Available: https://digital-library.theiet.org/content/journals/10.1049/iet-rpg_20060017

[67] C. Berzan, "Algorithms for cable network design on large-scale wind farms," 2011.

[68] M. Zhao, "Optimisation of electrical system for offshore wind farms via genetic algorithm," *IET Renewable Power Generation*, vol. 3, pp. 205–216(11), June 2009. [Online]. Available: https://digital-library.theiet.org/content/journals/10.1049/iet-rpg_20070112

[69] A. M. Jenkins, M. Scutariu, and K. S. Smith, "Offshore wind farm inter-array cable layout," in *2013 IEEE Grenoble Conference*, 2013, pp. 1–6.

[70] S. Lehmann, I. Rutter, D. Wagner, and F. Wegner, "A simulated-annealing-based approach for wind farm cabling," in *Proceedings of the Eighth International Conference on Future Energy Systems*, ser. e-Energy '17. New York, NY, USA: Association for Computing Machinery, 2017, p. 203–215. [Online]. Available: https://doi.org/10.1145/3077839.3077843

[71] Y. Eroglu and S. U. Seckiner, "Design of wind farm layout using ant colony algorithm," *Renewable energy*, vol. 44, pp. 53–62, 2012.

[72] Z. Chen, M. Zhao, and F. Blaabjerg, "Application of genetic algorithm in electrical system optimization for offshore wind farms," in *Proceedings of the 3rd International Conference on Electric Utility Deregulation and Restructuring and Power Technologies*. United States: IEEE, 2008, IEEE catalog 08EX1888; null ; Conference date: 06-04-2008 Through 09-04-2008.

[73] D. H. Minguijón, J.-A. Pérez-Rúa, K. Das, and N. A. Cutululis, "Metaheuristic-based design and optimization of offshore wind farms collection systems," in *2019 IEEE Milan PowerTech*, 2019, pp. 1–6.

[74] P. Hou, W. Hu, and Z. Chen, "Optimisation for offshore wind farm cable connection layout using adaptive particle swarm optimisation minimum spanning tree method," *IET renewable power generation*, vol. 10, no. 5, pp. 694–702, 2016.

[75] M. Sedighi, M. Moradzadeh, O. Kukrer, M. Fahrioglu, and L. Vandevelde, "Optimal electrical interconnection configuration of off-shore wind farms," *Journal of Clean Energy Technologies*, vol. 4, pp. 66–71, 2015.

[76] J.-S. Shin and J.-O. Kim, "Optimal design for offshore wind farm considering inner grid layout and offshore substation location," *IEEE Transactions on Power Systems*, vol. 32, no. 3, pp. 2041–2048, 2017.

[77] Cerveira et al., "Optimization design in wind farm distribution network," in *International Joint Conference SOCO'13-CISIS'13-ICEUTE'13*. Cham: Springer International Publishing, 2014, pp. 109–119.

[78] B. C. Neagu and G. Georgescu, "Wind farm cable route optimization using a simple approach," in *2014 International Conference and Exposition on Electrical and Power Engineering (EPE)*, 2014, pp. 1004–1009.

[79] L. Dong, H. Chao, and F. Yang, "Optimization of internal electric connection system of large offshore wind farm with hybrid genetic and immune algorithm," in *2008 Third International Conference on Electric Utility Deregulation and Restructuring and Power Technologies*, 2008, pp. 2476–2481.

[80] J.-A. Pérez-Rúa and N. Cutululis, "A framework for simultaneous design of wind turbines and cable layout in offshore wind," *Wind Energy Science*, vol. 7, no. 2, pp. 925–942, 2022.

[81] A. Cerveira, A. de Sousa, E. J. S. Pires, and J. Baptista, "Optimal cable design of wind farms: The infrastructure and losses cost minimization case," *IEEE Transactions on Power Systems*, vol. 31, no. 6, pp. 4319–4329, 2016.

[82] M. Fischetti and D. Pisinger, "Optimizing wind farm cable routing considering power losses," *European Journal of Operational Research*, vol. 270, no. 3, pp. 917–930, 2018. [Online]. Available: https://www.sciencedirect.com/science/article/pii/S037722171730704X

[83] M. Banzo and A. Ramos, "Stochastic optimization model for electric power system planning of offshore wind farms," *IEEE Transactions on Power Systems*, vol. 26, no. 3, pp. 1338–1348, 2011.

[84] Hertz et al., "Design of a wind farm collection network when several cable types are available." *J Oper Res Soc*, vol. 68, p. 62–73, 2017.

[85] Y. Chen, Z. Y. Dong, K. Meng, F. Luo, Z. Xu, and K. P. Wong, "Collector system layout optimization framework for large-scale offshore wind farms," *IEEE Transactions on Sustainable Energy*, vol. 7, no. 4, pp. 1398–1407, 2016.

[86] A. Klein and D. Haugland, "Obstacle aware optimization of offshore wind farm cable layouts." *Ann Oper Res*, no. 272, p. 373–388, 2019.

[87] A. Pillai, J. Chick, L. Johanning, M. Khorasanchi, and V. de Laleu, "Offshore wind farm electrical cable layout optimization," *Engineering Optimization*, vol. 47, no. 12, pp. 1689–1708, 2015. [Online]. Available: https://doi.org/10.1080/0305215X.2014.992892

[88] S. Lumbreras, A. Ramos, and S. Cerisola, "A progressive contingency incorporation approach for stochastic optimization problems," *Power Systems, IEEE Transactions on*, vol. 28, no. 2, pp. 1452–1460, May 2013.

[89] P. Fagerfjäll, "Optimizing wind farm layout - more bang for the buck using mixed integer linear programming," 2010.

[90] A. Wędzik, T. Siewierski, and M. Szypowski, "A new method for simultaneous optimizing of wind farm's network layout and cable cross-sections by milp optimization," *Applied energy*, vol. 182, pp. 525–538, 2016.

[91] A. Klein, D. Haugland, J. Bauer, and M. Mommer, "An integer programming model for branching cable layouts in offshore wind farms," in *Modelling, Computation and Optimization in Information Systems and Management Sciences*, ser. Advances in Intelligent Systems and Computing. Cham: Springer International Publishing, pp. 27–36.

[92] S. Lundberg, "Configuration study of large wind parks." Chalmers University of Technology, 2003.

[93] Duailibe et al., "Impact of the objective function on the construction of internal grids of wind farms using genetic algorithm." *Open Journal of Civil Engineering*, no. 6, pp. 705–721, 2016.

[94] H. J. Bahirat, B. A. Mork, and H. K. Høidalen, "Comparison of wind farm topologies for offshore applications," in *2012 IEEE Power and Energy Society General Meeting*, 2012, pp. 1–8.

[95] S. Wei, L. Zhang, Y. Xu, Y. Fu, and F. Li, "Hierarchical optimization for the double-sided ring structure of the collector system planning of large offshore wind farms," *IEEE Transactions on Sustainable Energy*, vol. 8, no. 3, pp. 1029–1039, 2017.

[96] P. Hou, W. Hu, C. Chen, and Z. Chen, "Overall optimization for offshore wind farm electrical system," *Wind energy (Chichester, England)*, vol. 20, no. 6, pp. 1017–1032, 2017.

[97] M. Zhao, Z. Chen, and F. Blaabjerg, "Optimization of electrical system for a large dc offshore wind farm by genetic algorithm." Nordic Workshop on Power and Industrial Electronics, 2004.

[98] O. Dahmani, S. Bourguet, M. Machmoum, P. Guerin, P. Rhein, and L. Josse, "Optimization of the connection topology of an offshore wind farm network," *Systems Journal, IEEE*, vol. 9, no. 4, pp. 1519–1528, December 2015.

[99] H. Lingling, F. Yang, and G. Xiaoming, "Optimization of electrical connection scheme for large offshore wind farm with genetic algorithm," in *2009 International Conference on Sustainable Power Generation and Supply*, 2009, pp. 1–4.

[100] W.-S. Moon, J.-C. Kim, A. Jo, and J.-N. Won, "Grid optimization for offshore wind farm layout and substation location," in *2014 IEEE Conference and Expo Transportation Electrification Asia-Pacific (ITEC Asia-Pacific)*, 2014, pp. 1–6.

[101] M. Zhao, Z. Chen, and J. Hjerrild, "Analysis of the behaviour of genetic algorithm applied in optimization of electrical system design for offshore wind farms," in *IECON 2006 - 32nd Annual Conference on IEEE Industrial Electronics*, 2006, pp. 2335–2340.

[102] S. Lumbreras and A. Ramos, "Optimal design of the electrical layout of an offshore wind farm applying decomposition strategies," *IEEE Transactions on Power Systems*, vol. 28, no. 2, August 2012.

[103] ——, "A Benders' Decomposition Approach for Optimizing the Electric System of Offshore Wind Farms," *IEEE Trondheim PowerTech conference*, 2011.

[104] J. Serrano González, M. Burgos Payán, and J. Riquelme Santos, "Optimum design of transmissions systems for offshore wind farms including decision making under risk," *Renewable energy*, vol. 59, pp. 115–127, 2013.

[105] H. Ergun, D. Van Hertem, and R. Belmans, "Transmission system topology optimization for large-scale offshore wind integration," *IEEE Transactions on Sustainable Energy*, vol. 3, no. 4, pp. 908–917, 2012.

[106] T. Trotscher and M. Korpås, "A framework to determine optimal offshore grid structures for wind power integration and power exchange," *Wind Energy*, vol. 14, pp. 977–992, 2011.

[107] H. G. Svendsen, "Planning tool for clustering and optimised grid connection of offshore wind farms," *Energy Procedia*, vol. 35, pp. 297–306, 2013, deepWind'2013 – Selected papers from 10th Deep Sea Offshore Wind RnD Conference, Trondheim, Norway, 24 – 25 January 2013. [Online]. Available: https://www.sciencedirect.com/science/article/pii/S187661021301268X

[108] V. C. Tai and K. Uhlen, "Design and optimisation of offshore grids in baltic sea for scenario year 2030," *Energy Procedia*, vol. 53, pp. 124–134, 2014, eERA DeepWind' 2014, 11th Deep Sea Offshore Wind RnD Conference. [Online]. Available: https://www.sciencedirect.com/science/article/pii/S1876610214010984

[109] H. Oh and W. Short, "Optimal expansion planning for the deployment of wind energy," *Journal of Energy Engineering*, vol. 135, no. 3, pp. 83–88, 2009.

[110] Y. Zhou, L. Wang, and J. D. McCalley, "Designing effective and efficient incentive policies for renewable energy in generation expansion planning," *Applied Energy*, vol. 88, no. 6, pp. 2201–2209, 2011. [Online]. Available: https://www.sciencedirect.com/science/article/pii/S0306261910005428

[111] S. J. Kazempour, A. J. Conejo, and C. Ruiz, "Strategic Generation Investment Using a Complementarity Approach," *IEEE Transactions on Power Systems*, vol. 26, no. 2, pp. 940–948, 2011.

[112] S. J. Kazempour and A. J. Conejo, "Strategic Generation Investment Under Uncertainty Via Benders Decomposition," *IEEE Transactions on Power Systems*, vol. 27, no. 1, pp. 424–432, 2012.

[113] F. H. Murphy and Y. Smeers, "Generation Capacity Expansion in Imperfectly Competitive Restructured Electricity Markets," *Operations research*, vol. 53, no. 4, pp. 646–661, 2005.

[114] P. Kaymaz, J. Valenzuela, and C. S. Park, "Transmission congestion and competition on power generation expansion," *IEEE Transactions on Power Systems*, vol. 22, no. 1, pp. 156–163, 2007.

[115] Kazempour, Jalal, "Advanced Optimization and Game Theory for Energy Systems - lecture 6," University Lecture, 2021, accessed: 05-09-22. [Online]. Available: https://www.jalalkazempour.com/teaching

[116] S. A. Gabriel, A. J. Conejo, J. D. Fuller, B. F. Hobbs, and C. Ruiz, *Complementarity Modeling in Energy Markets*, 2013th ed., ser. International Series in Operations Research and Management Science. New York, NY: Springer New York, vol. 180.

[117] C. Ruiz, A. J. Conejo, J. D. Fuller, S. A. Gabriel, and B. F. Hobbs, "A tutorial review of complementarity models for decision-making in energy markets," *EURO journal on decision processes*, vol. 2, no. 1-2, pp. 91–120, 2013.

[118] B. Hobbs, "Lcp models of nash-cournot competition in bilateral and poolco-based power markets," in *IEEE Power Engineering Society. 1999 Winter Meeting (Cat. No.99CH36233)*, vol. 1, 1999, pp. 303–308 vol.1.

[119] V. Grimm, A. Martin, M. Schmidt, M. Weibelzahl, and G. Zöttl, "Transmission and generation investment in electricity markets: The effects of market splitting and network fee regimes," *European journal of operational research*, vol. 254, no. 2, pp. 493–509, 2016.

[120] J. Wang, M. Shahidehpour, Z. Li, and A. Botterud, "Strategic Generation Capacity Expansion Planning With Incomplete Information," *IEEE Transactions on Power Systems*, vol. 24, no. 2, pp. 1002–1010, 2009.

[121] A. Chuang, F. Wu, and P. Varaiya, "A game-theoretic model for generation expansion planning: problem formulation and numerical comparisons," *IEEE Transactions on Power Systems*, vol. 16, no. 4, pp. 885–891, 2001.

[122] Roald et al., "Power systems optimization under uncertainty: A review of methods and applications." Power Systems Computations Conference PSCC2022 Porto, Portugal, July 2022.

[123] L. Baringo and A. J. Conejo, "Wind power investment: A benders decomposition approach," *IEEE Transactions on Power Systems*, vol. 27, no. 1, pp. 433–441, 2012.

[124] A. Marin and J. Salmeron, "Electric capacity expansion under uncertain demand: decomposition approaches," *IEEE Transactions on Power Systems*, vol. 13, no. 2, pp. 333–339, 1998.

[125] L. Baringo and A. Conejo, "Correlated wind-power production and electric load scenarios for investment decisions," *Applied Energy*, vol. 101, pp. 475–482, 2013, sustainable Development of Energy, Water and Environment Systems. [Online]. Available: https://www.sciencedirect.com/science/article/pii/S0306261912004400

[126] D. Bertsimas and M. Sim, "Robust discrete optimization and network flows," *Mathematical programming*, vol. 98, no. 1-3, pp. 49–71, 2003.

[127] X. Zhang and A. J. Conejo, "Robust Transmission Expansion Planning Representing Long- and Short-Term Uncertainty," *IEEE Transactions on Power Systems*, vol. 33, no. 2, pp. 1329–1338, 2018.

[128] R. A. Jabr, "Robust Transmission Network Expansion Planning With Uncertain Renewable Generation and Loads," *IEEE Transactions on Power Systems*, vol. 28, no. 4, pp. 4558–4567, 2013.

[129] Chen et al., "Robust Optimization for Transmission Expansion Planning: Minimax Cost vs. Minimax Regret," *IEEE Transactions on Power Systems*, vol. 29, no. 6, pp. 3069–3077, 2014.

[130] Alvaro Lorca, X. Andy Sun, Eugene Litvinov, Tongxin Zheng, "Multistage Adaptive Robust Optimization for the Unit Commitment Problem," *Operations Research*, vol. 64, pp. 32–51, 2016.

[131] D. Bienstock, M. Chertkov, and S. Harnett, "Chance-constrained optimal power flow: Risk-aware network control under uncertainty," *SIAM review*, vol. 56, no. 3, pp. 461–495, 2014.

[132] N. Barberis Negra, O. Holmstrom, B. Bak-Jensen, and P. Sorensen, "Aspects of relevance in offshore wind farm reliability assessment," *IEEE Transactions on Energy Conversion*, vol. 22, no. 1, pp. 159–166, 2007.

[133] M. Zhao, Z. Chen, and F. Blaabjerg, "Generation ratio availability assessment of electrical systems for offshore wind farms," *IEEE Transactions on Energy Conversion*, vol. 22, no. 3, pp. 755–763, 2007.

[134] R. Sun, G. Abeynayake, J. Liang, and K. Wang, "Reliability and economic evaluation of offshore wind power dc collection systems," *Energies*, vol. 14, no. 10, 2021. [Online]. Available: https://www.mdpi.com/1996-1073/14/10/2922

[135] G. Abeynayake, T. Van Acker, D. V. Hertem, and J. Liang, "Analytical model for availability assessment of large-scale offshore wind farms including their collector system," *IEEE Transactions on Sustainable Energy*, vol. 12, no. 4, pp. 1974–1983, 2021.

[136] B. Rasuo and A. Bengin, "Optimization of wind farm layout," *FME Transactions*, vol. 38, 01 2010.

[137] G. Quinonez-Varela, "Electrical collector system options for large offshore wind farms," *IET Renewable Power Generation*, vol. 1, pp. 107–114(7), June 2007. [Online]. Available: https://digital-library.theiet.org/content/journals/10.1049/iet-rpg_20060017

[138] P. Sanchez-Martin, A. Ramos, and J. Alonso, "Probabilistic midterm transmission planning in a liberalized market," *IEEE Transactions on Power Systems*, vol. 20, no. 4, pp. 2135–2142, 2005.

[139] P. Djapic and G. Strbac, "Centre for Sustainable Electricity and Distributed Generation Cost Benefit Methodology for Optimal Design of Offshore Transmission Systems," Tech. Rep., 2008.

[140] Saxena et al., "A review of clustering techniques and developments," *Neurocomputing*, vol. 267, pp. 664–681, 2017. [Online]. Available: https://www.sciencedirect.com/science/article/pii/S0925231217311815

[141] Bentley and Ottmann, "Algorithms for reporting and counting geometric intersections," *IEEE Transactions on Computers*, vol. C-28, no. 9, pp. 643–647, 1979.

[142] A. Pillai, J. Chick, L. Johanning, M. Khorasanchi, and V. de Laleu, "Offshore wind farm electrical cable layout optimization," *Engineering optimization*, vol. 47, no. 12, pp. 1689–1708, 2015.

[143] H. Ergun and R. Belmans, *Grid Planning for the Future Grid: optimizing Topology and Technology Considering Spatial and Temporal Effects*. Leuven: KU Leuven.Faculteit ingenieurswetenschappen, 2015. [Online]. Available: https://lirias.kuleuven.be/handle/123456789/472917

[144] H. Ergun, B. Rawn, R. Belmans, and D. Van Hertem, "Technology and topology optimization for multizonal transmission systems," *IEEE Transactions on Power Systems*, vol. 29, no. 5, pp. 2469–2477, 2014.

[145] I. Katic and J. Højstrup and Niels Otto Jensen , "A simple model for cluster efficiency," pp. 407–410, 1986.

[146] S. Donovan, "Wind farm optimization."   Department of Engineering Science University of Auckland New Zealand, 2005.

[147] H.-G. Kim, "A method of accelerating the convergence of computational fluid dynamics for micro-siting wind mapping," *Computation*, vol. 7, p. 22, 04 2019.

[148] "ENTSOE Project 120 - MOG II: connection of up to 2 GW additional offshore wind Belgium," https://tyndp2022-project-platform.azurewebsit es.net/projectsheets/transmission/120, accessed: 23-03-30.

[149] Smith, Bridget, "EU ALL for Belgian Energy Island," https://www.4coffs hore.com/news/eu-all-for-belgian-energy-island-nid23751.html, accessed: 2021-07-17.

[150] ENTSO-E, "Project 309 - neuconnect," 2022. [Online]. Available: https://tyndp2020-project-platform.azurewebsites.net/projectsheets/tra nsmission/309

[151] N. G. V. Elia Group, "Nautilus hybrid interconnecter," 2022. [Online]. Available: https://www.elia.be/en/infrastructure-and-projects/infrastructure-projects/nautilus

[152] E. Elia Group, "Triton link hybrid interconnecter," 2022. [Online]. Available: https://www.elia.be/en/news/press-releases/2021/11/20211 123_preliminary-study-on-hybrid-interconnector

[153] ENTSO-E, "Project 1051 - aminth energy ltd," 2022. [Online]. Available: https://tyndp2020-project-platform.azurewebsites.net/projectsheets/tra nsmission/1051

[154] E. Elia Group, "Project 335 - north sea wind power hub," 2022. [Online]. Available: https://tyndp2020-project-platform.azurewebsites.net/proje ctsheets/transmission/335

[155] Elia group, "Elia presents its plans for an energy island, which will be called the Princess Elisabeth Island – 3/10/22," https://www.elia.be/en/infrast ructure-and-projects/infrastructure-projects/princess-elisabeth-island/, accessed: 2023-30-03.

[156] FPS Economy, Government of Belgium, "Belgian offshore wind energy," https://economie.fgov.be/en/themes/energy/belgian-offshore-wind-energy, accessed: 2023-30-03.

[157] O. Dahmani, S. Bourguet, M. Machmoum, P. Guerin, P. Rhein, and L. Josse, "Optimization and reliability evaluation of an offshore wind farm architecture," *IEEE Transactions on Sustainable Energy*, vol. 8, no. 2, pp. 542–550, April 2017.

[158] Barot, H, "New Paradigms in Medium-Term Operations and Planning of Power Systems in Deregulation," Ph.D. dissertation, University of Waterloo, 2009.

[159] R. S. Olsen, J. Holboll, and U. S. Gudmundsdottir, "Dynamic temperature estimation and real time emergency rating of transmission cables," in *2012 IEEE Power and Energy Society General Meeting*.   IEEE, 2012, pp. 1–8.

[160] R. Olsen, G. J. Anders, J. Holboell, and U. S. Gudmundsdottir, "Modelling of dynamic transmission cable temperature considering soil-specific heat, thermal resistivity, and precipitation," *IEEE Transactions on Power Delivery*, vol. 28, no. 3, pp. 1909–1917, 2013.

[161] "IEC-60287-1: Electric cables - Calculation of the current rating," IEC International Electro-technical Commission, Tech. Rep., 2014.

[162] "Current ratings of cables for cyclic and emergency loads. Part 1. Cyclic Ratings (load factor Less than 100%) and response to a step function," CIGRE, Tech. Rep., 1976.

[163] "IEC-60853-2: Calculation of cyclic and emergency current rating of cables," IEC International Electro-technical Commission, Tech. Rep., 2008.

[164] CIGRE working group B1.40, "Offshore generation cable connections," CIGRE, Tech. Rep., 2015.

[165] J.-A. Pérez-Rúa, K. Das, and N. A. Cutululis, "Optimum sizing of offshore wind farm export cables," *International journal of electrical power and energy systems*, vol. 113, pp. 982–990, 2019.

[166] ENTSO-E. (2018) Transparency platform. [Online]. Available: https://transparency.entsoe.eu/transmission-domain/r2/dayAheadPrices/show

[167] ——, "Data set: Offshore wind time series," 2020. [Online]. Available: https://zenodo.org/record/3702418/files/PECD-MAF2019-wide-WindOffshore.feather?download=1

[168] Koivisto et al., "Using time series simulation tools for assessing the effects of variable renewable energy generation on power and energy systems," *Wiley Interdisciplinary Reviews: Energy and Environment*, vol. 8, no. 3, p. e329, 2019. [Online]. Available: https://onlinelibrary.wiley.com/doi/abs/10.1002/wene.329

[169] Sorensen, Koivisto, Murcia, "Final study report: MOGII System integration study," Elia Transmission Belgium, DTU Wind Energy, Tech. Rep., 2020.

[170] Chen, H. et al., "Assessing probabilistic modelling for wind speed from numerical weather prediction model and observation in the Arctic." *Sci Rep*, vol. 11, 2021.

[171] Barthelmie et al., "Modelling and measuring flow and wind turbine wakes in large wind farms offshore," *Wind Energy*, vol. 12, no. 5, pp. 431–444, 2009. [Online]. Available: https://onlinelibrary.wiley.com/doi/abs/10.1002/we.348

[172] Chandra Kant Jat, Stephen Hardy, Jay Kumar Dave, Hakan Ergun, Dirk Van Hertem, "Cost-Effective Planning of a Multi-Terminal HVDC Grid Considering Hybrid Offshore Assets," *IEEE Transactions on Industry Applications - under review*, 2021.

[173] "ENTSOE TYNDP Ten year network development plan." https://2022.entsos-tyndp-scenarios.eu/, accessed: 2022-05-17.

[174] "TYNDP 2020 Figure 36: RES LCOE in Distributed Energy 2040," https://2020.entsos-tyndp-scenarios.eu/electricity-costs/, accessed: 2019-08-05.

[175] ENTSO-E, "Data set: Reference grid 2025," 2020. [Online]. Available: https://www.entsoe.eu/Documents/TYNDP%20documents/TYNDP2020/Reference%20Grid%202025%20-%20TYNDP%202020.xlsx

[176] Coastal Division - Flemish Hydrography. Belgian hydrography data. [Online]. Available: https://bathy.agentschapmdk.be/spatialfusionviewer/mapViewer/map.action#

[177] EEA, "Europe's onshore and offshore wind energy potential an assessment of environmental and economic constraints," European Environmental Agency, Tech. Rep., 2009.

[178] European Commission, "Electricity network codes and guidelines," 2022.

[179] Cox et al. - KPMG LLP, "Offshore Transmission: An Investor Perspective - Update Report," https://www.ofgem.gov.uk, accessed: 20-06-18.

[180] European Commission, "United Kingdom: Post-Brexit relations on energy fall under the EU-UK Trade Cooperation Agreement and the Euratom-UK Agreement." 2022.

[181] Department for Business, Energy and Industrial Strategy, "Policy paper Trading electricity with the EU." 2021.

[182] "Denmark Greenlights North Sea Energy Island Hub," https://www.offshorewind.biz/2021/02/04/breaking-denmark-greenlights-north-sea-energy-island-hub/, accessed: 22-02-21.

[183] NSCOGI, "Offshore Transmission Technology," European Network of Transmission System Operators for Electricity, Tech. Rep., 2012.

[184] Flament et al., "North sea grid, final report." 3E, Tech. Rep., 2014.

[185] DNV GL, "PROMOTioN cost data collection report [internal document]," 2020.

[186] ABB's high voltage cable unit in Sweden, "XLPE Submarine Cable Systems Attachment to XLPE Land Cable Systems-User´s Guide Rev 5 2 XLPE Submarine Cable Systems | ABB," ABB, Tech. Rep. [Online]. Available: www.abb.com/cables

[187] C. Hill, "Offshore Transmission Benchmarking and Cost Monitoring," Catapult, Tech. Rep., 2016.

[188] Navigant Netherlands B.V., "Connecting offshore wind farms," Réseau de Transport d'Électricité and TenneT TSO B.V., Tech. Rep., 2019.

[189] Hardy, Ergun, Van Hertem, "A Greedy Algorithm for Optimizing Offshore Wind Transmission Topologies." *IEEE Transactions on Power Systems*, 2021.

[190] S.Hardy, H.Ergun, D.Van Hertem, K. Van Brusselen, "A Techno-Economic MILP Optimization of Multiple Offshore Wind Concessiosn." *Large-Scale Grid Integration of Renewable Energy in India*, 2019.

[191] W. C. Skamarock, J. B. Klemp, J. Dudhia, D. O. Gill, Z. Liu, J. Berner, W. Wang, J. G. Powers, M. G. Duda, D. M. Barker, and X.-Y. Huang,, "A description of the advanced research wrf version 4." 2019.

[192] Wächter, Andreas and Biegler, Lorenz T., "On the implementation of an interior-point filter line-search algorithm for large-scale nonlinear programming," *Mathematical programming*, vol. 106, no. 1, pp. 25–57, 2006.

[193] Coffrin et al., "PowerModels.jl: An Open-Source Framework for Exploring Power Flow Formulations," in *2018 Power Systems Computation Conference (PSCC)*, June 2018, pp. 1–8.

[194] L. Gurobi Optimization, "Gurobi optimizer reference manual," 2020. [Online]. Available: http://www.gurobi.com

[195] J.-A. Perez-Rua, M. Stolpe, K. Das, and N. A. Cutululis, "Global optimization of offshore wind farm collection systems," *IEEE Transactions on Power Systems*, vol. 35, no. 3, pp. 2256–2267, 2020.

[196] J.-A. Perez-Rua, M. Stolpe, and N. A. Cutululis, "Integrated global optimization model for electrical cables in offshore wind farms," *IEEE Transactions on Sustainable Energy*, vol. 11, no. 3, pp. 1965–1974, 2020.

[197] Z. Zhang, D. Zhang, and R. C. Qiu, "Deep Reinforcement Learning for Power System Applications: An Overview," *CSEE Journal of Power and Energy Systems*, vol. 6, no. 1, pp. 213–225, 2020.

[198] A. P. Marugán, F. P. G. Márquez, J. M. P. Perez, and D. Ruiz-Hernández, "A survey of artificial neural network in wind energy systems," *Applied energy*, vol. 228, pp. 1822–1836, 2018.

[199] Q. Sun and L. Yang, "From Independence to Interconnection-A Review of AI Technology Applied in Energy Systems," *CSEE Journal of Power and Energy Systems*, vol. 5, no. 1, pp. 21–34, 2019.

[200] R. Agrawal, T. Imieliński, and A. Swami, "Mining association rules between sets of items in large databases," in *SIGMOD Record (ACM Special Interest Group on Management of Data)*, vol. 22, no. 2, 1993, pp. 207–216.

[201] K. Lakshmi and G. Vadivu, "Extracting Association Rules from Medical Health Records Using Multi-Criteria Decision Analysis," *Procedia Computer Science*, vol. 115, pp. 290–295, 2017, 7th International Conference on Advances in Computing and Communications, ICACC-2017, 22-24 August 2017, Cochin, India.

[202] D. Liu, Y. Chen, Y. Fan, and G. Shen, "The application of association rule mining in power system restoration," in *2006 IEEE Power Engineering Society General Meeting*, 2006, p. 5.

[203] S. Pang and N. Kasabov, "Svmt-rule: Association rule mining over svm classification trees," in *Rule Extraction from Support Vector Machines*, ser. Studies in Computational Intelligence. Berlin, Heidelberg: Springer Berlin Heidelberg, 2008, vol. 80, pp. 135–162.

[204] M. J. Zaki, "Scalable algorithms for association mining," *IEEE Transactions on knowledge and data engineering*, vol. 12, no. 3, pp. 372–390, 2000.

[205] J. Han, J. Pei, Y. Yin, and R. Mao, "Mining Frequent Patterns without Candidate Generation: A Frequent-Pattern Tree Approach," *Data mining and knowledge discovery*, vol. 8, no. 1, pp. 53–87, 2004.

[206] P. Stey, M. McGrath, M. I. Restrepo, D. Aluthge, and B. Bot, "bcbi/arules.jl: v0.0.2," Feb. 2020. [Online]. Available: https://doi.org/10.5281/zenodo.3660120

[207] J. F. Seth Bromberger, "Juliagraphs/lightgraphs.jl: an optimized graphs package for the julia programming language," 2017. [Online]. Available: https://doi.org/10.5281/zenodo.889971

[208] J. Bezanson, A. Edelman, S. Karpinski, and V. B. Shah, "Julia: A fresh approach to numerical computing," *SIAM review*, vol. 59, no. 1, pp. 65–98, 2017. [Online]. Available: https://doi.org/10.1137/141000671

[209] "Project 120 - MOG II: connection of up to 2 GW additional offshore wind Belgium," https://tyndp2022-project-platform.azurewebsites.net/projectsheets/transmission/120, accessed: 23-03-30.

[210] S. P. Lloyd, "Least squares quantization in PCM," *IEEE Trans. Inf. Theory*, vol. 28, pp. 129–136, 1982.

[211] L. Hirth and I. Schlecht, "Market-based redispatch in zonal electricity markets," *IO: Empirical Studies of Firms and Markets eJournal*, 2018.

[212] A. Moser, N. Bracht, and A. Maaz, "Simulating electricity market bidding and price caps in the European power markets s18 report," European Commission and Directorate-General for Energy, Tech. Rep., 2017.

[213] J. Dave, H. Ergun, T. An, J. Lu, and D. Van Hertem, "TNEP of meshed HVDC grids: 'AC', DC and convex formulations," *IET Generation, Transmission and Distribution*, vol. 13, pp. 5523–5532(9), dec 2019.

[214] "4C Offshore Renewable Map," https://www.4coffshore.com/offshorewind/, 2018.

[215] PROMOTioN Workpackage 1, "Cost data collection report," KU Leuven, Tech. Rep., 2020, (Internal document).

[216] ABB high voltage cable unit, "HVDC light cables, submarine and land power cables," ABB, Tech. Rep., 2006.

[217] Wesley Cole, A. Will Frazier, and Chad Augustine, "Cost Projections for Utility-Scale Battery Storage: 2021 Update," NREL National Renewable Energy Laboratory, Tech. Rep., 2021.

[218] "ENTSOE TYNDP Ten year network development plan," accessed: 2022-05-17. [Online]. Available: https://2022.entsos-tyndp-scenarios.eu/

[219] European Commission, "Council regulation EU 2022/1854 of 6 October 2022 on an emergency intervention to address high energy prices," *Official Journal of the European Union*, 2022.

[220] L. Kaufman and P. Rousseeuw, *Partitioning Around Medoids (Program PAM).* John Wiley & Sons, Ltd, 1990, pp. 68–125.

[221] A. Themelis, L. Stella, and P. Patrinos, "Douglas-Rachford splitting and ADMM for nonconvex optimization: Accelerated and Newton-type algorithms," *Computational Optimization and Applications*, vol. 82, pp. 395–440, 2022.

[222] J. Schachner, "Power connections for offshore wind farms," Master's thesis, Delft University of Technology, January 2004.

[223] ABB, "XLPE Submarine Cable Systems," Tech. Rep., 2010.

[224] NKT, "High voltage cable systems cables and accessories up to 550 kv," Tech. Rep.

[225] P. B. Wyllie, Y. Tang, L. Ran, T. Yang, and J. Yu, "Low Frequency AC Transmission - Elements of a Design for Wind Farm Connection," Tech. Rep.

[226] W. Fischer, R. Braun, and I. Erlich, "Low frequency high voltage offshore grid for transmission of renewable power," in *2012 3rd IEEE PES Innovative Smart Grid Technologies Europe (ISGT Europe)*, Oct 2012, pp. 1–6.

[227] X. Xiang, M. M. C Merlin, and T. C. Green, "Cost Analysis and Comparison of HVAC, LFAC and HVDC for Offshore Wind Power Connection," in *The 12th IET International Conference on AC and DC*, 2016.

[228] D. Van Hertem and M. Ghandhari, "Multi-terminal VSC HVDC for the European supergrid: Obstacles," *Renewable and sustainable energy reviews*, vol. 14, no. 9, pp. 3156–3163, 2010.

[229] Y. Li and R. P. Gopalan, "Effective Sampling for Mining Association Rules," in *AI 2004: Advances in Artificial Intelligence*, ser. Lecture Notes in Computer Science. Berlin, Heidelberg: Springer Berlin Heidelberg, 2005, vol. 3339, pp. 391–401.

Curriculum vitae

Stephen Hardy born May 22nd 1983 in Victoria, British Columbia, Canada.

2001–2008	Marine Electrical Technician Fleet Maintenance Facility Cape Breton Esquimalt, BC, Canada
2008–2011	B.Eng Electrical Engineering Concordia University Montreal, QC, Canada
2011–2012	Diploma in Electrical Power Systems Engineering IGEE École Polytechnique de Montréal Montreal, QC, Canada
2012–2013	Power Systems Commissioning Engineer Dynamo Electric Regina, SK, Canada
2013–2014	International Development Engineer Engineers Without Borders/ACSES Malawi Lilongwe/Nkhotakhota, Malawi
2014–2016	English Teacher Su-san Eigo (Language school) Tokyo, Japan
2016–2017	M.Sc Mathematical Modelling Universitat Autònoma de Barcelona Barcelona, Catalunya, Spain
2018–2020	R&D Engineer C.G. Power Systems Mechelen, Belgium
2020–2023	Researcher in Engineering Science KU Leuven/EnergyVille Leuven/Genk, Belgium

List of publications

Publications included in this thesis

Peer reviewed journals

- J1: **Stephen Hardy**, Hakan Ergun, Dirk Van Hertem, "A Greedy Algorithm for Optimizing Offshore Wind Transmission Topologies," IEEE Transactions On Power Systems - November 2021.

- J2: **Stephen Hardy**, Hakan Ergun, Dirk Van Hertem, "Application of Association Rule Mining in Offshore HVAC Transmission Topology Optimization," Journal Electric Power Systems Research - July 2022.

- J3: **Stephen Hardy**, Hakan Ergun, Dirk Van Hertem, "Generation and transmission expansion planning under Zonal and Nodal market mechanisms," IEEE Transactions on Energy Markets, Policy and Regulation. – under review.

International conferences

- C1: **Stephen Hardy**, Hakan Ergun, Dirk Van Hertem, Stijn Hendrix, Kristof Van Brusselen, "Techno-Economic Analysis of HVAC, HVDC and OFAC Offshore Wind Power Connections." 2019 IEEE Milan PowerTech.

- C2: **Stephen Hardy**, Hakan Ergun, Dirk Van Hertem, "A Techno-Economic Analysis of meshed Topologies of Offshore Wind HVAC Transmission." 2021 IEEE Madrid PowerTech.

- C3: **Stephen Hardy**, Hakan Ergun, Dirk Van Hertem, "Application of Association Rule Mining in Offshore HVAC Transmission Topology Optimization" PSCC 2022 Porto, Portugal.

- C4: **Stephen Hardy**, Hakan Ergun, Dirk Van Hertem, "A Methodology for Offshore Transmission System Optimization Considering Spatial Constraints," 2023 IEEE Belgrade PowerTech – under review.

Publications not included in the thesis

Peer reviewed journals

- J4: Chandra Kant Jat, **Stephen Hardy**, Jay Kumar Dave, Hakan Ergun, Dirk Van Hertem, "Cost Effectiveness of a Multi-Terminal HVDC Demonstration Grid in the North Sea: Off-shore Bidding Zone Strategy For Wind Generators," Applied Energy – under review.

International conferences

- C5: **Stephen Hardy**, Hakan Ergun, Dirk Van Hertem, Kristof Van Brusselen, "A Techno-Economic MILP Optimization of Multiple Offshore Wind Concessions." 2nd International Conference on Large-Scale Grid Integration of Renewable Energy in India.

FACULTY OF ENGINEERING SCIENCE
DEPARTMENT OF ELECTRICAL ENGINEERING
ELECTA
Kasteelpark Arenberg 10, Bus 2445
B-3001 Leuven
stephen.hardy@kuleuven.be
https://www.esat.kuleuven.be/electa